DEVELOPMENT OF SOFT CHEMICAL PROCESSES:

PREPARATION OF TiO_2 FILMS AND POWDERS AT LOW TEMPERATURE

Memòria presentada per **David Gutiérrez Tauste** a l'Escola de Doctorat i Formació Continuada i al Departament de Química de la Universitat Autònoma de Barcelona, per optar al grau de Doctor en Química

Universitat Autònoma de Barcelona
Departament de Química
Unitat de Química Física

Bellaterra, febrer de 2008

José Antonio Ayllón Esteve, professor titular del Departament de Química de la Universitat Autònoma de Barcelona,

CERTIFICO:

Que aquesta memòria amb títol *Development of soft chemical processes: preparation of TiO_2 films and powders at low temperature* correspon al treball fet sota la meva direcció per **David Gutiérrez Tauste**, llicenciat en Ciències Químiques, i constitueix la seva tesi doctoral per optar al grau de Doctor en Química.

I perquè així consti, signo la present certificació.

Bellaterra, febrer de 2008.

Dr. José Antonio Ayllón Esteve

A la meva família

"My interest is in the future... because I am going to spend the rest of my life there"

Charles F. Kettering

"A mi no me gusta el vino ni el aguardiente serrana,
y el día que yo entré en quintas puse un ramo en tu ventana.
Puse un ramo en tu ventana de rosas y de claveles,
y hoy que vengo licenciado te lo pongo de laureles.
Te lo pongo de laureles por ser la más preferida,
con un letrero que diga: yo serví en infantería!
Yo serví en infantería el cuerpo más elegante,
que en todas las posiciones siempre íbamos delante,
medio descalzos y desnudos,
cargados de miseria y comiendo garbanzos crudos"

A José Tauste

AGRAÏMENTS

Diuen que tot principi té un final. No obstant, sembla mentida que estigui a punt d'acabar la meva tesi doctoral. I és que per un forat em veig el meu primer dia al laboratori intentant aprendre com netejar substrats segons protocols de neteja. Aquesta etapa de la meva vida ha estat plena d'intenses emocions. M'agradaria poder reflectir en aquestes línies totes aquelles contribucions que han fet possible que pogués tirar endavant aquest treball.

En primer lloc, vull agrair al Dr. Xavier Domènech el fet que m'obrís les portes a la recerca en el grup de Fotocatàlisi i Química Verda, la organització d'excursions de grup i les seves correccions d'estil amb l'anglès. Al Dr. José Peral el seu bon humor característic de les excursions de grup i també alguna ajudeta amb l'anglès. Del Dr. José A. Ayllón vull ressaltar tant el seu rigor científic com la seva motivació personal per a les tasques docents i investigadores.

Vull destacar en aquest apartat algunes contribucions directes en el treball. A la incansable Dra. Elena Vigil agrair-li les seves aportacions per a la caracterització de cel·les solars sensibilitzades i la possibilitat de l'estada a Cuba el 2003. Em marcarà per sempre i no oblidaré mai l'acollida que vaig tenir a casa de l'Inti a la Lisa, m'ho van oferir tot a canvi de res. A la Dra. Nieves Casañ li vull agrair la seva ajuda en la caracterització electroquímica de materials mitjançant voltametria cíclica. A la Dra. Concha Domingo gràcies pel suport rebut. Al Dr. Ángel Álvarez del Servei de Difracció de raigs X de la UAB, per la seva gran competència i el suport tècnic per a la caracterització de capes primes. Al Francesc Bohils del Servei de Microscòpia de la UAB, per la seva filosofia de vida i de treball, i per ensenyar-me la importància en la tria i preparació de mostres per a SEM. A la Dra. Emma Rossinyol (també del Servei de Microscòpia) pel tracte rebut i l'assessorament en observacions de TEM. Al Dr. Lorenzo Calvo dels SCT-UB, pel suport tècnic en espectroscòpia XPS. A la Dra. Mª Ángeles Hernández per l'enregistrament d'espectres de fotoluminiscència i el training en l'elaboració de fotocòpies. A L'Ivó Álvarez gràcies per permetre'm el luxe de tenir una portada de disseny per a la tesi.

I would like to thank SONY colleagues for their support and warm welcome in Germany, specially Dr. Gabi Nelles for giving me the opportunity I was looking for. In fact, my three months in Stuttgart went by too fast, and as you all know I would have stayed there for a longer time. I hope our future interests goes in the same direction. As Markus said, “you never know!” (because this is science). My regards to you all, but particularly to Markus, Gerda, Silvia, Ami, Yvonne and Salvatore. I will never forget new friendships started during this time: Luises, Sara, Chris, Nick, Özi, Max, David, Shera…

No és possible deixar de banda els companys de grup i despatx (i també de penes i alegries): Dra. Franch, Ivan, Mª José, Júlia, Xavi Batlle, Marc Estruga, Anna Serra, Nilbia, Neus, Laura, Adrián, Hugo... Tampoc d’altres doctorands de la torre tot i que alguns ja estiguin fora de la casa: Dani, Campillo, Juanma, Aleix Parra, Lluís, Elena, Mercè, Sergio, Adrià, Edu, Edgar, Juanmilla...; ni coneguts de Cerda: Mascaró, Caba, Dani Peüc, Javo, Llandro, Francesc, Sergi, Desi...; ni vigatans: Jus, Miki, Nasi, Silvia, Pep, Cati, Mon, Torres... Gràcies pels ànims i per allò de “com va?”, imprescindible per a la superació de les dificultats que cadascú es troba pel camí. Com no, també mercis per les convocatòries nocturnes, les sessions de SAF i tots els moments viscuts!

Diuen que si es pot dir el que un estima és que no estima de veritat. Gràcies Sara perquè sense tu mai ho hauria aconseguit; tu també et doctores amb mi. A partir d’ara, una nova etapa amb nous projectes... A la teva família, gràcies per acollir-me com un membre més.

Por último, debo agradecer todo lo que soy a mis padres. Ellos me han dado todo a cambio de nada: mi vida, mi educación y mi formación. Papa, gracias por las obras de reforma de nuestro piso, por tus consejos y por tu contribución a esta investigación en forma de herramientas de laboratorio improvisadas. Mama, gracias por esas fiambreras energéticas especialmente indicadas para trabajos de investigación y que todo el mundo recuerda como una característica mía. A la abuela gracias por estar siempre al “loro” de cuando llego y salgo.

Gràcies a tots pel vostre granet de sorra aportat en aquesta tesi, però sobretot gràcies a TU per llegir-la!

PREFACE

In the 21st century, scientific community faces challenges and opportunities concerning future development, where innovations will obviously play key roles. Over the past, evolution of western societies were based on incomplete models, only taking into account economical growth and not paying attention to environmental deterioration as a consequence of anthropogenic activity. We all have to learn from the mistakes of the past in order to not repeat them. Education and research of today, as the embryonic stages of the development models of tomorrow, should be redirected toward a sustainable mentality. In this sense, Green Chemistry has emerged as supportive instrument for minimizing environmental impact as well as economic cost in the field of chemical processes.

Titanium dioxide is a fascinating low-cost material exhibiting unique properties of stability and photoactivity, leading to clean technologies in environmental remediation and energy conversion of sunlight. However, conventional high-temperature processing of titania is a technological limitation beyond energy consumption, being a handicap for practical applications in areas such as the preparation of hybrid organic/TiO_2 materials or devices on thermolabile substrates. In this direction, the investigation presented in this doctoral dissertation deals with the development of soft chemical processes for preparing TiO_2 films and powders at low temperature.

The memory is divided in the following chapters: *Introduction*, *Goal and Scope of the Work*, *Materials and Methods*, *Results and Discussion*, *Concluding Remarks* and *Annexe*. The *Introduction* chapter highlights those aspects more significant for understanding the experimental work carried out. The main topics concerning fundamentals, practical applications as well as preparation methods of TiO_2 materials have been reviewed. A general outline of the *Goal and Scope of the Work* is included in the second chapter of the memory. The *Materials and Methods* chapter has been added to the memory for giving further information not explicitly described in the experimental sections of Publications, thus facilitating comprehension of this doctoral dissertation.

The *Results and Discussion* chapter is presented as a compendium of five publications. Note this chapter has been organized in four parts since discussion regarding to preparation of hybrid organic/TiO_2 films (Publication 3 and 4) has been comprised together in Section 4.3.

New low-temperature preparation method of the TiO_2 porous photoelectrode for dye-sensitized solar cells using UV irradiation.

J. Photochem. Photobiol. A: Chem. **2005**, *175*, 165-171.

Alternative fluoride scavengers to produce TiO_2 films by the liquid phase deposition (LPD) technique.

J. Mater. Chem. **2006**, *16*, 2249-2255.

Characterization of methylene blue/TiO_2 hybrid thin films prepared by the liquid phase deposition (LPD) method: Application for fabrication of light-activated colorimetric oxygen indicators.

J. Photochem. Photobiol. A: Chem. **2007**, *187*, 45-52.

Dopamine/TiO_2 hybrid thin films prepared by the liquid phase deposition method.

Thin Solid Films **2008**, *516*, 3831-3835.

Hexafluorotitanate salts containing organic cations: use as a reaction medium and precursor to the synthesis of titanium dioxide.

Chem. Commun. **2007**, 4659-4661.

Following the results part, the *Concluding Remarks* chapter examines general conclusions as well as perspectives derived from the present work. Finally, results awaiting publication are described in the *Annexe* chapter. These results comprise further studies continuing with the latter publication, some of them obtained during a research stay at the Material Science Laboratory of SONY Stuttgart Technology Center GmbH (Germany).

TABLE OF CONTENTS

GLOSSARY OF ABBREVIATIONS AND SYMBOLS

AM	Air Mass
AOPs	Advanced Oxidation Processes
At.%	Atomic percentage
ATR-FTIR	Attenuated Total Reflectance Fourier Transform Infrared
BET	Brunauer-Emmett-Teller
Bet	Betaine, $(CH_3)_3$-N^+-CH_2-COO^-
$BetH^+$	Betainium, $(CH_3)_3$-N^+-CH_2-COOH
CB	Conduction Band
CBD	Chemical Bath Deposition
Cho^+	Choline, $(CH_3)_3$-N^+-CH_2-CH_2OH
CV	Cyclic Voltammetry
DA	Dopamine
DSSCs	Dye-Sensitized Solar Cells
E	Irradiance, incident luminous power per area unit
E_λ	Spectral irradiance, incident luminous power per area unit at a fixed λ.
e^-_{CB} / h^+_{VB}	Electron-hole photogenerated in a semiconductor.
EPA	Environmental Protection Agency
EU	European Union
FF	Fill Factor
FTO	Fluorine Tin Oxide (SnO_2:F)
GCN	Green Chemistry Network
h	hour
HFTA	Hexafluorotitanic acid
HR	High Resolution
ILs	Ionic Liquids
IPCE	Incident Photon-to-Current Conversion Efficiency
IR	Infrared

ITO	Indium Tin Oxide (In_2O_3:Sn)
IUPAC	International Union of Pure and Applied Chemistry
I_{SC}	Short-circuit photocurrent
J_{SC}	Short-circuit photocurrent density
λ	Wavelength
λ_{max}	Maximum absorption wavelength
LPD	Liquid Phase Deposition
MB	Methylene Blue
min	minute
MLCT	Metal-to-Ligand Charge Transfer
MSL	Material Science Laboratory
η	Global conversion efficiency
NHE	Normal Hydrogen Electrode
OECD	Organization for the Economical Cooperation and Development
$OH^{\cdot}$	Hydroxyl radical
PEN	Poly(Ethylene Naphthalate)
PET	Poly(Ethylene Terephthalate)
PETEQUS	Plataforma Tecnológica Española de Química Sostenible
PFA	Per(fluoroalkoxy)
PTFE	Poly(tetrafluoroethylene)
REACH	Registration, Evaluation, Authorization and restriction of Chemicals
S	Photosensitizer
S*	Photoexcited sensitizer
SAMs	Self-assembled monolayers
SCE	Saturated Calomel Electrode
SED	Sacrificial Electron Donor
SEM	Scanning Electron Microscopy
SILAR	Successive Ionic-Layer Adsorption and Reaction
TALH	Titanium(IV) *bis*(ammonium lactato)dihydroxide
TBACl	Tetrabutylammonium chloride
TCO	Transparent Conductive Oxide
TEM	Transmission Electron Microscopy

TTB	Titanium tetrabutoxide
TTIP	Titanium tetra*iso*propoxide
TW	Terawatts
US	United States
UV	Ultraviolet
UVA	Ultraviolet A
UV-Vis	Ultraviolet-Visible
VB	Valence Band
V_{OC}	Open-circuit photovoltage
Wt.%	Weight percentage
XPS	X-Ray Photoelectron Spectroscopy
XRD	X-Ray Diffraction

CHAPTER 1:

INTRODUCTION

1.1. SUSTAINABLE DEVELOPMENT AND GREEN CHEMISTRY

Sustainability is a concept accepted nowadays by governments, industries, scientific community as well as public opinion, as a necessary goal in order to achieve a environmentally benign development. The discussion of sustainability essentially began at the end of the 80s, when the United Nations Commission on Environment and Development noted an accelerating deterioration of the natural environment and an acute depletion of resources, in contrast to the attained economic growth [1]. Consequences of natural media overexploitation had been omitted and developed societies had been constructed on the basis that natural resources could be unlimited as well as indefinitely renewable [2-4]. Anthropogenic activity has resulted in problems such as the ozone hole, the Earth's global warming, the decreasing of non-renewable energy resources and the elevated contamination levels in the atmosphere, water and soils.

The "sustainable development" concept has been defined as: "development which meets the needs of the present without compromising the ability of the future generations to meet their own needs" [1,5]. Within this broad definition, chemistry evidently plays a key role since almost all products we can consider, that are involved in maintaining and improving our quality of life, have been prepared or influenced somehow by chemistry [6,7]. The Green Chemistry movement was started in the early 90s by the US Environmental Protection Agency (EPA) in conjunction with the American Chemical Society, as a result of efforts carried out in the industrial and academic worlds for preventing the contamination. Green Chemistry means the implementation of the sustainable development model into chemical processes through twelve guide principles, originally developed by Anastas *et al.* [8] (see Scheme 1.1.1). These principles were conceived for the environmentally friendly design of chemical products and processes that reduce or eliminate the use and generation of hazardous substances [8]. Green Chemistry has to be seen as a new working philosophy (not as individual principles) based on the intuition and chemical common sense, trying to

prevent the pollution rather than cleaning up the mess later. A similar analogy is that of preventive medicine, which is widely recognized as being preferable rather than having to cure the disease. However, the biggest challenge of Green Chemistry is still to generalize its practice in order to innovate and design environmentally benign products and processes.

1. It is better to **prevent waste** than to treat or clean up waste after it is formed.
2. Synthetic methods should be designed to maximize the incorporation of all materials used in the process into the final product **(atom economy).**
3. Wherever practicable, synthetic methodologies should be designed to use and generate substances that possess **little or no toxicity** to human health and the environment.
4. Chemical products should be designed to **preserve efficacy of function while reducing toxicity.**
5. The use of **auxiliary substances** (*e.g.* solvents, separation agents, *etc.*) should be made **unnecessary** wherever possible and, **innocuous** when used.
6. **Energy requirements** should be recognized for their environmental and economic impacts and should be **minimized**. Synthetic methods should be conducted at ambient temperature and pressure.
7. A **raw material** of feedstock should be **renewable**, wherever technically and economically viable.
8. **Unnecessary derivatization** (blocking group, protection/deprotection, temporary modification of physical/chemical processes) should be **avoided** whenever possible.
9. **Catalytic reagents** (as selective as possible) are superior to stoichiometric reagents.
10. **Chemical products** should be designed so that at the end of their function they **do not persist** in the environment and break down into **innocuous degradation products**.
11. **Analytical methodologies** need to be further developed to allow for **real-time**, **in-process** monitoring and control prior to the formation of hazardous substances.
12. Substances and the form of a substance used in a chemical process should be chosen to **minimize the potential for chemical accidents**, including releases, explosions and fires.

Scheme 1.1.1. The twelve Green Chemistry principles [8].

In addition to EPA, several other national or international organizations and networks have incorporated Green Chemistry and sustainable development implementation within their main purposes. Just to cite a few as examples: Sustainable Development and Green Chemistry are included within United Nations Environmental Program milestones [9]. The Organization for the Economical Cooperation and Development (OECD) focus on implementing efficient environmental policies to solve problems and manage natural resources in a sustainable way [10]. The Royal Society of Chemistry launched in 1998 a new journal entitled Green Chemistry [11] and the Green Chemistry Network (GCN) for promoting awareness and facilitate education, training and practice of Green Chemistry in industry, commerce, academia and schools [12]. In Spain, the Spanish Technology Platform for Sustainable Chemistry (PETEQUS) stimulate the private and public research for sustainable chemical products and processes [13].

According to demographic projections of United Nations, a global human population increase from 2 to 4 billion people is expected by year 2050, giving rise to a major requirements of products and services (specially in non-industrialized countries) [14]. The demands of a growing and developing world population will soon exceed the capacity of our present fossil resources based infrastructure. Therefore, our industry faces unprecedented challenges for changing toward a more sustainable development model in the 21st century [15,16]. From last years of the 20th century up to now, an substantial increment in legislation affecting chemical manufacturing processes have been seen [15]. For example, as important driver for change in the UE, in June 2007 entered into force the new REACH legislation (Registration, Evaluation, Authorization and restriction of Chemical substances) [17]. It is though that around 10% of currently used chemicals will not pass REACH directives, which means that more than 3000 final products will be affected [15,17]. The legislation also calls for the progressive substitution of the most dangerous chemicals when suitable alternative have been identified. Therefore, in the design of molecules, materials, composites, and formulations as well as chemical engineering, there is a tremendous amount of basic research yet to be done [7,16].

1.1.1. TITANIUM DIOXIDE IN THE CONTEXT OF GREEN CHEMISTRY

Titania (TiO_2) is a cheap and innocuous inorganic material extensively employed in industrial and commercial applications such as pigment in the paint industry, as sunblocking material in cosmetics, as a binder in medicinal fields and so on [18-20]. For instance, more than 4 million tones of the white pigment are annually consumed by the paint industry worldwide, being the pigment most widely used because of its brightness, high refractive index and low-cost [19]. TiO_2 is a wide band gap semiconductor that presents photoactivity upon near UV or higher irradiation, absorbing photons and transforming them into chemical redox energy. Although TiO_2 is inert and do not promote chemical reactions without irradiation, the handling of very finely divided TiO_2 particles requires taking safety measures [21,22].

Interfacial electron transfer reactions on TiO_2 have centered the interest in strategic applications for solving several problems such as energy supply [23-25] (see Section 1.3.1 and 1.8) or remediation of contaminated air and water [20,26] (see Section 1.3.2). This practical applications are commonly cited as reference examples in the literature dealing with Green Chemistry, because closely fit some of its principles [27,28] (see Scheme 1.1.1): (i) TiO_2 is innocuous, low-cost and stable against chemical and photochemical corrosion (principles 3, 4, 5, 10, 12); (ii) TiO_2 photocatalyst operates under mild reaction conditions at room temperature and atmospheric pressure (principles 6, 9) and (iii) the semiconductor can be recovered and reused (principles 7, 10).

In order to attain a practical application of the TiO_2 photoactivity, it is normally needed a crystalline material, with an adequate particle size and morphology [29]. Photocatalysts with appropriate properties habitually require synthetic procedures or post-treatments at elevated temperature to induce the formation of crystalline phases and/or eliminate residual organics [30-32]. In general, the preparation of inorganic materials is not essentially a green process and its concordance with principles 1 (waste

prevention), 2 (atom economy), 5 (innocuous auxiliary substances), 6 (minimal energy requirements) and 12 (safety) is not usually followed. The major part of the existing examples of cleaner synthetic routes are focused on organic chemistry, whereas less work has been done for improving inorganic synthetic methods [1,7,33]. In case of developing soft methodologies for preparing an inorganic semiconductor like titania with the desired properties, then one can relate the as-prepared material to Green Chemistry because of a double reason: benign in the synthesis and environmentally correct in the use. At this point, TiO_2 applications as well as the material preparation would fit Green Chemistry guidelines.

1.2. FUNDAMENTALS OF TiO_2 PHOTOINDUCED PHENOMENA

1.2.1. TiO_2 CRYSTAL STRUCTURE

Four polymorphs of TiO_2 are found in nature (*i.e.* rutile (tetragonal), brookite (orthorhombic), anatase (tetragonal) and TiO_2-B (monoclinic)) [34,35]. In titania polymorphs, the basic building blocks consist of a titanium atom surrounded by six oxygen atoms in a more or less distorted TiO_6 octahedral configuration [36]. The crystal structure differ by the distortion of each octahedral and by the assembly patterns of the octahedral chains (Figure 1.2.1). In rutile, neighboring TiO_6 units share corners, being stacked with their long axis alternating by 90º [34]. Anatase framework consist of strongly distorted edge sharing TiO_6 octahedra. Corner sharing and edge sharing octahedral units give rise to the three-dimensional network of TiO_2-B. Differences in mass density and electronic band structure are explained in terms of the different lattice structures [37].

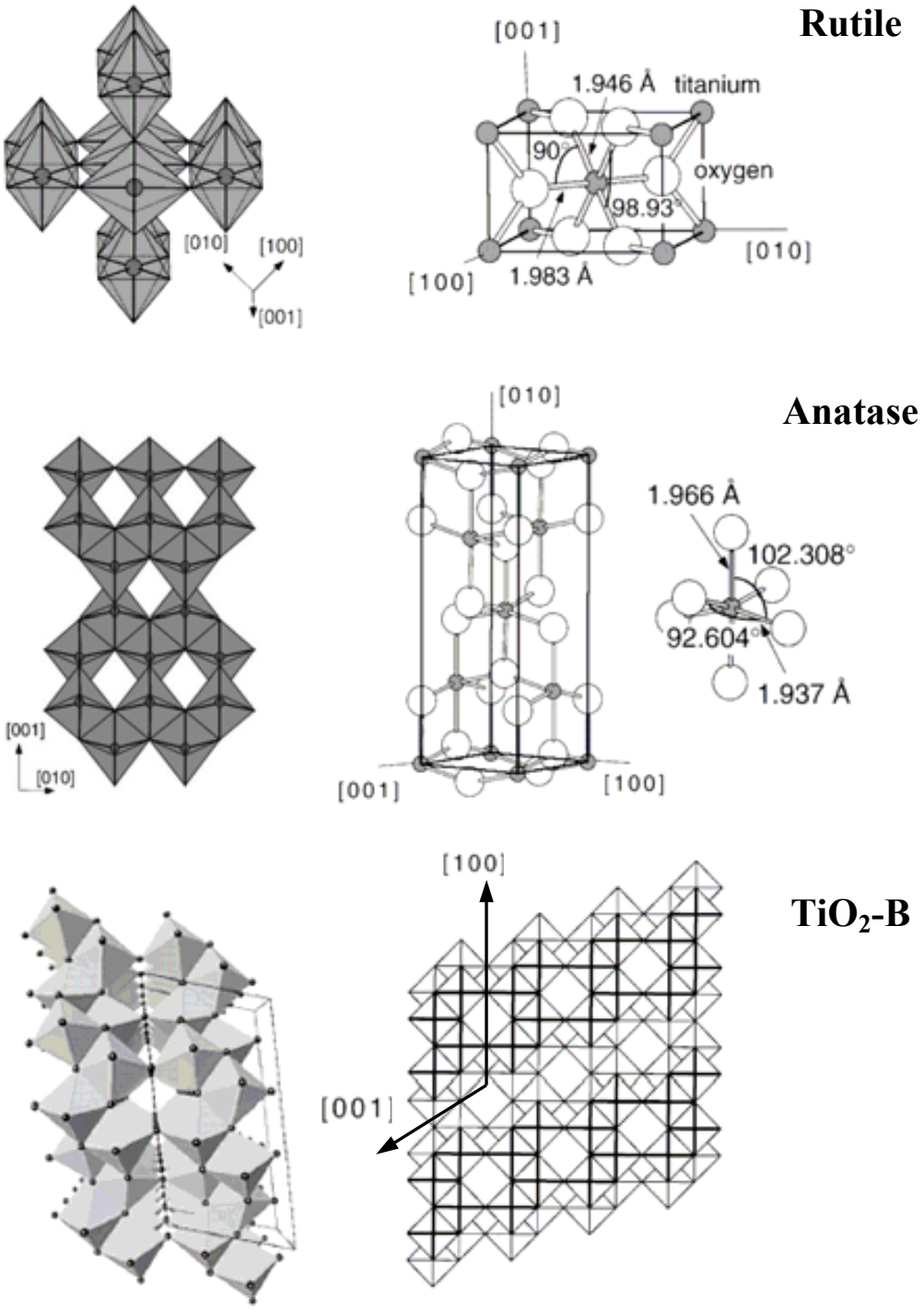

Figure 1.2.1. Bulk structure of rutile, anatase and TiO_2-B polymorphs [35,38,39-41]. Slightly distorted octahedra are the basic building units. Rutile (tetragonal; $P4_2/mnm$, a=b=4.584Å, c=2.953Å); anatase (tetragonal; $I4_1/amd$, a=b=3.785Å, c=9.514Å); TiO_2-B (monoclinic; C_2/m, a=12.163Å, b=3.735Å, c=6.513Å, β=107.29º).

The anatase and TiO_2-B phases are known to be thermodynamically less stable than the rutile phase so that they are converted into the other phases at high temperature. It is generally accepted that anatase is the most photoactive form of titania [42]. The bulk structure of titania networks is quite complex with various types of intrinsic defects including oxygen vacancies [35]. Such oxygen deficiency implies the presence of some Ti(III) centers that behave as electron-donating species, providing an n-type character to the semiconductor.

1.2.2. TiO_2 SURFACE AND WATER CHEMISORPTION

Chemisorption properties on titania surfaces has received much attention since interfacial electron transfer reactions are of special interest (see Section 1.2.4). The surface titanium centers exhibit coordination vacancies that in the presence of water are occupied by hydroxyl groups through dissociative water chemisorption. Resulting titanol groups (≡Ti-OH) are known to be amphoteric, similar to simple diprotic acids according to the following acid-base equilibria (Equations 1.2.A and 1.2.B) [20,37]:

$$\equiv Ti\text{-}OH_2^+ \rightleftharpoons \equiv Ti\text{-}OH + H^+; \quad pK_{a1} \tag{1.2.A}$$

$$\equiv Ti\text{-}OH \rightleftharpoons \equiv Ti\text{-}O^- + H^+; \quad pK_{a2} \tag{1.2.B}$$

Isoelectric (or zero point charge) of titania is given by one half sum of the superficial pK_a values (Equation 1.2.C). Acid-base behavior strongly depends on the intrinsic surface characteristics derived from the preparation method, having been reported isoelectric point values ranging from 5.6 to 6.2 [43].

$$pK_{isoelectric\ point} = 1/2\ (pK_{a1} + pK_{a2}) \tag{1.2.C}$$

1.2.3. TiO_2 LIGHT ACTIVATION

The properties of semiconductors can be understood by chemical interpretation of the band theory [20] (see Figure 1.2.2). On this theory, at 0 K, a perfect crystal of a semiconductor material possesses a group of very close filled electronic states (valence band, VB) and another group of close empty electronic states at higher energies (conduction band, CB). A region where no electronic states are available (band gap) exists between the VB and the CB.

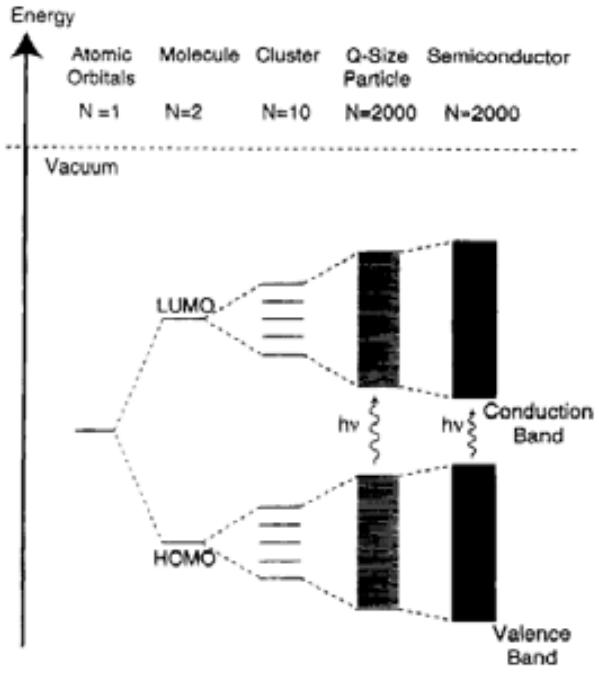

Figure 1.2.2. Representation of the effect of increasing the number of mixed molecular orbitals on the electronic structure. Adapted from reference [20].

Titania is a wide band gap semiconductor material (3.0-3.2 eV depending on the crystalline phase [44]), capable of converting energy from the light into chemical redox energy. When a photon with an energy equal or higher than the band gap of the semiconductor (E_g), an electron from the VB is promoted into the CB (e^-_{CB}) leaving a hole behind (h^+_{VB}). The number of photogenerated electron-hole pairs depends on the semiconductor band structure as well as the energy and the effective intensity of the incident light [20,45]. Unfortunately, light activation of titania occur in the near UV region (from $\lambda \leq 385$-400 nm), meaning that only a 5-8 % fraction of the sunlight can be

absorbed by the bare material [37] (see Figure 1.2.3). Due to the inherent relatively large band gap characteristic of TiO_2 materials, a great deal of research has focused on lowering the threshold energy for excitation in order to utilize a wider fraction of solar irradiation for conversion into chemical energy [46-48].

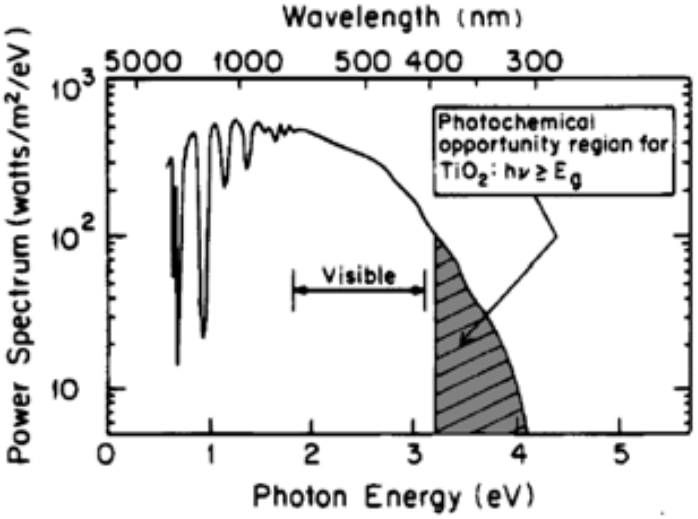

Figure 1.2.3. Direct normal spectral irradiance (AM=1)[Φ]. The area signaled with an arrow indicates the useful wavelength range for TiO_2 photoexcitation [37].

1.2.4. PHOTOSENSITIZED ELECTRON TRANSFER REACTIONS ON THE TiO_2 SURFACE

Photogenerated electron-hole pairs can follow two different pathways: interfacial electron transfer reactions or recombination (see Figure 1.2.4). In the absence of a suitable electron or hole scavenger, recombination of charge carriers occurs and the stored energy is dissipated (heat release) within a few nanoseconds, rendering a zero quantum yield with respect to photon consumption (*i.e.* reaction rate observed/photon absorption rate) [20,26].

[Φ] Air Mass (AM) value corresponds to the total irradiance (mW/cm^2) at a defined ratio between the atmosphere length crossed by the incident sunlight with respect to the atmosphere thickness *i.e.* a certain angle of incidence. For instance, typical standard values are AM=0 (extraterrestrial radiation), AM=1 (normal sunlight incidence) and AM=1.5 (sun-facing 37-degree titled surface, ~100 mW/cm^2) [37,49].

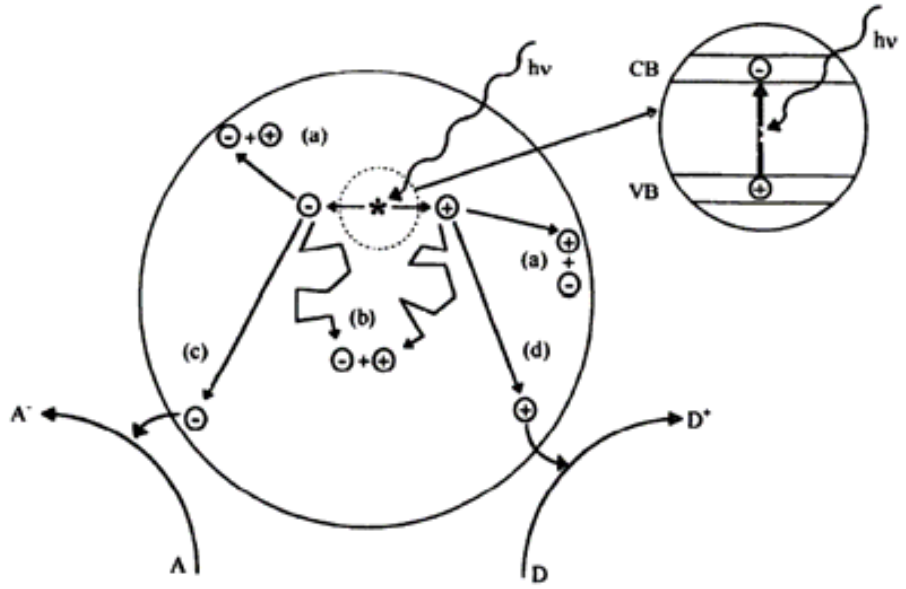

Figure 1.2.4. Schematic representation of the events at the light-activated TiO_2 particle. Electron-hole recombination can occur at the surface (a) or in the bulk (b) of the semiconductor. Interfacial electron transfer reactions at the surface of the particle: (c) photogenerated electrons reduce an electron acceptor A and (d) photogenerated holes oxidize and electron donor D. Adapted from ref. [45].

On the contrary, after migration of the charge carriers on the TiO_2 surface, subsequent interfacial redox reactions with adsorbed species take place when a suitable scavenger (or a charge carrier trapping site) is available. Thus, TiO_2 photosensitizes the reduction of an electron acceptor A (reaction (c) in Figure 1.2.4) and the oxidation of an electron donor D (reaction (d) in Figure 1.2.4), forming anion and cation radical species, respectively (Equation 1.2.D). These radicals are usually reactive and can react between them and with other adsorbed species, and they can even diffuse into a solution and participate in homogeneous-phase secondary reactions. Both surface adsorption as well as interfacial redox reactions can be enhanced by nano-sized semiconductors since more reactive surface area is available [45]. Semiconductor-assisted redox reactions are habitually referred as "heterogeneous photocatalysis" in the literature [26,45].

$$A + D \xrightarrow[E_{h\nu} \geq E_g]{TiO_2} A^{\cdot -} + D^{\cdot +} \qquad (1.2.D)$$

Redox potentials associated to the conduction and valence bands of titania define thermodynamic requirements for interfacial electron transfer reactions (Figure 1.2.5). While titania e^-_{CB} is a moderate reducing agent (E^o ~0V *vs* NHE), h^+_{VB} possesses strong oxidizing power (E^o ~3V *vs* NHE) [20]. In order to an electron acceptor A be spontaneously photoreduced, the CB reduction potential of the semiconductor must be more negative than the reduction potential of the $A/A^{\cdot-}$ pair. Following a similar reasoning, to assist the oxidation of an electron donor D, the potential of the semiconductor VB must be more positive than the reduction potential of $D^{\cdot+}/D$ pair. Therefore, assuming no kinetic limitations, light-induced semiconductor-assisted interfacial redox reactions will take place with acceptors and electron donors whose respective reduction potentials are comprised between CB and VB band positions [20,37].

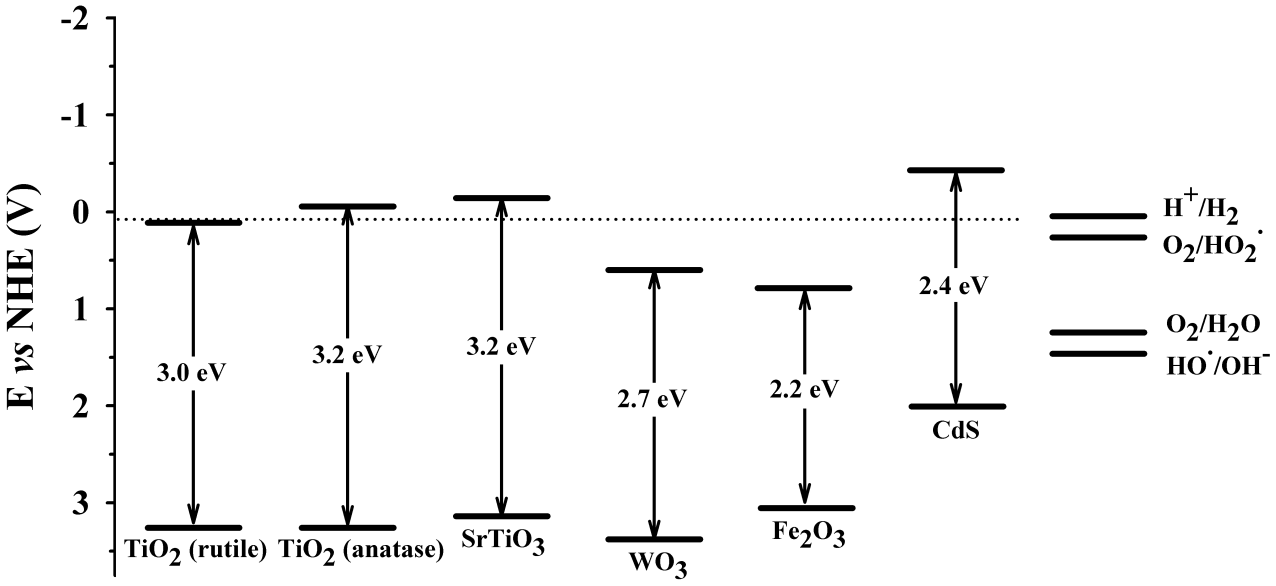

Figure 1.2.5. E_g values and reduction redox potentials of some semiconductor materials. Selected redox couples are also included. All values correspond to standard potentials measured *vs* NHE at pH=0 and T=298 K. Adapted from reference [45].

However, it should be taken into account that the contact between a semiconductor and another phase (*i.e.* liquid, gas or metal) generally involves a redistribution of electric charges and the formation of a double layer at the interface, resulting in upward bending of the bands potential in the case of an n-type semiconductor such as titania [50,51]. Among other semiconductors, inherent TiO_2 properties (inertness, low-cost, low-solubility, biocompatibility and relative high quantum yield) have situated this material in the pole position of applications based on semiconductor-assisted photoinduced processes.

1.3. TiO_2-ASSISTED ELECTRON TRANSFER REACTIONS: BRIEFLY REVIEWED APPLICATIONS

Interfacial electron transfer reactions on TiO_2 have received enormous attention from scientists and engineers over the past 30 years (see chronology of some major contributions in Scheme 1.3.1). Vigorous research has been carried out in fields as diverse as energy conversion, environmental remediation and other emerging applications. In a detailed web-based overview of semiconductor photochemistry-based applications, Mills *et al.* reported indications that commercial activity is growing worldwide, but being specially strong in Japan [42]. This Section pretends to be a brief overview of the most significant applications derived of TiO_2-sensitized systems without being exhaustive.

1972	Fujishima and Honda reported the first photoelectrochemical cell for water splitting ($2H_2O \rightarrow 2H_2 + O_2$) using a TiO_2 photoanode and Pt counter electrode [25,52].
1977	First implication of TiO_2 in environmental remediation: Frank and Bard examined the reduction of CN^- in water [53,54].
1978	First organic photosynthetic reaction: an alternative photoinduced Kolbe reaction ($CH_3COOH \rightarrow CH_4 + CO_2$) that opened the field of organic photosynthesis [55].
1983	Semiconductor-sensitized reactions for organic pollutant oxidative mineralization implemented by Ollis *et al.* [26,56].
1985	Application of TiO_2 as microbiocide: effective in photokilling of *Lactobacillus acidophilus*, *Saccharomyces cerevisiae* and *Esterichia coli* [57].
1986	Fujishima *et al.* described the first use of titania in photokilling of tumor cells [25].
1991	Grätzel *et al.* invented efficient solar cell using nano-sized TiO_2 particles [24,58] (see Section 1.8: Dye-Sensitized Solar Cells).
1997	Wang *et al.* obtained highly hydrophilic titania surfaces with excellent anti-fogging and self-cleaning properties [59].

Scheme 1.3.1. Some major contributions in the development of TiO_2 in photoactivated processes [34].

1.3.1. SOLAR HYDROGEN

Sustainable development and Green Chemistry principles should direct us to renewable energy sources. Hydrogen is considered as a non-pollutant fuel and a clean energy carrier for the future, much cleaner than fossil combustibles such as petroleum [60,61]. Nowadays, renewable hydrogen generation is not becoming widespread because the cost is still high and only represent a 5% of the total commercial hydrogen production [60].

TiO_2-assisted water-splitting has opened a promising way for low-cost and environmentally friendly production of hydrogen by solar energy [34]. Fujishima and Honda demonstrated for the first time that photoelectrolysis of water is possible, by using a system in which an n-type semiconductor electrode, connected to a platinum counter electrode, was exposed to near UV light [25,52] (Figure 1.3.1). However, the TiO_2/H_2O/Pt photoelectrochemical cell requires a degree of electrical or chemical bias (alkali in the TiO_2 photoanode half-cell and acid in the Pt cathode half-cell) to make it work [45].

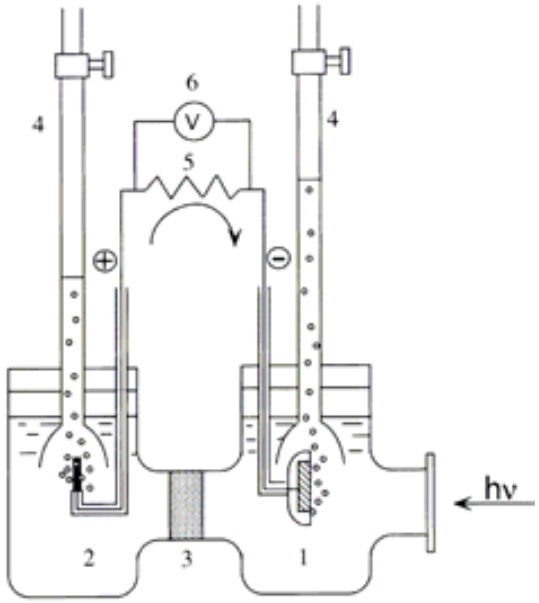

Figure 1.3.1. Schematic diagram of the first photoelectrochemical cell for water splitting (adapted from ref. [25]). (1) water oxidation at an n-type TiO_2 electrode ($H_2O + 2h^+ \rightarrow ½\ O_2 + 2H^+$); (2) H_2 production at an Pt counter electrode ($2H^+ + 2e^- \rightarrow H_2$); (3) ionically conducting separator; (4) gas buret; (5) load resistance and (6) voltmeter.

Presently, TiO_2-assisted hydrogen generation efficiency from solar energy still remain quite low mainly due to charge carrier recombination or inability to utilize visible light [60]. Many other researchers have investigated on sunlight and water conversion into storable chemical energy and significant progress has been attained [60,62]. So far, record quantum efficiencies reported are held by NiO-modified $La/KTaO_3$ (56%, pure water, UV light); Pt-modified ZnS (90%, $Na_2S/NaSO_3$, light with λ>300 nm); Cr/Rh-modified GaN/ZnO (2.5%, pure water, visible light) [62]. However, no material capable of reaching the 10% efficiency limit (for viable commercial applications) of hydrogen production under visible light has been found [62].

1.3.2. ENVIRONMENTAL REMEDIATION

At present, there is a chemical and technological demand of clean, safe and efficient decontamination methodologies since, in many cases, pollution has not been properly prevented and, toxic and hazardous agents are still released to water and air media. By far, the most active research area on TiO_2-assisted electron transfer reactions has been environmental remediation taking advantage of the photoinduced redox power. Satisfactory results have been obtained in wastewater treatment of effluents contaminated with toxic metals (*e.g.* Cr(IV) or Hg(II)) as well as recovery of precious metals by semiconductor-assisted reduction (*e.g.* Pt, Pd, Ag or Au) [20,51,63,64]. However, the major part of the research has been focused on the photosensitized oxidation of organic pollutants in the aqueous and gaseous phases by oxygen (Equation 1.3.A) [20,45,63]. TiO_2-assisted photodegradation has been successfully applied to abate refractory, very toxic and non-biodegradable molecules (some hazardous compounds listed in the EPA priority inventory, including pesticides, herbicides, surfactants or dyes) [65].

$$\text{Organic compound} + O_2 \xrightarrow[E_{h\nu} \geq E_g]{TiO_2} CO_2 + H_2O + \text{mineral acids} \quad (1.3.A)$$

Photooxidative degradation of organic matter takes place in subsequent steps derived from direct oxidation of adsorbed compounds by h^+_{VB} or generating hydroxyl radicals ($OH^{\bullet}$) from titanol groups (Figure 1.3.2) [42]. Under conventional aerobic conditions, e^-_{CB} (or a ≡Ti(III)OH electron trapping state on the semiconductor surface) reduces adsorbed O_2(ads) to the superoxide radical anion $O_2^{-\bullet}$(ads). This superoxide radical is an efficient oxygenating agent and experiences further electron transfer processes or chemical reactions over the surface or in the media after undergoing desorption [34].

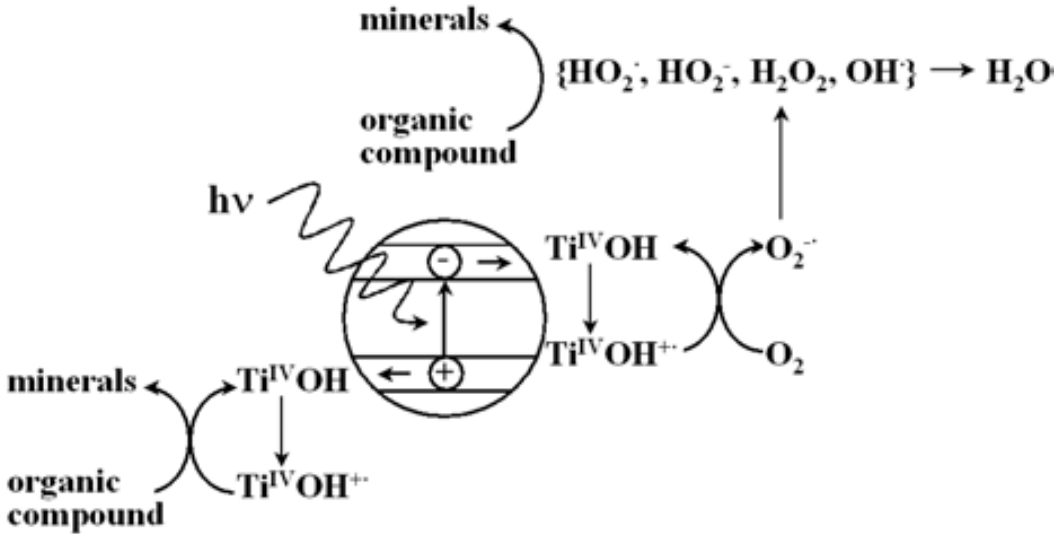

Figure 1.3.2. Major processes in TiO_2-assisted mineralization of organic pollutants by oxygen. Adapted from ref. [34].

In fact, chemical oxidation techniques able to produce high oxidant species (mainly the hydroxyl radical, E^o=2.8 V *vs* NHE, T=298 K) that non-selectively mineralize organic pollutants are generically known as AOPs (Advanced Oxidation Processes) [51]. Among other AOPs, heterogeneous photocatalysis is the one that more closely fit the Green Chemistry principles since TiO_2 does not require additional energy supply or reactants and, in principle, the catalyst can be recovered and reused [51]. Besides, TiO_2-assisted degradation of some compounds has been scaled up to pilot plant prototypes, for example, in PSA (Plataforma Solar Almeria), demonstrating that the system is a suitable way to decontaminate water in arid sunny areas and auguring a widespread application of the technology in the near future [28,66]. However, further development of heterogeneous photocatalysis is required since in some cases: (i) titania deactivation has been observed when strongly adsorbed species are present; (ii) photooxidative treatments present low quantum yield and should be coupled with other AOPs or biological systems [26,67].

1.3.3. ORGANIC SYNTHESIS

The chemical energy generated at light-activated TiO_2 has been explored for designing green reduction and oxidation routes for the production of organics [68]. The

development of efficient and selective chemical processes is on top on the Green Chemistry agenda (*i.e.* ideally avoiding organic solvents and using solar photons as green reactants instead of dangerous metal catalysts and further strong redox agents) [7,68].

Photocatalytic processes had been considered unselective in the past, specially in photooxidative processes in aqueous media (Equation 1.3.A). This is not surprising taking into account the generation of $OH^{\cdot}$ (best second universal oxidant) in the presence of water [28]. Hence, TiO_2-assisted synthetic routes have been mostly investigated by using inert organic solvents or the undiluted organic substrates, although some promising results have been reported in aqueous media as well [28,45,68]. The major part of the examples found in the literature refer to mild selective oxidation processes but reduction, isomerization or polymerization reactions have also been reported (Figure 1.3.3).

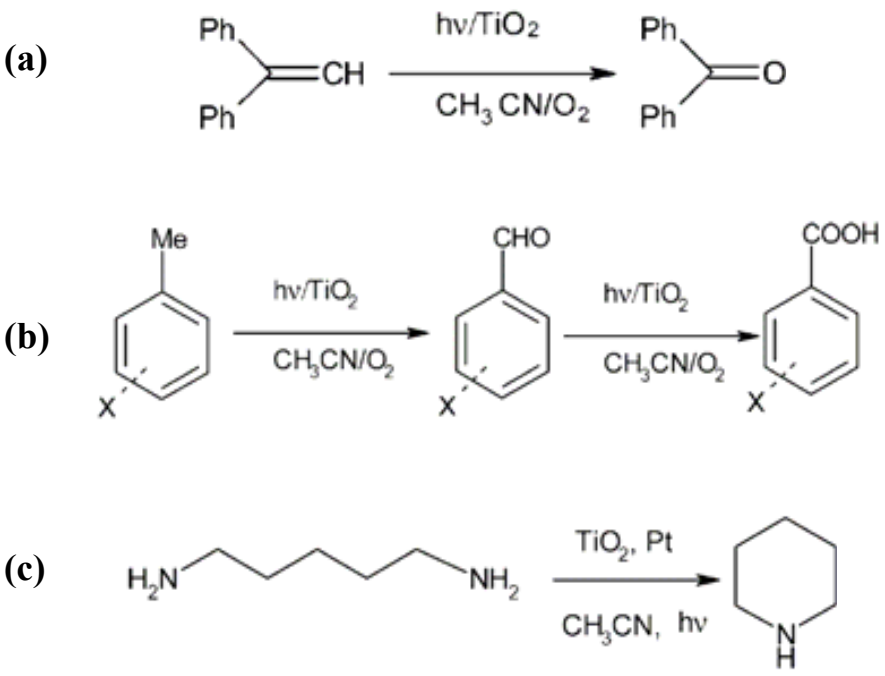

Figure 1.3.3. Selected examples of TiO_2-assisted transformation of organic compounds (see [34,45,68] and references cited therein): (a) oxidation of alkenes substituted with phenyl groups yielding corresponding ketones; (b) subsequent oxidation of substituted toluene to corresponding acetaldehyde and carboxylic acid and (c) amine intra *N*-alkylation.

1.3.4. PHOTOKILLING ACTIVITY

Several studies have proved remarkable cell killing power of illuminated titania, mainly ascribed to oxidative damage of the biological material, in a process similar to that in Equation 1.3.A [26]. The greatest level of research activity has focused on the destruction of *Escherichia coli*, which is a target bacterium traditionally used as an indicator of fecal contamination in water, although destruction of a wide range of other species has also been achieved [45,69]. Unfortunately, the lack of residual disinfection capacity and the generally slow kinetics represent major drawbacks for a practical application (*e.g.* in water treatment), compared with conventional chemical techniques employed [45]. However, self-sterilizing materials coated with TiO_2 in structural applications in hospitals such as ceramic tiles [70] (currently commercialized) and other potential applications in medical instruments or uniforms [25] have received special interest.

On the other hand, Fujishima's research group, in collaboration with some urologists at the School of Medicine of Yokohama City University, demonstrated an anti-tumor approach based on photocatalysis [25,26]. Subcutaneous injection of a titania suspension and near UV irradiation (that is biologically safe) were carried out by means of a modified endoscope into skin tumors of mice. Whereas a 10 times reduction of the tumor was observed after three weeks, control experiments (catalyst or light alone) exhibited tumor increase in volume by a factor of 30-50 [25,26]. However, further refinement of the devices is still required for practical application in human tumors [25].

1.3.5. SELF-CLEANING AND RELATED MATERIALS

In terms of commercial success, the biggest impact of semiconductor photochemistry is probably in the relative new area of self-cleaning and related materials, *i.e.* photoactive titania coated on ceramic or glass materials in which a dual-action occurs [42]. In such materials, well-known TiO_2-assisted photooxidation,

which leads to the breakdown of organics (Equation 1.3.A), takes place simultaneously with an intrinsically different phenomena termed UV-photoinduced superamphiphilicity, forcing detachment of any dust and organics by rainfall and also favoring a quick drying process [25,45]. Photoactive titania can possess both properties, in varying proportions, depending on the composition and the manufacturing process [45].

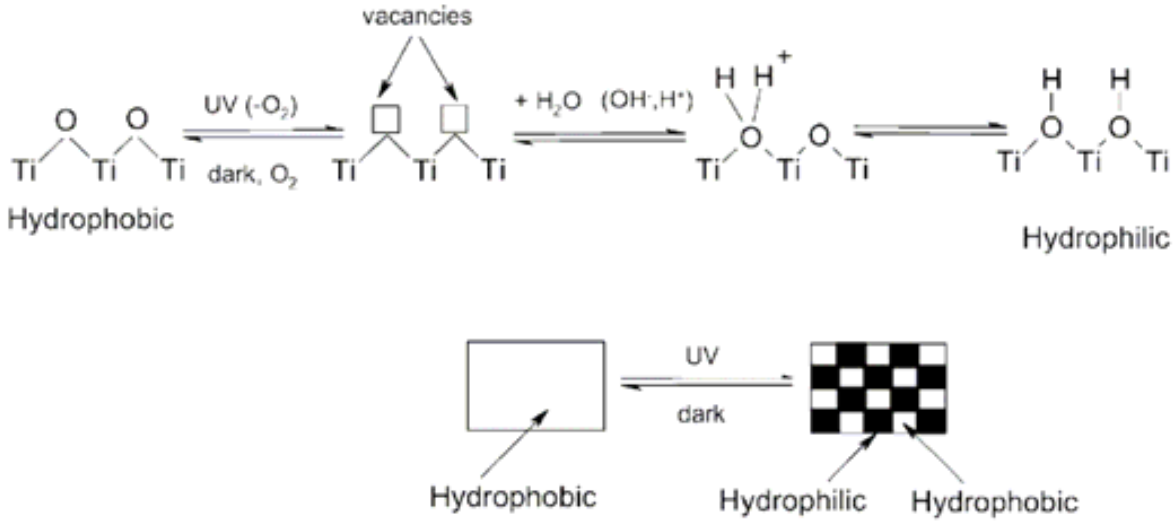

Figure 1.3.4. Mechanism of photoinduced superamphiphilicity of TiO_2. Adapted from ref. [34].

In light-activated titania in the absence of any appreciable level of adsorbed compounds such as an organic, the surface species available for reaction appear to be Ti(IV) together with bridging oxygen atoms. Photoinduced superamphiphilicity (see Figure 1.3.4) involves reduction of Ti(IV) cations to Ti(III) by electrons and simultaneous trapping of holes close to the surface of the semiconductor [25]. Such trapped holes weaken the bond between titanium and oxygen, allowing oxygen atoms to be liberated, thus creating vacancies. Subsequent adsorption of water at this sites renders further surface hydroxylation, with the result that hydrophilic nature of the surface is drastically increased (contact angles falls from 40-60º to almost zero) [25,42]. In other words, water can not exist in the shape of a drop and spreads flatly on the surface of the catalyst [70]. However, water adsorption does not occur uniformly and produces an amphiphilic surface with alternating regions at the scale of several

nanometers (usually <10 nm in size), surprisingly resulting in similar wetting capabilities for more oleophilic liquids [25]. The process is slowly reversed over some time in the dark (typically days), as Ti(III) are oxidized back to Ti(IV) by ambient oxygen, leading to the regeneration of bridging oxygen atoms. [34,42].

Contrarily, some authors have proposed a superhydrophilicity model uniquely based on photocatalysis [71]. This alternative model proposes photocatalytic degradation (Equation 1.3.A) of very small amounts of adventitious, hydrophobic and usually undetectable (by means of ATR-FTIR for example) organics, revealing the intrinsically hydrophilic surface of titania photocatalyst underneath. In addition, it is worth pointing here that surface roughness is a critical factor, making difficult comparison among the studies carried out [71]. The debate concerning the mechanism of superamphiphilic behavior of titania continues nowadays, claiming for additional basic research in the area although a dual-action seems plausible.

Interestingly, photoinduced superamphiphilicity of titania exhibits high quantum yield at low light levels and can thus be obtained upon the low UV light levels found in indoors (illuminated with conventional fluorescent lights) as well as outside (solar irradiation) [45]. At present, major ceramics and glass manufacturing companies such as TOTO (Japan) [70], Nippon Sheet Glass (Japan) [72], Pilkington Glass (UK) [73], Saint Gobain Glass [74] *etc.* already commercialize self-actuating materials based on the photocatalysis and photoinduced superamphiphilicity dual-action. For instance, anti-fogging surfaces for automobile side-view or bathroom mirrors, and self-cleaning windows, panels or glass roofs for buildings [70,72-74].

1.4. NANO-SIZED POWDERS AND NANO-STRUCTURED FILMS

Nano-structured materials have drawn much attention because of the dramatically different properties observed on going from bulk material to nano-sized particles. Nano-sized materials possess properties that lie between the quantum effects

of atoms and molecules and the bulk properties of materials [75]. In the nanometer range (1-100 nm) the particle size affects structural characteristics (*e.g.* lattice symmetry, unit-cell dimension), electronic properties (e.*g.* band gap, quantum size effect), and therefore also the physical and chemical properties [75,76]. Unfortunately, it is worth pointing that nano-toxicity and bioaccumulation can also be dramatically different with respect to micro-scale titania and, hence, toxicological evaluations should also be carried out [21,22]. Whereas nano-sized TiO_2 allows miniaturization and maximizes interfacial electron transfer reactions because of a high specific surface area, crystallites bellow 10 nm in size are generally not suitable since opportunities for recombination among electrons and holes are increased [77].

As commented in Section 1.3, most of the early work on titania-assisted applications focused mainly on the photomineralization of organics dissolved in aqueous solution, *i.e.* Equation 1.3.A, usually employing the semiconductor in the form of a powdered dispersion. In this field as well as in air remediation, supported TiO_2 have received a great deal of interest since, in practical systems, additional separation and regeneration methods of the photoactive semiconductor are habitually required [78-81]. In addition, self-actuating materials (*i.e.* self-cleaning and/or self-sterilizing, see Sections 1.3.4 and 1.3.5) as well as solar energy conversion devices into chemical (see Section 1.3.1, solar hydrogen) or electrical energy (see Section 1.8, Dye-Sensitized Solar Cells) inherently imply TiO_2 coatings on different substrates.

On the other hand, TiO_2 coatings have found extensive uses beyond already "classical" applications described in Section 1.3. A great variety of examples within present technological demands in fields as diverse as medicine, electronics, optics or sensors has been described. For instance, oxide layers on the surface of titanium alloys employed in modern reparative medicine are known to play key roles in corrosion resistance as well as biocompatility in bone implants [35,82]. Speed and degree of color change in WO_3-based electrochromic devices have been enhanced via complementary TiO_2-assisted oxidative coloration of dyes in counter electrodes [24]. Titania antireflective coatings have been found to efficiently increase light harvesting in silicon solar cells [83,84]. Titania promises excellent properties for technological use as

electrode material in lithium batteries [36,40]. Oxygen sensors for controlling air-fuel mixtures in car engines (based on change of the semiconductor resistance with partial pressure) have also been studied [85].

1.5. TiO_2 PREPARATION METHODS

The properties of TiO_2 materials strongly depend on the crystalline structure, phase composition, morphology, porosity and chemical composition as well as the final form (*i.e.* powder or films), which are determined by the corresponding synthetic method [33,76]. Therefore, many efforts have been made on exploring preparation routes in order to achieve desired features for a concrete application [34,76]. Both powders and films can be built from crystallites ranging from a few nanometers to several micrometers [86].

For instance, well-suspended deagglomerated nano-sized powder dispersions of highly-photoactive catalysts habitually maximize water decontamination and disinfection [28]. On the other hand, self-cleaning building materials ideally require compact thin films (60-400 nm thick) exhibiting photoactivity, superamphiphilicity, visible-light transparency (*i.e.* adequate particle size (<30 nm), not presenting light scattering), adherence as well as withstanding outdoor conditions [42,86,87]. Alternatively, micrometer-thick TiO_2 mesoporous[Φ] electrodes with appropriate electrical connection are preferably required for solar energy conversion in order to maximize global efficiency [24,25].

[Φ] According to IUPAC recommendations, a mesoporous material has pores of widths between 2 and 50 nm [88].

1.5.1. PREPARATION METHODS OF TiO_2 POWDERS

One can found a wide variety of commercial titanium precursors including titanium alkoxides, halides, complexes, titanyl derivates and mixed compounds [89]. The corresponding hydrolysis, metathesis, thermal decomposition or ligand displacement reactions carried out in gas as well as liquid phase have been extensively explored as synthetic routes for preparing titania powdered products as is reflected by the sheer volume of available literature [34,51,76]. In the major part of the cases, nano-sized main particles (exhibiting a narrow distribution) with high specific surface area is the desired morphological feature [51].

Industrially, titania is produced via two major routes from titanium ores: sulfate process and chloride process [51,90,91]. In the former, *Ilmenite* ("titanic iron", 40-60% titania and 30-50% iron oxide) or titanium slag (iron contained in *Ilmenite* largely reduced with carbon to the metal in a furnace at 1200-1600ºC and separated) finely ground are employed. Raw materials are digested in H_2SO_4(c), iron reduced by a Ti(III) solution and separated as $FeSO_4 \cdot 7H_2O$(s). Afterwards, the resulting titanyl sulfate is hydrolyzed feeding in steam at 95-100ºC in the presence of seed crystals. The hydrolysis product is washed, bleached and finally fired at 1000ºC approximately. On the other hand, in the chloride process, rutile raw materials are treated with Cl_2(g) and carbon to produce $TiCl_4$. As-produced $TiCl_4$ is mixed with reducing agents to convert impurities such as vanadium oxychloride to lower valence state vanadium compounds and $TiCl_4$ is purified afterwards by distillation. Finally, $TiCl_4$(g) combustion in the presence of oxygen gives rise to the desired TiO_2 and Cl_2(g) (that is reused in the chlorination process). Although the economics of the two routes are strongly dependent upon the raw materials availability, chloride process is preferred due to easier purification processes are required for providing the titania precursor $TiCl_4$ [51].

Special interest has been paid to wet-chemistry approaches due to their attractive advantages in terms of versatile control of the final product by using structure growth directing agents such as surfactants or complexing agents in combination with different reaction processing such as conventional heating, solvothermal treatments and microwave or ultrasonic assistance [34,76]. However, wet-chemistry routes present particular disadvantages (*i.e.* expensive precursors, the presence of carbon as an impurity as well as high temperature and long processing times) that need to be solved for effective economical competitiveness with industrial gas-phase production methods [34,51]. In fact, wet-chemistry synthesis of high quality TiO_2 nanocrystals on a large scale is still a challenge nowadays [92].

Among wet-chemistry methods, sol-gel routes are by far the most extended approaches mainly due to their relative higher versatility, and a brief description should be addressed [51,76,93]. However, versatility goes to the detriment of simplicity since sol-gel routes intrinsically consist of multi-step procedures [34,76]. In a typical sol-gel synthesis a colloidal suspension (sol) is initially formed from the hydrolysis and polimerization reactions of a alkoxide precursor (*e.g* titanium tetra*iso*propoxide (TTIP) or titanium tetrabutoxide (TTB)) or $TiCl_4$. Complete polymerization and loss of solvent give rise to the transition from the liquid sol into a quasi-solid gel phase. In order to achieve a better control over the evolution of the microstructure, it is desirable to separate and temper the steps of hydrolysis and condensation by means of coordinating agents, peptization (at acidic or basic pH), controlling the water content or decreasing the working temperature [76]. Finally, titania can be obtained via a thermal (400-600ºC) or an hydrothermal treatment (200-300ºC) of the gel phase under proper conditions [34]. Additionally, thin films can be produced on a substrate by spin-coating or dip-coating either the sol or gel phase prior to this thermal annealing. A highly porous and extremely low-density TiO_2 aerogels can also be prepared by combining sol-gel processing with supercritical drying [76].

1.5.2. PREPARATION METHODS OF TiO_2 FILMS

The great variety of methods applied to the preparation of titania films can be broadly divided into two major categories [51]. On one hand, TiO_2 particles previously formed can be mechanically or electrophoretically deposited forming the resulting films. Nevertheless, such strategy habitually needs a thermal post-treatment in order to achieve desired mechanical or electrical properties (see discussion in Section 4.1).

On the other hand, titania films can be subsequently grown *in situ* by involving either a physical (*e.g.* Physical Vapor Deposition, sputtering, plasma processes, *etc.*) or a chemical process (*e.g.* Chemical Vapor Deposition, spray pyrolysis, electrodeposition, *etc.*) [94,95]. So-called dry methods (*i.e.* purely physical strategies as well as chemical processes in the vapor phase) are generally preferred since they produce high-quality films due to a better control over the film composition, crystalline structure and growth rate [94,96]. However, complex instrumentation, vacuum systems as well as high energy consumption are commonly required, resulting in high-cost methodologies [32,94]. In addition, in many cases, substrates are maintained at elevated temperatures, being even higher than 500ºC [97-99], and it is also difficult to coat complex-shaped substrates [96]. Alternatively, wet chemical techniques such as sol-gel or Chemical Bath Deposition have been intensively explored as simpler and lower-cost approaches [32].

1.6. LOW-TEMPERATURE WET-CHEMISTRY TiO_2 PREPARATION METHODS: STATE OF THE ART

Independently of the preparation method employed and the final form, TiO_2 preparation methods conventionally include a thermal post-treatment at elevated temperatures (>400ºC) in order to remove the organic content and/or crystallize the as-prepared amorphous material, a procedure accompanied by grain coarsening and a

reduction in surface area [34,100]. Additionally, in the case of films, mechanical robustness as well as electrical contact are habitually improved via the same post-annealing [31]. This latter case is of special interest in the preparation of TiO_2 photoelectrodes for DSSCs from pre-synthesized nanoparticles and will be discussed in more detail in Section 4.1. High-temperature processing of titania represents a technological limitation, for example, for preparing hybrid organic/TiO_2 composites [101,102] as well as titania deposition on thermolabile substrates [31]. Therefore, the development of low-temperature wet-chemistry synthesis of titania is essential for its implementation across a wider range of applications. In this Section, a general overview including some relevant examples of the contributions reported in this research area is presented.

1.6.1. LOW-TEMPERATURE SOL-GEL ROUTES

Some authors have focused on introducing modifications in the relatively well established sol-gel methodologies for preparing TiO_2 in both the powdered and film forms at low temperature. Alternative sol-gel processing or post-treatments such as long time at moderated temperatures [100,103,104], supercritical CO_2 [105,106], low-temperature hydrothermal [107] or microwave irradiation [108] have been reported. In addition, sol-gel methods employing ionic liquids (ILs) as co-solvents have shown significant implications for the direct synthesis of titania (see Section 4.4.1).

For instance, Langlet *et al.* prepared compact and robust antireflective 100 nm-thick TiO_2 coatings by means of consecutive gel aging at 45ºC for 15 minutes, 110ºC for 2 hours and 60 ºC for 5 days [103]. Li *et al.* achieved nanocrystalline anatase particles with crystallite sizes ranging 6-10 nm by subsequently drying (60ºC, 5h) and aging (100ºC, 12h) of as-prepared titania gels [100]. Surfactant-templated TiO_2 mesoporous films of 100-400 nm of thickness were prepared aging at 150ºC for 2h in combination with an UV post-treatment for organics removal [104]. Langlet *et al.* also studied water/ethanol solvothermal (90-140ºC, 1-20h) crystallization and coalescence of titania gels deposited on different polymer substrates [107]. Phase and shape controller

behavior of amines due to Ti(IV) coordination capability under hydrothermal aging of gels at 140ºC for 3 days was demonstrated by Sugimoto *et al.* [109]. 100-300 nm anatase particles were synthesized via thermohydrolysis of titanium di*iso*propoxide *bis*(acetylacetonate) in supercritical CO_2 in the range of 10-20 MPa and 200-300ºC [106]. Ayllón *et al.* prepared colloidal solutions of ~8x5 nm box-shaped anatase by microwave-assisted hydrolysis, refluxing for 2h a TTIP ethanol-rich solution stabilized with tetrabutylammonium hydroxide [108]. Other authors have found that *in situ* generation of water from esterification reactions in non-aqueous media result in controlled hydrolysis of titanium alkoxides [110].

Unfortunately, as seen in the former examples, avoiding high-temperature steps is not obvious and alternative proposals in sol-gel routes present intrinsic drawbacks such as longer time-consuming steps, further requirements of expensive instrumentation and increase in safety risk (because of employing pressured reactors).

1.6.2. OTHER LOW-TEMPERATURE WET-CHEMISTRY ROUTES

To overcome these drawbacks, synthetic routes other than multi-step sol-gel strategies have also been described. For example, in the non-aqueous method reported by Niederberger *et al.*, solvolysis of $TiCl_4$ in anhydrous benzyl alcohol results in the formation of nanocrystalline anatase particles at temperatures as low as 40ºC, but employing long processing times of 7-21 days [111,112]. However, the use of an organic solvent and the rather violent initial reaction between concentrated $TiCl_4$ and benzyl alcohol seem to move away from Green Chemistry guidelines. Cozzoli *et al.* prepared different sized and shaped organic-capped anatase nanorods by controlling the hydrolysis process of TTIP with oleic acid as surfactant (80-100ºC, 6-12h) [113]. In our research group, anatase nanopowders with high surface area were prepared by hydrolyzing titanium 1,2-diolates in hot water by means of microwave irradiation [114]. Several authors have explored the formation of TiO_2 particles by the peroxotitanic acid approach, in which hydrated precipitates from the hydrolysis of a titanium alcoxide are

simultaneously digested in H_2O_2 and subsequently treated hydrothermally [115-117]. As recent achievement, Beok *et al.* prepared nano-sized powdered rutile by autoclaving a peroxotitanic acid solution at 100ºC for 12h [117].

Low-temperature Chemical Bath Deposition (CBD) techniques for preparing titania films have also been widely investigated [32]. CBD terminology refers to depositions from solutions (usually aqueous) where the titania deposit is both chemically generated from the controlled destabilization of a titania precursor and directly deposited on the substrate in the same bath. Hence, precursors such as titanium alkoxides and $TiCl_4$ are not commonly employed due to the existing difficulties to prevent the solution from spontaneous bulk precipitation [96,118]. Conceptually, CBD rank as the simplest approach for preparing coatings although direct deposition of nanocrystalline titania films is not obvious [119]. For example, Baskaran *et al.* successfully prepared titania UV filters on both sulfonated polymeric substrates and silicon functionalized with self-assembled monolayers[Φ] via a biomimetic approach involving acidic or basic destabilization (70-100ºC, 1-24h) of aqueous solutions of titanium (IV) *bis*(ammonium lactato)dihydroxide [96]. Imai *et al.* studied the deposition of transparent films consisting of anatase crystallites on various kinds of substrates by controlled hydrolysis of TiF_4 acidic solutions (pH=1-3) at 40-70ºC for 0.5-260h [120]. Besides, the same authors also explored experimental conditions for depositing rutile films by hydrolyzing $TiOSO_4$ acidic solutions (pH=1-2) at 60ºC for 1-20 days [121]. Recently, White *et al.* have described the Successive Ionic-Layer Adsorption and Reaction (SILAR) anatase deposition, in which a substrate is subsequently dipped in an ammonium titanyl oxalate solution alternating with an hydrolyzing NaOH solution for various cycles (100-480), followed by an hydrothermal treatment at 120ºC for 16h [122]. Oekermann *et al.* have reported anodic electrodeposition of rutile porous films from aqueous $TiCl_3$ solution under the influence of the surfactant sodium dodecyl sulfate at temperatures between 60-80ºC [123]. Apart from the cited works, there is a

[Φ] Highly ordered and oriented molecular assemblies formed by the chemisorption of a bifunctional surfactant. While the head functional group presents chemical affinity toward the surface of the substrate (*e.g.* H-S- and $(Cl)_3$-Si-, for Au and native oxide layer on Si, respectively), the tail group (*e.g.* –COOH, $-SO_3H$ or $–PO_4H_2$) facilitates titania deposition on the molecular assembly [96,124].

particular case of low-temperature CBD in which metal oxide thin films are grown by forcing the hydrolysis of a fluoro-complex precursor with a fluoride scavenger (see the following Section 1.7 for more details). In the literature, the term Liquid Phase Deposition is habitually kept for this concrete methodology.

1.7. LIQUID PHASE DEPOSITION

1.7.1. GENERAL DESCRIPTION

Liquid Phase Deposition (LPD) refers to the formation of metal oxide thin films from a metal fluoro-complex $[MF_n]^{(m-n)}$ (being *m* the cation charge and *n* the number of coordinating fluoro ligands), whose hydrolysis equilibria are displaced by scavenging processes of fluorine anions. The strong coordination capability of fluoride anions toward acidic and highly charged cations such as Si(IV) or Ti(IV) gives rise to aqueous solutions that are stable over months [119,121], in contrast to common titania precursors *i.e.* titanium alkoxides or $TiCl_4$ [96,118]. Nevertheless, dynamic metathesis equilibria are established between fluoro and hydroxo ligands in $[MF_n]^{(m-n)}$ aqueous solutions [32]. According to Equation 1.7.A, in case of increasing the water concentration or decreasing fluoride concentration, the equilibrium will be shifted toward the metal oxide [119]. Typically, boric acid is added to the media as fluoride scavenger, destabilizing the metal fluoro-complex and finally producing a very stable anion *i.e.* BF_4^- (Equation 1.7.B) [32]. Thus, the formation of the corresponding metal oxide is forced by shifting the dynamic hydrolysis equilibria 1.7.A.

$$[MF_n]^{(m-n)}\,(aq) + m/2\ H_2O \rightleftharpoons MO_{m/2}\,(s) + n\ F^-\,(aq) + m\ H^+\,(aq) \qquad (1.7.A)$$

$$H_3BO_3\,(aq) + 4\ HF\,(aq) \longrightarrow BF_4^-\,(aq) + H_3O^+\,(aq) + 2\ H_2O \qquad (1.7.B)$$

Suitable surface chemistry induces film formation at levels of supersaturation[Φ] that do not sustain homogeneous nucleation [32,124]. If the solution is highly supersaturated, precipitation takes place dominantly through homogeneous nucleation. On the contrary, the solution is metastable because of an extremely low reaction rate. Compared with the formation of oxide films by other CBD, the fluoride scavenging process allows a much better control of the synthetic reaction, the supersaturation of the solution as well as the growth rate of the films [32]. LPD is a soft aqueous-based chemical method performed under atmospheric pressure at low temperatures, which do not require neither special equipment (only a thermostatic reactor) nor high energy supply [101,102,125]. By the LPD method, relatively large area coatings have been successfully obtained on glass, conductive glass, silicon as well as complex-shaped substrates such as stainless steel or glass fiber [126,127]. Thus, LPD exhibits a clear advantage with respect to dry-methods employing vacuum, in which coating areas are limited [96].

LPD technique was firstly reported in the patent literature for preparing titania films [128] and has been mainly employed for depositing SiO_2 films afterwards [124,129]. Other examples include V_2O_5 [130], VO_2 [131], β-FeOOH (Fe_2O_3) [132], Nb_2O_5 [133], SnO_2 [134], ZrO_2 [135] as well as multicomponent metal oxide films [124,134]. It is worth pointing that, in the major part of the cases, amorphous films have been obtained [130,131,133]. Therefore, if a certain degree of crystallinity is required for a practical application, a further annealing step has to be carried out.

1.7.2. TiO_2 LIQUID PHASE DEPOSITION

Deki *et al.* reported first comprehensive publications dealing with titania LPD, carried out from $(NH_4)_2TiF_6$ and H_3BO_3 solutions [136,137]. For the ligand exchange hydrolysis of $[TiF_6]^{2-}$ ion in aqueous solution, the following equibrium scheme has been proposed (Equation 1.7.C):

[Φ] Metastable situation in which the concentration of a substance in solution exceeds the equilibrium concentration with respect to their solid phase [32].

$$[TiF_6]^{2-}\ (aq) + x\ H_2O \rightleftharpoons [TiF_{6-x}(OH)_x]^{2-}\ (aq) + x\ HF\ (aq) \qquad (1.7.C)$$

The deposition mechanism from these reactants is considered to occur via dehydratation of unstable $[TiF_{6-x}(OH)_x]^{2-}$ species generated by the hydrolysis reaction of $[TiF_6]^{2-}$, right hand shifted by the fluoride scavenging process [136,137]. Hence, supersaturation degree and deposition rate of titania films depend on the concentration of titanium hydroxide complex ions [138]. Polycrystalline anatase thin films exhibiting visible light transparency and excellent adherence are obtained on glass upon appropriate $(NH_4)_2TiF_6/H_3BO_3$ ratios [136] (Figure 1.7.1). It has been found that fluoride sorption on TiO_2 surface seems to moderate the polymerization of the growing material, favoring crystallization of the anatase phase under proper conditions [120].

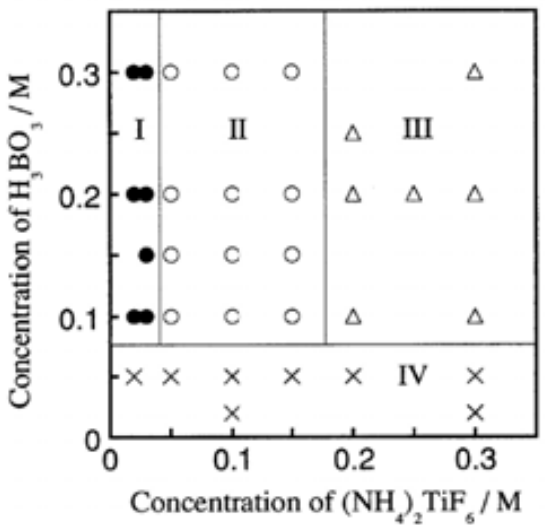

Figure 1.7.1. Relationship between aspect and chemical composition of titania films and the concentration range of $(NH_4)_2TiF_6$ and H_3BO_3. Temperature 25ºC. (I) hazy anatase; (II) transparent anatase; (III) NH_4TiOF_3; (IV) no deposition. Adapted from reference [136].

Since then, other research groups have studied the influence of different experimental parameters such as surface chemistry [43,124,138], pH [138,139] or deposition temperature [43] on the growth rate, morphology, composition and crystalline nature of the films. Yu *et al.* reported a systematic study regarding to the effect of the calcination temperature on the microstructure and photocatalytic activity of amorphous TiO_2 films prepared by LPD [140]. Typically, TiO_2 LPD is performed at 25-80ºC in acidic media (pH=1-4) with an average growth rate of 3-300 nm/h, resulting in coatings with a maximum thickness of 100-500 nm [32]. However, in order to

achieve as-prepared films crystalline enough, long deposition times (from tens of hours up to days) [136,137,139] or thermal post-treatments are required [140]. In our research group, it has been found that MW activation highly enhances both growth rate and crystallinity degree of titania thin films and powders [141-143].

Practical applications of TiO_2 films prepared by LPD have been proven in diverse fields. For instance, titania deposited on different substrates have exhibited self-actuating properties [126,127,144]. Koumoto *et al.* have developed bioinspired micro and nano-patterning of titania films on different substrates functionalized with self-assembly monolayers [124,139]. Vigil *et al.* have analyzed the behavior of TiO_2 deposited on conductive glass by MW-assisted LPD as blocking layers in Dye-Sensitized Solar Cells [145]. Finally, LPD technique has also recently broadened horizons toward the preparation of hybrid organic/TiO_2 materials (see Section 4.3).

1.8. DYE-SENSITIZED SOLAR CELLS

Current energy demands in order to sustain the lifestyle of 6.5 billion people worldwide is about 13 terawatts (TW), although additional power needs of 10-30 TW has been projected by year 2050 [146,147]. Fortunately, the Sun supplies to the Earth a gigantic value of energy *i.e.* 170,000 TW striking us every moment [147,148]. In case of 0.16 % of the Earth's land surface was covered with solar panels offering an efficiency of 10% turning sunlight to electricity, present energetic needs would be satisfied by far [147].

Dye-Sensitized Solar Cells (DSSCs) based on wide band gap nanocrystalline semiconductor oxides have been intensively studied and developed during the 90s and the present decade, since their discovery in 1991 by Grätzel *et al.* [58]. These devices were conceived as an environmentally friendly and economically viable alternative to conventional inorganic devices, based on solid-state p-n junctions. So far, best laboratory scale cells have attained certified efficiencies up to 11 % under standard reporting conditions (simulated AM 1.5 sunlight at 100 mW/cm^2 intensity, 298 K) using

TiO_2 as semiconductor in liquid junction devices [24,149]. Moreover, full-scale outdoor performance tests have shown advantages over commercial silicon cells, in terms of increased performance at high temperature and efficiency at low solar angles [150].

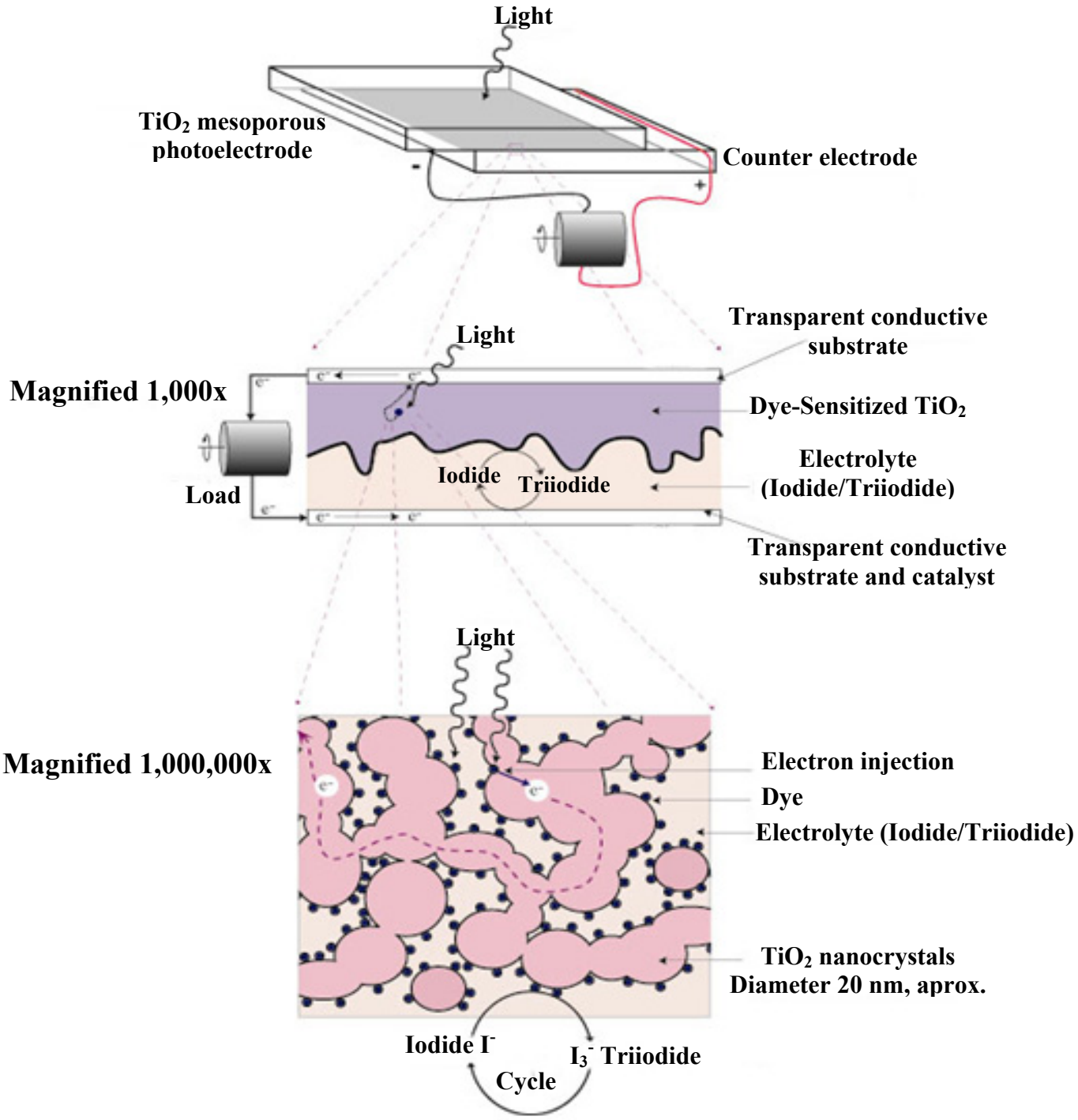

Figure 1.8.1. Representation at different scales of the components of a DSSC. Adapted from reference [151].

Figure 1.8.1 shows a representation at different scales of a DSSC and its components. The photoactive electrode consists of a nanocrystalline and mesoporous network of a wide band gap semiconductor (usually TiO_2), which is covered with a monolayer of photosensitizer molecules. The cell is illuminated through a Transparent Conductive Oxide (TCO) electrode, where the semiconductor is deposited. The TiO_2 pores are filled with a redox electrolyte (I_3^-/I^-) which acts as redox mediator and establishes electrical contact with a redox catalyst in the counter electrode [152].

DSSCs differ from conventional semiconductor devices (p-n heterojunctions), since in these photoelectrochemical devices the function of light absorption and the transport occur separately. The light absorption takes place in a monolayer of the photosensitizer (S), which is chemically adsorbed on the surface of the semiconductor (Equation 1.8.A). The photoexcited dye (S*) is then able to transfer an electron into the semiconductor (Equation 1.8.B) that move toward the TCO electrode through the TiO_2 porous network. Electrons lost by the sensitizer are recovered using the reduced specie present in the electrolyte (I^-), according to Equation 1.8.C. Finally, the circuit is closed by the oxidized specie of the mediator (I_3^-), that obtains electrons which flows to the counter electrode through the electrical load (Equation 1.8.D). Taking advantage of the redox mediator, photogenerated electron-hole pairs are transported in a cyclic process. The heart of the device is a TiO_2 mesoporous electrode with large internal area in order to make the most of the solar fotons per volume unit [151]:

$$\text{Sensitizer} + h\nu \rightarrow \text{Sensitizer*} \quad (1.8.A)$$

$$\text{Sensitizer*} + TiO_2 \rightarrow e^-(TiO_2) + \text{Oxidized Sensitizer}^+ \quad (1.8.B)$$

$$\text{Oxidized Sensitizer}^+ + 3/2\ I^- \rightarrow \text{Sensitizer} + 1/2\ I_3^- \quad (1.8.C)$$

$$1/2\ I_3^- + e^-(\text{counter electrode}) \rightarrow 3/2\ I^- \quad (1.8.D)$$

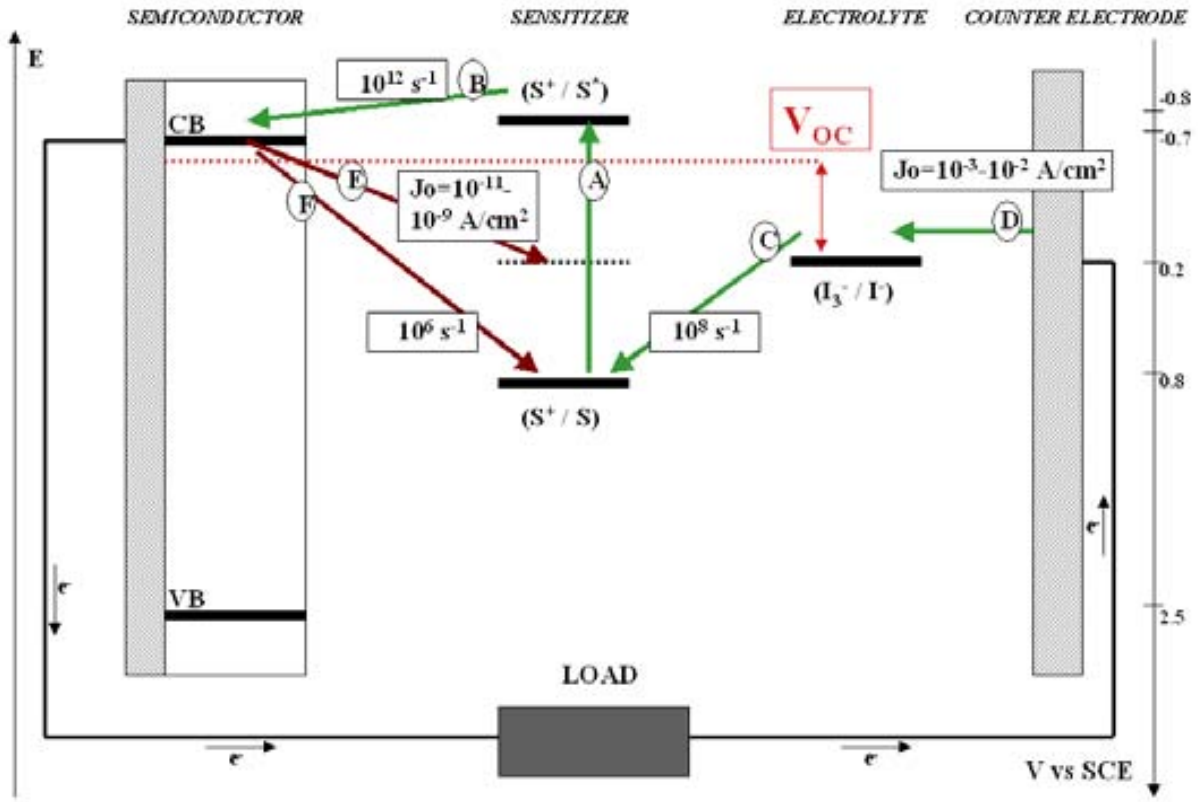

Figure 1.8.2. Schematic representation of the operating principles in DSSCs [24,50]. Green arrows: processes A-D (corresponding to Equations 1.8.A-1.8.D, respectively); brown arrows: non-desired processes, F (back electron transfer) and E (back reaction). Potentials are referred to the Saturated Calomel Electrode (SCE). The open-circuit voltage (V_{OC}) of the solar cell corresponds to the difference between the redox potential of the mediator and the quasi-Fermi level[Φ] of the nanocrystalline film (indicated with a dotted line). Adapted from ref. [50].

A schematic representation of the operating principles in DSSCs is given in Figure 1.8.2. Typical photosensitizers are ruthenium complexes anchored to the TiO_2 surface by a carboxylate bipyridyl ligand. The carboxylate groups are directly coordinated to the surface titanium(IV) ions, producing intimate electronic contact between the sensitizer and the semiconductor [24,50]. Upon illumination, the visible light absorption of these types of complexes is a metal-to-ligand charge transfer

[Φ] Qualitatively, the Fermi level (E_F) is the energy at which the probability of an energy level being occupied by an electron is exactly 1/2. Above the Fermi level the probability of occupancy drops to zero, and the energy levels are empty, while below E_F the energy levels are filled. In n-type semiconductors, a shift of E_F toward E_{CB} occur since the probability of occupancy of energy levels at the CB increases [153]. Upon light irradiation, the distribution of charge carriers in the semiconductor is altered due to electron storage, resulting in a higher apparent E_F energy (quasi-Fermi level) [50,146,154].

(MLCT) transition that takes place in the femtosecond scale (A) [50]. The electron injection from the photoexcited dye into the TiO_2 is carried out in the picosecond scale (B), while the back electron transfer (F) is six orders of magnitude slower, giving a quantum yield near 100% although process F is thermodynamically favorable [155]. However, back reduction reaction of triiodide anions by electrons transferred in the semiconductor can also occur, giving rise to non-desired current densities of 10^{-11}-10^{-9} A/cm^2, approximately. Employing a conventional Pt coated counter electrode, current densities of 10^{-3}-10^{-2} A/cm^2 are reached. Finally, the reduction of the oxidized sensitizer by iodide present in the electrolyte takes place in 10^{-8} s approximately [50].

Many companies and institutions have been engaged in research and development to address practical solutions to remaining challenges for practical applications of the DSSCs technology [150,156-160]. The weakest point of the present DSSCs is the limited long-term stability of the liquid junction devices with high conversion efficiency. Possible desorption of loosely attached dyes, and photodegradation in the desorbed state as well as corrosion of the Pt counter electrode by the iodide/triioidide couple have been suggested as some of the critical factors limiting the long-term performance of the devices, specially at elevated temperature [150,161,162]. In order to match specifications required for practical outdoors applications, light soaking and thermal stability tests performed under realistic conditions have been carried out [150,160-163]. Best results in sealed laboratory devices have been obtained using non-volatile electrolytes based on ionic liquids, whose initial top efficiency (η=8.3%) remains almost invariable after standard aging tests at 80ºC and light soaking at 65ºC, over a period of 1000 h [160].

1.9. REFERENCES

[1] Clark, J.; Macquarrie, D. *Handbook of green chemistry and technology.* Blackwell publishing. **2002**. ISBN 0-632-05715-7.

[2] Smith, J.H. *Science* **2003**, *302*, 1171.

[3] Gleick, P.H. *Science* **2003**, *302*, 1524-1527.

[4] Chow, J. *Science* **2003**, *302*, 1528-1531.

[5] EPA, Green Chemistry: www.epa.gov/greenchemisty.

[6] Clark, J.H. *Green Chem.* **1999**, *1*, 1-8.

[7] Poliakoff, M.; Licence, P. *Nature* **2007**, *450*, 810-812.

[8] Anastas, P.; Warner, J.C. *Green Chemistry Theory and Practice.* Oxford University Press. New York, **1998**. ISBN 0-19-850698-8.

[9] United Nations Environmental Programme: www.unep.org/wssd/.

[10] Organization for the Economical Cooperation and Development (OECD): www.oecd.org/wsd/.

[11] www.rsc.org/Publishing/Journals/gc/index.asp.

[12] www.chemsoc.org/networks/gcn/.

[13] www.pte-quimicasostenible.org/en/index.html.

[14] Cohen, J.E. *Science* **2003**, *302*, 1172-1175.

[15] Clark, J.H. *J. Chem. Technol. Biotechnol.* **2007**, *82*, 603-609.

[16] Horvath, I.T.; Anastas, P. *Chem. Rev.* **2007**, *107*, 2169-2173.

[17] www.ec.europa.eu/environment/chemicals/reach/reach_intro.htm.

[18] Tahiri, H.; Serpone, N.; Le van Mao, R. *J. Photochem. Photobiol. A: Chem.* **1996**, *93*, 199-203.

[19] Thompson, R. *Industrial Inorganic Chemicals: Production and Uses.* Royal Society of Chemistry. **1995**. ISBN 0-85404-514-7.

[20] Hoffmann, M.R.; Martin, S.T.; Choi, W.; Bahnemann, D.W. *Chem. Rev.* **1995**, *95*, 69-96.

[21] Zhu, R.R.; Wang, S.L.; Zhang, R.; Sun, X.Y.; Yao, S.D. *Chin. J. Chem.* **2007**, *25*, 958-961.

[22] Li, J.; Li, Q.; Xu, J.; Li, J.; Cai, X.; Liu, R.; Li, Y.; Ma, J.; Li, W. *Environ. Toxicol. Pharmacol.* **2007**, *24*, 239-244.

[23] Grätzel, M. *Nature.* **2001,** *414*, 338-344.

[24] Grätzel, M. *Prog. Photovolt: Res. Appl.* **2006**, *14*, 429-442.

[25] Fujishima, A.; Rao, T.N.; Tryk, D.A. *J. Photochem. Photobiol. C: Rev.* **2000**, *1*, 1-21.

[26] Ollis, D.F. *C. R. Acad. Sci. Paris, Chemistry.* **2002**, *3*, 405-411.

[27] Tundo, P.; Anastas, P. *Green Chemistry: challenging perspectives.* Oxford University Press. **2000**. ISBN 0-19-850455-1.

[28] Herrmann, J.M.; Duschamp, C.; Karkmaz, M.; Hoai, B.T.; Lachheb, H.; Puzenat, E.; Guillard, C. *J. Hazard. Mat.* **2007**, *146*, 624-629.

[29] Ohtani, B.; Ogawa, Y.; Nishimoto, S. *J. Phys. Chem. B* **1997**, *101*, 3746-3752.

[30] Ettlinger, M. *Technical Bulletin Pigments. Highly Dispersed Metallic Oxides Produced by the AEROSIL® Process.* No. *56*.

[31] Gutiérrez-Tauste, D.; Zumeta, I.; Vigil, E.; Hernández-Fenollosa, M.A.; Domènech, X.; Ayllón, J.A. *J. Photochem. Photobiol. A: Chem.* **2005**, *175*, 165-171.

[32] Niessen, T.P.; De Guire, M.R. *Solid State Ionics* **2002**, *151*, 61-68.

[33] Mao, Y.; Park, T.J.; Zhang, F.; Zhou, H.; Wong, S.S. *Small* **2007**, *3*, 1122-1139.

[34] Carp, O.; Huisman, C.L.; Reller, A. *Prog. Solid State Chem.* **2004**, *32*, 33-177.

[35] Diebold, U. *Surf. Sci. Rep.* **2003**, *48*, 53-229.

[36] Nuspl, G.; Yoshizawa, K.; Yamabe, T. *J. Mater. Chem.* **1997**, *7*, 2529-2536.

[37] Linsebigler, A.L.; Lu, G.; Yates, J.T. *Chem. Rev.* **1995**, *95*, 735-758.

[38] www.webmineral.com.

[39] Kolen'ko, Y.V.; Kovnir, K.A.; Gavrillov, A.I.; Garshev, A.V.; Frantti, J.; Lebedev, O.I.; Churagulov, B.R.; Tendeloo, G.V.; Yoshimura, M. *J. Phys. Chem. B* **2006**, *110*, 4030-4038.

[40] Zukalova, M.; Kalbac, M.; Kavan, L.; Exnar, I.; Grätzel, M. *Chem. Mater.* **2005**, *17*, 1248-1255.

[41] Banfield, J.F.; Veblen, D.R.; Smith, D.J. *Am. Mineral.* **1991**, *76*, 343-353.

[42] Mills, A.; Lee, S.K. *J. Photochem. Photobiol. A: Chem.* **2002**, *152*, 233-247.

[43] Pizem, H.; Sukenik, C.N.; Sampathkumaran, U.; McIlwain, A.K.; De Guire, M.R. *Chem. Mater.* **2002**, *14*, 2476-2485.

[44] Hurum, D.C.; Agrios, A.G.; Gray, K.A.; Rajh, T.; Thurnauer, M.C. *J. Phys. Chem. B* **2003**, *107*, 4545-4549.

[45] Mills, A.; Le Hunte, S. *J. Photochem. Photobiol. A: Chem.* **1997**, *108*, 1-35.

[46] Gole, J.L.; Stout, J.D.; Burda, C.; Lou, Y.; Chen, X. *J. Phys. Chem. B* **2004**, *108*, 1230-1240.

[47] Nagaveni, K.; Hegde, M.S.; Ravishankar, N.; Subbana, G.N.; Madras, G. *Langmuir* **2004**, *20*, 2900-2907.

[48] Thompson, T.L.; Yates, J.T. *Chem. Rev.* **2006**, *106*, 4428-4453.

[49] ASTM *Standard tables for terrestrial direct normal solar spectral irradiance for air mass 1.5.* E891-87. **1987**.

[50] Hagfelt, A.; Grätzel, M. *Chem. Rev.* **1995**, *95*, 49-68.

[51] Blesa, M.A. *Eliminación de contaminantes por Fotocatálisis heterogénea.* Programa CYTED. **2001**. ISBN 987-43-3809-1.

[52] Fujishima, A.; Honda, K. *Nature* **1972**, *238*, 37-38.

[53] Frank, S.N.; Bard, A.J. *J. Am. Chem. Soc.* **1977**, *99*, 303-304.

[54] Frank, S.N.; Bard, A.J. *J. Phys. Chem.* **1977**, *81*, 1484-1488.

[55] Kraeutler, B.; Bard, A.J. *J. Am. Chem. Soc.* **1978**, *100*, 5985-5992.

[56] Pruden, A.L.; Ollis, D.F. *Environ. Sci. Technol.* **1983**, *17*, 628-631.

[57] Matsunaga, T.; Tomoda, R.; Nakajima, T.; Wake, H. *FEMS Microb. Lett.* **1985**, *29*, 211-214.

[58] O'Regan, B.; Grätzel, M. *Nature* **1991,** *353*, 737.

[59] Wang, R.; Hashimoto, K.; Fujishima, A.; Chikuni, M.; Kojima, E.; Kitamura, A.; Shimohigoshi, M.; Watanabe, T. *Nature* **1997**, *388*, 431-432.

[60] Ni, M.; Leung, M.K.H.; Leung, D.Y.C.; Sumathy, K. *Renew. Sust. Energ. Rev.* **2007**, *11*, 401-425.

[61] Dunn, S. *Int. J. Hydrogen Energy*. **2002**, *27*, 235-264.

[62] Osterloh, F.E. *Chem. Mater.* **2008**, *20*, 35-54.

[63] Kabra, K.; Chaudhary, R.; Sawhney, R.L. *Ind. Eng. Chem. Res.* **2004**, *43*, 7683-7696.

[64] Herrmann, J.M. *Top. Catal.* **2005**, *34*, 49-65.

[65] Blake, D.M; Maness, P.C.; Huang, Z.; Wolfrum, E.J.; Huang, J.; Jacoby, W.A. *Bibliography of work on photocatalytic removal of hazardous compounds from water and air.* National Renewable Energy Laboratory (NREL/TP-430-22197). Golden, **1999**.

[66] Plataforma Solar de Almeria (PSA): www.psa.es.

[67] Franch, M.I.; Peral, J.; Domènech, X.; Ayllón, J.A. *Chem. Commun.* **2005**, 1851-1853.

[68] Palmisano, G.; Augugliaro, V.; Pagliaro, M.; Palmisano, L. *Chem. Comunn.* **2007**, 3425-3437.

[69] McCullagh, C.; Robertson, J.M.C.; Bahnemann, D.W.; Robertson, P.K.J. *Res. Chem. Intermed.* **2007**, *33*, 359-375.

[70] TOTO Inc.: www.toto.co.jp.

[71] Mills, A.; Crow, M. *J. Phys. Chem. C* **2007**, *111*, 6009-6016.

[72] Nippon Sheet Glass Co., Ltd.: www.nsg.co.jp/en/.

[73] Pilkington Glass Co., Ltd.: www.pilkington.com/international+products/activ/default.htm.

[74] Saint Gobain Glass Co., Ltd.; www.selfcleaningglass.com.

[75] Hodes, G. *Adv. Mater.* **2007**, *19*, 639-655.

[76] Chen, X.; Mao, S.S. *Chem. Rev.* **2007**, *107*, 2891-2959.

[77] Zhong, Z.; Ang, T.P.; Luo, J.; Gan, H.C.; Gedanken, A. *Chem. Mater.* **2005**, *17*, 6814-6818.

[78] McMurray, T.A.; Byrne, J.A.; Dunlop, P.S.M.; Winkelman, J.G.M.; Eggins, B.R.; McAdams, E.T. *Appl. Catal. A: Gen.* **2004**, *262*, 105-110.

[79] Rao, K.V.; Subrahmanyam, M.; Boule, P. *Appl. Catal. B: Environ.* **2004**, *49*, 239-249.

[80] Roméas, V.; Pichat, P.; Guillard, C.; Chopin, T.; Lehaut, C. *Ind. Eng. Chem. Res.* **1999**, *38*, 3878-3885.

[81] Hwang, S.; Lee, M.C.; Choi, W. *Appl. Catal. B: Environ.* **2003**, *46*, 49-63.

[82] Karpagavalli, R.; Zhou, A.; Chellamuthu, P.; Nguyen, K. *J. Biomed. Mat. Res., Part A* **2007**, 1087-1095.

[83] Richards, B.S. *Sol. Energ. Mat. Sol. C.* **2003**, *79*, 369-390.

[84] Lien, S.Y.; Wuu, D.S.; Yeh, W.C.; Liu, J.C. *Sol. Energy Mater. Sol. Cells* **2006**, *90*, 2710-2719.

[85] Francioso, L.; Presicce, D.S.; Taurino, A.M.; Rella, R.; Siciliano, P.; Ficarella, A. *Sens. Actuators B* **2003**, *95*, 66-72.

[86] Mills, A.; Lepre, A.; Elliott, N.; Bhopal, S.; Parkin, I.P.; O'Neill, S.A. *J. Photochem. Photobiol. A: Chem.* **2003**, *160*, 213-224.

[87] Chae, S.Y.; Park, M.K.; Lee, S.K.; Kim, T.Y.; Kim, S.K.; Lee, W.I. *Chem. Mater.* **2003**, *15*, 3326-3331.

[88] Sing, K.S.W.; Everett, D.H.; Haul, R.A.W.; Moscou, L.; Pierotti, R.A.; Rouquérol, J.; Siemieniewska, T. *Pure Appl. Chem.* **1985**, *57*, 603-619.

[89] Sigma-Aldrich: www.sigmaaldrich.com.

[90] Büchel, K.H.; Moretto, H.H.; Woditsch, P. *Industrial Inorganic Chemistry.* 2nd edition. Ed. Wiley-VCH. Weinheim, **2000**. ISBN 3-527-29849-5.

[91] Rayner-Canham, G. *Descriptive Inorganic Chemistry.* 2nd edition. Ed. W. H. Freeman and Company. New York, **2000**. ISBN 0-7167-3553-9.

[92] Ding, K., Miao, Z.; Liu, Z.; Zhang, Z.; Han, B.; An, G.; Miao, S.; Xie, Y. *J. Am. Chem. Soc.* **2007**, *129*, 6362-6363.

[93] Cushing, B.L.; Kolesnichenko, V.L.; O'Connor, C.J. *Chem. Rev.* **2004**, *104*, 3893-3946.

[94] Schuegraff, K.K. *Handbook of thin-film deposition processes and technologies: principles, methods, equipment and applications.* Noyes plublications, materials science and process technology series. New Jersey, **1988**. ISBN 0-8155-1153-1.

[95] Peiró, A.M.; Brillas, E.; Peral, J., Domènech, X.; Ayllón, J.A. *J. Mater. Chem.* **2002**, *12*, 2769-2773.

[96] Baskaran, S.; Song, L.; Liu, J.; Chen, Y.L.; Graff, G.L. *J. Am. Ceram. Soc.* **1998**, *81*, 401-408.

[97] Seifred, S.; Winterer, M.; Hahn, H. *Chem. Vap. Deposition* **2000**, *6*, 239-244.

[98] Lee, S.M.; Park, J.H.; Hong, K.S.; Cho, W.J.; Kim, D.L. *J. Vac. Sci. Technol.* **2000**, *18*, 2384-2388.

[99] Castañeda, L., Alonso, J.C.; Ortiz, A.; Andrade, E.; Saniger, J.M.; Bañuelos, J.G. *Mater. Chem. Phys.* **2002**, *77*, 938-944.

[100] Li, Y.; White, T.J.; Lim, S.H. *J. Solid State Chem.* **2004**, *177*, 1372-1381.

[101] Gutiérrez-Tauste, D.; Domènech, X.; Casañ-Pastor, N.; Ayllón, J.A. *J. Photochem. Photobiol. A: Chem.* **2007**, *187*, 45-52.

[102] Gutiérrez-Tauste, D.; Domènech, X.; Domingo, C.; Ayllón, J.A. *Thin Solid Films* **2008**, *516*, 3831-3835.
[103] Langlet, M.; Burgos, M.; Coutier, C.; Jimenez, C.; Morant, C.; Manso, M. *J. Sol-Gel Sci. Technol.* **2001**, *22*, 139-150.
[104] Bosc, F.; Ayral, A.; Albouy, P.; Guizard, C. *Chem. Mater.* **2003**, *15*, 2463-2468.
[105] Jensen, H.; Bremholm, M.; Nielsen, R.P.; Joensen, K.D.; Pedersen, J.S.; Birkedal, H.; Chen, Y.S.; Almer, J.; Sogaard, E.G.; Iversen, S.B.; Iversen, B.B. *Angew. Chem. Int. Ed.* **2007**, *46*, 1113-1116.
[106] Alonso, E.; Montequi, I.; Lucas, S.; Cocero, M.J. *Supercrit. Fluids* **2007**, *39*, 453-461.
[107] Langlet, M.; Kim, A.; Audier, M.; Herrmann, J.M. *J. Sol-Gel Sci. Technol.* **2002**, *25*, 223-234.
[108] Peiró, A.M.; Peral, J.; Domingo, C.; Domènech, X.; Ayllón, J.A. *Chem. Mater.* **2001**, *13*, 2567-2573.
[109] Sugimoto, T.; Zhou, X.; Maramatsu, A. *J. Colloid Interface Sci.* **2003**, *259*, 53-61.
[110] Zhu, J.; Zhang, J.; Chen, F.; Anpo, M. *Mater. Lett.* **2005**, *59*, 3378-3381.
[111] Niederberger, M.; Bartl, M.H.; Stucky, G.D. *J. Am. Chem. Soc.* **2002**, *124*, 13642-13643.
[112] Niederberger, M.; Bartl, M.H.; Stucky, G.D. *Chem. Mater.* **2002**, *14*, 4364-4370.
[113] Cozzoli, P.D.; Kornowski, A.; Weller, H. *J. Am. Chem. Soc.* **2003**, *125*, 14539-14548.
[114] Saadoun, L.; Ayllón, J.A.; Jiménez-Becerril, J.; Peral, J.; Domènech, X.; Rodríguez-Clemente, R. *Appl. Catal., B* **1999**, *21*, 269-277.
[115] Wang, Z.C.; Chen, J.F.; Hu, X.F. *Mater. Lett.* **2002**, *43*, 87-90.
[116] Liu, Y.J.; Aizawa, M.; Peng, W.Q.; Wang, Z.M.; Hatori, H.; Uekawa, N.; Kanoh, H. *Chem. Lett.* **2007**, *36*, 1094-1095.
[117] Beok, S.; Ahn, B.Y.; Pramanik, N.C.; Kim, H. *J. Am. Ceram. Soc.* **2006**, *89*, 1147-1149.
[118] Niessen, T.P.; Bill, J.; Aldinger, F. *Chem. Mater.* **2001**, *13*, 1552-1559.
[119] Hodes, G. *Phys. Chem. Chem. Phys.* **2007**, *9*, 2181-2196.
[120] Shimizu, K.; Imai, H.; Hirashima, H.; Tsukuma, K. *Thin Solid Films* **1999**, *351*, 220-224.

[121] Yamabi, S.; Imai, H. *Chem. Mater.* **2002**, *14*, 609-614.

[122] Johnson, S.E.; Burgoon, W.P.; Wang, Q.; White, J.M. *Langmuir* **2006**, *22*, 6570-6577.

[123] Wessels, K.; Feldhoff, A.; Wark, M.; Rathousky, J.; Oekermann, T. *Electrochem. Solid-State Lett.* **2006**, *9*, C93-C96.

[124] Gao,Y.; Koumoto, K. *Crys. Growth Des.* **2005**, *5*, 1983-2017.

[125] Gutiérrez-Tauste, D.; Domènech, X.; Hernández-Fenollosa, M.A.; Ayllón, J.A. *J. Mater. Chem.* **2006**, *16*, 2249-2255.

[126] Yu, H.; Lee, S.C.; Yu, J.; Ao, C.H. *J. Mol. Catal. A: Chem.* **2005**, *246*, 206-211.

[127] Lee, S.C.; Yu, H.; Yu, J.; Ao, C.H. *J. Cryst. Growth* **2006**, *295*, 60-68.

[128] Kawahara, H.; Honda, H. Japanese patent 59141441 A (Nippon Sheet Glass), August 14, **1984**.

[129] Sakai, Y.; Norimatsu, H.; Saito, Y.; Inomata, H.; Mizuno, T.; *Thin Solid Films* **2001**, *392*, 294-298.

[130] Deki, S.; Aoi, Y.; Miyake, A.; Gotoh, A.; Kajinami, A. *Mater. Res. Bull.* **1996**, *31*, 1399-1406.

[131] Deki, S.; Aoi, Y.; Kajinami, A. *J. Mater. Sci.* **1997**, *32*, 4269-4273.

[132] Deki, S.; Aoi, Y.; Okibe, J.; Yanagimoto, H.; Kajinami, A.; Mizuhata, M. *J. Mater. Chem.* **1997**, *7*, 1769-1772.

[133] Ko, H.Y.Y.; Mizuhata, M.; Kajinami, A.; Deki, S. *J. Fluorine Chem.* **2003**, *120*, 157-163.

[134] Deki, S.; Iizuka, S.; Mizuhata, M.; Kajinami, A. *J. Electroanal. Chem.* **2005**, *584*, 38-43.

[135] Kuratani, K.; Mizuhata, M.; Kajinami, A.; Deki, S. *J. Alloys Compd.* **2006**, *408*, 711-716.

[136] Deki, S.; Aoi, Y.; Hiroi, O.; Kajinami, A. *Chem. Lett.* **1996**, *6*, 433-434.

[137] Deki, S.; Aoi, Y.; Asaoka, Y.; Kajinami, A.; Mizuhata, M. *J. Mater. Chem.* **1997**, *7*, 733-736.

[138] Masuda, Y.; Ieda, S.; Koumoto, K. *Langmuir* **2003**, *19*, 4415-4419.

[139] Masuda, Y.; Sugiyama, T.; Seo, W.S.; Koumoto, K. *Chem. Mater.* **2003**, *15*, 2469-2476.

[140] Yu, J.G.; Yu, H.G.; Cheng, B.; Zhao, X.J.; Yu, J.C.; Ho, W.K. *J. Phys. Chem.* **2004**, *107*, 13871-13879.
[141] Vigil, E.; Saadoun, L.; Ayllón, J.A.; Domènech, X.; Zumeta, I.; Rogríguez-Clemente, R. *Thin Solid Films* **2000**, *365*, 12-18.
[142] Ayllón, J.A.; Peiró, A.M. ; Saadoun, L.; Vigil, E.; Domènech, X.; Peral, J. *J. Mater. Chem.* **2000**, *10*, 1911-1914.
[143] Vigil, E.; González, B.; Zumeta, I.; Docteur, S.; Peiró, A.M.; Gutiérrez-Tauste, D.; Domingo, C.; Domènech, X.; Ayllón, J.A. *J. Crys. Growth* **2004**, *262*, 366-374.
[144] Wang, X.P.; Yu, Y.; Hu, X.F.; Gao, L. *Thin Solid Films* **2000**, *371*, 148-152.
[145] Vigil, E.; Zumeta, I.; Ayllón, J.A.; González, B.; Domènech, X.; Domingo, C. *Phys. State Sol.* **2005**, *242*, 1807-1811.
[146] Kamat, P.V. *J. Phys. Chem. C* **2007**, *111*, 2834-2860.
[147] Service, R.F. *Science* **2005**, *309*, 548-551.
[148] Crabtree, G.W.; Lewis, N.S. *Physics Today* **2007**, *60*, 37-42.
[149] Nazeeruddin, M.K.; Péchy, P.; Renouard, T.; Zakeeruddin, S.; Humphry-Baker, R.; Comte, P.; Liska, P.; Cevey, L.; Costa, E.; Shklover, V.; Spiccia, L.; Deacon, G.B.; Bignozzi, C.A.; Grätzel, M. *J. Am. Chem. Soc.* **2001**, *123*, 1613-1624.
[150] Toyoda, T.; Sano, T.; Nakajima, J.; Doi, S.; Fukumotoa, S.; Ito, A.; Tohyama, T.; Yoshida, M.; Kanagawa, T.; Motohiro, T.; Shiga, T.; Higuchi, K.; Tanaka, H.; Takeda, Y.; Fukano, T.; Katoh, N.; Takeichi, A.; Takechi, K.; Shiozawa, M. *J. Photochem. Photobiol. A: Chem.* **2004**, *164*, 203-207.
[151] Smestad, G.P. *Sol. Energ. Mat. Sol. C.* **1998**, *55*, 157-178.
[152] Bisquert, J.; Cahen, D.; Hodes, G.; Rühle, S.; Zaban, A. *J. Phys. Chem. B.* **2004**, *108*, 8106-8118.
[153] Finklea, H.O. *J. Chem. Educ.* **1983**, *60*, 325-327.
[154] Peter, L.M. *J. Phys. Chem. C* **2007**, *111*, 6601-6612.
[155] Nazeeruddin, M.K.; Kay, A.; Rodicio, I.; Humphry-Baker, R.; Müller, E.; Liska, P.; Vlachopoulos, N.; Grätzel, M. *J. Am. Chem. Soc.* **1993**, *115*, 6382-6390.
[156] Sustainable Technologies International Ltd. www.sta.com.au.
[157] Fraunhofer Institut für Solare Energies Systeme (ISE): www.ise.fhg.de.
[158] SONY Stuttgart Technology Center. SONY Deutschland GmbH: www.stuttgart.sony.de.

[159] Tribusch, H. *Coord. Chem. Rev.* **2004**, *248*, 1511-1530.

[160] Kuang, D.; Klein, C.; Ito, S.; Moser, J.E.; Humphry-Baker, R.; Evans, N.; Duriaux, F.; Grätzel, C.; Zakeeruddin, S.M.; Grätzel, M. *Adv. Mater.* **2007**, *19*, 1133-1137.

[161] Wang, P.; Zakeeruddin, S.M.; Moser, J.E.; Nazeeruddin, M.K.; Sekiguchi, T.; Grätzel, M. *Nature* **2003**, *2*, 402-406.

[162] Hinsch, A.; Kroon, J.M.; Kern, R.; Uhlendorf, I.; Holzbock, J.; Meyer, A.; Ferber, J. *Prog. Photovolt: Res. Appl.* **2001**, *9*, 425-438.

[163] Sommeling, P.M.; Späth, M.; Smit, H.J.P.; Bakker, N.J.; Kroon, J.M. *J. Photochem. Photobiol. A: Chem.* **2004**, *164*, 137-144.

CHAPTER 2:

GOAL AND SCOPE OF THE WORK

The purpose of the present work is offering novel contributions to wet-chemistry preparation methods for obtaining TiO_2 films and powders within Green Chemistry guidelines, developing simple, environmentally benign and low-cost approaches and, putting special emphasis on low-temperature processing. Low-temperature methods (ideally up to a maximum closer to 100ºC) should give rise to materials exhibiting properties similar than those processed at high temperature or solvothermally treated. It is worth remarking here that crystalline nature of titania is habitually a key requirement for practical applications based on light-activated photoinduced interfacial reactions.

On one hand, mechanical stability and electrical contact of mesoporous titania photoelectrodes prepared by depositing pre-synthesized TiO_2 nanoparticles are of vital importance in Dye-Sensitized Solar Cells, and habitually attained only with a high temperature post-treatment (450-500ºC). In this context, low-temperature processing of such photoelectrodes would represent to unlock the door for light and flexible DSSCs on plastic substrates. Chemical necking of commercial TiO_2 P-25 nanoparticles is attempted as low-temperature alternative processing.

On the other hand, the interest in the present work is also focused on novel contributions to Liquid Phase Deposition technique, concerning the enhancement of deposition rate, crystallinity and homogeneity of as-prepared TiO_2 thin films. In addition, broadening horizons of LPD toward one-step deposition of hybrid/TiO_2 films is high on our agenda in order to prepare functional composites with practical applications as actuating materials and/or materials directly sensitized to visible light.

Finally, designing novel green synthetic routes for direct low-temperature synthesis of nanocrystalline TiO_2 particles is pursued in order to apply them, for example, in constituting DSSCs photoelectrodes or as photocatalyst for environmental remediation. In this direction, versatile and high-yield methods giving rise to particles with controlled size and morphology are ideally desired.

CHAPTER 3:

MATERIALS AND METHODS

3.1. SUBTRATES AND CLEANING PROCEDURES

Three different types of substrates have been used: common glass, conductive glass and conductive plastic. Conductive substrates consist of an isolating substrate covered with a Transparent Conductive Oxide (TCO). The conductive oxides more widely employed are ITO (Indium Tin Oxide, In_2O_3:Sn) and FTO (Fluorine Tin Oxide, SnO_2:F). Suppliers as well as technical characteristics of the substrates used are shown in Table 3.1.1.

Table 3.1.1. Technical data of the employed substrates.

Substrate	Technical data	Supplier
Common glass	25x75x1 mm standard cover slides	IDL GmbH & Co.
Glass-ITO	50x50x1.1 mm pieces; transmittance 92 %; 13-18 Ω/□	Optical Filters Ltd.
Glass-FTO	25x25x2.0 mm pieces; 15 Ω/□	Pilkington Glass Ltd.
PET-ITO	200 x 300 mm films; PET thickness 175 μm; 60 Ω/□	Innovate Sputtering Technology N.V.

Substrates were carefully cut into pieces of suitable size and were cleaned afterwards. Cleanliness of substrates is a critical factor for both correct homogeneity and adherence of the future coatings deposited over them and it is absolutely essential to follow strict cleaning protocols in order to assure there are no impurities on the surface of the substrates. Substrates were cleaned just before using according to procedures previously reported [1,2], based on ultrasonic treatments with different solvents. On the other hand, no cleaning procedure was chosen in the case of the conductive plastic substrate and was used as-received because of, as was observed experimentally, the ITO conductive coating on the polymer foil presented low mechanical stability under similar sonnication treatments with solvents. However, special care was taken in manipulating PET-ITO substrates and maintaining their surface clean.

3.2. TiO_2 DEGUSSA P-25

TiO_2 Degussa P-25 is synthesized via the AEROSIL® process at temperatures above 1200ºC, in which $TiCl_4$ is hydrolyzed in the presence of oxygen and hydrogen [3-5] (Equation 3.2.A). As-prepared titania is treated with steam to remove HCl, which is also produced as by-product [3].

$$TiCl_4\ (g) + 2\ H_2\ (g) + O_2\ (g) \longrightarrow TiO_2\ (s) + 4\ HCl\ (g) \qquad (3.2.A)$$

The product is 99.5% pure TiO_2 (anatase:rutile ratio, 70:30), which is non-porous, with cubic particles with rounded edges [6]. The remaining percentage of composition include other oxides (SiO_2<0.2%, Al_2O_3<0.3%, Fe_2O_3<0.01%) as well as HCl<0.3% [4]. TiO_2 P-25 powder has a surface area of 50±15 m^2/g and an average particle diameter of 21 nm, forming aggregates of 0.1 μm [3].

Degussa P-25 has became the "gold standard" material in semiconductor photochemistry research since presents high photoactivity [6]. Investigations concerning such high photoactivity of P-25 with respect to other commercial titania photocatalysts (including pure anatase phases) coincide with the existence of some synergistic effects in the interaction between the two different polymorphs. According to the model proposed by Hurum *et al.*, charge separation occurs on the rutile phase, that extends P-25 response into visible wavelengths (E_g(rutile)=3.0 eV (410 nm); E_g(anatase)=3.2 eV (385 nm)) and behave as antenna. The particular structure of P-25, in which two crystal structures present high surface contact, allows rapid electron transfer from rutile to lower energy trapping sites located in anatase environment, yielding an efficient charge separation [7].

3.3. EXPERIMENTAL PROCEDURES

3.3.1. REFERENCE TiO_2 POROUS PHOTOELECTRODES FOR DSSCs

The conventional high-temperature sintering method for preparing TiO_2 P-25 porous photoelectrodes described by Nazeeruddin *et al.* [8] was adopted as reference method in Publication 1 (see Section 4.1). In order to break P-25 aggregates into separate particles, the powder (6 g) was vigorously ground in a porcelain mortar with a small amount of acetylacetone aqueous solution (0.2 ml in 2 ml) to prevent reaggregation of the particles. Afterwards, the resulting viscous paste was slowly diluted with 8 ml of water under continued grinding. Finally, 1 ml of a 1:10 Triton X-100 (polyethylene glycol *tert*-octylphenyl ether) solution in water was added to facilitate the spreading of the colloid on the TCO substrate. This latter process was carried out by the Doctor Blade method (Figure 3.3.1), in which the paste with the adequate viscosity is spread using a glass rod on the area delimited by an adhesive tape in the substrate edges [9].

Figure 3.3.1. Representation of the Doctor Blade method, adapted from reference [9].

3.3.2. LIQUID PHASE DEPOSITION

Liquid Phase Deposition processes were performed in polyethylene vessels with the substrate (*i.e.* glass or ITO-covered glass previously cleaned) immersed vertically. Deposition media were prepared from fresh aqueous solutions of the corresponding components. LPD processes were carried out at 80ºC in an standard Memmert oven for variable times depending on the case (ranging from 2 to 7.5 h). In all the experiments,

the commercial Ti precursor employed was $(NH_4)_2TiF_6$ (ammonium hexafluorotitanate, AHFT) with a fixed concentration of 10 mM. Reference TiO_2 films were prepared upon the same temperature and deposition time with boric acid as fluoride scavenger ($Ti:H_3BO_3$ ratio=3, initial pH adjusted to 2.8 with diluted $HClO_4$), according to previous values used [1,10]. In order to only deposit coatings on one side, the substrates were back-side covered with a clean glass slide subjected with PTFE Teflon. Determination of pHs in LPD media were carried out by means of a Crison pH meter equipped with a 52-06 HF-resistant electrode (up to 1g/l, pH=3, T=20ºC) [11].

3.3.3. TiO_2 SYNTHESIS FROM IONIC LIQUID LIKE PRECURSOR SOLUTIONS

$[BetH]_2TiF_6$ and $[Cho]_2TiF_6$ hexafluorotitanate salts were prepared by reacting betaine (Bet; $(CH_3)_3$-N^+-CH_2-COO^-) and choline (Cho^+; $(CH_3)_3$-N^+-CH_2-CH_2OH) chloride with commercial H_2TiF_6 (hexafluorotitanic acid, HFTA) in a 2:1 ratio. The reactor was a 30 ml plastic bottle covered with PFA Teflon (Nalgene®) and was heated in a double boiler system. In the former case, 2.93 g of Bet (24.9 mmol) were dissolved in 3.35 g of 60 wt.% HFTA (12.3 mmol) giving rise to an exothermic reaction, while when 3.53 g of ChoCl (24.9 mmol) were added to the same amount of HFTA, an endothermic reaction was noticed. The tetraalkylmmonium hexafluorotitanate ($[NR_4]_2TiF_6$) solutions were kept hot by means of the double boiler system and homogenized for 30 min. Afterwards, 1.5 equivalents of boric acid (1.14 g, previously ground in a porcelain mortar) were added little by little to the corresponding $[NR_4]_2TiF_6$ precursor solution heated in the double boiler. Afterwards, the reaction media were aged at 85ºC in a standard Memmert oven for variable time periods (ranging from 18 to 90 h), gradually acquiring a white paste texture. As-prepared TiO_2 was washed with 25 ml of water and the solid part was recovered by centrifugation. Then, the non-dried solid part was divided into two centrifuge tubes, dispersed with 25 ml of water on each half (TiO_2 approx. 2 wt.%) and separated by centrifugation, a cleaning procedure that was repeated a total of 5 times. In selected cases, the final solid product was dried at 85 ºC in the oven.

3.4. MATERIALS CHARACTERIZATION

3.4.1. OPTICAL ESTIMATION OF BAND GAP ENERGY

UV-Vis absorbance spectra of titania thin films were processed in order to estimate band gap energy (E_g) from the threshold absorption values. In the high absorption region (>10^4 cm^{-1}), titania absorption coefficient α is related to the energy ($h\nu$) of incident photons by the relation shown in Equation 3.4.A, where B is the corresponding absorption constant [12,13]:

$$\alpha = B\,(h\nu - E_g)^2 / h\nu \qquad (3.4.A)$$

If scattering losses are negligible with respect to fundamental absorption, observed absorbance can be assumed to be proportional to optical absorption coefficient α [13]. Reorganizing terms, a lineal dependence between $Abs^{1/2}(h\nu)^{1/2}$ and incident radiation ($h\nu$) is established (Equation 3.4.B). In the absorption range, the E_g value of the semiconductor coincides with the value of the incident radiation ($h\nu$) when $Abs^{1/2}(h\nu)^{1/2}$ is extrapolated to zero.

$$Abs^{1/2}(h\nu)^{1/2} = B'h\nu - B'E_g \qquad (3.4.B)$$

3.4.2. CRYSTALLITE SIZE ESTIMATION: SCHERRER EQUATION

In 1918, P. Scherrer showed that, when X-ray monochromatic radiation falls on a randomly oriented mass of crystals, the diffracted beam is broadened when the particle size is small [14]. Thus, the angular spread of X-Ray Diffraction (XRD) signals beyond instrumental effects can give a useful measure of the crystallites size in polycrystalline specimens [14,15]. The linear dimension of crystallite $L_{[hkl]}$ can usually be related to the

broadening of the corresponding signal via the semiempirical Scherrer equation [13,15,16] (Equation 3.4.C), in which K is a correction factor (depending on the particle shape and is usually about 0.9), λ the wavelength of X-ray (Cu K_α = 0.154056 nm), β_L the peak full-width at half-maximum and θ the diffraction angle.

$$L_{[hkl]} = K \lambda / \beta_L \ \mathrm{Cos}\ \theta \qquad (3.4.C)$$

In fact, Scherrer formula can be applied successfully only over a limited crystallite size range since particles smaller than about 5 nm usually lead to reflection peaks too broad and diffuse for accurate measurement [14,16]. On the other hand, as the number of regularly spaced scattering centers increases, the angles at which diffracted beams are observed become more and more sharply defined [16].

3.5. DYE-SENSITIZED SOLAR CELLS CHARACTERIZATION

A series of magnitudes and terms necessary hereafter for the photoelectrochemical characterization of DSSCs are defined [9,17].

I_{SC} Short-circuit electrical photocurrent: maximum output current of the device, obtained when the external load resistance is zero (or negligible with respect to the resistance of the device). J_{SC} refers to the corresponding photocurrent density ($J_{SC}=I_{SC}$/illuminated area).

V_{OC} Open-circuit photovoltage: light-created voltage output for infinite load resistance.

I_{opt}, V_{opt} Optimal photocurrent and photovoltage values giving rise to the maximum available output power.

FF Fill Factor: ratio between the maximum output power available ($I_{opt} \cdot V_{opt}$) and the maximum power, combining the short-circuit and open-circuit situations ($I_{SC} \cdot V_{OC}$).

E Irradiance or incident luminous power per area unit.

E_λ Spectral irradiance or incident luminous power per area unit at a fixed λ.

3.5.1. SPECTRAL RESPONSE: IPCE

In the literature is commonly employed the value IPCE (Incident Photon-to-Current Conversion Efficiency) for determining quantitatively the spectral response. IPCE is defined according to Equation 3.5.A [8,18,19], which measures the percentage of photons that generate electrical current with respect to the total number of incident photons at a fixed wavelength.

$$IPCE\ (\%) = 1240 / \lambda\ [nm] \cdot J_{SC}\ [A/cm^2] / E_\lambda\ [W/cm^2] \cdot 100 \qquad (3.5.A)$$

Monochromatic radiation were obtained from a 35 W halogen lamp coupled with a Pye Unicam SP 600 UV monochromator system. On one hand, spectral irradiance was determined by the incidence of the corresponding monochromatic radiation on a spectrally calibrated photodiode (Hamamatsu S1337-66BQ, 6x6 cm^2). Generated electrical photocurrent was measured and, taking into account the supplied calibration ($I_{photodiode}$ *vs* incident luminous power, [A/W]), spectral irradiance ($E_\lambda = J_{photodiode}$/calibration) was determined. On the other hand, electrical current generated was evaluated in a two-electrode photoelectrochemical cell with a Pt counter electrode (Figure 3.5.1). The studied photoelectrode was impregnated with the electrolyte and an area of 6x7 mm^2 was front-side illuminated with monochromatic radiation. Non-sensitized photoelectrodes were irradiated in 300-400 nm range, while sensitized photoelectrodes were irradiated in the 400-800 nm range. The measured photocurrents ranged from nA to μA and were registered with a Keithley 6487 picoammeter.

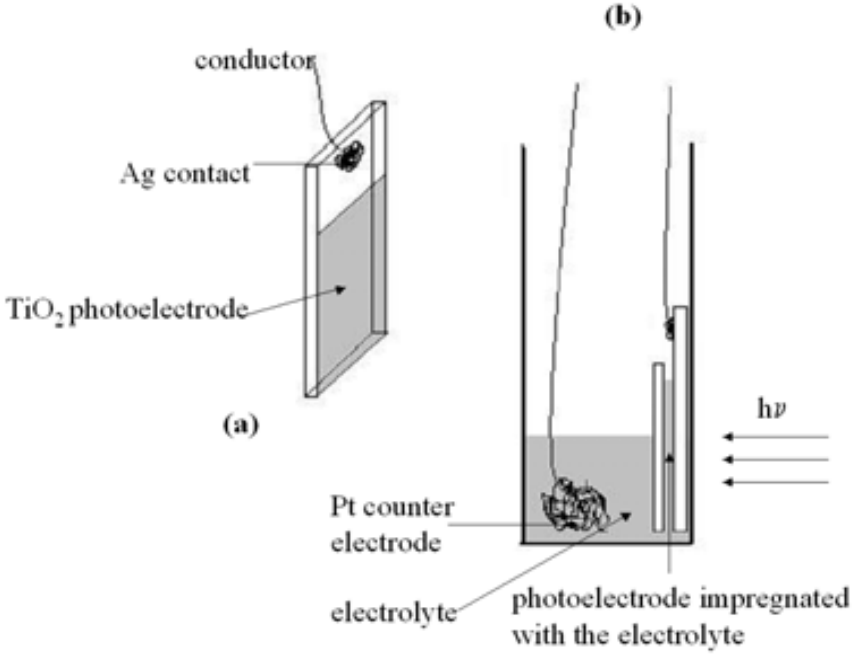

Figure 3.5.1. Two-electrode photoelectrochemical cell used for measuring IPCE: (a) TiO_2 photoelectrode preparation and (b) experimental set-up in a standard quartz cuvette.

3.5.2. GLOBAL CONVERSION EFFICIENCY

Percentage of the incident visible light converted to electricity by the DSSC is defined according to Equation 3.5.B as follows:

$$\eta\ (\%) = J_{SC}\ [mA/cm^2] \cdot V_{OC}\ [V] \cdot FF\ /\ E\ [100\ mW/cm^2] \cdot 100 \qquad (3.5.B)$$

The following two-electrode sandwich solar cell configuration was employed: TiO_2 porous photoelectrode / electrolyte / platinized counter electrode. A TiO_2 porous photoelectrode was fabricated on a 2.5x2.5 cm^2 TCO substrate. Non-resistive electrical contacts were assured by using Cu foil-Sn clad conductive tape with an Ag adhesive (BDF Tesa). The TiO_2 porous photoelectrode was impregnated with the electrolyte and the cell was finally assembled with the platinized counter electrode by using clips of adequate size, placing between the two electrodes an spacer in order to avoid

short-circuit and then a final 1.9 cm^2 active area was thus obtained. Devices were irradiated with UV-visible light from a 50 W halogen lamp with partial UV and IR filtering and the corresponding I-V characteristic curves were registered taking the lectures with multimeters Promax FP-2b. V_{OC} and J_{SC} values were determined in open-circuit and short-circuit conditions, respectively, and the rest of points of the curve were obtained by varying the value of a variable resistance (Bourns 1-5 kΩ) in the external circuit. The distance between the light source and the devices was fixed at 6.6 cm according to the calibrated response of the photodiode, whose value was calibrated at the *Universitat Politècnica de Catalunya* with a standard AM 1.5 sun simulator (Oriol Stanford Corporation 81102, $I_{photodiode\ AM\ 1.5}$=5.27 mA upon E=100 mW/cm^2).

3.6. REFERENCES

[1] Vigil, E.; Saadoun, L.; Ayllón, J.A.; Domènech, X.; Zumeta, I.; Rodríguez-Clemente, R. *Thin Solid Films*. **2000**, *365*, 12-18.

[2] Peiró, A. M.; Peral, J.; Domingo, C.; Domènech, X.; Ayllón, J.A. *Chem. Mater.* **2001**, *13*¸ 2567-2573.

[3] Mills, A.; Le Hunte, S. *J. Photochem. Photobiol. A: Chem.* **1997**, *108*, 1-35.

[4] Ettlinger, M. *Technical Bulletin Pigments. Highly Dispersed Metallic Oxides Produced by the AEROSIL® Process.* No. *56*.

[5] Blesa, M.A. *Eliminación de contaminantes por Fotocatálisis heterogénea.* Programa CYTED. **2001**. ISBN 987-43-3809-1.

[6] Mills, A.; Lee, S.K. *J. Photochem. Photobiol. A: Chem.* **2002**, *152*, 233-247.

[7] Hurum, D.C.; Agrios, A.G.; Gray, K.A.; Rajh, T.; Thurnauer, M.C. *J. Phys. Chem.* **2003**, *107*, 4545-4549.

[8] Nazeeruddin, M.K.; Kay, A.; Rodicio, I.; Humphry-Baker, R.; Müller, E.; Liska, P.; Vlachopoulos, N.; Grätzel, M. *J. Am. Chem. Soc.* **1993**, *115*, 6382-6390.

[9] Smestad, G.P. *Sol. Energ. Mat. Sol. C.* **1998**, *55*, 157-178.

[10] Masuda, Y.; Sugiyama, T.; Koumoto, K. *Chem. Mater.* **2003**, *15*, 2469-2476.

[11] Crison, catalog of pH electrodes: www.crison.es/pdfs/electrodos_pH.pdf.

[12] Serpone, N.; Lawless, D.; Khairutdinov, R. *J. Phys. Chem.* **1995**, *99*, 16646-16654.

[13] Sreemany, M.; Sen, S. *Mater. Chem. Phys.* **2004**, *83*, 169-177.

[14] Buschow, K.H.J.; Cahn, R.W.; Flemings, M.C.; Ilschner, B.; Kramer, E.J.; Mahajan, S. *Encyclopedia of Materials: Science and Technology.* Ed. Elsevier. **2001**. ISBN 0-08-043152-6.

[15] Hammond, C. *The Basics of Crystallography and Diffraction.* International Union of Crystallography, Oxford University Press. New York, **1997**. ISBN 0-19-855966-6.

[16] Pope, C.G. *J. Chem. Educ.* **1997**, *74*, 129-131.

[17] Hovel, H.J. *Semiconductors and semimetals: solar cells.* Academic Press. New York, **1978**. ISBN 0-12-752111-9.

[18] Grätzel, M. *Prog. Photovolt: Res. Appl.* **2006**, *14*, 429-442.

[19] Kamat, P.V. *J. Phys. Chem. C* **2007**, *111*, 2834-2860.

CHAPTER 4:

RESULTS AND DISCUSSION

PART 4.1:

UV PREPARATION METHOD OF TiO_2 POROUS PHOTOELECTRODES FOR DSSCs

Publication 1:

New low-temperature preparation method of the TiO_2 porous photoelectrode for dye-sensitized solar cells using UV irradiation.

J. Photochem. Photobiol. A: Chem. **2005**, *175*, 165-171.

4.1.1. INTRODUCTION

One important goal in the development of DSSCs technology is the fabrication of lightweight and flexible solar cells because of their advantages for transportation of power-supply equipments. New designs and applications such as renewable and mobile power sources for laptops, mobile phones, watches, pocket calculators, *etc.* are expected in the future [1]. Besides, replacing a rigid substrate by a flexible material allows a low-cost fabrication by roll-to-roll mass production [2]. Hence, developing soft, simple and low-temperature preparation methods for TiO_2 porous photoelectrodes is of special interest, in order to apply flexible-device technologies to DSSCs. In this sense, flexible substrates such as ITO (Indium Tin Oxide)-covered PET [3-6] or ITO-covered PEN [1,7] have been proposed.

In the literature, a great variety of methods are described for depositing TiO_2 films from pre-synthesized nanoparticles on conductive substrates, *e.g.* dip-coating [8], drain-coating [9], spin-coating [10], screen printing [1,5,11], inkjet printing [5], spray painting [12,13] or electrophoretic deposition [14-17]. Nevertheless, doctor blading is the most widely employed due to its simplicity and versatility [18,19]. However, these methods habitually need a thermal post-treatment at 450-500ºC for obtaining mechanically stable and electrically connected TiO_2 photoelectrodes (*i.e.* among nanoparticles and between the porous network and the TCO substrate), being the presence of organic residues from the paste formulation and incomplete connection (necking) the key reasons [4]. Obviously, typical flexible plastic substrates cannot withstand conventional sintering processes and electrode processing in a low-temperature range less than 150ºC is required [7].

Up to the end of 2004, at the time of writing Publication 1: **New low-temperature preparation method of the TiO_2 porous photoelectrode for dye-sensitized solar cells using UV irradiation.** *J. Photochem. Photobiol. A: Chem.* **2005**, *175*, 165-171, various processing methods for low-temperature fabrication of DSSCs TiO_2 photoelectrodes had been reported. Representative examples include

low-temperature heating at 100-150ºC for long times [10,20,21], compression at moderate temperatures [2,22,23], hydrothermal crystallization at 100ºC [6], chemical necking [17] and electron beam shower [15]. Researching new strategies in low-temperature preparation of TiO_2 photoelectrodes had been justified since top efficiencies attained under standard simulated sunlight AM 1.5 (100 mW/cm^2) had remained quite low, ranging from 1.2 [20] to 4.2 % [6] for photoelectrodes prepared on FTO-glass rigid substrates.

During the period comprised between 2005 up to present relevant contributions have appeared in the literature. In this way, a brief description of the most relevant contributions is given. Uchida *et al.* described a sintering process induced by 28 GHz microwave irradiation, achieving 2.16% maximum conversion efficiency for all-plastic cells [12]. The combination of different deposition techniques plus compression of the resulting films have shown no significant improvement of global efficiency on FTO electrodes (η=3% approx.) [13,16] with respect to pioneering works of Hadgfeldt *et al.* [2,22,23]. Several authors have obtained 2-3% global efficiency designing approaches for chemical connection of TiO_2 photoelectrodes on rigid electrodes by newly formed TiO_2 [24] or polysiloxane binding [25]. Application of laser-direct write sintering process have been explored but only showed 1.84% efficiency on FTO-glass, in spite of complex instrumentation and high energy consumption requirements [26]. Miyasaka *et al.* have reported acceptable efficiency values of η=5.8% in low-temperature processed flexible DSSCs electrodes by coating binder-free nanocrystalline TiO_2 pastes capable of interparticle connection at 120-150ºC, via dehydration of titania sols [7]. Recently, Meng *et al.* have reported effective ammonia activation process for fabricating ZnO DSSCs on ITO-PET yielding 3.8% conversion efficiency, that is a very promising result taking into account that maximum values for high-temperature sintered ZnO electrodes are 4-5% [27]. So far, Arakawa *et al.* have demonstrated a record conversion efficiency (η=7.4%) in all-plastic DSSCs by pressing a binder-free TiO_2 film composed of different sized nanoparticles, exhibiting light confinement effects [19].

Other authors have developed alternative technologies for continuing with the application of high–temperature sintering processes applicable to flexible substrates in closer works [1,3,28,29]. Grätzel *et al.* have demonstrated high efficiency (η=7.2%) for TiO_2 electrodes on a Ti foil by using a back illumination configuration in all-flexible solar cells [1]. Nelles *et al.* have proposed a lift-off and transfer method of pre-sintered porous layers on Au/glass supporting substrate, resulting in a respectable efficiency on all-plastic devices (η=5.8%) [3], although this procedure may need simplification before practical applications [1]. However, these approaches are a back-step in terms of energy consumption in the fabrication of TiO_2 photoelectrodes. Summarizing, to the best of our knowledge, reaching high conversion efficiency in low-temperature sintered electrodes for flexible DSSCs applications is still a challenge nowadays and the ideal method have not been invented yet.

4.1.2. MAIN RESULTS AND DISCUSSION

A new low-temperature method for sintering TiO_2 P-25 nanoparticles by chemical necking through additional TiO_2 freshly grown was presented in this work. The formation of the connecting agent took place via photocatalytic decomposition of a titania precursor: Titanium(IV) *bis*(ammonium lactato)dihydroxide, TALH (Equation 4.1.A). However, direct photolysis pathway had to be also considered, since high energetic UV irradiation of the light source (*i.e.* λ≤300 nm, see Figure 4.1.1) is capable of giving rise to this phenomena [30].

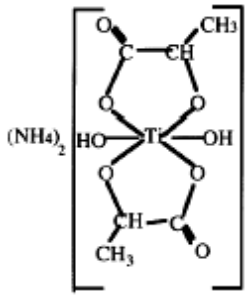

$$+\ O_2 \xrightarrow[E_{hv} \geq E_g]{TiO_2\ P\text{-}25} TiO_2 + \text{decomposition products} \quad (4.1.A)$$

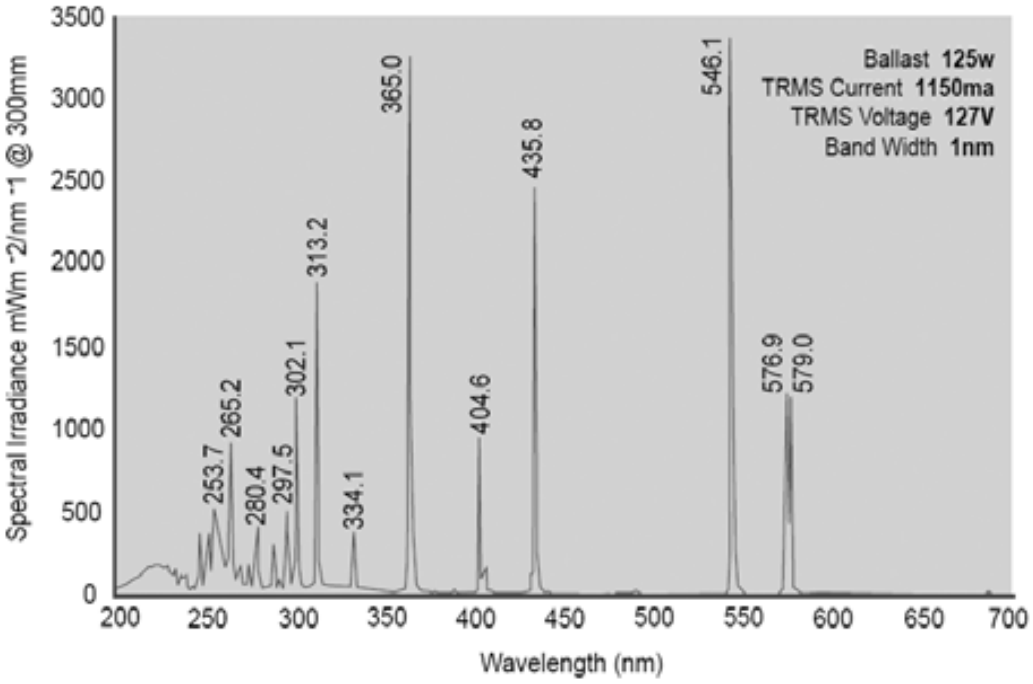

Figure 4.1.1. Spectral emission lines of the medium-pressure Hg UV light source employed in the TiO_2 porous films fabrication process [31].

TiO_2 P-25 presents high photocatalytic activity because of the synergism due to the presence of anatase and rutile crystalline phases, which promotes electron-hole separation inhibiting their recombination [32]. Habitually, P-25 type TiO_2 has been used as reference catalyst in works regarding to heterogeneous photocatalysis [33]. The proposed method took advantage of this high photocatalytic activity of TiO_2 P-25 for the degradation of the titania precursor present in the initial mixed suspension. Thus, additional TiO_2 acted as a cement, capable of providing the required mechanical stability and electrical contact in the photoelectrodes, as is sketched in Figure 4.1.2. A maximum temperature of 80ºC was estimated in the films during the irradiation time and, hence, TiO_2 photoelectrodes on ITO-PET substrates could be prepared following our low-temperature sintering procedure. The UV preparation method agrees with Green Chemistry principles, since it is simple, low-cost, the solvent used is water and energy consumption reasonably low.

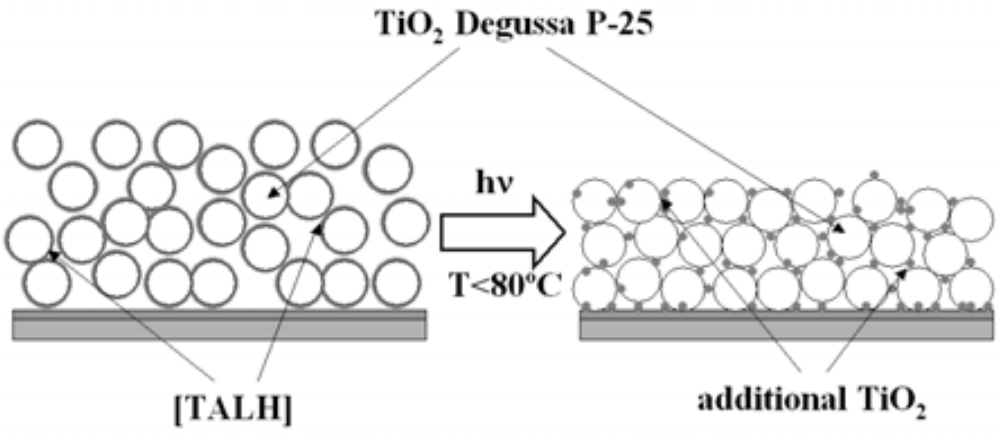

Figure 4.1.2. Schematic representation of the UV sintering process. A maximum temperature of 80ºC was estimated in the films during the irradiation time.

In foregoing investigations, the impregnation with titania precursors plus resintering at 450ºC in order to grow additional TiO_2 in photoelectrodes previously annealed had shown positive effects in the performance of DSSCs. This additional TiO_2 grown among the particles had led to a better interconnection and improved photoinduced charge carrier kinetics [34,35]. Moreover, UV post-treatments had also revealed usefulness as cure treatment for eliminating residual organics in TiO_2 porous films preparation [5,17,36]. However, it must be remarked that, to the best of our knowledge, direct UV degradation of titania precursors to form TiO_2 cement had never been reported.

4.1.2.A. Materials characterization

A qualitative test of homogeneity and adherence of the films (after ultrasound disruption) was used for determining optimal TiO_2 P-25 / TALH ratio in the formulation of the suspension. For this purpose, the concentration of the titania precursor was varied, and samples were prepared under the same experimental conditions ([TiO_2 P-25], [surfactant], protocol of homogenization, irradiation, *etc.*). A TiO_2 P-25 / TALH molar ratio of 7.4 was selected as the optimal value, presenting similar

mechanical stability than samples obtained with a conventional method including an annealing step. Quasi-total elimination of the organic content of the films were demonstrated by means of infrared spectroscopy after irradiating for 6 hours with the medium-pressure Hg UV light source.

Crystalline or amorphous nature of the additional TiO_2 formed after the UV treatment of the doctor bladed coatings could not be discerned. Although no differences between samples before and after UV irradiation were found in terms of X-Ray Diffraction due to the high intensity of the TiO_2 P-25 signals, we believe TiO_2 freshly grown would have probably reproduced the structure of the main crystalline component.

Morphology of both UV treated and conventional high-temperature sintered samples were observed by Scanning Electron Microscopy (SEM). UV preparation method gave rise to samples with a hazy appearance since larger particles and pores were obtained due to the absence of disaggregating agents in the formulation of the initial suspension. On the other hand, in some investigations a second scattering layer of larger particles is added to transparent films in order to increase light harvesting efficiency [19,37-39]. Therefore, the presence of an optimum proportion of large-size light scattering TiO_2 aggregates can be very effective for increasing DSSCs efficiency [19].

Additionally, non-significant differences were obtained in low-temperature photoluminescence spectra of UV processed samples with respect to the thermally sintered ones. Photoluminescence data at low temperature (T=4-15K) have been widely used for detecting presence and identify the nature of defect and impurities in semiconductors [40]. Emissions observed at 550 nm can be ascribed to transitions from donor levels (which are consequence of internal surfaces or boundaries formed by particles necking) to the VB [41-43]. According to photoluminescence spectra, UV procedure gave rise to a similar kind and degree of emissive centers than a conventional sintering process at 450ºC, pointing to similar recombination rates under illumination.

4.1.2.B. DSSCs characterization

In a set of preliminary experiments, the applicability of the UV-prepared photoelectrodes in DSSCs were confirmed by comparing their IPCE with respect to conventional high-temperature annealed electrodes. No differences between both methods, beyond those ascribed to the thickness variability, were obtained for non-sensitized and low-cost sensitized electrodes (anthocyanin dyes extracted from the fruit of *Coriaria Myrtifolia* [44] and the commercial dye 2',7'-dichlorofluorescein [45]).

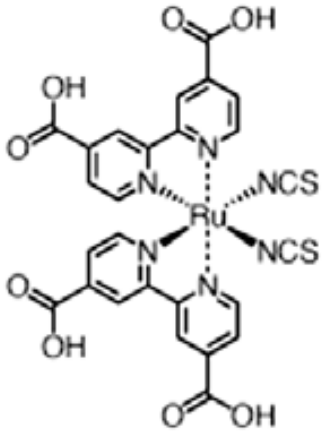

Figure 4.1.3. Structure of *cis*-*bis*(*iso*thiocyanato) *bis*(2,2'-bipyridyl-4,4'-dicarboxylic acid) ruthenium(II) sensitizer, commercially named "N3" or "Ru 535".

In order to report higher conversion efficiencies with respect to values obtained with low-cost sensitizers, IPCE data were finally measured afterwards sensitizing photoelectrodes with an standard N3 Ru(II) dye (Figure 4.1.3). The choice of the N3 dye was justified by the high energy conversion reached (efficient TiO_2 sensitization up to 750 nm) and proven stability of N3-sensitized photoelectrodes [46-48]. Firstly, higher spectral efficiencies were obtained for UV-prepared versus photoelectrodes annealed at 450 ºC on ITO-glass substrates, as was expected, since it is well-known that resistivity of ITO-based substrates is increased during processing at high temperature [6]. This phenomenon did not allow a direct comparison of both methods by means of IPCE. Secondly, adherence and electrical contact in photoelectrodes on flexible ITO-PET was enough for maintaining spectral efficiency in acceptable levels.

Current-voltage response was also evaluated in order to establish a direct comparison between both UV and high-temperature prepared photoelectrodes on FTO-glass substrates. Thus, the conventional method was not penalized for resistivity increasing. FTO shows good stability against conventional thermal treatments and its use has been favored in DSSCs, although ITO substrates present higher availability and lower price [6]. Table 4.1.1 summarizes J_{SC}, V_{OC}, FF, and η typical performance values of DSSCs devices fabricated with electrodes on FTO-glass using both methods and UV-prepared samples on ITO-PET.

Table 4.1.1. Characteristic performance parameters of DSSCs fabricated with TiO_2 porous photoelectrodes prepared by the UV and conventional methods.

Method	Substrate	J_{SC} (mA/cm^2)	V_{OC} (mV)	FF (%)	η (%)
UV, low temperature	FTO-glass	3,95	785	61.5	1.9
Conventional, high temperature	FTO-glass	3,85	769	62.4	1.8
UV, low temperature	ITO-PET	3,80	791	34,3	1.0

Only minimal differences associated to thickness variability were obtained under the same experimental conditions, demonstrating similar performance of UV photoelectrodes against conventional annealed ones. However, obtained J_{SC} and FF values in both cases were lower than those reported in the literature [46,49] and, consequently, global efficiencies only reached 2%, approximately. Firstly, experimental limitations on measuring intensity forced the employment of useful areas approximately 10 times larger than common size of laboratory cells (around 0.2 cm^2) [46,49]. As known, in relative large area photoelectrodes, charge collection decreases because of insufficient substrate conductivity, resulting in noticeably penalized values of current density and fill factor [50-53]. Alternatively, metal current collectors are prepared in DSSCs scaled up to modules, in analogy with conventional silicon solar cells [50,52].

The absolute global efficiency of DSSCs devices is also influenced by series of other parameters such as electrical properties of the TCO substrate, sensitization, electrolyte characteristics or quality of the platinization in the counter electrode [49]. As previously commented, demonstrating that UV approach was suitable for preparing TiO_2 DSSCs electrodes was the main goal of the work, instead of optimizing the absolute global efficiency reached.

DSSCs fabricated employing UV-treated photoelectrodes on ITO-PET presented a drastic reduction of FF (being approximately the half of the value obtained on FTO-glass). These devices presented large series resistance mainly due to both factors the intrinsic high sheet resistance of the plastic substrate and the quality of the ITO/TiO_2 interface contact, favoring for example electron recombination with the electrolyte at the contact. It must be signaled that ITO-PET employed (dated from 2001) presented 60 Ω/□ nominal sheet resistance, clearly higher than TCO-glass (13-18 Ω/□). In fact, the price of ITO-PET substrates with higher conductivities was prohibitive in the past, although plastic substrates with sheet resistance as low as 13 Ω/□ are reasonably accessible nowadays [7]. On the other hand, further factors contributed to the increase of ITO/TiO_2 contact resistance: incomplete necking, the flexible nature of the substrate and the impossibility of substrate cleaning. Concerning this latter, Miyasaka *et al.* have proposed a preliminary ozone/UV cleaning procedure, demonstrating positive effects [7].

Finally, in this work, DSSCs were always assembled using counter electrodes thermally platinized on FTO-glass and, therefore, all-plastic devices were not fabricated. However, it must be pointed that low-temperature alternatives (typically Pt sputtering) exist in the literature [7,54]. Moreover, Pt has also satisfactorily been replaced by other materials such as chemically polymerized *p*-toluensulfonate doped poly(3,4-ethylenedioxythiophene) films [55]. These latter studies focus on the reduction of the cost and the energy consumption in the fabrication of the devices (due to high market price of Pt), also justifying the research carried out.

4.1.3. CONCLUSIONS

The soft method based on the UV decomposition of the TALH titania precursor impregnating the surface of TiO_2 P-25 nanoparticles allows the preparation of mechanically stable and electrically connected TiO_2 porous photoelectrodes at low temperature (<80ºC). Thus, titania photoelectrodes on conductive glass and plastic are satisfactorily fabricated. The method is simple, low-cost, aqueous-based and do not require neither sophisticated equipment nor high energy supply, reasonably fitting Green Chemistry principles.

The resulting chemical necking in TiO_2 P-25 photoelectrodes gives rise to an electrical contact comparable to that generated by conventional sintering procedures at high temperature. In spite of the observed irregular adhesion of the porous layer on the substrate, P-25 nanoparticles seem to be firmly hold together suggesting a good interconnection among them. Finally, the applicability of the UV-processed photoelectrodes in DSSCs has been demonstrated, resulting in devices exhibiting acceptable features.

4.1.4. REFERENCES

[1] Ito, S.; Cevey Ha, N.; Rothenberger, G.; Liska, P.; Comte, P.; Zakeeruddin, S.M.; Péchy, P.; Nazeeruddin, M.K.; Grätzel, M. *Chem. Comm.* **2006**, 4004-4006.

[2] Lindström, H.; Holmberg, A.; Magnusson, E.; Lindquist, S.-E.; Malmqvist, L.; Hagfeldt, A. *Nano Lett.* **2001**, *2*, 97-100.

[3] Dürr, M.; Schmid, A.; Obermaier, M.; Rosselli, S.; Yasuda, A.; Nelles, G. *Nat. Mater.* **2005**, *4*, 607-611.

[4] Zhang, D.; Yoshida, T.; Minoura, H. *Adv. Mater.* **2003**, *15*, 814-817.

[5] Oekermann, T.; Zhang, D.; Yoshida, T.; Minoura, H. *J. Phys. Chem. B* **2004**, *108*, 2227-2235.

[6] Zhang, D.; Yoshida, T.; Furuta, K.; Minoura, H. *J. Photochem. Photobiol. A: Chem.* **2004**, *164*, 159-166.

[7] Kijitori, Y.; Ikegami. M.; Miyasaka, T. *Chem. Lett.* **2007**, *36*, 190-191.

[8] Bosc, F.; Ayral, A.; Albouy, P.A.; Guizard, C. *Chem. Mater.* **2003**, *15*, 2463-2468.

[9] Peiró, A.M.; Peral, J.; Domingo, C.; Domènech, X.; Ayllón, J.A. *Chem. Mater.* **2001**, *13*, 2567-2573.

[10] Ito, S.; Takeuchi, T.; Katayama, T.; Sugiyama, M.; Matsuda, M.; Kitamura, T.; Wada, Y.; Yanagida, S. *Chem. Mater.* **2003**, *15*, 2824-2828.

[11] Dürr, M.; Rosselli, S.; Yasuda, A.; Nelles, G. *J. Phys. Chem. B* **2006**, *110*, 21899-21902.

[12] Uchida, S.; Tomiha, M.; Takizawa, H.; Kawaraya, M. **2004**, *164*, 93-96.

[13] Toivola, M.; Ahlskog, F.; Lund, P. *Sol. Energ. Mat. Sol. C.* **2006**, *90*, 2881-2893.

[14] Peiró, A.M.; Brillas, E.; Peral, J.; Domènech, X.; Ayllón, J.A. *J. Mater. Chem.* **2002**, *12*, 2769-2773.

[15] Miyasaka, T.; Kijitori, Y.; Murakami, T.N.; Kimura, M.; Uegusa, S. *Chem. Lett.* **2002**, 1250-1251.

[16] Yum, J.-H.; Kim, S.-S.; Kim, D.-Y.; Sung, Y.-E. *J. Photochem. Photobiol. A: Chem.* **2005**, *173*, 1-6.

[17] Murakami, T.N.; Kijitori, Y.; Kawashima, N.; Miyasaka, T. *J. Photochem. Photobiol. A: Chem.* **2004**, *164*, 187-191.

[18] Smestad, G.P. *Sol. Energ. Mat. Sol. C.* **1998**, *55*, 157-178.

[19] Yamaguchi, T.; Tobe, N.; Matsumoto, D.; Arakawa, H. *Chem. Commun.* **2007**, 4767-4769.

[20] Pichot, F.; Roland Pitts, J.; Gregg, B.A. *Langmuir* **2000**, *16*, 5626-5630.

[21] Sommeling, P.M.; Späth, M.; Kroon, J.; Kinderman, R.; Van Roosmalen, J. *European Photovoltaic Solar Energy Conference, Proceedings of the International Conference.* Glasgow, UK, May 1-5. **2000**, *1*, 91-101.

[22] Lindström, H.; Holmberg, A.; Magnusson, E.; Malmqvist, L.; Hagfeldt, A. *J. Photochem. Photobiol. A: Chem.* **2001**, *145*, 107-112.

[23] Lindström, H.; Magnusson, E.; Holmberg, A.; Södergren, S.; Lindquist, S.-E.; Hagfeldt, A. *Sol. Energ. Mat. Sol. C.* **2002**, *73*, 91-101.

[24] Du Pasquier, A. *Electrochim. Acta* **2007**, *52*, 7469-7474.

[25] Soeda, k.; Kosugi, D.; Kado, T.; Hayase, S. *Chem. Lett.* **2005**, *34*, 650-651.

[26] Kim, H., Auyeung, R.C.Y.; Ollinger, M.; Kushto, G.P.; Kafafi, Z.H.; Piqué, A. *Appl. Phys. A* **2006**, *83*, 73-76.

[27] Liu, X.; Luo, Y.; Li, H.; Fan, Y.; Yu, Z.; Lin, Y.; Chen, L. Meng, Q. *Chem. Commun.* **2007**, 2847-2849.

[28] Jun, Y.; Kim, J.; Kang, M.G. *Sol. Energ. Mat. Sol. C.* **2007**, *91*, 779-784.

[29] Fan, X.; Wang, F.; Chu, Z.; Chen, Lin.; Zhang, C.; Zou, D. *Appl. Phys. Lett.* **2007**, *90*, 073501.

[30] Mills, A.; Wang, J. *J. Photochem. Photobiol. A: Chem.* **1999**, *127*, 123-134.

[31] Spectral irradiance provided by the supplier: Cathodeon Ltd.
However, this company was acquired in 2005 by Heraeus Noblelight GmbH(Germany): www.heraeus-noblelight.com.

[32] Hurum, D.C.; Agrios, A.G.; Gray, K.A.; Rajh, T.; Thurnauer, M.C. *J. Phys. Chem. B* **2003**, *107*, 4545-4549.

[33] Hoffman, M.R.; Martin, S.T.; Choi, W.; Bahnemann, D.W. *Chem. Rev.* **1995**, *95*, 69-96.

[34] Barbé, C.J.; Arendse, F.; Comte, P.; Jirousek, M.; Lenzmann, F.; Shklover, V.; Grätzel, M. *J. Am. Ceram. Soc.* **1997**, *80*, 3157-3171.

[35] Lin, Y.; Xiao, X.R.; Li, W.B.; Wang, W.B.; Li, X.P.; Cheng, J.Y. *J. Photochem. Photobiol. A: Chem.* **2003**, *159*, 41-45.

[36] Longo, C.; Freitas, J.; De Paoli, M.A. *J. Photochem. Photobiol. A: Chem.* **2003**, *159*, 33-39.

[37] Kubo, W.; Sakamoto, A.; Kitamura, T.; Wada, Y.; Yanagida, S. *J. Photochem. Photobiol. A: Chem.* **2004**, *164*, 33-39.

[38] Dürr, M.; Bamedi, A.; Yasuda, A.; Nelles, G. *Appl. Phys. Lett.* **2004**, *84*, 3397-3399.

[39] Tachibana, Y.; Hara, K.; Sayama, K.; Arakawa, H. *Chem. Mater.* **2002**, *14*, 2527-2535.

[40] Buschow, K.H.J.; Cahn, R.W.; Flemings, M.C.; Ilschner, B.; Kramer, E.J.; Mahajan, S.; *Encyclopedia of Materials: Science and Technology.* Ed. Elsevier. **2001**. ISBN: 0-08-043152-6.

[41] Li, F.B.; Li, X.Z. *Chemosphere* **2002**, *48*, 1103-1111.

[42] Yu, J.C.; Ho, W.; Yu, J.; Hark, S.K.; Iu, K. *Langmuir* **2003**, *19*, 3889-3896.

[43] Toyoda, T.; Hayakawa, T.; Shen, Q. *Mat. Sci. Eng. B* **2000**, *B78*, 84-89.

[44] Cherepy, N.J.; Smestad, G.P.; Grätzel, M.; Zhang, J.Z. *J. Phys. Chem. B.* **1997**, *101*, 9342-9351.

[45] Benkö, G.; Skarman, B.; Wallenberg, R.; Hagfeldt, A.; Sundström, V.; Yartsev, A.P. *J. Phys. Chem. B* **1997**, *107*, 1370-1375.

[46] Nazeeruddin, M.K.; Kay, A.; Rodicio, I.; Humphry-Baker, R.; Müller, E.; Liska, P.; Vlachopoulos, N.; Grätzel, M. *J. Am. Chem. Soc.* **1993**, *115*, 6382-6390.

[47] Kallioinen, J.; Benkö, G.; Myllyperkö, P.; Khriachtchev, L.; Skarman, B.; Wallenberg, R.; Tuomikoski, M.; Korppi-Tommola, J.; Sundström, V.; Yarstev, A.P. *J. Phys. Chem. B* **2004**, *108*, 6365-6373.

[48] Solaronix S.A. (Switzerland): www.solaronix.com.

[49] Grätzel, M. *Nature* **2001,** *414*, 338-344.

[50] Okada, K.; Matsui, H.; Kawashima, T.; Ezure, T.; Tanabe, N. *J. Photochem. Photobiol. A: Chem.* **2004**, *164*, 193-198.

[51] Lee, W.J.; Ramasamy, E.; Lee, D.Y.; Song, J.S. *J. Photochem. Photobiol. A: Chem.* **2006**, *183*, 133-137.

[52] Lee, W.J.; Ramasamy, E.; Lee, D.Y.; Song, J.S. *Sol. Energy Mater. Sol. Cells* **2007**, *91*, 1676-1680.

[53] Dai, S.; Weng, J.; Sui, Y.; Shi, C.; Huang, Y.; Chen, S.; Pan, X.; Fang, X.; Hu, L.; Kong, F.; Wang, K. *Sol. Energy Mater. Sol. Cells* **2004**, *84*, 125-133.

[54] Fang, X.; Ma, T.; Akiyama, M.; Guan, G.; Tsunematsu, S.; Abe, E. *Thin Solid Films* **2005**, *472*, 242-245.

[55] Nakade, S.; Matsuda, M., Kambe, S.; Saito, Y.; Kitamura, T.; Sakata, T.; Wada, Y.; Mori, H.; Yanagida, S. *J. Phys. Chem. B.* **2002**, *106*, 10004-10010.

Available online at www.sciencedirect.com
SCIENCE DIRECT
Journal of Photochemistry and Photobiology A: Chemistry 175 (2005) 165–171
Journal of Photochemistry and Photobiology A:Chemistry
www.elsevier.com/locate/jphotochem

New low-temperature preparation method of the TiO_2 porous photoelectrode for dye-sensitized solar cells using UV irradiation

David Gutiérrez-Tauste [a], Inti Zumeta [b], Elena Vigil [b], Maria Angeles Hernández-Fenollosa [c], Xavier Domènech [a], José A. Ayllón [a,*]

[a] *Departamento de Química, Universidad Autónoma de Barcelona, Campus UAB, Edificio Cn, 08290 Cerdanyola del Valles, Spain*
[b] *Instituto de Materiales, Facultad de Física, Universidad de La Habana, Colina Universitaria, Ciudad Habana 10 400, Cuba*
[c] *Departament de Física Aplicada, Universitat Politècnica de València, E-46071 València, Spain*

Received 20 January 2005; received in revised form 15 April 2005; accepted 25 April 2005
Available online 6 June 2005

Abstract

Thick porous TiO_2 films have been prepared at low temperature from a mixture of a commercial TiO_2 powder (Degussa P25) and an easy-to-handle water-soluble titania precursor: titanium(IV) *bis*(ammonium lactato)dihydroxide. Films have been obtained spreading the mixture using "doctor blade" technique. UV light treatment using a medium-pressure mercury vapor lamp leads to decomposition of the titania precursor as a result of the photocatalytic activity of nanocrystalline TiO_2 present in the blend. The additional titanium oxide thus formed assures both, necking between particles and film adhesion to the substrate. Porous nano-structured TiO_2 films were fabricated by this low-temperature method (always lower than 80 °C) on transparent conducting oxide-covered glass and flexible plastic substrates (indium-tin-oxide on glass and on PET, and fluorine-doped tin oxide on glass). The photoelectrodes obtained by this method have been characterized by scanning electron microscopy, attenuated total reflection Fourier transform infrared spectroscopy, photoluminiscence, monochromatic incident photon-to-current conversion efficiency (IPCE) and *I–V* measurements. Results obtained with dye-sensitized solar cells (DSSC) built with these films are promising.

Keywords: Titanium oxide; Photocatalysis; Dye-sensitized solar cells; Low-temperature film preparation

1. Introduction

Dye-sensitized solar cells (DSSC) based on nano-structured TiO_2 photoelectrodes are intensively studied due to their low cost and promising efficiency values reached so far. At the present time, research pursues the development of this inexpensive solar cell based on a nanocrystalline TiO_2 layer deposited on a flexible plastic substrate [1–2]. This type of substrate allows a continuous-mode production process, which should lower production costs; in addition, it facilitates fabrication of light-weight and thin DSSC [3–5]. Conventional DSSC technology includes an annealing step in which temperatures as high as 400–500 °C are needed. This temperature range, adequate for glass substrates, is above the allowed temperature for possible polymer-based flexible substrates. It must also be mentioned that these temperatures increase the resistivity of the conducting substrate, particularly ITO (In_2O_3:Sn). This has favored the use of conducting SnO_2 glass (FTO) over ITO in DSSC, even though the last one has a greater availability in the market and lower price.

These relatively high temperatures normally used in the annealing step are needed for two key reasons concerning TiO_2 photoelectrodes production. The first one is to eliminate the organic substances present in the colloidal TiO_2 suspension or paste used to make the photoelectrodes. Organics are added to the TiO_2 precursor formulations to improve the quality of the film by breaking down agglomerates, to stabilize TiO_2 suspensions, and to increase the wetting capacity of the precursor mixture. Thus, more regular TiO_2 thick

* Corresponding author. Tel.: +34 935812176; fax: +34 935812920.
E-mail address: joseantonio.ayllon@uab.es (J.A. Ayllón).

1010-6030/$ – see front matter © 2005 Published by Elsevier B.V.
doi:10.1016/j.jphotochem.2005.04.031

films are produced without too large pores or cracks. The second key reason is to improve the connection between the nanocrystallites that constitute the film (necking), as well as, to guarantee their adherence to the transparent conducting oxide (TCO) film acting as substrate. Annealing at high temperatures improves the diffusion coefficient of electrons, and thus the efficiency of DSSC [6,7]. It is to be expected that the quality of these contacts determines both, electrical properties of the porous thick film and also its mechanical sturdiness. Some authors [8,9] have used chemical treatment of TiO_2 porous electrodes, with titania molecular precursor solutions, followed by re-annealing to produce a freshly grown titania. Depositing TiO_2 all over the porous layer should improve the necking of the grains, and it should decrease carrier-trapping defects.

On the other hand, there are reports on TiO_2 film fabrication procedures that are compatible with the use of non-conducting plastic substrates, although the purpose has been to exploit TiO_2 photocatalytic or UV blocking properties [10–18]. However, they produce thin films not suitable for DSSC fabrication due to their thickness and non-porosity. Besides, deposition on TCO-covered substrates poses an extra requirement of no modification of the TCO layer, which limits the experimental conditions to be employed. For example, deposition from solution with extreme pH values is not possible because the conducting layer is damaged.

Different approaches appear in the literature to avoid high-temperature annealing of the thick porous TiO_2 layer. Pichot et al. have studied the performance of electrodes treated at temperatures as low as 100 °C, avoiding the use of organic surfactants in the formulation of the precursor paste, but the performance of the cells thus obtained is limited compared to the annealed ones [19]. A promising alternative to substitute sinterization at high temperature is to compress the particle layers using high pressure during a short time interval. Mechanically stable, electrically conducting, nano-structured porous films are thus obtained [3–5,20]. Recently, a sophisticated method that employs a shower of low-accelerating electron beams has been demonstrated as a further option to cure TiO_2 films [21].

Some authors employ a mixture containing both nanocrystalline TiO_2 and a molecular TiO_2 precursor [22–23]. Under hydrothermal treatment at low temperature (100 °C) in the solid–gas (water vapor) interphase, the molecular precursor hydrolyzes acting as glue. This method has some drawbacks, such as incomplete necking of the particles and presence of residual organics in the film [24]. These organics can be eliminated later using UV/ozone treatment [25]. A different low-temperature method proposed by De Paoli and co-workers [1] takes advantage of the photocatalytic activity of TiO_2 in order to eliminate organic substances present in the commercial TiO_2 colloidal precursor used. TiO_2 thick film fabrication is completed by a heat treatment at 140 °C during 2 h. UV treatment has also been employed by Murakami et al. [26] in order to eliminate adsorbed organic impurities in the TiO_2 obtained using an electrophoretic method and thus improves the efficiency of their DSSC.

In this paper, we propose an alternative method to prepare TiO_2 porous thick films, suitable to work as photoelectrodes in DSSC. It combines photocatalytic activity of TiO_2 with the use of a mixture of nanocrystalline TiO_2 powder and a soluble precursor of TiO_2. This precursor, after photodegradation, will produce new TiO_2 that allows necking between particles and also provides adherence to the substrate. A stable water-soluble titania precursor, titanium(IV) *bis*(ammonium lactato)dihydroxide (TALH), is used to preserve the simplicity of the method.

2. Experimental

2.1. Reagents

All chemicals mentioned hereafter were, at least, of reagent grade and used as received. All water used in the experiments was previously purified in a Millipore Milli-Q system. TiO_2 Degussa P-25 (80% anatase–20% rutile) was kindly gifted by Degussa (Spanish delegation). Titanium(IV) *bis*(ammonium lactato)dihydroxide (Aldrich) was purchased as a 50% aqueous solution and diluted with water prior to its utilization.

2.2. Substrate cleaning

The substrates used were ITO (In_2O_3:Sn)-covered glass 13–18 Ω/sq, 1.1 mm thick optical glass (Opticalfilters UK), F-doped SnO_2-covered glass 15 Ω/sq (Flabeg, Pilkington Group) and poly(ethylene terephthalate) coated with In_2O_3:Sn (PET-ITO, T-MOX 60/175, 60 Ω/sq on 175 μm thick PET)—a sample kindly supplied by Innovative Sputtering Technology N.V. Glass-based substrates were cleaned just before performing the deposition process. Samples of adequate size were subjected to 5-min ultrasonic cleaning first in acetone, then in absolute ethanol, next for 1 min in 30% nitric acid and finally for 5 min in water. After that the substrates were dried under a nitrogen flow. PET-ITO substrates, which do not support this kind of treatment (ITO films are detached from the substrate), were used as received. Maximum precautions were taken to maintain their surface clean.

2.3. TiO_2 porous film preparation

A mixture of TiO_2 Degussa P-25 (2.0 g) and 0.416 M TALH solution (10 mL) were stirred mechanically and then introduced into an ultrasonic bath for 15 min. Then, 0.50 mL of a Tritron X-100 solution in water (1:10) was added and the mixture sonicated for 15 min. Water in the ultrasonic bath was changed periodically to avoid temperature increase. The mixture thus obtained was allowed to stand for a few minutes. With the help of Scotch (3 M) adhesive tape spacers

and microscope slides, the paste was deposited using "doctor blade" technique as was described by Smestad [27]. After the films dried at room temperature, they were irradiated. Films were located at 8 cm from a medium-pressure Hg lamp (125 W, HPK Cathodeon) and no filter was placed between the lamp and the sample. For comparison, reference TiO_2 films were prepared by the conventional procedure described as method B by Nazeeruddin et al. [9].

2.4. TiO_2 films characterization techniques

The composition of TiO_2 films was analyzed by ATR-FTIR performed with a Bruker apparatus (Tensor model equipped with MKII Golden Gate). TiO_2 powder samples were obtained by scrapping off the film and pulverizing the sample in an agate mortar. To test the adhesion of TiO_2 films to the substrate, we used ultrasound disruption: the electrodes were immersed completely in a beaker with water and sonicated for different time intervals (Ultrasonic bath Selecta, 50 W). Surface characteristics of gold-covered films were further investigated by SEM, using a Hitachi S-570 electron microscope. TiO_2 film thickness was studied with SEM. TiO_2 films were easily distinguished from the substrate because of their different roughness. Low-temperature unpolarized photoluminescence (PL) experiments were performed in a backscattering geometry. Samples were placed inside a helium close-cycle cryostat and the 325.2 nm line of a 30 mW He–Cd laser was used. The emitted light was analyzed by a Jobin-Yvon HR460 spectrometer using a GaAs PMT detector optimized for the 350–650 nm range.

2.5. Sensitization of the films and photoelectrochemical measurements

The dye, *cis–bis*(isothiocyanato)*bis*(2,2′-bipyridyl-4,4′-dicarboxylato)ruthenium(II) (Greatcell Solar S.A., Switzerland) commonly named N3, was used as sensitizer. For the purpose of eliminating water in the TiO_2, before sensitization, samples were heated for 1 h near 100 °C (80 °C in the case of ITO-PET samples). They were dipped while still warm, in a 0.5 mM solution of N3 in ethanol for 24 h and subsequently rinsed with ethanol. They were dipped in ethanol to desorb any excess dye. These films were dried in a nitrogen stream before using them as photoelectrodes. Photocurrent action spectra were measured with a Pye Unicam SP 600 UV monochromator system to which a 35 W halogen lamp for sample illumination was added. A Keithley 6487 picoammeter was coupled to this system for photocurrent measurements. For obtaining IPCE values from measured photocurrent, samples were substituted by a spectrally calibrated photodiode to measure incident light intensity at each wavelength. A two-electrode photoelectrochemical cell was used for photocurrent measurements with a Pt counter electrode. Radiation was incident on the TCO side. The redox electrolyte consisted 0.50 M LiI, 0.050 M I_2, and 0.50 mM *tert*-butylpyridine in 3-metoxy-propionitrile.

Photocurrent–voltage measurements were made in a two-electrode sandwich configuration. The active area of the cells was 1.9 cm^2. Counter electrodes were prepared by spreading a drop of 10 mM hexachloroplatinic acid solution in 2-propanol on a SnO_2:F covered glass, followed by heating at 380 °C for 30 min in air [28–29]. A spacer was placed between the two electrodes to avoid short-circuit and the previously mentioned electrolyte was used. Visible light was generated with a 50 W halogen lamp with a UV filter ($\lambda < 325$ nm). In order to decrease the temperature change caused by IR heating, a water filter (3.0 cm optical path length) was used. Lamp distance was adjusted in order to obtain a light intensity of 100 mW/cm^2. *I–V* curves were traced with the help of a simple multimeter and variable resistances.

3. Results and discussion

Our first objective was to define a good TiO_2 precursor suspension, which must contain a mixture of photoactive nanocrystalline TiO_2 and a molecular titania precursor. The first ingredient must supply the necessary photoactivity to decompose the second component, the titania precursor. The additional titanium oxide formed after TALH photodegradation must act as cement and assure electrical connection among particles, as well as, between titania and the substrate. The criteria used to find an optimal formulation was uniformity and adherence of the film obtained after UV treatment. TiO_2 Degussa P-25, easily available and with a high photocatalytic activity was chosen as the crystalline TiO_2 powder component of the mixture. TALH was chosen as titania molecular precursor because it is a stable compound even under open atmosphere and special care must not be taken during its manipulation. Besides, it is commercially available and it allows the use of water as a solvent.

The mass of TiO_2 obtained from the decomposition of the molecular precursor must be enough to assure necking among preformed nanocrystals. On the other hand, the time required for TALH decomposition increases with its concentration in the initial mixture. Besides, TALH could cover the entire catalyst surface if present in a high percentage in the mixture and this probably causes photocatalytic activity decay. Therefore, it seems reasonable that the amount of TiO_2 to be formed from the molecular precursor must be low compared to TiO_2 added as a crystalline powder. After several paste compositions were essayed, the optimized composition found contains 1 mol of TALH per 7.4 mol of TiO_2 present as powder. The qualitative criteria used for this optimization was endurance of the obtained layer with sonication time, i.e., area that remained covered after 10 min in the ultrasonic bath. The TiO_2 powder to precursor molar ratio selected is approximately half the value used by Yoshida and co-workers with their hydrothermal method [24]. A smaller percentage of TALH does not allow the production of stable films. A small amount of Triton X-100 was added to the mixture to facil-

itate substrate wetting and to produce uniform films using "doctor blade" technique. The organic nature of the surfactant allows its elimination after UV activation of photocalytic TiO_2. Ultrasound was used to break as much as possible the large agglomerates usually present in TiO_2 Degussa P-25 aqueous suspensions, and to facilitate the intimate mixture of the three components. It was found that additives normally employed to break TiO_2 aggregates, like acetylacetone, acetic acid, etc., lead to loosely adhered films. Probably, their presence and/or their degradation products avoid or make difficult the adsorption of the titania molecular precursor to the TiO_2 nanocrystallites. Besides, the presence of these substances, which strongly adsorb on the TiO_2 surface, can block activity center and the photodegradation processes [30–31].

The temperature attained in the film during UV irradiation was lower than 80 °C. As no UV filters are used, it must be considered that both direct photolysis and TiO_2-activated photocatalytic degradation are possible pathways for precursor decomposition. It is well known that under TiO_2 irradiation with photon energy higher than its band gap, strong oxidant species are formed that promote the complete mineralization of organic compounds. Different UV treatment times were essayed from 1 to 6 h. ATR-FTIR spectroscopy was used to assess the effect of the UV treatment, using samples representative of the whole film thickness. The reference sample was obtained simply by drying the precursor paste, i.e., prior to irradiation treatment, when all the TALH was still present. In the spectra (Fig. 1), intense peaks assignable to TALH are clearly visible (2983 and 2940 cm^{-1} C–H stretch; 1376 cm^{-1} symmetric stretch carboxylate group, 1114 and 1051 cm^{-1} methyl group skeletal vibration). After only 1 h treatment, their intensity has diminished strongly. Broadening of peaks is to be expected considering that a blend of different degradation products could be formed. The rapid elimination of the organic species could be due to the formation and diffusion of volatile intermediates. Treatment was performed for 6 h to eliminate more refractive compounds responsible of weak signals that remain and require longer treatment (Fig. 1). After this longer treatment, most of the organic substances are eliminated.

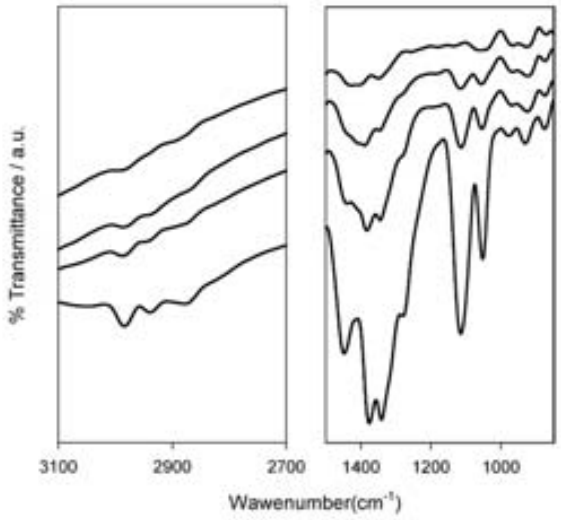

Fig. 1. ATR-FTIR spectra of the TiO_2 film after different times of irradiation (from bottom to top: 0, 1, 2, and 6 h, respectively). Spectra are representative of the whole film thickness composition as samples were obtained pulverizing film portions scrapped from the substrate.

If we consider the low optical transmittance of TiO_2 for λ lower than 385 nm approximately, then the upper layer of the film hinder the illumination of the material below. Nonetheless, the lactate that remains in the deeper layers, where the intensity of incoming radiation is smaller, could also be degraded because oxidizing species are able to diffuse through the pores to deeper regions of the film [32–33].

Films prepared by this new method are more opaque than those prepared by the conventional method, which are translucent. This indicates that bigger aggregates are still present in our method. In the Nazeeruddin's method [9], the use of acetylacetone helps to break the agglomerates present in P-25. As mentioned before, the use of acetylacetone or other disaggregating substances must be avoided in our method because it worsens the adherence of the films produced. SEM analysis (Fig. 2a and b) shows larger aggregates but comparable crystallite dimensions when comparing

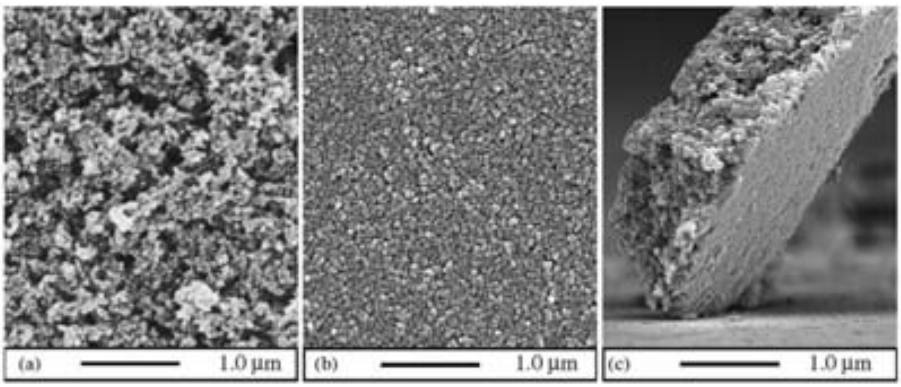

Fig. 2. SEM images of porous TiO_2 films produced by (a) the method reported in the present work, after 6 h. UV light irradiation; (b) sample obtained using Nazeeruddin method B [9]; and (c) small film fragment prepared as in (a) detached from the substrate after ultrasound treatment.

samples prepared by the present technique with samples prepared using acetylacetone for disaggregating TiO_2. The larger aggregates give rise to larger pores, since they do not pack as well as small particles. This should reduce the total real area of the device. In Fig. 2c, the typical thickness of layers obtained is shown—around 12 μm.

Adhesion to the conducting glass substrate was tested studying resistance to sonication. Tests showed that adhesion is irregular, some areas been detached while others remain firmly attached. Although the percentage of area lost after a certain time varies from sample to sample, it was possible to obtain results comparable to those obtained with the conventional method that includes an annealing step. Spots in the TiO_2 film are detached as platelets (see Fig. 2c). This shows that powder nanocrystallites hold firmly together; that a good necking among particles is obtained. It also indicates that the ITO/TiO_2 interface contact is not uniform. The same problem was found in other low-temperature sintered TiO_2 films [19]. The fact that in some areas the adhesion is much better than that in others suggests that an adequate substrate activation or pre-treatment could probably homogenize the firm adhesion of the film to the conducting glass. This aspect is under investigation. It is also possible to deposit films on ITO-PET substrates. In this case, the sonication test is not possible because the ITO layer detaches. It must be stressed, though, that the film does not peel off when the substrate is bent.

The absence of strong IR bands, as well as the fact that the hydroxides and carbonates of titanium are not stable, suggest that TiO_2 has been formed as a final TALH photodegradation byproduct. We have tried XRD to know more about the crystal structure of the generated material. The pattern is dominated by the intense signals due to the nanocrystalline TiO_2 present in the initial mixture (Degussa P-25), which constitutes most of the TiO_2 layer. One tends to think that, as it is to be expected, the deposited materials reproduces the crystalline structure on top of which it grows given the similarity between XRD of the layer obtained with "paint-on" and the one obtained with our method. The presence of a minor XRD-silent component (amorphous phase) could not be completely excluded, though.

Photoluminescence spectra were also used to characterize the TiO_2 films. In Fig. 3, we can see the low-temperature spectra ($T = 15$ K) of a film made from the TiO_2 + TALH mixture before (dashed line) and after the 6 h UV treatment (solid line). For comparison, the spectrum of a film produced by Nazeeruddin method including 450 °C annealing is also showed (dotted line). Considering the same photoluminescent emission, the peak intensity depends on the concentration of other competing non-radiative recombination centers. The lower intensity of the sample prior to UV treatment (about 20% less) is due to the fact that the TiO_2 surface is covered with photodegradable substances, and the recombination process is less probable, i.e., adsorption of the TALH precursor on the crystalline TiO_2 quenches partially their PL [34–35]. The intensity of the PL signal at 550 nm of the sample after the UV treatment is very similar to

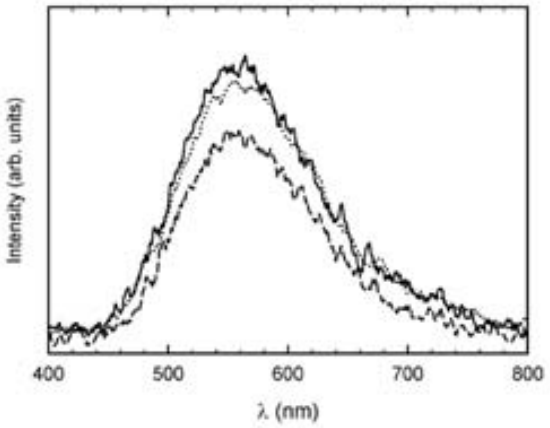

Fig. 3. PL spectra of porous thick TiO_2 films prepared by produced by (a) the method reported in the present work (dashed line) before UV light treatment and (solid line) after 6 h. UV light irradiation; (dotted line) sample obtained using Nazeeruddin's method B [9].

that corresponding to the film prepared by thermal annealing (dotted line). This indicates that defect concentration is very similar in both samples, since non-radiative recombinations are favored at defects, e.g., those due to internal surfaces or boundaries formed by particles necking. Since the shape of the PL emission is the same for different treatments, this indicates that the kind of defects (or emissive centers) responsible of the PL signal has not changed due to the treatment.

The photovoltaic properties of the electrodes obtained by our method were characterized and compared to electrodes made by the more conventional method, which includes annealing at high temperature. First, we measured IPCE of N3-sensitized (Fig. 4) electrodes prepared on ITO-glass sub-

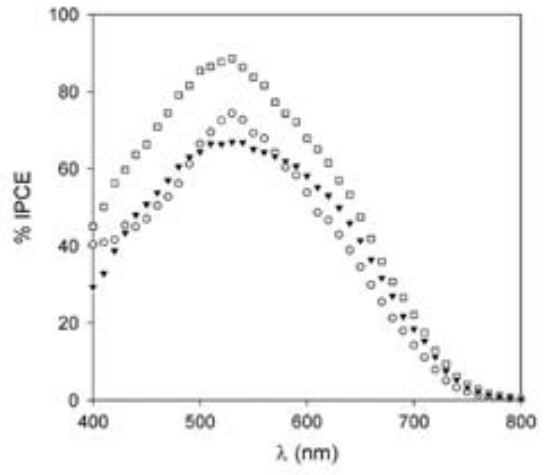

Fig. 4. Dependence of the IPCE values for N3 sensitized TiO_2 electrodes prepared on ITO-glass substrates by our UV-based method (squares); conventional method including annealing at high temperature (open circles), and photoelectrode prepared by our UV-based method on ITO-PET substrate (inverted triangles). The redox electrolyte consisted of 0.50 M LiI, 0.050 M I_2, and 0.50 mM *tert*-butylpyridine in 3-metoxy-propionitrile.

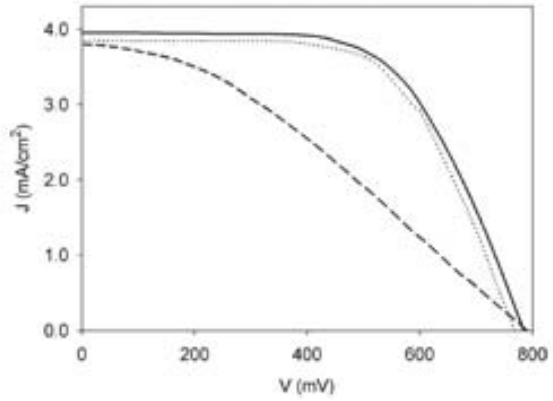

Fig. 5. Current–potential curves for N3-sensitized TiO_2 electrodes prepared on SnO_2:F glass substrates (solid line) by our method; (dotted line) conventional method including annealing at high temperature (dashed line) photoelectrode prepared by our method on ITO-PET substrate. The redox electrolyte consisted of 0.50 M LiI, 0.050 M I_2, and 0.50 mM *tert*-butylpyridine in 3-metoxy-propionitrile. The radiant power is 100 mW/cm^2. For comparative intention, in all the cases the counterelectrode was a platinized SnO_2:F glass substrate.

strates. Results indicate that the photoelectrodes prepared by the TiO_2–TALH mixture method have a satisfactory behavior comparable with electrodes prepared by the traditional method. However, it must be pointed that, since we used ITO based substrates, the traditional method is penalized as the resistivity of this oxide increases during the annealing step.

To facilitate comparison of both methods, photocurrent density (J) versus voltage (V) curves were measured for cells obtained but in this case, SnO_2:F covered glass was used, which maintains its low resistivity with temperature. As can be observed in Fig. 5, very similar results were obtained. It must be said that we have not attempted to optimize the cells contacts and geometry. Our first objective is only to compare the two methods of TiO_2 film preparation; this is why the efficiency of the cell is only around 2% and the fill factor is in the 0.60–0.65 interval. Results corresponding to electrodes prepared at low temperature are slightly better. Poorer results, though, have been obtained with electrodes prepared on plastic substrates. As known, the inverse of the slopes at points where $V = 0$ (short-circuit current I_{sc}) and where $I = 0$ (open-circuit voltage V_{oc}) give the so called, parallel resistance R_p and series resistance R_s, respectively. Ideally, the parallel resistance should be infinitely large and the series resistance 0. Therefore, for the plastic substrate, as seen in Fig. 5, the parallel resistance is too low and the series resistance too high. This must be due to the higher resistivity of the ITO layer on this flexible substrate, which is four times larger than that of the glass substrates as said before. Evidently, higher contact resistance increases series resistance; but also, high contact resistance might lower electron extraction. This could lead to electron recombination with the electrolyte at the contact, which represents a leakage current and decreases parallel resistance. Further studies are required using lower resistivity plastic substrates.

4. Conclusions

A new procedure to the preparation of porous thick TiO_2 photoelectrodes is proposed and studied. Its essence is the use of the photocatalytic properties of nanocrystalline TiO_2 to decompose a molecular titania precursor. The thus produced titania serves to neck previously crystallized TiO_2, as well as to improve TiO_2 porous layer adherence to the TCO. The highest temperature reached with this method is approximately 80 °C; therefore, it is suitable for ITO-covered plastic substrates. The use of an open-atmosphere-stable and water-soluble titania precursor is another clear advantage. A first evaluation of the performance of the films obtained as photoelectrodes for DSSC has given promising results: photoelectrodes obtained using the proposed technique show characteristics equal to or better than those obtained with the traditional method. Good mechanical properties were shown by the films obtained with the new method related to satisfactory necking among nanocrystallites and very strong adhesion in some areas (which could be made uniform for the whole area in the future). These characteristics should also favor electron transport from particle to particle and finally, to the TCO.

Acknowledgements

This work has been financed by the Spanish National Plan of Research (BQU2003-01280 project). Part of the work was conducted thanks to the grant of the Spanish Secretaría de Estado de Educación y Universidades to E. Vigil (SAB2002-0081).

References

[1] C. Longo, J. Freitas, M.-A. De Paoli, J. Photochem. Photobiol. A: Chem. 159 (2003) 33–39.
[2] A.F. Nogueira, C. Longo, M.-A. De Paoli, Coord. Chem. Rev. 248 (2004) 1455–1468.
[3] H. Lindström, E. Magnusson, A. Holmberg, S. Södergren, S.-E. Lindquist, A. Hagfeldt, Sol. Energy Mater. Sol. Cells 73 (2002) 91–101.
[4] H. Lindström, A. Holmberg, E. Magnusson, S.-E. Lindquist, L. Malmqvist, A. Hagfeldt, Nano Lett. 1 (2001) 97–100.
[5] A. Hagfeldt, G. Boschloo, H. Lindström, E. Figgemeier, A. Holmberg, V. Aranyos, E. Magnusson, L. Malmqvist, Coord. Chem. Rev. 248 (2004) 1501–1509.
[6] S. Nakade, M. Matsuda, S. Kambe, Y. Saito, T. Kitamura, T. Sakata, Y. Wada, H. Mori, S. Yanagida, J. Phys. Chem. B 106 (2002) 10004–10010.
[7] K.-J. Kim, K.D. Benkstein, J. van de Lagemaat, A.J. Frank, Chem. Mater. 14 (2002) 1042–1047.
[8] C.J. Barbe, F. Arendse, P. Comte, M. Jirousek, F. Lenzmann, V. Shklover, M. Gratzel, J. Am. Ceram. Soc. 80 (1997) 3157–3171.
[9] M.K. Nazeeruddin, A. Kay, I. Rodicio, R. Humphry-Baker, E. Mueller, P. Liska, N. Vlachopoulos, M. Graetzel, J. Am. Chem. Soc. 115 (1993) 6382–6390.
[10] S. Yamabi, H. Imai, Thin Solid Films 434 (2003) 86–93.

[11] F. Bosc, A. Ayral, P.-A. Albouy, C. Guizard, Chem. Mater. 15 (2003) 2463–2468.
[12] M. Langlet, A. Kim, M. Audier, C. Guillard, J.M. Herrmann, Thin Solid Films 429 (2003) 13–21.
[13] J. Huang, I. Ichinose, T. Kunitake, A. Nakao, Langmuir 18 (2002) 9048–9053.
[14] N. Kaliwoh, J.-Y. Zhang, I.W. Boyd, Surf. Coat. Technol. 125 (2000) 424–427.
[15] K. Shimizu, H. Imai, H. Hirashima, K. Tsukuma, Thin Solid Films 351 (1999) 220–224.
[16] S. Baskaran, L. Song, J. Liu, Y.L. Chen, G.L. Graff, J. Am. Ceram. Soc. 81 (1998) 401–408.
[17] A. Dutschke, C. Diegelmann, P. Löbmann, J. Mater. Chem. 13 (2003) 1058–1063.
[18] Y. Aoi, H. Kambayashi, E. Kamijo, S. Deki, J. Mater. Res. 18 (2003) 2832–2836.
[19] F. Pichot, J.R. Pitts, B.A. Gregg, Langmuir 16 (2000) 5626–5630.
[20] G. Boschloo, H. Lindström, E. Magnusson, A. Holmberg, A. Hagfeldt, J. Photochem. Photobiol. A: Chem. 148 (2002) 11–15.
[21] T. Kado, M. Yamaguchi, Y. Yamada, S. Hayase, Chem. Lett. 32 (2003) 1056–1057.
[22] D. Zhang, T. Yoshida, H. Minoura, Adv. Mater. 15 (2003) 814–817.
[23] R. Gaudiana, J. Macromol. Sci. A39 (2002) 1259–1264.
[24] D. Zhang, T. Yoshida, K. Furuta, H. Minoura, J. Photochem. Photobiol. A: Chem. 164 (2004) 159–166.
[25] T. Oekermann, D. Zhang, T. Yoshida, H. Minoura, J. Phys. Chem. B 108 (2004) 2227–2235.
[26] T.N. Murakami, Y. Kijitori, N. Kawashima, T. Miyasaka, J. Photochem. Photobiol. A: Chem. 164 (2004) 187–191.
[27] G.P. Smestad, Sol. Energy Mater. Sol. Cells 55 (1998) 157–178.
[28] N. Papageorgiou, Coord. Chem. Rev. 248 (2004) 1421–1446.
[29] N.J. Cherepy, G.P. Smestad, M. Grätzel, J.Z. Zhang, J. Phys. Chem. B 101 (1997) 9342–9351.
[30] R. Morand, K. Noworyta, J. Augustynski, Chem. Phys. Lett. 364 (2002) 244–250.
[31] S.T. Martin, J.M. Kesselman, D.S. Park, N.S. Lewis, M.R. Hoffmann, Environ. Sci. Technol. 30 (1996) 2535–2542.
[32] W. Kubo, T. Tatsuma, A. Fujishima, H. Kobayashi, J. Phys. Chem. B 108 (2004) 3005–3009.
[33] S.-K. Lee, S. McIntyre, A. Mills, J. Photochem. Photobiol. A: Chem. 162 (2004) 203–206.
[34] F.B. Li, X.Z. Li, Chemosphere 48 (2002) 1103–1111.
[35] J.C. Yu, W. Ho, J. Yu, S.K. Hark, K. Iu, Langmuir 19 (2003) 3889–3896.

PART 4.2:

ALTERNATIVE FLUORIDE SCAVENGERS FOR TiO_2 LPD

Publication 2:

Alternative fluoride scavengers to produce TiO_2 films by the liquid phase deposition (LPD) technique.

J. Mater. Chem. **2006**, *16*, 2249-2255.

4.2.1. INTRODUCTION

As commented, hexafluoro titanium(IV) aqueous solutions are stable over months due to the strong coordination of the ligand fluoro, whereas common titania precursors are quickly hydrolyzed in aqueous media [1,2]. However, such fluoro-complexes can be destabilized by means of a defluorinating agent (Equations 1.7.B and 1.7.C) [3,4]. In spite of Liquid Phase Deposition is becoming a consolidated wet-chemistry methodology for metal oxide deposition at low temperature, the nature of the fluoride scavenger has received little attention, although the defluorinating agent plays a key role in the deposition process. *A priori*, any substance with enough affinity for being coordinated by free fluoride anions is a suitable candidate. In fact, alternatives in the use of boric acid as fluoride scavenger (the commonly used) are poorly described in the literature.

On one hand, there are a few reports dealing with the preparation of titania nano-hole arrays by employing nano-structurated anodic alumina as fluoride scavenger (Equation 4.2.A) [5-8]. However, anodic alumina additionally acts as template in this strategy, which is not versatile for coating other substrates.

$$Al_2O_3(s) + 12\ HF(aq) \longrightarrow 2\ H_3AlF_6(aq) + 3\ H_2O \qquad (4.2.A)$$

On the other hand, although aluminum metal had also been proposed as fluoride scavenger in the past by some authors [6,9,10], practical applications of this metal seem to have been discouraged by two major reasons. The redox reaction between Al(s) and HF(aq) (Equation 4.2.B) gives rise to the production of $H_2(g)$, which in combination with solid particles of the scavenger induces heterogeneity in the deposition medium. Consequently, this heterogeneity makes difficult the correct coating of the substrate with the corresponding metal oxide and, deposition medium should be pumped through an additional vessel where Al(s) is compartmentalized [11].

$$Al(s) + 6\ HF\ (aq) \longrightarrow H_3AlF_6(aq) + 3/2\ H_2(g) \qquad (4.2.B)$$

In the paper **Alternative fluoride scavengers to produce TiO_2 films by the liquid phase deposition (LPD) technique.** *J. Mater. Chem.* **2006**, *16*, 2249-2255, trivalent Al(III) and Fe(III) cations were proposed as defluorinating agents others than boric acid (Equations 4.2.C and 4.2.D). In this work, for the first time, the viability of Al(III) nitrate and Fe(III) chloride salts as fluoride scavengers for TiO_2 LPD was studied and compared with respect to boric acid.

$$Al^{3+}(aq) + 6\,HF\,(aq) \longrightarrow [AlF_6]^{3-}(aq) + 6\,H^{+}(aq) \qquad (4.2.C)$$

$$Fe^{3+}(aq) + 5\,HF\,(aq) \longrightarrow [FeF_5]^{2-}(aq) + 5\,H^{+}(aq) \qquad (4.2.D)$$

4.2.2. MAIN RESULTS AND DISCUSSION

Table 4.2.1 compiles the successive formation constants of $[AlF_n]^{(3-n)}$, $[FeF_n]^{(3-n)}$ and $[TiF_n]^{(4-n)}$ complexes (where *n* refers to the number of fluoro ligands), according to values extracted from the literature [12-14]. The stability of Al(III) and Fe(III) coordination complexes with the fluoro ligand is orders of magnitude larger than those for the analogous complexes with Ti(IV). Additionally, each β_n of $[AlF_n]^{(3-n)}$ complexes are approximately one order of magnitude higher than those for $[FeF_n]^{(3-n)}$. Hence, these thermodynamic constants suggested the choice of these trivalent cations as candidates for alternative fluoride scavengers.

Table 4.2.1. Successive formation constants of $[AlF_n]^{(3-n)}$, $[FeF_n]^{(3-n)}$ and $[TiF_n]^{(4-n)}$ complexes at 298 K [12-14].

Cation	Log β_1	Log β_2	Log β_3	Log β_4	Log β_5	Log β_6
Al(III)	6.1	11.1	14.9	17.6	19.2	19.7
Fe(III)	5.5	9.7	12.7	14.9	15.4	-
Ti(IV)	6.0	2.2	3.2	4.0	13.0	2.3

4.2.2.A. TiO_2 deposition on glass

Composition, concentrations and temperature of the deposition bath determine the final properties of deposits obtained by means of LPD [15]. Temperature and $(NH_4)_2TiF_6$ precursor concentration were fixed at 80ºC and 10 mM, respectively. Series of preliminary experiments were carried out in order to establish optimized Ti:scavenger molar ratios and deposition times for being systematically used in the rest of the experiments. Optimal conditions were chosen in base of a primary characterization of the obtained deposits: visual observations of adherence (after ultrasound disruption), macroscopic appearance and, in some cases, X-Ray Diffraction. Al(III) and Fe(III) concentrations of 5, 10, 20 and 30 mM in combination with deposition times of 2, 3, 4.5 and 7.5 h were tested. As a result of these previous experiments, the following optimized LPD conditions were adopted: (i) Ti: scavenger stoichiometric ratio 1:1 and 1:2 for Fe(III) and 1:1 for Al(III); and (ii) deposition time of 3 h. The pHs of the deposition baths were unmodified, being in the usual 1.5-3 range [16-18]. For comparison purposes, TiO_2 films were obtained under the same experimental conditions but employing a $Ti:H_3BO_3$ molar ratio of 1:3, and adjusting the pH of the medium to 2.8.

Macroscopic observations of TiO_2 films deposited on bare glass revealed a hazy appearance. As shown SEM photographs, low nucleation density on this substrate resulted in the growth of TiO_2 forming sub-micrometric hemispherical deposits instead of a continuous coverage. The chemical nature of the fluoride scavenger determined the nucleation sites available. The growth rate of TiO_2 coatings was estimated as an average, taking into consideration the radius of the hemispherical deposits and deposition time. Radial growth rate for Al(III) became the largest (in agreement with the highest thermodynamic stability of $[AlF_n]^{(3-n)}$ complexes, see Table 4.2.1), almost doubling the corresponding rate of boric acid.

It was totally necessary to find a manner to increase the nucleation sites density in order to obtain more regular coatings. Thus, bare glass substrates were pretreated (30 min, 80ºC) in a 0.1 M aqueous solution of H_2TiF_6 partially neutralized with NH_3.

Hydrofluoric acid (pK_a=3.2) in equilibrium concentration with H_2TiF_6 corrodes glass, most probably yielding tiny $Ti_{1-x}Si_xO_2$ deposits on the surface of the processed substrate (Equation 4.2.E) [19-21]. This freshly-formed seed layer served as initial growth points for titania and allowed the desired deposition of well-adhered, transparent, uniform and compact sub-micrometric coatings on the glass in the posterior LPD process.

$$SiO_2(s) + 6\,HF(aq) \longrightarrow [SiF_6]^{2-}(aq) + 2\,H_3O^+ \qquad (4.2.E)$$

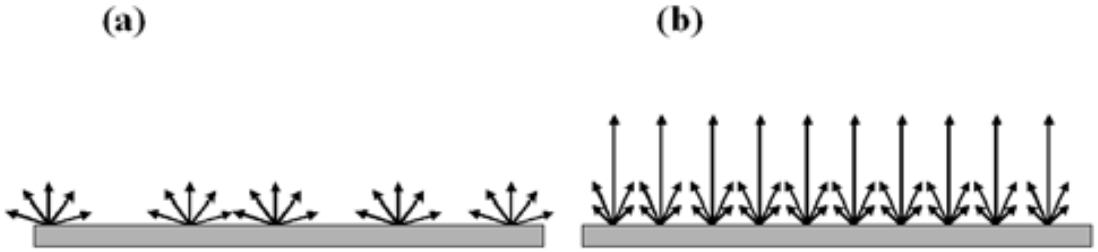

Figure 4.2.1 Schematic representation of the growth mechanism of TiO_2 LPD (the black arrows represent the *c* axis preferential growth of the anatase crystallites): (a) LPD process on bare glass, growth of isolated hemispherical deposits consisting of elongated and twinned crystals; (b) LPD process on a seed layer in a pretreated glass, high degree of coalescence among crystallites of closer aggregates and preferential orientation with the *c* axis direction perpendicular to the substrate surface.

SEM and UV-Vis transmittance spectra of the films prepared by the two-step procedure stated the positive effect of the pretreatment in terms of total surface coverage and transparency, respectively. Grazing angle XRD confirmed as-deposited films on bare glass were partially crystalline in the form of anatase phase and, evidenced typical LPD preferential growth along the *c* axis direction, due to stronger fluoride coordination in perpendicular crystal faces [22,23]. It should be remarked here again that in order to obtain coatings crystalline enough, long deposition times (up to days) at lower temperatures [3,4,9,24] or posterior annealing steps are required [20]. Besides, samples deposited on a seed layer exhibited a preferential orientation of the TiO_2 nanocrystallites perpendicular to the substrate surface, as a consequence of a majority degree of coalescence of the elongated crystallites when high nucleation sites

density is available. The thicker coatings (prepared using Al(III) as scavenger), showed this effect more pronounced. Proposed growth mechanisms of TiO_2 LPD on bare glass (a) and on pretreated glass (b) are sketched in Figure 4.2.1.

4.2.2.B. TiO_2 deposition on ITO-glass

The crystalline coating of the ITO-glass TCO substrate favored in this case the LPD process, acting as nucleation layer for TiO_2 deposition due to a similar nature between both metal oxides. Therefore, regular and well-adhered films were obtained on ITO-glass with no pretreatment. However, a short (30 min) LPD pretreatment employing the same conditions of the second LPD process were tested but transparency and uniformity of the samples became worse. It must be pointed this LPD seed process was adopted because, as observed experimentally, hexafluorotitanic pretreatment used for glass substrates increased the resistivity of ITO-glass. Figure 4.2.2 pretends to give an idea of the macroscopic appearance of the samples, showing photographs of the coatings prepared on glass and ITO-glass substrate with and without the tested pretreatments in each case.

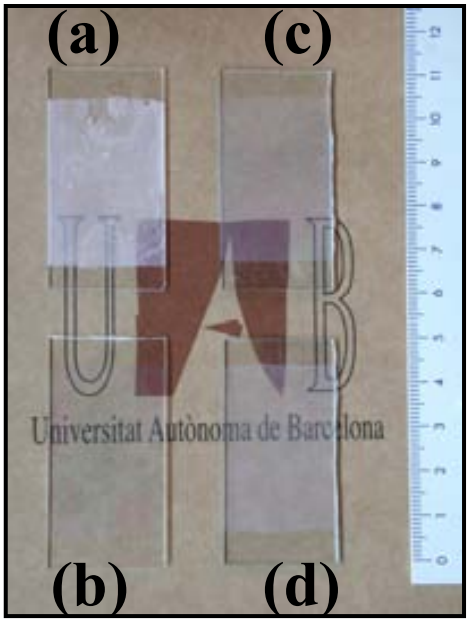

Figure 4.2.2. Photograph of TiO_2 films deposited by LPD employing Al(III) as fluoride scavenger: (a) on bare glass, (b) on glass H_2TiF_6-pretreated, (c) on bare ITO-glass and (d) on LPD-pretreated ITO-glass.

Although XRD signals of TiO_2 coatings were partially masked by ITO peaks, preferential orientation of crystallites was also observed in samples deposited on the conductive substrate, also being more intense for the thicker films (prepared using Al(III)).

An evaluation of the composition was required in order to analyze the content of both Al(III) and Fe(III) cations in the deposited materials. Two facts had already pointed towards the incorporation of iron in samples prepared using this cation: (i) yellow coloration and light absorption shifted to the visible zone, and (ii) inhibition of thermally induced crystal growth due to partial segregation of iron(III) oxide clusters. XPS analysis of samples deposited on ITO-glass confirmed a significant amount of iron, mainly inside the coatings (Ti/Fe atomic ratio around 3). In this case, most probably a $Fe_xTi_{1-x}O_{2-x/2}$ solid solution was formed and, iron oxide segregation observed after annealing can be ascribed to a lower solubility of this compound in the anatase phase rather than in the initial amorphous matrix [25]. On the other hand, Al(III) did not seem to be incorporated during TiO_2 LPD, being its level lower than the detection limit of the employed instrumental (*i.e.* 0.5 at.% approximately). A significant fluoride contamination was also found, although in atomic percentages similar to those previously reported by using boric acid as fluoride scavenger [4,20,22].

4.2.3. CONCLUSIONS

Al(III) and Fe(III) cations allow an efficient fluoride scavenging process for destabilizing fluoro-complexes of titanium(IV). Partially crystalline TiO_2 anatase is deposited by LPD in a relative short time (3 h) at low temperature (80ºC), although major average deposition rate is obtained for Al(III) cation. Whereas Fe(III) as fluoride scavenger yields a final material in which this metal is incorporated in high degree, aluminum content in the deposited samples was not detectable by means of XPS.

Under the experimental conditions studied, the LPD process only allows an incomplete surface coverage on common glass in form of isolated hemispherical deposits consisting of elongated and twinned crystals and, consequently, exhibiting a hazy appearance. On the other hand, the coating of ITO-glass surface is continuous, since structural similarities between both metal oxides favor LPD nucleation. The pretreatment of the glass substrate with H_2TiF_6 allows the creation of a seed layer with high nucleation sites density. In a posterior LPD process, total and homogeneous surface coating with a preferential orientation of TiO_2 nanocrystallites is reached, exhibiting an acceptable transparency.

4.2.4. REFERENCES

[1] Niessen, T.P.; De Guire, M.R. *Solid State Ionics* **2002**, *151*, 61-68.

[2] Gutiérrez-Tauste, D.; Domènech, X.; Hernández-Fenollosa, M.A.; Ayllón, J.A. *J. Mater. Chem.* **2006**, *16*, 2249-2255.

[3] Deki, S.; Aoi, Y.; Hiroi, O.; Kajinami, A. *Chem. Lett.* **1996**, *6*, 433.

[4] Kishimoto, H.; Takahama, K.; Hashimoto, N.; Aoi, Y.; Deki, S. *J. Mater. Chem.* **1998**, *8*, 2019-2024.

[5] Imai, H.; Takei, Y.; Shimizu, K.; Matsuda, M.; Hirashima, H. *J. Mater. Chem.* **1999**, *9*, 2971-2972.

[6] Yamanaka, S.; Hamaguchi, T.; Muta, H.; Kurosaki, K.; Uno, M. *J. Alloys Compd.* **2004**, *373*, 312-315.

[7] Hamaguchi, T.; Uno, M.; Yamanaka, S. *J. Photochem. Photobiol. A: Chem.* **2005**, *173*, 99-105.

[8] Cochran, R.E.; Shyue, J.J.; Padture, N.P. *Acta Mater.* **2007**, *55*, 3007-3014.

[9] Deki, S.; Aoi, Y.; Asaoka, Y. Kajinami, A.; Mizuhata, M. *J. Mater. Chem.* **1997**, *7*, 733-736.

[10] Deki, S.; Aoi, Y.; Okibe, J.; Yanagimoto, H.; Kajinami, A.; Mizuhata, M. *J. Mater. Chem.* **1997**, *7*, 1769-1772.

[11] Sakai, Y.; Norimatsu, H.; Saito, Y.; Inomata, H.; Mizuno, T. *Thin Solid Films* **2001**, *392*, 294-298.

[12] Burriel, L.; Lucena, F., Arribas, S.; Hernández, J. *Química Analítica Cualitativa.* 16th edition. Ed. Paraninfo. Madrid, **2001**. ISBN 84-9732-140-5.

[13] Martín, R.B. *Coord. Chem. Rev.* **1996**,*141*, 23-32.

[14] Serre, C.; Corbière, T.; Lorentz, C.; Taubelle, F.; Férey, G. *Chem. Mater.* **2002**, *14*, 4939-4947.

[15] Pizem, H.; Sukenik, C.N.; Sampathkumaran, U.; McIlwain, A.K.; De Guire, M. *Chem. Mater.* **2002**, *14*, 2476-2485.

[16] Pizem, H.; Sukenik, C.N. *Chem. Mater.* **2002**, *14*, 2476-2485.

[17] Masuda, Y.; Sugiyama, T.; Seo, W.S.; Koumoto, K. *Chem. Mater.* **2003**, *15*, 2469-2476.

[18] Masuda, Y.; Ieda, S.; Koumoto, K. *Langmuir* **2003**, *19*, 4415-4419.

[19] Lee, M.K.; Lei, B.H. *Jpn. J. Appl. Phys.* **2000**, *39*, L101-L103.

[20] Yu, J.G.; Yu, H.G.; Cheng, B; Zhao, X.J.; Yu, J.C.; Ho, W.K. *J. Phys. Chem. B* **2004**, *107*, 13871-13879.

[21] Rayner-Canham, G. *Descriptive Inorganic Chemistry.* 2nd edition. Ed. W. H. Freeman and Company. New York, **2000**. ISBN 0-7167-3553-9.

[22] Ayllón, J.A.; Peiró, A.M.; Saadoun, L.; Vigil, E.; Domènech, X.; Peral, J. *J. Mater. Chem.* **2000**, *10*, 1911-1914.

[23] Peiró, A.M.; Brillas, E.; Peral, J.; Domènech, X.; Ayllón, J.A. *J. Mater. Chem.* **2002**, *12*, 2769-2773.

[24] Koumoto, K.; Seo, S.; Sugiyama, T.; Seo, W.S. *Chem. Mater.* **1999,** *11*, 2305-2309.

[25] Gracia, F.; Holgado, J.P.; Caballero, A.; Gonzalez-Elipe, A.R. *J. Phys. Chem. B* **2004**, *108*, 17466-17476.

PAPER www.rsc.org/materials | Journal of Materials Chemistry

Alternative fluoride scavengers to produce TiO_2 films by the liquid phase deposition (LPD) technique

David Gutiérrez-Tauste,[a] Xavier Domènech,[a] Maria Angeles Hernández-Fenollosa[b] and José A. Ayllón*[a]

Received 28th October 2005, Accepted 15th March 2006
First published as an Advance Article on the web 12th April 2006
DOI: 10.1039/b515367k

TiO_2 films have been deposited on bare glass and on glass coated with indium tin oxide (ITO) by the liquid phase deposition (LPD) method, using Al(III) nitrate and Fe(III) chloride as alternative fluoride scavengers. Films were characterized by grazing angle X-ray diffraction, scanning electron microscopy, UV-vis spectra, X-ray photoelectron spectroscopy and photoluminescence. Results are compared with those obtained using boric acid, which is commonly used as a scavenger in the LPD technique. Well adhered films, 250–450 nm thick, were obtained after 3 h of deposition process at 80 °C (353 K). While Al(III) is not significantly incorporated on the film, in the case of Fe(III) considerable incorporation of this element is observed. When Al(III) nitrate is used as a scavenger instead of boric acid, the deposition rate is nearly doubled. Furthermore, the effect of the substrate on the TiO_2 crystal growth has been addressed. On bare glass, the low number of nucleation sites, slightly influenced by the scavenger nature, causes a partial coverage of the substrate. Glass pretreatment for 30 min with a H_2TiF_6 aqueous solution at 80 °C noticeably increases the nucleation site density, leading to continuous transparent film deposition. Coherent films were deposited on ITO surfaces as this substrate favors the nucleation of TiO_2.

1 Introduction

Titanium dioxide based materials have gained much attention due to the application of these materials in fields as diverse as photocatalysis,[1,2] dye sensitized solar cells,[3,4] superhydrophilic self-cleaning surfaces,[5] UV protection films,[6] and deposition of inorganic micropattern on flexible substrates.[7] Development of soft-solution methods that provide low-cost routes to synthesize dense and well-adhered titanium dioxide films for different applications is nowadays gaining much attention. Low temperature deposition techniques for TiO_2, not requiring high temperature annealing post-treatments, are particularly interesting because material deposition on thermolabile substrates is necessary to fabricate dye sensitized solar cells or electrochromic devices on flexible substrates or to deposit photoactive catalyst on light support as fibers or plastics.[8] Liquid phase deposition (LPD) is a process based on the controlled hydrolysis of metallic fluoro-complexes and has been developed as a low temperature route to obtain several oxide films, including TiO_2.[9] LPD processes conform with the green chemistry principles because it functions at low temperatures, uses low-cost and low energy-spending equipment and water as a solvent.

While common titania precursors like alcoxides or $TiCl_4$ are readily hydrolyzed even with traces of water, the great affinity of fluoride to titanium(IV), allows its stabilization in aqueous solution in the form of fluoro-complexes like hexafluorotitanate. However, dynamic equilibrium exchange between fluoro and water ligands is established. This equilibrium is displaced towards the more hydrated species in the presence of a fluoride scavenger; these species are unstable and evolve to titanium oxide as final product. The global process, which is slow at ambient temperature, can be accelerated by increasing the deposition temperature. Boric acid, which reacts with fluoride in several steps to yield BF_4^-, is the fluoride scavenger commonly used. The key reactions can be expressed as follows:

$$TiF_6^{2-}(aq) + 2\,H_2O \rightleftharpoons TiO_2(s) + 4\,HF(aq) + 2\,F^-(aq)$$

$$H_3BO_3(aq) + 4\,HF(aq) \rightarrow BF_4^-(aq) + 3\,H_2O(l) + H^+(aq)$$

LPD of TiO_2 is performed usually in the 25–50 °C temperature range.[10–13] These low temperatures allow TiO_2 deposition on thermolabile substrates like organic polymers.[14–16] Organic-polymer-core TiO_2-shell composite particles and TiO_2 hollow spheres have been also fabricated using LPD.[17–18] While wet deposition methods usually require a thermal post-treatment in order to induce crystallization of the deposited material and/or eliminate organics, films obtained by LPD can be at least partially crystalline depending on the precursor concentration, initial pH, temperature and surface characteristics.[19–20] Moreover, deposition rate and crystal orientation can be controlled by an appropriate choice of experimental parameters.[20] Using microwave irradiation to activate the precursor solution, highly crystalline materials have been obtained; the temperature of the process remains relatively low, being limited to the boiling temperature of the precursor solution to aprox. 100 °C in bath processes[21] and below 50 °C if a flowing precursor solution is employed.[22]

TiO_2 films prepared by LPD have shown their usefulness in the most attractive TiO_2 films applications: as

[a]*Departament de Química, Universitat Autònoma de Barcelona, 08290 Cerdanyola del Vallès, Spain. E-mail: JoseAntonio.Ayllon@uab.es; Fax: 34 93581 2919; Tel: 34 935812176*
[b]*Departament de Física Aplicada, Universitat Politècnica de València, E-46071 València, Spain*

photocatalyst,[12,23] as superhydrophilic surface[24,25] or as electrode in photovoltaic devices.[26,27] The great versatility of LPD has allowed its use in TiO_2 patterning at the micro and nano scale.[7,13,19,28–33] Moreover, LPD has recently been used to develop a L-glutamic acid sensor based on a molecularly imprinted TiO_2 film.[34]

For any oxide materials deposition technology a good understanding and control of film growth is desirable.[35] After the pioneering work by Deki *et al.*,[10–12] the effects of pH and substrate surface modification by self-assembled monolayers on the TiO_2 deposition by LPD have been studied by other authors.[13,20,28,36–37] The use of fluoride scavengers others than boric acid has received little attention. Aluminium is an alternative scavenger; however, two facts discourages its use: it is a solid insoluble reagent, and it introduces heterogeneous conditions in the bath, and hydrogen gas is obtained as a by-product. Recently, the use of nanostructured anodic alumina as a solid scavenger has allowed the preparation of titania nano-hole arrays.[38–39] On the other hand, there are many metallic cations, stable in the aqueous acid medium used in LPD, that form strong fluoro-complexes and thus will consume the free fluoride anions present in solution. These complexes are soluble and as such will not interfere with the deposition process. Consequently, these cations can be envisaged as alternative soluble fluoride scavengers. Furthermore, it is expected that the chemical nature of the fluoride scavenger will have an influence on the characteristics of the TiO_2 films produced by LPD. In this work, the use of soluble salts of Al(III) or Fe(III) as alternative fluoride scavengers has been studied and films produced have been compared with those obtained using boric acid. A deposition temperature of 80 °C and a relatively dilute precursor solution were used in order to favor the crystallinity of the film as well as to reduce the amount of precursor lost due to homogeneous precipitation.

2 Experimental

2.1 Reagents

Ammonium hexafluorotitanate (AHFT, Aldrich), aluminum(III) nitrate (Fluka), iron(III) chloride (Aldrich), boric acid (Panreac) and hexafluorotitanic acid (Aldrich) were used as received. Water purified with a Milli-Q (Millipore) system (conductivity $< 0.05\ \mu S\ cm^{-1}$) was employed both in solution preparation and cleaning procedures. Analytical grade acetone and ethanol (Panreac) were also used for substrate cleaning.

2.2 Substrates

The substrates used were ITO (In_2O_3 : Sn) conducting glass 13–18 Ω square^{-1}, 1.1 mm thick (Optical Filters) and bare glass (microscope slides IDL, Germany). Substrates were cleaned just before performing the deposition process. Glass slides were successively immersed for 15 min in boiling 50% sulfuric acid and 15 min in boiling water, followed by 5 min ultrasonic cleaning in acetone, then absolute ethanol and finally water. ITO-glass substrates were subjected to 5 min ultrasonic cleaning in acetone, then in absolute ethanol, then in 30% nitric acid for 1 min and finally in water for 5 more min.

2.3 Deposition of TiO_2 films

Bath solutions were prepared by mixing new AHFT solutions with fresh solutions of the different compounds used as fluoride scavenger: boric acid, Al(III) nitrate or Fe(III) chloride. Several compositions of the chemical bath were essayed; their compositions, stoichiometric relations between titanium and scavenger and initial pHs are summarized in Table 1. Each bath composition has been denoted according to the nomenclature "<TiO_2/scavenger>" (first column in Table 1). When boric acid is used, the pH of the precursor solution was adjusted to 2.8 with diluted $HClO_4$. Substrates were placed vertically into a polyethylene vessel containing the precursor solution and the whole system was kept at 80 °C during the deposition process. After deposition the films were gently washed with water and dried in a nitrogen gas flow.

In additional experiments, the substrate (bare glass slide) was pretreated in a 0.10 M H_2TiF_6 solution, with the pH adjusted to 3.2 using diluted NH_3, at 80 °C for 30 min. After this treatment, the substrate was sonicated in water and used immediately. For additional characterization, some films were annealed at 500 °C on air for 3 h.

2.4 Characterization techniques

The film surface characteristics were investigated by SEM on gold covered samples, using a Hitachi S-570 microscope (operating voltage, 10–30 keV). For thickness measurements, samples were cut into pieces resulting in the break of the TiO_2 film near the cut edge of the substrate. Film thickness was studied in these edges, taking into consideration the sample inclination with respect to the electron beam. TiO_2 films were easily distinguished from the substrate due to their different roughness. The XRD spectra were registered on a Philips X'Pert diffractometer equipped with a monochromator and using Cu Kα radiation ($\lambda = 0.154056$ nm). In order to increase the sensitivity of the thin film signal, a grazing incident configuration was used (2.0°). Transmittance of films deposited on glass was measured with a UV-vis Helios series γ spectrophotometer (Bonsai Technologies), using the bare glass substrate as the blank.

XPS experiments were performed in a PHI 5500 Multitechnique System (from Physical Electronics) with a monochromatic X-ray source (Aluminium Kα line of

Table 1 Baths composition used for TiO_2 deposition

Bath	Scavenger (source)	$[(NH_4)_2TiF_6]_{initial}$	$[Scavenger]_{initial}$	Ti : scavenger molar ratio	$pH_{initial}$
<TiO_2/Al>	Al^{3+} ($Al(NO_3)_3 \cdot 9H_2O$)	10 mM	10 mM	1:1	2.1
<TiO_2/1-Fe>	Fe^{3+} ($FeCl_3$)	10 mM	10 mM	1:1	2.2
<TiO_2/2-Fe>	Fe^{3+} ($FeCl_3$)	10 mM	20 mM	1:2	2.0
<TiO_2/B>	H_3BO_3	10 mM	30 mM	1:3	2.8

1486.6 eV energy and 350 W), placed perpendicular to the analyzer axis and calibrated using the $3d^{5/2}$ line of Ag with a full width at half maximum (FWHM) of 0.8 eV. The analyzed area was a 0.8 mm diameter circle, and the selected resolution for the fitted spectra was 23.5 of pass energy and 0.1 eV $step^{-1}$. Additional measurements were done after a slight stripping that were performed sputtering the surface with an Ar^+ ion source (4 keV energy). All these measurements were made in a ultra high vacuum chamber (pressure between 5×10^{-8} and 5×10^{-9} Torr).

3 Results and discussion

3.1 Deposition on glass

The first objective was to select experimental conditions that allow film deposition at a relatively high rate and favor the crystalline nature of the coatings. A set of preliminary experiments showed that strongly adhered films on bare glass substrates were produced at 80 °C using a 10 mM titanium precursor solution. Temperature was increased somewhat, compared to those usually employed in LPD processes (comprised between 25 and 50 °C), with the aim to favor the crystallization of TiO_2.[20,23] The precursor concentration used was five to ten times lower than those habitually used in LPD. This low precursor concentration benefits heterogeneous deposition *vs.* homogeneous nucleation and consequently allows to reduce the amount of precursors consumed due to powder precipitation by homogenous phase nucleation. The reduction of solids in suspension is advantageous taking into account that these particles can be trapped in the film resulting in a poor quality of the coating. Furthermore, the low precursor concentration favors the production of more crystalline materials.[20,40]

When the deposition time is noticeable increased fragments of the film detach from the substrate, remaining as little sheets in the bottom of the container, pointing towards increased mechanical stress for thicker films. The moment at which this phenomenon occurs depends on the bath composition: though never has been observed at the deposition time selected (3 h), always occurs after seven hours of deposition period. As a consequence, the thickness of the deposits obtainable by the LPD process is limited, as has been observed previously.[9,20] The molar ratio of fluoride scavenger with respect to Ti(IV) was fixed to one for Al(III), while in the case of iron(III) two Ti : Fe molar ratio alternatives, 1 : 1 and 1 : 2, were studied. The number of equivalents of boric acid was fixed at 3.0, that is a common value used in previous works.[7,13–16,19,25,34]

The TiO_2 films deposited on bare glass substrates using any of these three different fluoride scavengers have a hazy aspect. Additionally, a yellow color is observed for films produced using Fe(III) as fluoride scavenger, pointing toward some degree of iron incorporation in the deposited material (see later). The surface morphology was studied by SEM (Fig. 1). In all cases only a partial substrate coverage was observed. The morphology of the films consisted of hemispherical deposits; a similar morphology has been observed in TiO_2 films obtained by LPD processes when the nucleation sites density is low.[16,19] Bath composition has some influence in the density of nucleation sites, being clearly lower for <TiO_2/B> and higher for <TiO_2/2-Fe> (see Fig. 1). On the other hand, the average size of the hemispherical deposits is much higher when Al(III) is used as fluoride scavenger (Fig. 1a), compared to boric acid (Fig. 1d), leading to a better substrate coverage. Radial growth average rates for Al(III), around 175 nm h^{-1}, almost double the corresponding to boric acid, 90 nm h^{-1}. 110 and 82 nm h^{-1} radial growth rates are observed using <TiO_2/1-Fe> and <TiO_2/2-Fe>, respectively. Although the rate diminished when the amount of iron(III) is doubled (<TiO_2/2-Fe>), an increased degree of substrate coverage is achieved as a consequence of the higher number of nucleation sites (compare Fig. 1c and 1b).

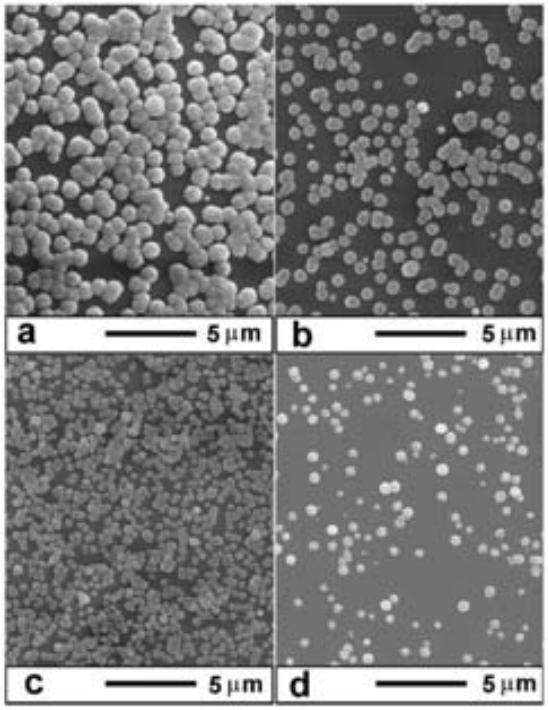

Fig. 1 SEM micrographs of TiO_2 films deposited on bare glass by LPD using different bath compositions: (a) <TiO_2/Al>; (b) <TiO_2/1-Fe>; (c) <TiO_2/2-Fe> and (d) <TiO_2/B>.

It must be taken into account that the different bath compositions have slightly different initial pH values. In the <TiO_2/B> bath the pH was adjusted to 2.8 with perchloric acid. This pH modification, also adopted by other authors, gives films with improved transparency than those obtained at natural pH (*ca.* 3.5). In the other baths, the pH values are lower without added acid (<TiO_2/Al> , 2.1; <TiO_2/1-Fe>, 2.2 and <TiO_2/2-Fe>, 2.0). To simplify the work methodology, the pH of these baths were unmodified. It has been established that using boric acid as a scavenger, a pH reduction from 2.8 to 1.5 implies a noticeable decrease of the TiO_2 deposition rate.[36] This implies that the higher deposition rate observed using Al(III) or Fe(III) as a fluoride scavenger, can not be directly ascribed to the more acidic character of the chemical bath in these experiments. A different factor must be the origin of these enhanced deposition rates. Lower pH values favor the chemical attack of the glass substrate by HF traces and must assist the initial nucleation of TiO_2. Nevertheless, it is not

possible to establish a direct relationship between the density of nucleation sites and the initial pH of the bath, denoting a clear influence of the chemical nature of the other species present in the bath.

A two-step process was designed in order to intentionally increase the nucleation sites density and thus obtain more regular films. The first step is a relatively short (30 min) substrate immersion in a 0.10 M H_2TiF_6 solution, at 80 °C. During this pretreatment, the glass substrate itself could act as fluoride scavenger, leading to some TiO_2 deposition. It is known that HF, present in small equilibrium concentrations in H_2TiF_6 solutions, can corrode SiO_2, producing silicon fluoride complexes.[23] However, after this short treatment the glass substrates seem unaltered to naked eye and no appreciable amount of deposited material could be observed. Although the modification of the substrate is too slight to be clearly measured or identified by the characterization techniques used during this work (UV-vis spectra, grazing angle XRD, SEM), the positive effect of this pretreatment is evident by the fact that posterior LPD process on thus treated substrates gives optically transparent TiO_2 films (as mentioned, films deposited on untreated substrates present a hazy appearance). SEM characterization confirmed that the two-steps method allows a more regular coating (Fig. 2). In these samples, films homogeneity is improved and accordingly, thickness is much better defined (Fig. 3). The average deposition rate is again much higher using Al(III) as a scavenger (150 nm h^{-1}) compared to boric acid (85 nm h^{-1}). The other measured values were 105 and 85 nm h^{-1} for film deposited using <TiO_2/1-Fe> and <TiO_2/2-Fe>, respectively. All these data are close to the radial growth rates estimated from the size of the hemispherical deposits obtained on non-treated glass.

The most compact and regular films produced by this two-step method were used to perform UV-vis transmittance spectra (Fig. 4). Films obtained using boric acid or

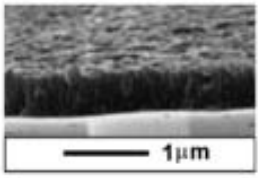

Fig. 3 SEM micrograph showing a step on a TiO_2 films deposited on bare glass pretreated with a solution of hexafluorotitanic acid. The step was done intentionally by cracking the glass substrate after deposition.

aluminum(III) as scavenger are highly transparent in the visible spectrum. The absorbance in the visible range spectrum, at lower wavelength interval, of the samples obtained from <TiO_2/1-Fe> and <TiO_2/2-Fe> baths suggests the incorporation of this cation in the material. Absorption oscillations, due to interference phenomena, are more evident on samples obtained in <TiO_2/Al> baths, indicating that more regular films are produced in these samples. Spectra have been processed in order to estimate the absorption threshold values from the expression corresponding to indirect band gap semiconductors (Table 2).

In the as-deposited film from the <TiO_2/Al> and the <TiO_2/B> bath, absorption threshold values are slightly higher than anatase band gap (Eg). After annealing, a shift to the visible is produced and the new values agree with the Eg values expected for anatase, suggesting an increase of film crystallinity. On the other hand, absorption threshold values determined for films obtained using iron(III) as scavenger are considerably shifted towards the visible. After annealing, a more pronounced shift is observed. These data strongly suggest the incorporation of iron(III) species on the film, as was confirmed by XPS analysis (see later). The changes observed after annealing could be due to a partial segregation of iron(III) to form tiny iron(III) oxide aggregates. Similar

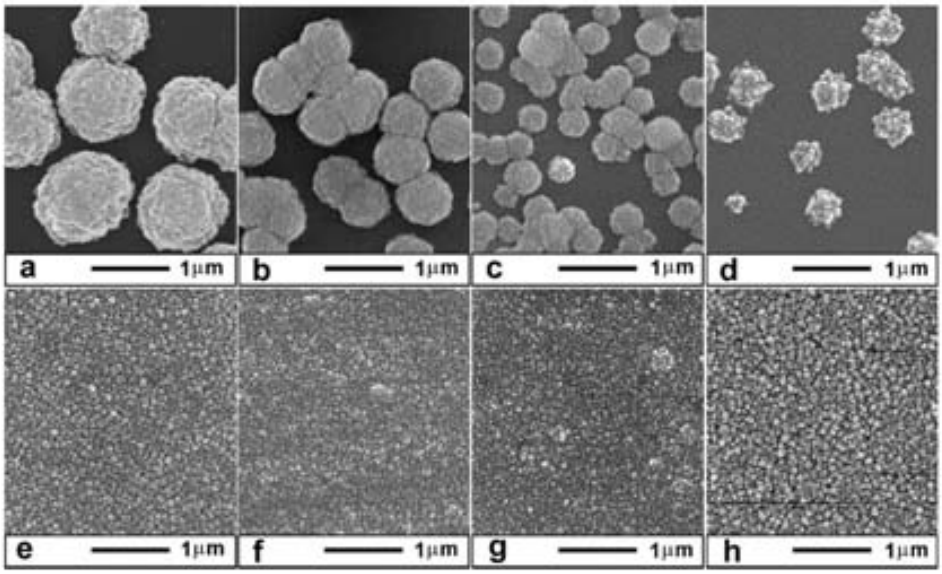

Fig. 2 Comparison between TiO_2 films deposited on bare glass (up) and films deposited on glass pretreated with a solution of hexafluorotitanic acid (bottom). SEM micrographs correspond to samples obtained using bath compositions: <TiO_2/Al>, (a) and (e); <TiO_2/1-Fe>, (b) and (f); <TiO_2/2-Fe>, (c) and (g); and <TiO_2/B>, (d) and (h).

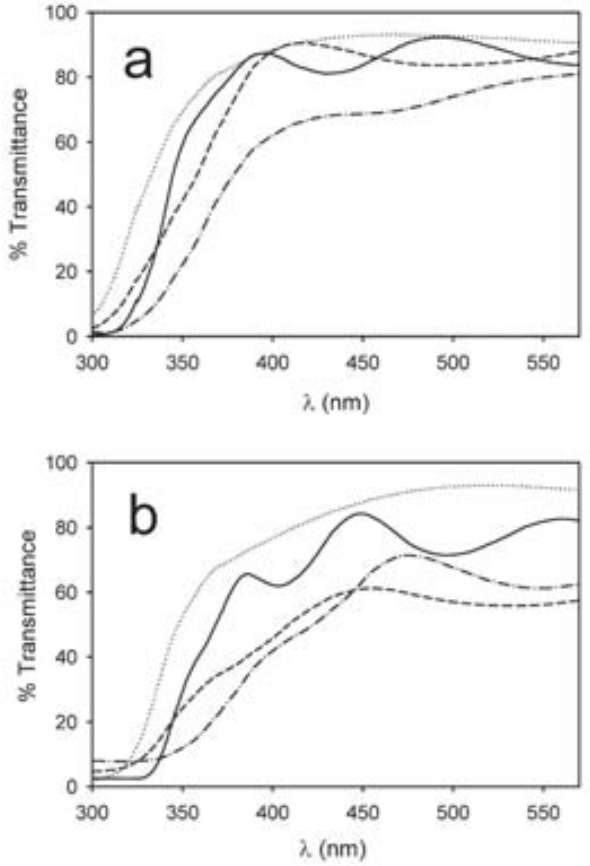

Fig. 4 UV-visible transmittance spectra of TiO_2 thin films deposited on glass pretreated with a solution of hexafluorotitanic acid, as obtained (a) and after calcinations (b). Films were prepared by the two-step method using different bath compositions: <TiO_2/Al>, solid line; <TiO_2/1-Fe>, dotted–dashed line; <TiO_2/2-Fe>, dashed line, and <TiO_2/B>, dotted line.

Table 2 Absorption threshold values (eV units) corresponding to different TiO_2 films deposited in glass pretreated with H_2TiF_6

Bath	As-deposited film	Annealed film
<TiO_2/Al>	3.35	3.15
<TiO_2/1-Fe>	3.00	2.50
<TiO_2/2-Fe>	3.00	2.80
<TiO_2/B>	3.40	3.20

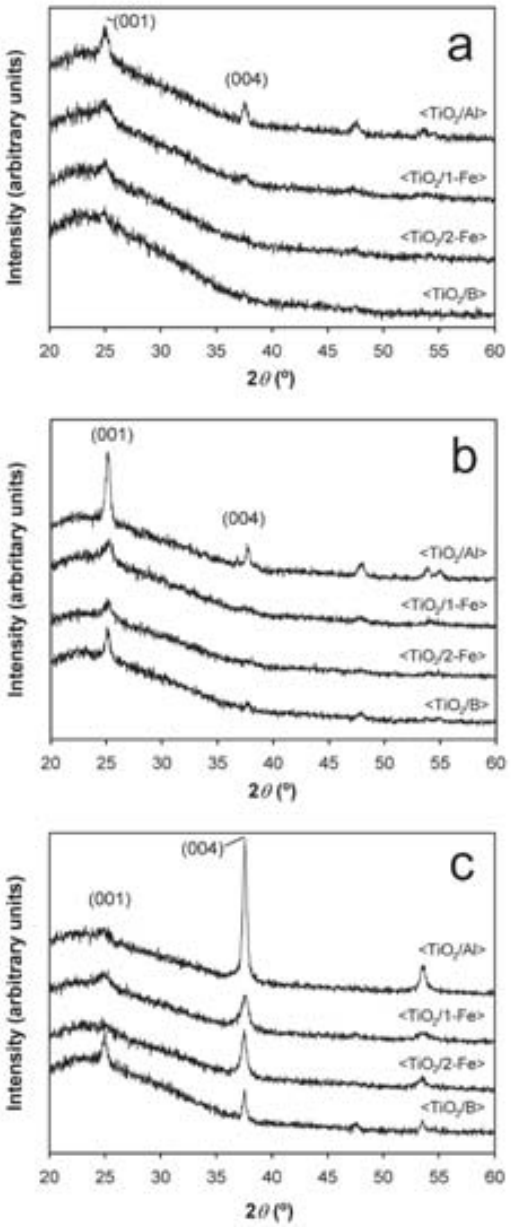

Fig. 5 Grazing angle XRD diffractograms of TiO_2 films deposited on bare glass (a) before and (b) after annealing, and (c) TiO_2 films deposited on glass pretreated with a solution of hexafluorotitanic acid. Bath composition employed for each sample is indicated on the figure.

results have been found in Fe^{3+}–TiO_2 films obtained by CVD.[41]

X-ray analysis of the different TiO_2 films revealed peaks assignable to the anatase structure, although only weak signals were observed for the films that contain less amount of material. Anatase formation is favored in the presence of titanium strongly complexing ions such as fluoride, this phase being usually produced by TiO_2 LPD.[9,42] Diffractograms of as-deposited films on bare glass (Fig. 5a) show poorly defined peaks that are relatively best defined in the case of thicker TiO_2 film obtained using Al(III). After annealing (Fig. 5b), XRD patterns of films prepared using baths <TiO_2/Al> or <TiO_2/B> show thinner and more intense peaks as a consequence of the thermally induced crystal growth. In contrast, annealing has little effect on the diffractogram of films deposited from baths containing Fe(III), pointing that the segregation of iron prevents the crystal growth in these samples. However, no signal assignable to an iron oxide phase was observed, no even on annealed samples diffractograms.

The XRD patterns of the films deposited on bare glass (Fig. 5a and 5b) differ noticeably with respect to those of the more compact films obtained on glass pretreated with H_2TiF_6 (Fig. 5c). On Fig. 5c peaks are more intense and present clearly different relative intensities than those of the anatase patron

(JCPDS pattern 21–1272). In the anatase patron, corresponding to complete random order, a 5 : 1 intensity ratio is observed between the most intense peak (plane (101); 25.3°), and the peak that appears at $2\theta = 37.8°$ (plane (004)). In the diffractograms of our samples, the relative intensity of the peak at 37.8° appears notably increased with respect to the anatase patron. This effect is more intense in the case of the films produced using Al(III), which are the thicker films. On the other hand, patterns corresponding to films produced using boric acid and iron(III), that have a similar thickness, present very different intensity ratios between these two peaks, indicating that other parameters influence the crystal growth and/or orientation.

The preferential *c*-axis orientation of the anatase film growth on glass can not be the result of a specific nucleation mechanism, as the substrate lacks an ordered structure. Preferential crystal growth in the [004] direction has been observed previously both for TiO_2 powders and films obtained from AHFT.[43,21] This has been associated with preferential adsorption of fluoride to planes parallel to this direction.[36]

It has been shown that preferential crystal growth is enough to explain a preferential crystal orientation with respect to a substrate.[16,44] In TiO_2 LPD, initially hemispherical deposits are formed. Each hemispherical deposit consists of numerous elongated crystals, with the long axis parallel to the *c*-axis and disposed on radial symmetry around an initial nucleation site. Coalescence of such deposits, reached earlier or later depending on the density of nucleation centers, favors the growth of the crystals, with the *c*-axis perpendicular to the substrate.[16,44] Thus, a high density of nucleation sites deals to smooth, dense and oriented film (Fig 3). On the contrary, if only a limited number of nucleation sites is available, hemispherical deposits grow before to coalesce, *i.e.* not oriented waved films were produced and only partial substrate coverage is obtained (Fig. 1).

3.2 TiO_2 deposition on ITO

TiO_2 deposition on ITO is favored due to structural similarities between both materials; as a consequence, coherent films are deposited on ITO covered glass. It must be taken into account that in the XRD diffractograms the peak corresponding to the anatase plane (004) ($2\theta = 37.8°$) is not resolved from the substrate signal (peak at $2\theta = 37.9°$). However, comparing the XRD patterns of the substrate and the TiO_2 coated substrate (Fig. 6), it is evident that the intensity of the peak at 37.8° greatly increases relative to the other visible peaks for the samples with the TiO_2 film, so the contribution of the anatase signal is evident. In this case, thicker films are produced using Al(III) as scavenger, also showing a more pronounced crystal preferential orientation.

The composition of the TiO_2 thin film deposited on ITO covered glass using Al(III) or Fe(III) as scavengers were characterized with XPS (Table 3). As-deposited films were analyzed before and after Ar sputtering (in the first case, the contribution from adventitious carbon has not been considered to calculate the composition of the film). Soft stripping conditions are used to eliminate only 25–50 nm of the film. Aluminum is not detected in the samples produced from

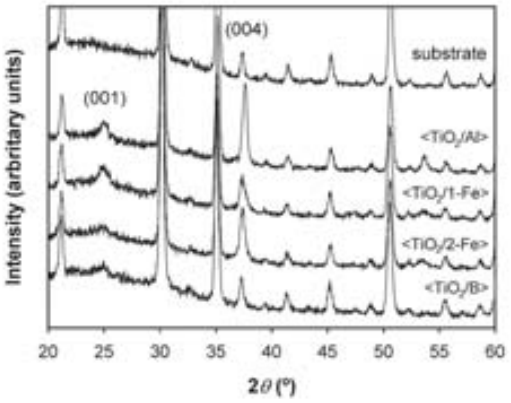

Fig. 6 Grazing angle XRD diffractograms of TiO_2 films deposited on ITO covered glass. Bath composition employed for each sample is indicated on the figure. The diffractogram corresponding to the substrate is also included (up) for comparison.

Table 3 Composition (at.%) of TiO_2 films deposited on ITO covered glass using different chemical bath compositions

Bath	O	Ti	F	Si	N	Fe	In
<TiO_2/Al>	68.0	26.7	3.9	0.5	0.9	—	—
<TiO_2/Al>[a]	55.5	40.4	3.5	—	0.6	—	—
<TiO_2/1-Fe>	67.6	23.1	2.7	2.0	0.5	4.0	—
<TiO_2/1-Fe>[a]	53.4	32.5	2.2	—	—	11.2	—
<TiO_2/2-Fe>			2.4	1.7	0.7	2.4	0.8
<TiO_2/2-Fe>[a]			1.6	—		10.2	1.2

[a] Data corresponding to measures done after a slight sample stripping.

bath <TiO_2/Al>, whilst the samples produced from the baths containing iron(III) have a significant amount of this element incorporated. Remarkably, iron concentration is higher inside the films. Fluoride, the most usual contaminant in TiO_2 obtained by titanium fluoro-complexes,[23,43] was also found at a significant level and higher in the samples obtained in the <TiO_2/Al> bath. The presence of Si can be related to the attack of the glass substrate by the HF present in the precursor solution, yielding silicon fluoro-complexes. These silicon derivatives are unstable due to the presence of fluoride scavenger and yielding then insoluble oxide material that is incorporated in the film.[23] A similar process can account for the presence of indium traces, while ammonium and nitrate ions are the source for the traces of nitrogen detected.

4 Conclusions

Presented results demonstrate that soluble salts of Al(III) and Fe(III) can be used as fluoride scavenger. Al(III) allows to obtain partially crystallized films at low temperature (80 °C) and at higher deposition rates than boric acid. Fe(III) used as scavenger produces yellow colored films containing a significant amount of iron dispersed in the titanium oxide matrix. For both scavengers, the films contain significant concentrations of fluorine, lesser in the case of Fe(III). Comparable fluorine levels are found when boric acid is used as scavenger.[23,43] The chemical nature of the fluoride scavenger also determines the number of nucleation sites

accessible. Glass pretreatment with H_2TiF_6 greatly increases the number of accessible nucleation centers. LPD on thus pretreated substrates allows to obtain compact films that present a preferential orientation of the TiO_2 crystallites, with the *c*-axis perpendicular to the substrate. The degree of this preferential orientation is influenced by the chemical nature of the fluoride scavenger.

Acknowledgements

This work has been financed by the Spanish National Plan of Research (BQU2003-01280 project).

References

1 O. Carp, C. L. Husiman and A. Reller, *Prog. Solid State Chem.*, 2004, **32**, 33–177.
2 A. Mills and S. Le Hunte, *J. Photochem. Photobiol., A*, 1997, **108**, 1–35.
3 M. Grätzel, *Nature*, 2001, **414**, 338–344.
4 B. Peng, G. Jungmann, C. Jäger, D. Haarer, H.-W. Schmidt and M. Thelakkat, *Coord. Chem. Rev.*, 2004, **248**, 1479–1489.
5 A. Mills, A. Lepre, N. Elliott, S. Bhopal, I. P. Parkin and S. A. O'Neil, *J. Photochem. Photobiol., A*, 2003, **160**, 213–224.
6 S. Baskaran, L. Song, J. Liu, Y. L. Chen and G. L. Graff, *J. Am. Ceram. Soc.*, 1998, **81**, 401–408.
7 J. Xiang, P. Zhu, Y. Masuda and K. Koumoto, *Langmuir*, 2004, **20**, 3278–3283.
8 A. F. Nogueira, C. Longo and M-A De Paoli, *Coord. Chem. Rev.*, 2004, **248**, 1455–1468.
9 T. P. Niesen and M. R. De Guire, *Solid State Ionics*, 2002, **151**, 61–68.
10 S. Deki, Y. Aoi, O. Hiroi and A. Kajinami, *Chem. Lett.*, 1996, **6**, 433–434.
11 S. Deki, Y. Aoi, Y. Asaoka, A. Kajinami and M. Mizuhata, *J. Mater. Chem.*, 1997, **7**, 733–736.
12 H. Kishimoto, K. Takahama, N. Hashimoto, Y. Aoi and S. Deki, *J. Mater. Chem.*, 1998, **8**, 2019–2024.
13 K. Koumoto, S. Seo, T. Sugiyama, W. S. Seo and W. J. Dressick, *Chem. Mater.*, 1999, **11**, 2305–2309.
14 A. Dutschke, C. Diegelmann and P. Löbmann, *J. Mater. Chem.*, 2003, **13**, 1058–1063.
15 B. Herbig and P. Löbmann, *J. Photochem. Photobiol., A*, 2004, **163**, 359–365.
16 A. Dutschke, C. Diegelmann and P. Löbmann, *Chem. Mater.*, 2003, **15**, 3501–3506.
17 Y. Aoi, H. Kambayashi, E. Kamijo and S. Deki, *J. Mater. Res.*, 2003, **18**, 2832–2836.
18 H. Strohm, M. Sgraja, J. Bertling and P. Loebmann, *J. Mater. Sci.*, 2003, **38**, 1605–1609.
19 J. Xiang, Y. Masuda and K. Koumoto, *Adv. Mater.*, 2004, **16**, 1461–1464.
20 H. Pizem, C. N. Sukenik, U. Sampathkumaran, A. K. McIlwain and M. R. De Guire, *Chem. Mater.*, 2002, **14**, 2476–2485; H. Pizem, O. Gershevitz, Y. Goffer, A. A. Frimer, C. N. Sukenik, U. Sampathkumaran, X. Milhet, A. McIlwain and Mark R. De Guire, *Chem. Mater.*, 2005, **17**, 3205–3213.
21 A. M. Peiró, E. Vigil, J. Peral, C. Domingo, X. Domènech and J. A. Ayllón, *Thin Solid Films*, 2002, **411**, 185–191.
22 E. Vigil, J. A. Ayllón, A. M. Peiró, R. Rodríguez-Clemente, X. Domènech and J. Peral, *Langmuir*, 2001, **17**, 891–896.
23 J.-G. Yu, H.-G. Yu, B. Cheng, X.-J. Zhao, J. C. Yu and W.-K. Ho, *J. Phys. Chem. B*, 2004, **107**, 13871–13879.
24 X.-P. Wang, Y. Yu, X.-F. Hu and L. Gao, *Thin Solid Films*, 2000, **371**, 148–152.
25 Y. Gao, Y. Masuda and K. Koumoto, *Langmuir*, 2004, **20**, 3188–3194.
26 H. Tokuhisa and P. T. Hammond, *Adv. Funct. Mater.*, 2003, **13**, 831–839.
27 L. I. Halaoui, N. M. Abrams and T. E. Mallouk, *J. Phys. Chem. B*, 2005, **109**, 6334–6342.
28 Y. Masuda, S. Ieda and K. Koumoto, *Langmuir*, 2003, **19**, 4415–4419; Y. Masuda, N. Saito, R. Hoffmann, M. R. De Guire and K. Koumoto, *Sci. Technol. Adv. Mater.*, 2003, **4**, 461–467; Y. Masuda, T. Sugiyama and K. Koumoto, *J. Mater. Chem.*, 2002, **12**, 2643–2647.
29 N. Ozawa, H. Yabe and T. Yao, *J. Am. Ceram. Soc.*, 2003, **86**, 1976–1978.
30 N. Ozawa and T. Yao, *Solid State Ionics*, 2002, **151**, 79–87.
31 S. Deki, S. Iizuka, A. Horie, M. Mizuhata and A. Kajinami, *Chem. Mater.*, 2004, **16**, 1747–1750.
32 S. Deki, S. Iizuka, A. Horie, M. Mizuhata and A. Kajinami, *J. Mater. Chem.*, 2004, **14**, 3127–3132.
33 H. Tokuhisa and P. T. Hammond, *Langmuir*, 2004, **20**, 1436–1441.
34 L. Feng, Y. Liu and J. Hu, *Langmuir*, 2004, **20**, 1786–1790.
35 Z. H. Barber, *J. Mater. Chem.*, 2006, **16**, 334–344.
36 Y. Masuda, T. Sugyama, W. S. Seo and K. Koumoto, *Chem. Mater.*, 2003, **15**, 2469–2476.
37 Y. Gao and K. Koumoto, *Cryst. Growth Des.*, 2005, **5**, 1983–2017.
38 H. Imai, Y. Takei, K. Shimizu, M. Matsuda and H. Hirashima, *J. Mater. Chem.*, 1999, **9**, 2971–2972.
39 T. Hamaguchi, M. Uno, K. Kurosaki and S. Yamanaka, *J. Alloys Compd.*, 2005, **386**, 265–269.
40 N. Ozawa, Y. Kumazawa and T. Yao, *Thin Solid Films*, 2002, **418**, 102–111.
41 F. Gracia, J. P. Holgado, A. Caballero and A. R. Gonzalez-Elipe, *J. Phys. Chem. B*, 2004, **108**, 17466–17476.
42 A. Kay and M. Grätzel, *Sol. Energy Mater. Sol. Cells*, 1996, **44**, 99–117.
43 J. A. Ayllón, A. M. Peiró, L. Saadoun, E. Vigil, X. Domènech and J. Peral, *J. Mater. Chem.*, 2000, **11**, 1911–1914.
44 G. K. L. Goh, S. K. Donthu and P. K. Pallathadka, *Chem. Mater.*, 2004, **16**, 2857–2861.

PART 4.3:

ONE-STEP ORGANIC/TiO_2 HYBRID THIN FILMS PREPARED BY LPD

Publication 3:

Characterization of methylene blue/TiO_2 hybrid thin films prepared by the liquid phase deposition (LPD) method: Application for fabrication of light-activated colorimetric oxygen indicators.

J. Photochem. Photobiol. A: Chem. **2007**, *187*, 45-52.

Publication 4:

Dopamine/TiO_2 hybrid thin films prepared by the liquid phase deposition method.

Thin Solid Films **2008**, *516*, 3831-3835.

4.3.1. INTRODUCTION

Electronic conductivity, high surface affinity toward certain ligands and large surface area have situated TiO_2 in a privileged place in many interesting applications based on the surface modification of semiconductor nanoparticles (in many cases deposited on a TCO substrate and forming a film) with organic derivates. The development of soft and low-temperature chemical routes for preparing metal oxide materials has been an important issue at the end of the 90s and the present decade [1,2]. Preparation methods at mild conditions (pH, temperature, solvent) have recently broadened new horizons toward the field of hybrid organic/inorganic materials prepared in one step, since organic additives can be easily added to the preparation bath and incorporated with the inorganic material, as long as the two components present sufficient affinity to give rise to the hybrid material [3,4].

LPD had already opened the door to the preparation of organic/inorganic materials with a threesome of publications when both papers forming this part were conceived [5-7]. However, several key reasons motivated the interest in the research of one-step hybrid TiO_2 LPD approaches. Firstly, common TiO_2 preparation routes need a high temperature post-treatment in order to induce crystallization, eliminate residual organics or sinter nanoparticles. Consequently, habitual routes become incompatible with thermolabile substrates, forcing the surface modification process to be carried out separately [8]. Secondly, since TiO_2 crystallization at mild conditions is usually required and not obvious to achieve, functional hybrid organic/TiO_2 materials prepared in one-step approaches are hardly reported in the literature, in contrast with the great variety of existing examples for other oxides such as ZnO [3,4,9-11] and SiO_2 [12-17]. Thirdly, controlling LPD media supersaturation, hybrid organic/metal oxides composites are directly prepared only on the substrate surface (without precipitation from the bulk solution), being, for instance, a clear advantage compared to low-temperature encapsulating sol-gel methods [18]. And last but not least, some authors claim improved and/or different emerging applications of hybrid composite materials with respect to simple surface modification. For example, selective

recognition abilities for L-glutamic acid [7] or proteins [18] of moleculary imprinted TiO_2 thin films by LPD have been proved. Increased efficiency due to higher dye loading has been demonstrated in electrochemically self-assembled nanoporous metal-free dye/ZnO hybrid films [4].

On one hand, the cationic dye Methylene Blue (MB or MB^+, 3,7-*bis*(dimethylamino)phenazathionium), that is a brightly colored thiazine dye ($\varepsilon_{664}=9\cdot10^4$ $M^{-1}cm^{-1}$), presenting λ_{max} values at 664, 610 and 292 nm in aqueous solutions [19,20], was firstly chosen for the work done in Publication 3: **Characterization of methylene blue/TiO_2 hybrid thin films prepared by the liquid phase deposition (LPD) method: Application for fabrication of light-activated colorimetric oxygen indicators.** *J. Photochem. Photobiol. A: Chem.* **2007**, *187*, 45-52. MB has been extensively employed in many applications such as dye for different staining procedures in biology, redox indicator in analytical chemistry or mediator in electrochemical biosensors, own to its good electrochemical reversibility and colorization properties [19-23] (Figure 4.3.1) In the context of heterogeneous photocatalysis, photobleaching of MB has been widely used as model test for demonstrating both UV and visible light activity in home-made TiO_2 catalysts, although some controversy regarding to the ambiguity of this system exists in the literature, since: (i) MB can be either oxidized or reduced under aerobic or anaerobic conditions, respectively [19,24]; (ii) direct photolysis of this model dye pollutant has been proved even upon low-energy UV irradiation [19] and (iii) MB also sensitizes the TiO_2 semiconductor toward visible light [25,26]. Mills *et al.* patented a new intelligent ink composed of a mixture of MB and TiO_2 P-25 powder for oxygen gas sensing [27] (which is essential for the proliferation of aerobic microorganisms, the main cause of habitual food spoilage). These authors claimed the necessity of developing inexpensive, non-toxic and irreversible oxygen indicators, with practical application in modified atmosphere food packaging industry [24,28,29].

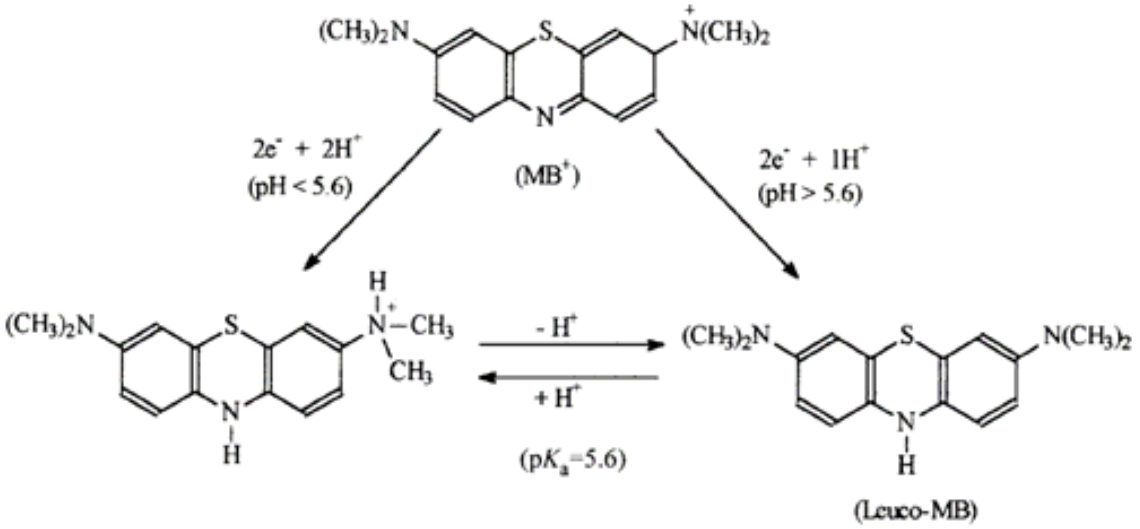

Figure 4.3.1. MB structure and scheme of behavior in aqueous solutions at various pH values. MB reduction gives rise to the non-colored Leuco-MB form. Adapted from ref. [20].

On the other hand, in Publication 4: **Dopamine/TiO_2 hybrid thin films prepared by the liquid phase deposition method.** *Thin Solid Films* **2008**, *516*, 3831-3835, the catecholamine Dopamine or 2-(3,4-dihydroxyphenil)ethylamine (DA, Figure 4.3.2) was secondly selected as candidate for forming an hybrid material with titania. DA is a compound of great biochemical and neurochemical interest, playing a key role in the functioning of the central nervous system, cardiovascular, renal and hormonal systems as well as in drug addiction and Parkinson's disease [30,31]. Rajh *et al.* have deeply studied the surface modification of TiO_2 nanoparticles with bidentate ligands containing enediol units which have the optimal geometry for strongly chelating surface Ti atoms, resulting in a five-membered ring coordination complex (restoring bulk-like six-coordinated octahedral geometry of surface Ti atoms) and forming ligand-to-metal charge-transfer complexes [32-34]. DA (as catecholamine) is intrinsically attractive within the enediol family of compounds as bridging ligand; *i.e.* it can additionally be functionalized through amide bonds with other molecules of interest via alkyl-NH_2 group [35-37]. Compared to the unmodified semiconductor, the formation of these charge-transfer complexes on TiO_2 has been shown to change the electronic properties of the nanoparticles: (i) extending the semiconductor response toward the visible range (leading to an effective band gap of 1.6 eV in DA-modified

TiO_2) [34]; (ii) enhancing interfacial electron-transfer rate, via a direct dye-to-TiO_2 pathway from the ground state of the dye [34,38,39]; (iii) improving charge separation between the semiconductor (or electron acceptors) and the enediol modifier (or electron donors linked via dopamine), giving rise to light-induced TiO_2 redox architectures with selective chemistry [40-44]. Therefore, DA seemed specially suitable for preparing low-cost metal-free TiO_2 photoelectrodes for DSSCs in one step [39].

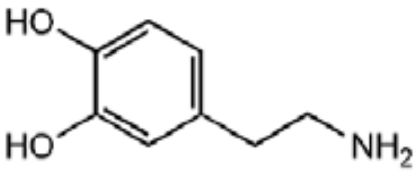

Figure 4.3.2. Dopamine (DA) structure.

4.3.2. MAIN RESULTS AND DISCUSSION

As starting point of the preparation of hybrid/TiO_2 materials by LPD, the experimental conditions used in our previous work were adopted (see Section 4.2, $[(NH_4)_2TiF_6]$ = 10 mM and T=80ºC). However, the deposition times were increased from 3 to 4.5 h in order to obtain films thick enough, since organic modifiers clearly decreased the average deposition rates. Firstly, MB/TiO_2 thin films were prepared on both glass and ITO-glass substrates employing H_3BO_3 as fluoride scavenger ($[H_3BO_3]$ = 30 mM, pH adjusted to 2.8 with diluted $HClO_4$). Secondly, aluminum nitrate salt ([Al(III)] = 10 mM, natural pH of 2.0) was the selected scavenger for hybrid DA/TiO_2 LPD (only on ITO-glass in this case), since higher deposition rates had been proven in our former studies and, taking into account that strong enediol coordination would have probably decreased so much the hybrid material growth rate. It should be pointed here that previous pretreatment of the substrate (H_2TiF_6 corrosion on glass and short-time LPD on ITO-glass) was required for hybrid LPD in the case of MB due to a low nucleation density in the initial stages of the process. Optimal modifier concentrations ([MB] = 0.5 mM and [DA] = 20 mM) were also selected according to a primary characterization (mechanical stability, appearance and XRD) of samples prepared over a range of concentrations.

4.3.2.A. MB/TiO_2 hybrid thin films by LPD

Uniform, well-adhered and intense blue-colored MB/TiO_2 films were deposited by employing the optimized 0.5 mM MB concentration in the LPD bath, although the effective dye concentration in the bath was lower due to the precipitation of the violet $MBClO_4$ precipitate (as confirmed by IR spectroscopy). Analogous hybrid deposition by adjusting the pH of the bath with diluted HCl was attempted but no satisfactory film deposition was obtained, suggesting a positive role of the $MBClO_4$ precipitate, most probably guaranteeing a nearly constant concentration of soluble MB cation.

LPD of TiO_2 gives rise to an important fluoride chemisorption on the freshly grown material [45,46]. By means of IR spectroscopy, no significant differences in the MB absorption mode was found on both bare TiO_2 P-25 and the fluorinated TiO_2 in the hybrid material. Accordingly, electrostatic interaction between negative density charge at the TiO_2 fluorinated surface grown by LPD and the cationic dye ($\equiv Ti\text{-}F^{\delta-}:::MB^{+}$) was suggested as driving force for the formation of the nanocomposite. However, the hybrid material differed from simple physisorption since high stability was found against relative long time aqueous desorption tests (even in 0.5 M electrolyte salt solutions). Additionally, analogous MB absorption (from aqueous solutions) within blank TiO_2 films prepared by LPD was not possible.

Visible light absorption of MB/TiO_2 films evidenced the aggregation of the cationic dye in the hybrid material as revealed by an hypsochromic shift of λ_{max} from 664 nm (isolated molecule) to 605 (dimer) and 580 nm (trimer). It is well known that MB molecules in spite of repulsion due to similar charges, undergo self-aggregation to form dimers, trimers or higher aggregates, significantly affecting its optical properties [47-53]. Whereas the H-type or face-to-face association of this cationic dye shows a blue shift (favored at high aggregation numbers), the J-type or head-to-tail configuration shows an extra red shift in the dimer form (additional maximum at 697 nm) [50,53]. The environment where MB is located has a strong influence on its aggregation state. In general, negatively charged surfaces, micelles and interfaces may favor MB

self-aggregation increasing its local concentration and incorporation within the growing LPD film, since this associations can be stabilized due to the compensation of the electrostatic repulsion between the positive charges [51,52]. As a result, high concentrations of MB were incorporated during TiO_2 LPD, decreasing the anatase crystallite and the main particle size (although the average deposition rate of the film was slightly enhanced) and giving rise to films with more oriented anatase crystallites with respect to TiO_2 blank samples.

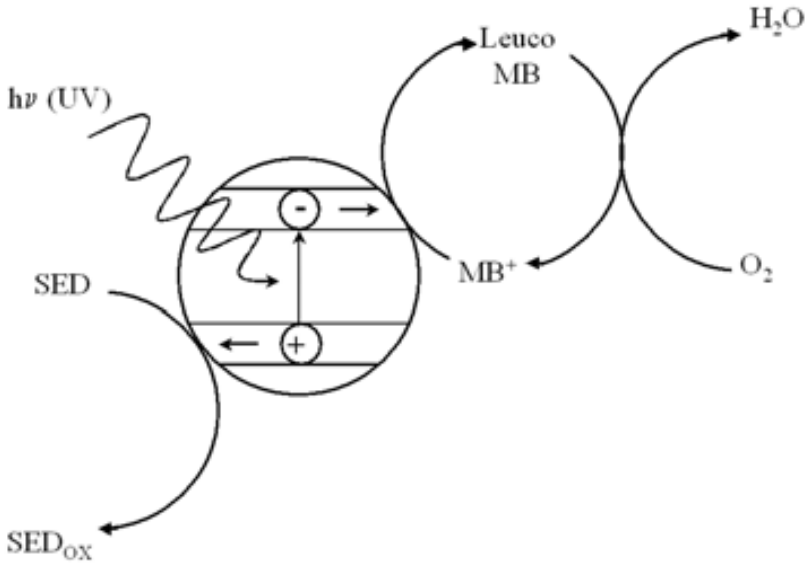

Figure 4.3.3. Schematic representation of the basic processes associated with a UV-activated oxygen indicator. MB is photobleached (reduction) and the SED is oxidized upon UV irradiation. Once the device is light-activated, blue coloration recovering indicates oxygen presence due to Leuco-MB reoxidation.

Photochemical activity of the hybrid MB/TiO_2 films was demonstrated in preliminary experiments in which the samples were totally photobleached (due to MB reduction to form the non-colored Leuco-MB) upon UVA irradiation using triethanolamine as sacrificial electron donor (SED). Following the same strategy of Mills *et al.* in their intelligent ink for oxygen sensing [27-29], that is based on the classical "blue bottle" demonstration [54,55] (see Figure 4.3.3), light-activated oxygen indicators with high optical transparency and delayed response were satisfactory

fabricated from the MB/TiO_2 films (by spin-coating an aqueous solution of the same sacrificial compound in hydroxyethyl cellulose encapsulating polymer). As working principle, light-activated indicators become non-colored upon exposure to UV light (photobleaching), gradually recovering blue coloration under aerobic conditions when the source of UV is removed (MB reoxidation). Thus, blue coloration recovering is indicative of the presence of oxygen, that is the main responsible of food-spoilage due to microorganisms proliferation [24,29].

Finally, cyclic voltammetry experiments of MB/TiO_2 films deposited on ITO-glass evidenced electroactive properties of the nanocomposite material. However, nanocomposite working electrodes showed irreversible redox activity in the time scale studied, since Leuco-MB reoxidation was not possible and significant MB desorption observed. Hence, electrochemical redox processes significantly differed with respect to photochemical reduction and Leuco-MB reoxidation by atmospheric oxygen in the UV-activated indicators.

4.3.2.B. DA/TiO_2 hybrid thin films by LPD

Uniform, well-adhered and brown-colored DA/TiO_2 films were deposited by employing the optimized 20 mM DA concentration in the LPD bath. It is well-known that DA by itself is extremely susceptible to oxidation either electrochemically or by atmospheric oxygen, forming the corresponding *o*-quinone according to Equation 4.3.A. [56]. However, Rajh *et al.* had already reported that enediol ligands gain stability and are not so easily oxidized due to the bidentate binding to titania nanoparticles [33].

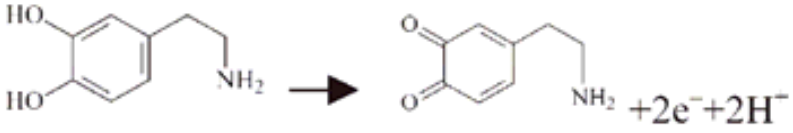

Equation 4.3.A. Dopamine oxidation in aqueous solution to form the corresponding *o*-quinone.

Dopamine addition to the precursor bath alters the LPD chemical equilibria due to the coordination of Ti(IV) cations by the enediol unit, giving rise to a characteristic brown-colored appearance to the solution. However, it should be pointed that according to the data calculated by Bi *et al.* [57,58] (see Figure 4.3.4), Al(III)-$(DA)_n$ coordination did not take place at the acidic pH at which LPD was carried out.

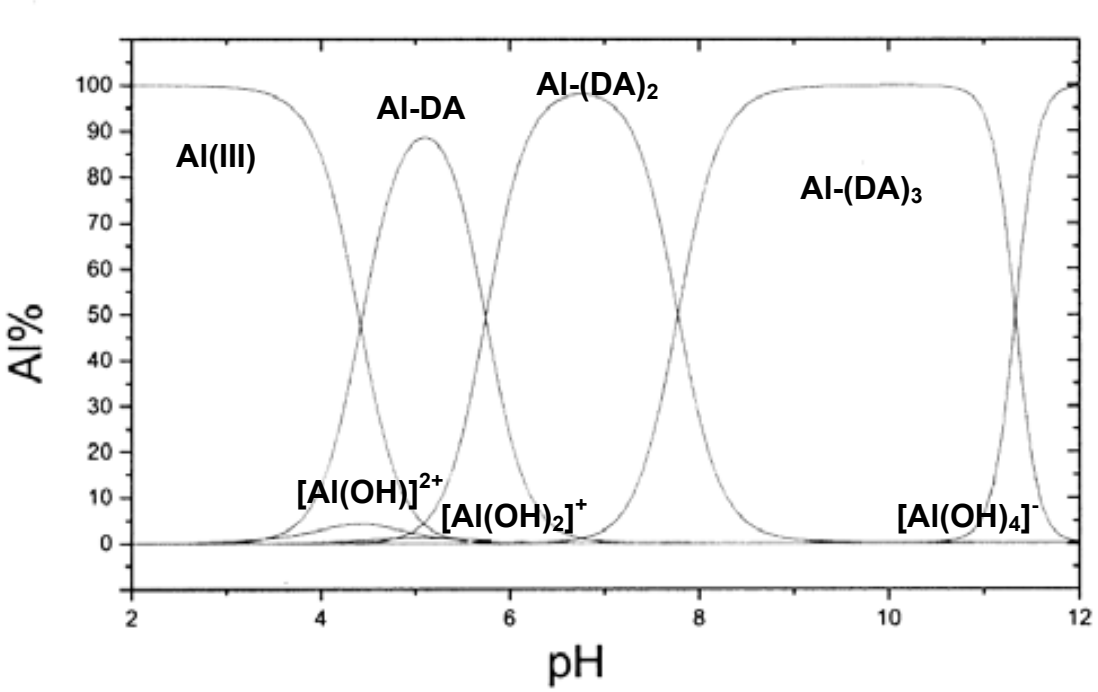

Figure 4.3.4. Calculated distribution of the species of Al(III)-DA complexes in aqueous solution: 0.04 mM Al(III) and 1.2 mM DA. Adapted from reference [57].

As occurred in the MB/TiO_2 material, no significant differences in the DA absorption mode was found on both bare TiO_2 P-25 and the fluorinated TiO_2 by means of IR spectroscopy and, hence, the same bidentate enediol coordination was confirmed. Additionally, by-product powder samples were also collected in the case of DA/TiO_2 by scrapping off low-adhered coatings on the polyethylene vessels. An incorporation of 7% of DA in the hybrid material was estimated by means of elemental analysis of these powder samples, evidencing a high dye incorporation during TiO_2 LPD. DA incorporation in the growing TiO_2 limited the size of both anatase crystallites and the main particle of the nanocomposite, and slightly decreased the average deposition rate

of the films. XRD showed that the hybrid material preferentially grow in both *a* and *c* anatase directions in the powder samples, although selective *c* axis orientation perpendicular with respect of the substrate still dominated in the hybrid film deposition on ITO-glass.

TEM suggested both enediol and alkyl-NH_2 linkage in the hybrid material since a continuous and aggregated structure of randomly oriented crystallites was observed in DA/TiO_2, being noticeably different from the isolated crystallites in an amorphous matrix in the case of MB/TiO_2 films. In spite of this phenomenon had already reported for *in situ* non-aqueous functionalization of nanocrystalline titania [59] or DA molecularly imprinted silica-alumina gel [60], crystallite-crystalline repulsion would have probably expected *a priori* since amino group of DA exists in the protonated form (pK_a=8.9 [61]) at the acidic pH that LPD was performed.

Practical applications of DA/TiO_2 hybrid thin films on ITO-glass were attempted as molecularly imprinted material and photoelectrode for DSSCs. On one hand, removing Dopamine from the films was studied in order to test if the DA/TiO_2 material was useful for selectively detecting such catecholamine afterwards. In fact, as-prepared DA/TiO_2 films were noticeably stable, supporting our hypothesis concerning crystallite linkage: (i) DA desorption in either acidic and basic solutions as well as commercial phosphate buffer was not achieved even for long times (over months) and (ii) medium-pressure Hg UV irradiation resulted in completely cracked films. However, films photobleaching (from brown-colored DA/TiO_2 to highly transparent "only TiO_2" samples) was attained upon black light UV irradiation due to DA photocatalytic degradation. But DA reincorporation within the photobleached films became too slow and limited, only exhibiting a slight brown coloration recovery. On the other hand, DA/TiO_2 photoelectrodes showed no IPCE spectral response (redox electrolyte: [KI]=0.50 M, [I_2]=0.050 M in ethylene glycol). In principle, at least a minimum of response would have reasonably expected since porous TiO_2 photoelectrodes sensitized toward visible light with Dopamine had shown light conversion in DSSCs [39].

4.3.3. CONCLUSIONS

MB/TiO_2 and DA/TiO_2 hybrid nanocomposite materials have been prepared with a low-temperature and one-step approach based on trapping these compounds within a LPD growing TiO_2. In the former, the driving force for MB/TiO_2 formation can be reasonably ascribed to continuous electrostatic interaction among negative density charges at the TiO_2 fluorinated surface and the cationic MB dye. In the latter, it seems plausible to attribute material formation to bidentate enediol plus amine linkage of TiO_2 nanocrystallites via Dopamine during LPD, according to the noticeably stability observed.

MB and DA incorporate in the respective hybrid materials in high concentration, inducing changes in the typical growth mechanism of the titania material prepared by LPD. As a general result, crystallite and main particle size are decreased in both cases. The practical application of MB/TiO_2 hybrid thin films for fabricating light-activated indicators for oxygen sensing has also been demonstrated.

4.3.4. REFERENCES

[1] Niessen, T.P.; De Guire, M.R. *Solid State Ionics* **2002**, *151*, 61-68.

[2] Gao, Y.; Koumoto, K. *Cryst. Growth Des.* **2005**, *5*, 1983-2017.

[3] Goux, A.; Pauporté, T.; Yoshida, T.; Lincot, D. *Langmuir* **2006**, *22*, 10545-10553.

[4] Oekermann, T.; Yoshida, T.; Minoura, H.; Wijayantha, K.G.U.; Peter, L.M. *J. Phys. Chem. B* **2004**, *108*, 8364-8370.

[5] Li, L.; Mizuhata, M.; Kajinami, A.; Deki, S. *Synth. Met.* **2004**, *146*, 17-27.

[6] Li, L.; Mizuhata, M.; Deki, S. *Appl. Surf. Sci.* **2005**, *239*, 292-301.

[7] Feng, L.; Liu, Y.; Hu, J. *Langmuir* **2004**, *20*, 1786-1790.

[8] Gutiérrez-Tauste, D.; Zumeta, I.; Vigil, E.; Hernández-Fenollosa, M.A.; Domènech, X.; Ayllón, J.A. *J. Photochem. Photobiol. A: Chem.* **2005**, *175*, 165-171.

[9] Nonomura, K.; Yoshida, T.; Schlettwein, D.; Minoura, H. *Electrochim. Acta* **2003**, *48*, 3071-3078.

[10] Pauporté, T.; Bedioui, F.; Lincot, D. *J. Mater. Chem.* **2005**, *15*, 1552-1559.

[11] Pauporté, Th. *Cryst. Growth Des.* **2007**, *7*, 2310-2315.

[12] Moreau, J.J.E.; Vellutini, L.; Chi Man, M.W.; Bied, C. *J. Am. Chem. Soc.* **2001**, *123*, 1509-1510.

[13] Moreau, J.J.E.; Vellutini, L.; Chi Man, M.W.; Bied, C.; Dieudonné, P.; Bantignies, J.L.; Sauvajol, J.L. *Chem. Eur. J.* **2005**, *11*, 1527-1537.

[14] Usui, T.; Suzuki, S.; Kojima, M.; Nakajima, T.; Ino, J.; Takemura, K. *Mol. Cryst. Liquid Cryst. Sci. Technol.* **1996**, *277*, 575-586.

[15] Mabuchi, T.; Suzuki, S.; Nakajima, T.; Ino, J.; Takemura, K.; Shimizu, E. *J. Photosci.* **1998**, *5*, 105-109.

[16] Corriu, R.J.P.; Mehdi, A.; Reyé, C.; Thieuleux, C. *Chem. Commun.* **2004**, 1440-1441.

[17] Bodoardo, S.; Borello, L.; Fiorilli, S.; Garrone, E.; Onida, B.; Otero Arean, C.; Penazzi, N.; Turnes Palomino, G. *Micropor. Mesopor. Mater.* **2005**, *79*, 275-281.

[18] Tatemichi, M.; Sakamoto, M.; Mizuhata, M.; Deki, S.; Takeuchi, T. *J. Am. Chem. Soc.* **2007**, *129*, 10906-10910.

[19] Mills, A.; Wang, J. *J. Photochem. Photobiol. A: Chem.* **1999**, *127*, 123-134.

[20] Dias, S.L.P.; Fujiwara, S.T.; Gushikem, Y.; Bruns, R.E. *J. Electroanal. Chem.* **2002**, *531*, 141-146.

[21] Yao, H.; Li, N.; Xu, S.; Xu, J.Z.; Zhu, J.J.; Chen, H.Y. *Biosens. Bioelectron.* **2005**, *21*, 372-377.

[22] Satoh, A.Y.; Trosko, J.E.; Masten, S.J. *Environ. Sci. Technol.* **2007**, *41*, 2881-2887.

[23] Liu, C.; Hu, J.; Hu, J.; Tanga, H. *Electroanalysis* **2006**, *18*, 478-484.

[24] Lee, S.K.; Sheridan, M.; Mills, A. *Chem. Mater.* **2005**, *17*, 2744-2751.

[25] Epling, G.A.; Lin, C. *Chemosphere* **2002**, *46*, 561-570.

[26] Chatterjee, D.; Dasgupta, S.; Rao, N.N. *Sol. Energy Mat. Sol. Cells* **2006**, *90*, 1013-1020.

[27] Mills, A.; Lee, S.K. PCT. Int. Appl. **2003**. WO 03/021252 A1.

[28] Lee, S.K.; Mills, A.; Lepre, A. *Chem. Commun.* **2004**, 1912-1913.

[29] Mills, A. *Chem. Soc. Rev.* **2005**, *34*, 1003-1011.

[30] Alpat, S.; Alpat, S.K.; Telefoncu, A. *Anal. Bioanal. Chem.* **2005**, *383*, 695-700.

[31] Kadieva, M.G.; Oganesyan, E.T.; Mutsueva, S.K. *Pharm. Chem. J.* **2005**, *39*, 453-465.

[32] Rajh, T.; Nedeljkovic, J.M.; Chen, L.X.; Poluektov, O.; Thurnauer, M.C. *J. Phys. Chem. B* **1999**, *103*, 3515-3519.

[33] Rajh, T.; Chen, L.X.; Lukas, K.; Liu, T.; Thurnauer, M.C.; Tiede, D.M. *J. Phys. Chem. B* **2002**, *106*, 10543-10552.

[34] Garza, L.; Saponjic, Z.V.; Dimitrijevic, N.M.; Thurnauer, M.C.; Rajh, T. *J. Phys. Chem. B* **2006**, *110*, 680-686.

[35] Xu, C.; Xu, K.; Gu, H.; Zheng, R.; Liu, H.; Zhang, X.; Guo, Z.; Xu, B. *J. Am. Chem. Soc.* **2004**, *126*, 9938-9939.

[36] Fan, X.; Lin, L.; Dalsin, J.L.; Messersmith, P.B. *J. Am. Chem. Soc.* **2005**, *127*, 15843-15847.

[37] Shultz, M.; Reveles, J.U.; Khanna, S.N.; Carpenter, E.E. *J. Am. Chem. Soc.* **2007**, *129*, 2482-2487.

[38] Dimitrijevic, N.M.; Saponjic, Z.V.; Bartels, D.M.; Thurnauer, M.C.; Tiede, D.M.; Rajh, T. *J. Phys. Chem. B* **2003**, *107*, 7368-7375.

[39] Tae, E.L.; Lee, S.H.; Lee, J.K.; Yoo, S.S.; Kang, E.J.; Ion, K.B. *J. Phys. Chem. B* **2005**, *109*, 22513-22522.

[40] Rajh, T.; Saponjic, Z.; Liu, J.; Dimitrijevic, N.M.; Scherer, N.F.; Vega-Arroyo, M.; Zapol, P.; Curtiss, L.A.; Thurnauer, M.C. *Nano Lett.* **2004**, *4*, 1017-1023.

[41] Dimitrijevic, N.M.; Saponjic, Z.V.; Rabatic, B.M.; Rajh, T. *J. Am. Chem. Soc.* **2005**, *127*, 1344-1345.

[42] Garza, L.; Saponjic, Z.V.; Rajh, T.; Dimitrijevic, N.M. *Chem. Mater.* **2006**, *18*, 2682-2688.

[43] Paunesko, T.; Vogt, S.; Lai, B.; Maser, J.; Stojicevic, N.; Thurn, K.T.; Osipo, C.; Liu, H.; Legnini, D.; Wang, Z.; Lee, C.; Woloschack, G.E. *Nano Lett.* **2007**, *7*, 596-601.

[44] Dimitrijevic, N.M.; Poluektov, O.G.; Saponjic, Z.V.; Rajh, T. *J. Phys. Chem. B* **2006**, *110*, 25392-25398.

[45] Gutiérrez-Tauste, D.; Domènech, X.; Hernández-Fenollosa, M.A.; Ayllón, J.A. *J. Mater. Chem.* **2006**, *16*, 2249-2255.

[46] Yu, J.G.; Yu, H.G.; Cheng, B; Zhao, X.J.; Yu, J.C.; Ho, W.K. *J. Phys. Chem. B* **2004**, *107*, 13871-13879.

[47] Brasell, E. *J. Phys. Chem.* **1968**, *72*, 2477-2483.

[48] Zhao, Z.; Malinowski, E.R. *J. Chemometr.* **1999**, *13*, 83-94.

[49] Gessner, F.; Schmitt, C.C.; Neumann, M.G. *Langmuir* **1994**, *10*, 3749-3753.

[50] Heger, D.; Jirkovsky, J.; Klan, P. *J. Phys. Chem. A* **2005**, *109*, 6702-6709.

[51] Jockusch, S.; Turro, N.J.; Tomalia, D.A. *Macromolecules* **1995**, *28*, 7416-7418.

[52] Severino, D.; Junqueira, H.C.; Gugliotti, M.; Gabrielli, D.S.; Baptista, M.S. *Photochem. Photobiol.* **2003**, *77*, 459-468.

[53] Patil, K.; Pawar, R.; Talap, P. *Phys. Chem. Chem. Phys.* **2000**, *2*, 4313-4317.

[54] Mowry, S.; Ogren, P.J. *J. Chem. Ed.* **1999**, *76*, 970-973.

[55] Wellman, W.E.; Noble, M.E. *J. Chem. Ed.* **2003**,*80*, 537-540.

[56] Zeng, Y.; Li, C.; Tang, C.; Zhang, X.B.; Shen, G.; Yu, R. *Electroanalysis* **2006**, *18*, 440-448.

[57] Zhang, F.; Yang, L.; Bi, S.; Liu, J.; Liu, F.; Wang, X.; Yang, X.; Gan, N.; Yu, T.; Hu, J.; Li, H.; Yang, T. *J. Inorg. Biochem.* **2001**, *87*, 105-113.

[58] Liu, J.; Bi, S.; Yang, L.; Gu, X.; Ma, P.; Gan, N.; Wang, X.; Long, X.; Zhang, F. *Analyst* **2002**, *127*, 1657-1665.

[59] Niederberger, M.; Garnweitner, G.; Krumeich, F.; Nesper, R.; Cölfen, H.; Antonietti, M. *Chem. Mater.* **2004**, *16*, 1202-1208.

[60] Ling, T.R.; Syu, Y.Z.; Tasi, Y.C.; Chou, T.C.; Liu, C.C. *Biosens. Bioelectron.* **2005**, *21*, 901-907.

[61] Kiss, T.; Sovago, I.; Martin, B. *J. Am. Chem. Soc.* **1989**, *111*, 3611-3614.

Available online at www.sciencedirect.com
ScienceDirect
Journal of Photochemistry and Photobiology A: Chemistry 187 (2007) 45–52
Journal of Photochemistry and Photobiology A:Chemistry
www.elsevier.com/locate/jphotochem

Characterization of methylene blue/TiO_2 hybrid thin films prepared by the liquid phase deposition (LPD) method: Application for fabrication of light-activated colorimetric oxygen indicators

David Gutiérrez-Tauste [a,*], Xavier Domènech [a], Nieves Casañ-Pastor [b], José A. Ayllón [a]

[a] Chemistry Department, Autonomous University of Barcelona, Campus UAB, Building Cn, 08290 Cerdanyola del Vallès, Barcelona, Spain
[b] Institute of Materials Science (CSIC), Campus UAB, 08290 Cerdanyola del Vallès, Barcelona, Spain

Received 6 July 2006; received in revised form 20 September 2006; accepted 21 September 2006
Available online 30 September 2006

Abstract

Methylene blue (MB)/TiO_2 hybrid nanocomposite material has been successfully deposited on both bare glass and indium tin oxide (ITO) covered glass by the liquid phase deposition (LPD) technique. LPD method is applied to one-step hybrid dye/TiO_2 deposition. An optimized amount of MB is added to the fluoride titania precursor aqueous solution in order to entrap this dye within the growing thin film of TiO_2, yielding a MB/TiO_2 nanocomposite material. Stable, well-adhered, intense blue-colored and optically transparent coatings have been obtained. The formation of the material can be explained by electrostatic interaction between negative charge density at the fluorinated surface of TiO_2 and the cationic dye. MB/TiO_2 nanocomposite material has been characterized by ATR-FT-IR, UV–vis spectroscopy, SEM, TEM, grazing angle XRD and cyclic voltammetry (CV). Deposited hybrid films exhibit photochemical activity: MB is photobleached upon UVA irradiation, using triethanolamine (TEOA) as mild sacrificial electron donor. Moreover, light-activated oxygen indicators with high optical transparency and delayed response can also be satisfactory fabricated by spin-coating a solution of TEOA with an encapsulating polymer (hydroxyethyl cellulose) over the MB/TiO_2 hybrid films.

Keywords: Titanium oxide; Methylene blue; Liquid phase deposition; Hybrid nanocomposite; Light-activated oxygen indicator

1. Introduction

Liquid phase deposition (LPD) is a soft chemical technique first described in the patent literature to deposit titania films [1] and have been successfully applied to the deposition of many oxides. LPD of titania thin films has been studied throroughly by several groups [2–12]. Titanium dioxide (TiO_2) thin films deposited by this method are of interest for diverse applications including deposition of inorganic micropattern on flexible substrates [4], inorganic barrier layer to physically block oxidation of polymeric materials [7], photocatalyst-supported materials [11,12], blocking layer on dye sensitized solar cells [13], or superhydrophilic self-cleaning surfaces [14].

LPD is a process based on the controlled hydrolysis of metallic fluoro-complexes. The dynamic equilibrium exchange established between fluoro and water ligands is displaced towards TiO_2 formation in the presence of a fluoride scavenger such as boric acid. Partially crystallized TiO_2 deposition can be obtained by LPD at relatively low temperature (below 80 °C) [15,16]. Anatase formation is favored in presence of titanium complexing ions such as fluoride, being this phase usually produced by LPD [17]. This wet process allows to deposit TiO_2 over large and complex surfaces without thermal annealing. The key reactions can be expressed as follows:

$$TiF_6^{2-}(aq) + 2H_2O \rightleftarrows TiO_2(s) + 4\,HF(aq) + 2F^-(aq)$$

$$H_3BO_3(aq) + 4HF(aq) \rightarrow BF_4^-(aq) + 3H_2O(l) + H^+(aq)$$

Surface modification of TiO_2 semiconductor particles has gained much attention due to the application of these materials in fields as diverse as electrochromic [17] and photochromic [18] devices, dye-sensitized solar cells [19] and light-induced site-specific DNA redox chemistry [20]. In these applications, transparent conductive materials must be used as substrates for

* Corresponding author. Tel.: +34 93 5812176; fax: +34 93 5812920.
E-mail address: davidg@qf.uab.es (D. Gutiérrez-Tauste).

1010-6030/$ – see front matter © 2006 Published by Elsevier B.V.
doi:10.1016/j.jphotochem.2006.09.011

modified TiO_2 particles films. More than one step is usually required to produce these complex nanostructures: the linking of semiconductor particles to form a more or less porous film and, ideally, the adsorption of a monolayer of the surface modifier. When typical TiO_2 deposition processes as sol–gel or doctor blade are used, post-annealing treatments at 400–500 °C are required to sinterize TiO_2 particles or to induce crystallization [17,21]. Thus, thermolabile substrates cannot be used. On the other hand, the surface modification process is a time consuming step, as TiO_2 films must be put in contact with surface modifier solution for a long period to allow diffusion and equilibration into the intricate porous structure. Development of simpler, low temperature and one-step methods is attractive to advance in the application of hybrid organic-TiO_2 films.

One-step deposition methods for hybrid TiO_2 films are poorly reported in the literature. Electrochromic electrodes were prepared by electrochemical deposition of Prussian Blue in the presence of a suspension of TiO_2 particles [22]. Rhodamine-doped SiO_2/TiO_2 composite films were fabricated by the sol–gel technique with low temperature heat treatment at 150 °C [23]. Organic dyes were entrapped within TiO_2 thin films prepared on conductive substrates by electrodeposition from classical sol–gel titania precursors [24]. Stucky et al. have reported a new fluorocarbon-based synthesis route for hybrid rhodamine/TiO_2 mesostructured optical materials for waveguided photoluminescence emission device [25]. Recently, Deki et al. have reported the deposition of alkyl sulfate and alkylbenzene sulfonate surfactants/TiO_2 [26] and copper phthalocyanine/TiO_2 [27] hybrid films by the LPD method. Hu et al. have reported molecularly imprinted TiO_2 thin films by LPD for the determination of L-glutamic acid [28]. However, one-step hybrid film deposition has been described for other transition oxides such as ZnO [29,30] and SiO_2 [31,32].

Methylene blue (MB) is a cationic dye whose redox formal potential, comprised between 0.08 and −0.25 V (versus SCE) in solution with pH 2–8, respectively, is close to those of several biomolecules [33]. MB has been widely used for electrochemical applications, for example, as catalyst/mediator in electrochemical biosensors [33]. Moreover, TiO_2 has been satisfactory sensitized with MB for photodegradation of various halocarbons using visible light [34]. Recently, a mixture of commercial TiO_2 powder and MB has been used to fabricate an intelligent ink sensible to oxygen [35,36]. Oxygen allows to grow aerobic microorganism during food storage, being the main cause of most food-spoilage. There is an increasing interest to develop inexpensive, non-toxic and irreversible oxygen sensors in fields as modified atmosphere food (MAP) packaging to assure oxygen absence [35,36].

Here, we report, for the first time, an one-step route to entrap MB with TiO_2 chemically deposited in situ by the LPD technique. MB/TiO_2 resulting films consist of anatase nanocrystals with adsorbed MB molecules. MB/TiO_2 nanocomposite hybrid films were characterized by ATR-FT-IR, UV–vis spectroscopy, SEM, TEM, grazing angle XRD and cyclic voltammetry (CV). Photochemical activity of the films were tested and light-activated oxygen indicators were satisfactory fabricated from the deposited nanocomposite material.

2. Experimental section

2.1. Reagents

Ammonium hexafluorotitanate, boric acid, methylene blue (MB) and hexafluorotitanic acid were analytical grade (Aldrich, Panreac) and used as received without further purification. Acetone and ethanol (Panreac) were used for substrate cleaning. TiO_2 Degussa P-25 (80% anatase–20% rutile) was kindly provided by Degussa (Spanish branch). Deionized water from a Milli-Q system (Millipore, conductivity <0.05 μS/cm) was used both in solution preparation and cleaning procedures.

2.2. Substrates

The substrates used were ITO (In_2O_3:Sn) conducting glass, 13–18 Ω/sq, 1.1 mm thick (Optical Filters) and bare glass (microscope slides, IDL). Substrates were cleaned just before performing the deposition process [15]. Glass slides were sequentially immersed for 15 min in boiling 50% sulfuric acid and 15 min in boiling water, followed by 5 min ultrasonic cleaning in acetone, then absolute ethanol and finally water. ITO-glass substrates were subjected to 5 min ultrasonic cleaning in acetone, then in absolute ethanol, then in 30% nitric acid for 1 min and finally in water 5 more min.

2.3. Deposition of TiO_2 films

TiO_2 films were deposited on both, glass slides and ITO-covered glass, according to LPD procedure described in our previous work [15]. These samples were used for comparative purposes. Bare glass substrates were pretreated in a 0.10 mM H_2TiF_6 solution, with pH adjusted to 3.2 using diluted NH_3, at 80 °C for 30 min. After this pretreatment, the substrate was sonicated in water and used immediately. Substrates were placed vertically into a polyethylene vessel containing the fresh precursor solution (10 mM $(NH_4)_2TiF_6$ and 30 mM H_3BO_3, pH adjusted to 2.8 using diluted $HClO_4$). The whole was sonicated for 1 min and kept at 80 °C for 3 h. After deposition, films were gently washed with water and dried with a nitrogen gas flow.

2.4. Deposition of MB/TiO_2 films

In this case, both substrates had to be pretreatred. Bare glass slides were pretreated as in the former case. ITO-glass substrates were pretreated for 1 h at 80 °C in an aqueous solution 10 mM $(NH_4)_2TiF_6$ and 30 mM H_3BO_3 at natural pH of 3.6. In both cases, substrates were sonicated after the pretreatment and the subsequent deposition process were also performed immediately. The optimized precursor bath consisted of 10 mM $(NH_4)_2TiF_6$, 30 mM H_3BO_3 and 0.5 mM MB; its initial pH was adjusted to 2.8 with diluted $HClO_4$. A range of MB concentrations between 0.1 mM and 2 mM were also tried. The substrates were immersed in the bath, sonicated for 1 min, and kept at 80 °C for 4.5 h. After LPD process, samples were also gently washed with water and dried with a nitrogen gas flow.

2.5. Characterization

ATR-FT-IR spectrums were performed with a Bruker apparatus (Tensor model equipped with MKII Golden Gate). TiO_2 powder samples from the films were obtained by scrapping the coating off. UV–vis absorbance data were obtained with a Helios series γ spectrophotometer (Bonsai Technologies), using the respective bare substrate as the blank. Films surface characteristics were investigated by SEM on gold covered samples, using a Hitachi S-570 microscope (operating voltage, 10–30 kV). For thickness measurements, samples were cut into pieces which results in breaking the TiO_2 film near the cut edge of the substrate. Films thickness was studied in these edges, taking into consideration the sample inclination with respect to the electron beam. Electron diffraction patterns and transmission electron microscopy (TEM) images were recorded in a JEOL 2011 microscope that was operated at 200 kV. Energy dispersive spectroscopy (EDS) X-ray microanalysis were carried out using an INCA-X detector (Oxford Instruments). XRD spectra were registered on a Philips X'Pert diffractometer equipped with a monochromator and using Cu Kα radiation ($\lambda = 0.154056$ nm). In order to increase the sensitivity of the thin film signal, a grazing incident configuration was used (2.0°). Cyclic voltammetry (CV) studies were carried out on an EG&G PAR 273A potentiostat/galvanostat at room temperature. A three-electrode electrochemical cell were used on a single compartment: MB/TiO_2 films deposited on ITO-covered glass were used as working electrode (a Cu foil-Sn clad conductive tape with an Ag adhesive (BDF Tesa) was employed to assure good electrical contact on ITO), a platinum wire (1 mm diameter) served as counter electrode and a Ag/AgCl double bridged (1 M KCl) electrode was used as the reference. The electrolyte was a 0.25 M aqueous solution of tetrabutylammonium chloride (TBACl) with pH adjusted to 2.5 with diluted hydrochloric acid. Cathodic run and anodic run were performed at scan rate of 5 and 10 mV/s, respectively. Argon was flowed through the electrolyte solution just before performing the CV.

To test the adhesion and stability of the MB/TiO_2 films ultrasound disruption was used: coated substrates were immersed completely in a beaker with water and sonicated for 5 min (Ultrasonic bath Selecta, 50 W). For comparison purposes, MB were adsorbed on TiO_2 Degussa P-25 from a suspension 10 mM TiO_2 P-25 and 0.5 mM MB. The initial pH was adjusted to 2.8 with diluted $HClO_4$ and the suspension was kept at 80 °C for 4.5 h. The powder obtained was separated by centrifugation, washed with deionized water and dried at 60 °C.

UV-activated colorimetric oxygen indicators devices were fabricated using MB/TiO_2 films deposited on glass. An upper layer of triethanolamine (TEOA) embedded in hydroxyethyl cellulose (HEC) polymer were spin-coated at 1000 rpm for 5 min, using an aqueous solution of 7.5 g TEOA and 2.5 g HEC in 50 ml of water. Photobleaching experiments were carried out upon exposure of UVA light from a 6 W Phillips black light (held 2.5 cm away) on both MB/TiO_2 oxygen sensors and MB/TiO_2 bare coatings (immersed in a 0.1 M TEOA aqueous solution). Lamp intensity at the coatings was 1.4 mW/cm^2, measured using a UV radiometer Lutron UVA-365. Samples photobleaching were followed by UV–vis absorbance spectra in the 400–800 range.

3. Results and discussion

3.1. MB/TiO_2 films preparation and characterization

Our first goal was to find bath compositions and substrate preparation procedures that allow to obtain optically transparent and well adhered coatings of a MB/TiO_2 nanocomposite material, that is TiO_2 nanocrystals grown on the substrate with MB modifier adsorbed on their surface. For that purpose, several assays varying MB concentrations in the LPD precursor bath were carried out.

It is important to remark that high coating thickness covering the substrate or excessive MB incorporation within the TiO_2 growing film impede the deposition of well adhered coatings. In addition, to guarantee its further use in several applications it is desirable that all TiO_2 nanoparticles are directly connected between them. On the other hand, at very low MB concentration, its incorporation into the coating is very poor and thus practically almost pure TiO_2 film is obtained. Using an optimized 0.5 mM MB concentration in the precursor bath, uniform intense blue-colored films were obtained without TiO_2 homogeneous precipitation. Films adhesion and MB desorption were tested using ultrasound disruption.

In fact, the actual MB concentration in solution is slightly lower than the nominal one due to the formation of a flocculent violet precipitate corresponding to the perchlorate salt of MB cation that is less soluble that the chloride salt used as starting. This precipitate was observed in the LPD precursor bath just after adjusting initial pH to 2.8 with diluted perchloric acid. $MBClO_4$ was also identified by IR spectroscophy (Fig. 1d) [37]. Although the formation of this precipitate can be prevented by using a different acid to adjust the pH of the bath, experimental

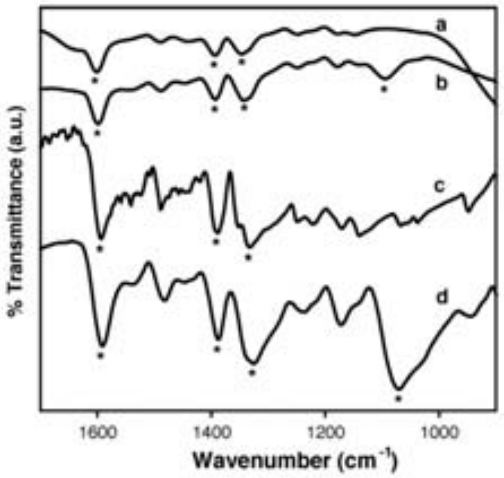

Fig. 1. ATR-FT-IR spectra of: (a) MB/TiO_2 film scrapped off, (b) MB adsorbed on Degussa P-25, (c) commercial MB, and (d) $MBClO_4$ precipitate from the LPD solution after MB/TiO_2 film deposition. Mean absorption peaks are also marked with '*'.

results show that this precipitate, that remain at the bottom of the container does not interfere with the formation of an uniform coating. A set of additional experiments were performed avoiding the precipitation of the perchlorate salt of MB, using dye concentrations near the reported solubility value for $MBClO_4$ ($1–3 \times 10^{-5}$ M) [44] and adjusting the pH of the bath to 2.8 with HCl. In these experiments, no satisfactory hybrid film deposition was observed, suggesting that precipitated $MBClO_4$ allow to preserve a MB concentration during the LPD process. Moreover, the existence of an optimal MB concentration suggest that $MBClO_4$ redisolution when MB soluble is incorporated within the TiO_2 film can be limited kinetically.

TiO_2 prepared by LPD process present a high degree of surface fluorination (≡Ti–F) [10,15]. The fluoride chemisorption is favored at acidic pH (maximum of approximately 99% at pH 3–4) and greatly reduces the positive surface charge on TiO_2 by replacing $\equiv Ti–OH_2^+$ by ≡Ti–F species [38]. Due to the great affinity of fluoride for the TiO_2 surface, MB direct adsorption on the oxide surface is avoided in a high fluorinated surface.

Characteristic infrared absorption peaks of MB [33,39] (Fig. 1c) at ~1600 cm^{-1} (ring stretch), ~1390 cm^{-1} (C–N symmetric stretch) and ~1335 cm^{-1} (–CH_3 symmetric deformation) appear in the MB/TiO_2 nanocomposite material (Fig. 1a). MB/TiO_2 and MB adsorbed on Degussa P-25 present almost the same IR spectra (Fig. 1a and b, respectively). The only difference is the peak at ~1087 cm^{-1} of P-25/MB powder, associated to stretching vibrations of perchlorate anion [37] and is not observed in the MB/TiO_2 fluorinated material. These results point to a similar adsorption mode for the cationic dye on both a clean and a fluorinated surface. It is thought therefore, that the electrostatic interaction between negative density charge at the TiO_2 fluorinated surface generated during the LPD process and the cationic dye ($(\equiv Ti\text{-}F^{\delta-}:::MB^+)$) will be the force responsible of MB adsorption, yielding the final MB/TiO_2 nanocomposite material.

The intense coloration of the MB/TiO_2 hybrid films deposited suggest that the nanocomposite contains dye molecules in a high concentration. MB adsorbed on clean (non-fluorinated) TiO_2 surface desorbs quickly in an aqueous medium. However, MB of MB/TiO_2 films only desorbs appreciably after approximately 10 days of immersion in water, even if an electrolyte salt is added to the medium, i.e. KCl, NaCl, NH_4Cl or Na(OOC–H_3C). A reference experiment trying to incorporate MB from an aqueous solution to a TiO_2 blank film also obtained by LPD over one night showed very low MB adsorption.

UV–vis optical absorption of a typical MB/TiO_2 film presents a non-symmetrical peak with a maximum at 580 nm and a shoulder at approximately 700 nm (Fig. 2). The shift towards shorter wavelength, with respect to the MB monomer (λ_{max} = 664 nm), clearly denotes that MB cations are aggregated. The position of the maximum and the shape of the signal suggest that MB is mainly present as trimers, while the presence of monomers is significantly low [40–43]. Performance studies of oxygen indicators fabricated using MB/TiO_2 films confirm that MB cations are aggregated (see discussion of Fig. 6 in Section 3.2). On the other hand, UV–vis spectrum of the deposition bath shows mainly presence of monomer, according to the $MBClO_4$ solubility in water reported [44] ($1–3 \times 10^{-5}$ M) and taking into account that formation of MB aggregates is reported for [MB] $>10^{-4}$ to 10^{-3} M [41]. Self-aggregation is then favored by adsorption and concentration within the film. The aggregation of MB and the consequent hypsochromic shift of the visible spectra has been reported when cationic dyes are adsorbed on negatively charged surfaces [45,46]. In the MB/TiO_2 nanocomposite material, the TiO_2 nanocrystals can wear a neat negative charge due to excess fluoride adsorbed on the titania surface that counteract the positive charge of the MB cations. Thus, most probably, the dye is adsorbed on the fluoride layer and not directly on the oxide surface. The base line of MB/TiO_2 spectrum shows a slight decrease of transmittance with respect the case of TiO_2 (compare in the 400–450 nm interval), due to some degree of light dispersion as consequence of the film morphology.

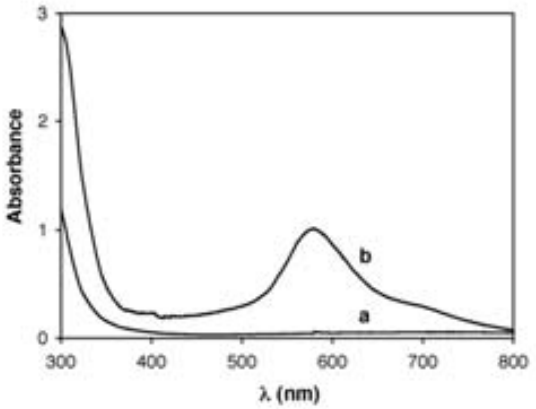

Fig. 2. Typical UV–vis absorption spectra of films deposited on glass slides by LPD: (a) TiO2 and (b) MB/TiO_2.

Surface morphology and thickness of MB/TiO_2 hybrid films deposited on glass slides were studied by SEM (Fig. 3a and b). MB/TiO_2 films show dense and compact substrate coverage, nevertheless their film surface are slightly waved. However, MB/TiO_2 samples show no cracks and present high optical transparency (see Fig. 2, absorbance UV–vis). The particle size in the MB/TiO_2 samples is in the 15–50 nm range, being clearly lower with respect to TiO_2 samples [15]. An average deposition rate of 105 nm/h is estimated taking into account the films thickness (Fig. 3b) and the deposition time in MB/TiO_2 samples. For comparison, a deposition rate of 85 nm/h was reported for TiO_2 films in our previous work [15]. SEM observations point that MB adsorption on the fluorinated TiO_2 surface limit the particle size of the new material and also increase slightly the average deposition rate of the film.

To improve our understanding of the MB/TiO_2 hybrid nanocomposite material, TEM and selected-area electron diffraction (SAED) studies were carried out (Supporting Information). The film studied was deposited using a 1 mM MB concentration in the deposition bath in order to obtain a coating with less adherence. Film was sonicated for 15 min in ethanol to detach nanocomposite aggregates of appropriate size to be observed by TEM. The diffraction pattern indicates a polycrystalline structure with diffraction rings corresponding to lattice

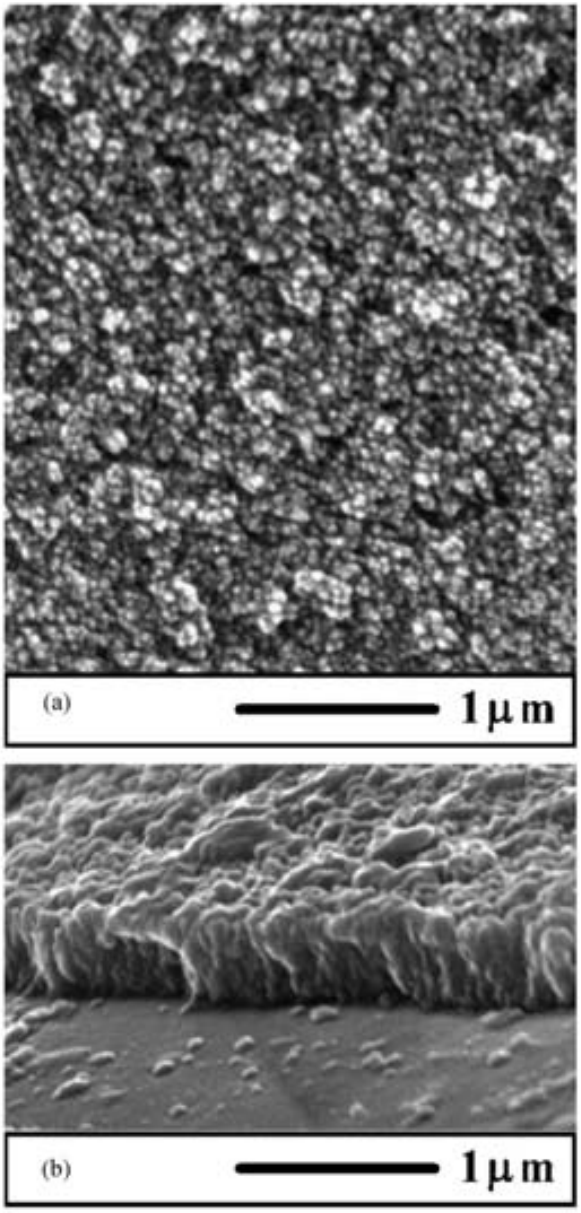

Fig. 3. SEM photographs showing surface morphology (a) and film thickness (b) of MB/TiO_2 samples deposited on glass by LPD.

spacings of 3.5 and 2.4 Å that are assigned to (1 0 1) and (0 0 4) reflections of anatase TiO_2 (JCPDS pattern 21–1272). These lattice fringes of the anatase grains are easily distinguished in the corresponding TEM image. The associated EDS microanalysis (Supporting Information) show a sulfur atomic percentage of approximately 2%. Taking into account that every MB molecule only have one sulfur atom, microanalysis results point the incorporation of the dye at high concentration within the film.

X-ray diffraction of TiO_2 and MB/TiO_2 films deposited on glass slides are shown in Fig. 4, revealing peaks that may be assigned to the anatase structure. It is well known that anatase is the TiO_2 phase usually favored by LPD, due to the presence of

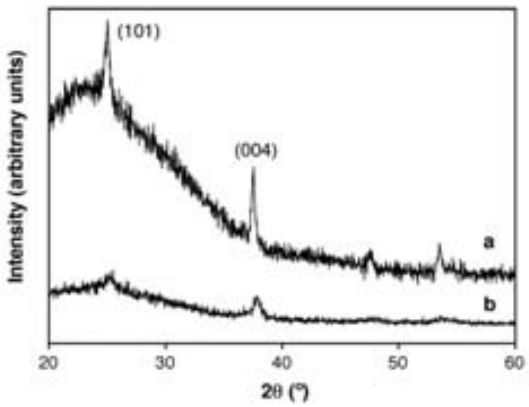

Fig. 4. Grazing-incidence XRD diffractogram of films deposited on glass slides by LPD: (a) TiO_2 and (b) MB/TiO_2.

titanium strongly complexing ions such as the fluoride [6,15,16]. Relative intensities of the peaks differ noticeable respect to the anatase standard (JCPDS pattern 21–1272), corresponding to complete random order. Thus, the standard presents a relative intensity of 5:1 for the (1 0 1) and the (0 0 4) peaks. However, in the diffractrograms obtained, the relative intensity of the (0 0 4) signal appears notably increased. Preferential *c* axis orientation has been reported previously both for TiO_2 films and powders prepared by LPD, and has been attributed to the preferential adsorption of fluoride to planes parallel to this direction [7,8]. On the other hand, although MB/TiO_2 films are thicker than TiO_2 ones, their diffraction signals are weaker and wider. In addition, while MB/TiO_2 films present approximately a 2:1 relative intensity for (0 0 4) and (1 0 1) signals, the TiO_2 samples only present a 1:1 ratio. XRD results confirm that MB adsorption on fluorinated surface of the new material is favored, limiting the size of anatase crystallites (and also decreasing the main particle size as was observed by SEM) and yielding more oriented films.

3.2. Photochemical activity: light-activated oxygen indicators

A set of preliminary experiments were performed to evaluate the photochemical activity of the new material. MB/TiO_2 films were immersed in a TEOA solution and were UV-irradiated. In these experiments, electron–hole pairs are generated in the semiconductor particles. Photogenerated holes are able to oxidize irreversibly the TEOA mild sacrificial electron donor while photogenerated electrons reduce the MB dye to its leuco form. Upon irradiation with UVA light, under aerobic or anaerobic conditions, initial highly blue-colored samples were completely bleached showing excellent transparency. Samples remain indefinitely bleached in the absence of oxygen, whereas blue color begin to return as soon as ambient oxygen reoxidize leuco-MB. Maximum coloration recovery is attained after approximately 1 h under ambient conditions. It is important to remark that MB desorption in the TEOA solution is not observed in any case.

UV-activated colorimetric oxygen indicators devices were satisfactory fabricated from MB/TiO_2 films, by spin-coating a TEOA solution containing HEC as encapsulating polymer over

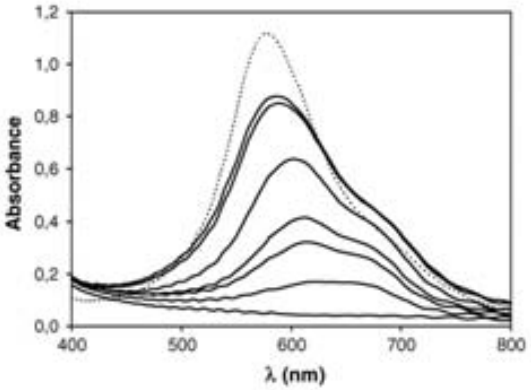

Fig. 5. Absorbance changes in a typical MB/TiO_2 UV-activated oxygen indicator between 400 and 800 nm, after different times under ambient conditions (solid line from bottom to top): 0, 4, 8, 12, 24, 48 and 72 h, respectively. Initial spectra of the non-activated TiO_2/MB oxygen indicator is also included (dotted line).

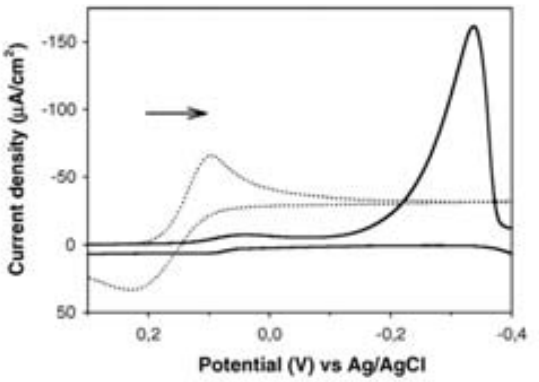

Fig. 6. Typical CV of MB/TiO_2 films deposited on ITO-coated glass (solid line) and CV of the blank experiment with MB in solution (dotted line). Electrolyte: 0.25 M TBACl; cathodic scan rate: 5 mV/s; anodic scan rate: 10 mV/s.

the nanocomposite material in an analogous way to intelligent inks previously reported by Mills et al. [35,36] MB/TiO_2 oxygen indicators are UV-activated (totally bleached state) in an irradiation time of 18 to 48 h. The low photocatalytic activity of the TiO_2 deposited due to its low crystallinity seems to increase the irradiation time required to activate the indicator. A decrease in activation time is expected using UVA lamps with higher power.

Leuco-MB reoxidation under ambient atmospheric conditions was studied following evolution of the UV–vis spectra (Fig. 5, solid lines). Displacement of the maximum of the peak to shorter wavelengths as reoxidation advance denotes reaggregation of MB. MB/TiO_2 sensors show a delayed response to oxygen presence, pointing a slow oxygen diffusion through the indicator. A delayed response of the indicator could be useful to estimate the exposition time to air [36]. Maximum absorbance recovery at 580 nm is typically 75–80% with respect to the initial absorbance (Fig. 5, dotted line). However, spectra corresponding to a reoxidized sample after 48 or 72 h under ambient conditions present higher MB monomer absorbance at 664 nm than the original spectra, indicating a higher amount of monomer. Therefore, the change in absorbance spectra is due to a different distribution of aggregates rather than to partial decomposition. It must be considered that molecular diffusion of MB may be prevented or made more difficult because of the solid nature of the MB/TiO_2 nanocomposite. Minor MB direct photolysis can also partially account for the spectra variations [47]. Therefore, although MB/TiO_2 oxygen indicators can be reused there are minor variations after each cycle, pointing a limited stability of the device.

3.3. Cyclic voltammetry experiments

MB/TiO_2 films were also satisfactory prepared on a conductive substrate, i.e. ITO-covered glass. While regular and dense TiO_2 coatings were deposited on ITO without any pretreatment [14], only hazy and low-colored MB/TiO_2 samples could be obtained on ITO substrate. Pretreatment of the surface is absolutely necessary to prepare MB/TiO_2 coatings on ITO; MB adsorption on ITO seems to make difficult the nucleation of TiO_2 particles. Thus, a preliminary seed process is required to assure enough TiO_2 nucleation sites density before the deposition process. Otherwise, only a partial substrate coverage can be attained and low-transparency samples are obtained. Modification of the substrate upon treatment is too slight to be clearly measured or identified by the characterization techniques used in this work.

Cyclic voltammetry (CV) experiments of MB/TiO_2 films deposited on ITO-covered glass (Fig. 6, solid line) show redox activity, evidencing the electroactive properties of the nanocomposite material. Two cathodic waves that shift their potential value upon repeated cycling are observed, showing the irreversibility of the electrochemistry of the MB/TiO_2 nanocomposite material in the CV time scale. A couple of cathodic/anodic peaks of marginal current density is seen with a midpoint potential of approximately +70 mV. A CV blank experiment of dissolved MB using ITO as electrode (Fig. 6, dotted line) show a cathodic/anodic couple with a midpoint potential of +163 mV. Taking into account that only MB monomers are expected in the TBAC1 solution [48], the couple has to be assigned to MB redox activity in the monomer form. In addition, Garrone et al. observed a similar couple in CV of MB solutions using a paste graphite electrode and ascribed it to traces of MB in the salt form, strongly interacting with its chloride counted on physisorbed on carbon grains [49]. Therefore, the marginal couple in the MB/TiO_2 nanocomposite have to be ascribed to MB traces in the salt form on the ITO surface. However, the marginal anodic peak in the nanocomposite is preferably observed at higher scan rates (10 mV/s) than the cathodic one (5 mV/s), suggesting that reoxidation of traces of this MB salt form is a faster process.

A second cathodic wave of high current density at −338 mV versus Ag/AgCl is seen in the MB/TiO_2 material (Fig. 6, solid line). This cathodic signal is assigned to MB reduction in the MB/TiO_2 nanocomposite and, consequently, total bleaching of the film is observed. The MB reduction potential is noticeably increased in the nanocomposite with respect to the MB reduction of the monomer form in solution seen in the blank experiment ($E_{cathodic}$ = +96 mV, dotted line in Fig. 6). Different facts can contribute to difficult the MB reduction in the nanocomposite:

MB self-aggregation, MB electrostatic interaction on the fluorinated TiO_2 surface or the low conductivity of the TiO_2 due to its semiconductor nature. The main reduction peak in the MB/TiO_2 nanocomposite presents a non-symmetrical appearance, also suggesting irreversibility of the MB reduction process in the time scale studied. The anodic couple of this main MB cathodic peak is not present in the 0.5–10 mV/s scan rate range studied, pointing the leuco-MB reoxidation cannot be accelerated electrochemically. While after the cathodic run total bleaching of the MB/TiO_2 electrode is observed due to reduction of the greater part of the MB molecules, after the anodic run only a slight blue coloration can be distinguished in the electrode that can be assigned to the secondary oxidation process of the MB salt form. However, under atmospheric conditions blue coloration returned to the film after the CV experiment and self-aggregation of MB is also observed by UV–vis spectroscopy.

It has also been observed that electrolytic reduction of MB induces its desorption from the coating, with clear evidence of electrolyte-blue coloring after oxidation. MB desorption values of 1.5–4 $\times 10^{-9}$ mol/cm^2 are estimated by UV–vis spectroscopy in the electrolyte solution considering that only MB monomers are present ($\varepsilon_{664} = 9 \times 10^{-4}\,M^{-1}\,cm^{-1}$) [41]. Air was flowed through the electrolyte solution to assure leuco-MB reoxidation to MB form. No MB readsorption is observed in CV experiments time scale. Therefore, the absence of the main MB anodic peak could be attributed to a very slow electrochemical oxidation kinetics and changes in the interaction among the electroactive MB molecules and the fluorinated TiO_2 surface, that favor the MB desorption after the cathodic run. It must be remembered that no MB desorption was observed in photobleaching experiments using TEOA as sacrificial electron donor (see Section 3.2, *Photochemical activity*). MB/TiO_2 nanocomposite seems to follow different redox mechanisms in CV electrochemical processes with respect to photochemical reduction and chemical oxidation by atmospheric oxygen.

4. Conclusions

MB/TiO_2 nanocomposite thin films have been successfully prepared by LPD on both bare glass and ITO-covered glass, concluding that new applications of LPD method are possible in the field of the preparation of organic-inorganic hybrid thin films. High concentrations of MB are incorporated in the new nanocomposite material, yielding stable, well-adhered, intense blue-colored and optically transparent coatings. MB adsorption on the fluorinated TiO_2 surface promotes MB aggregation, limits the size of anatase crystallites and the main particle of the nanocomposite, while slightly increases the average deposition rate of the film. The results seem to be reasonably explained by continuous electrostatic interaction among negative density charges at the fluorinated surface and the cationic dye molecules during the LPD process. The MB/TiO_2 films exhibit photochemical activity respect to the oxidation of TEOA mild sacrificial electron donor upon UVA irradiation. Light-activated oxygen indicators with high optical transparency and delayed response can also be satisfactory fabricated from the MB/TiO_2 hybrid films. CV experiments show irreversible redox activity of the MB/TiO_2 nanocomposite in the time scale studied and provide indications that different mechanisms can take place in CV electrochemical processes (MB desorption) with respect to photochemical reduction and chemical oxidation by atmospheric oxygen (non MB desorption).

Acknowledgements

This work has been financed by the Spanish National Plan of Research (BQU2003-01280 project). We thank Jose Manuel Amigo for useful discussion about the UV–vis spectra.

Appendix A. Supplementary data

Supplementary data associated with this article can be found, in the online version, at doi:10.1016/j.jphotochem.2006.09.011.

References

[1] H. Kawahara, H. Honda, Japanese Patent 59141441 A (Nippon Sheet Glass), August 14, 1984.
[2] S. Deki, Y. Aoi, O. Hirió, A. Kajinami, Chem. Lett. 6 (1996) 433–434.
[3] H.Y.Y. Ko, M. Mizuhata, A. Kajinami, S. Deki, J. Flu. Chem. 120 (2003) 157–163.
[4] A. Dutschke, D. Diegelmann, P. Löbmann, J. Mater. Chem. 13 (2003) 1058–1063.
[5] Y. Masuda, T. Sugiyama, W.S. Seo, K. Koumoto, Chem. Mater. 15 (2003) 2469–2476.
[6] H. Pizem, C.N. Sukenik, U. Sampathkumaran, A.K. McIlwain, M.R. De Guire, Chem. Mater. 14 (2002) 2476–2485.
[7] H. Pizem, O. Gershevitz, Y. Goffer, A.A. Frimer, C.N. Sukenik, U. Sampathkumaran, X. Milhet, A. McIlwain, M.R. De Guire, M.A.B. Meador, J.K. Sutter, Chem. Mater. 17 (2005) 3205–3213.
[8] A.M. Peiró, E. Vigil, J. Peral, C. Domingo, X. Domènech, J.A. Ayllón, Thin Solid Films 411 (2002) 185–191.
[9] J.A. Ayllón, A.M. Peiró, L. Saadoun, E. Vigil, X. Domènech, J. Peral, J. Mater. Chem. 11 (2000) 1911–1914.
[10] J.G. Yu, H.G. Yu, B. Cheng, X.J. Zhao, J.C. Yu, W.K. Ho, J. Phys. Chem. B 107 (2004) 13871–13879.
[11] B. Herbig, P. Löbmann, J. Photochem. Photobiol. A: Chem. 163 (2004) 359–365.
[12] H. Yu, S.C. Lee, J. Yu, C.H. Ao, J. Mol. Catal. A: Chem. 246 (2005) 206–211.
[13] I. Zumeta, B. González, R. Espinosa, J.A. Ayllón, E. Vigil, Semicond. Sci. Technol. 19 (2004) L52–L55.
[14] (a) X.P. Wang, Y. Yu, X.F. Hu, L. Gao, Thin Solid Films 371 (2000) 148–152;
(b) Y. Gao, Y. Masuda, K. Koumoto, Langmuir 20 (2004) 3188–3194.
[15] D. Gutiérrez-Tauste, X. Domènech, M.A. Hernández-Fenollosa, J.A. Ayllón, J. Mater. Chem. 16 (2006) 2249–2255.
[16] (a) T.P. Niessen, M.R. De Guire, Solid State Ionics 151 (2002) 61–68;
(b) Y. Gao, K. Koumoto, Cryst. Growth Des. 5 (2005) 1983–2017.
[17] S.Y. Choi, M. Mamak, N. Coombs, N. Chopra, G.A. Ozin, Nano Lett. 4 (2004) 1231–1235.
[18] M. Biancardo, R. Argazzi, C.A. Bignozzi, Inorg. Chem. 44 (2005) 9619–9621.
[19] M. Grätzel, Nature 414 (2001) 338–344.
[20] T. Rajh, Z. Saponjic, J. Liu, N.M. Dimitrijevic, N.F. Scherer, M. Vega-Arroyo, P. Zapol, L.A. Curtiss, M.C. Thurnauer, Nano Lett. 4 (2004) 1017–1023.
[21] D. Gutiérrez-Tauste, I. Zumeta, E. Vigil, M.A. Hernández-Fenollosa, X. Domènech, J.A. Ayllón, J. Photochem. Photobiol. A: Chem. 175 (2005) 165–171.

[22] M. Nishizawa, S. Kuwabata, H. Yoneyama, J. Electrochem. Soc. 143 (1996) 3462–3465.
[23] H. Yanagi, T. Hishiki, T. Tobitani, A. Otomo, S. Mashiko, Chem. Phys. Lett. 292 (1998) 332–338.
[24] R. Shacham, D. Avnir, D. Mandler, J. Sol–Gel Sci. Technol. 31 (2004) 329–334.
[25] M.H. Bartl, S.W. Boettcher, E.L. Hu, G.D. Stucky, J. Am. Chem. Soc. 126 (2004) 10826–10827.
[26] L. Li, M. Mizuhata, S. Deki, Appl. Surf. Sci. 239 (2005) 292–301.
[27] L. Li, M. Mizuhata, A. Kajinami, S. Deki, Synth. Met. 146 (2004) 17–27.
[28] L. Feng, Y. Liu, J. Hu, Langmuir 20 (2004) 1786–1790.
[29] T. Oekermann, T. Yoshida, H. Minoura, K.G.U. Wijayantha, L.M. Peter, J. Phys. Chem. B 18 (2004) 8364–8370.
[30] T. Pauporté, F. Bedioui, D. Lincot, J. Mater. Chem. 15 (2005) 1552–1559.
[31] T. Mabuchi, S. Satoshi, T. Nakajima, J. Ino, K. Takemura, E. Shimizu, J. Photosci. 5 (1998) 105–109.
[32] T. Usui, S. Suzuki, M. Kojima, T. Nakajima, J. Ino, K. Takemura, Mol. Cryst. Liquid Cryst. Sci. Technol. 277 (1996) 215–226.
[33] H. Yao, N. Li, S. Xu, J.Z. Xu, J.J. Zhu, H.Y. Chen, Biosens. Bioelectron. 21 (2005) 372–377.
[34] D. Chatterjee, S. Dasgupta, N.N. Rao, Sol. Energy Mater. Sol. C 90 (2006) 1013–1020.
[35] S.K. Lee, A. Mills, A. Lepre, Chem. Commun. (2004) 1912–1913.
[36] S.K. Lee, M. Sheridan, A. Mills, Chem. Mater. 17 (2005) 2744–2751.
[37] K. Nakamoto, Infrared and Raman Spectra of Inorganic and Coordination Compounds. Part A: Theory and Applications in Inorganic Chemistry, 5th ed., Wiley-Interscience, New York, 1997.
[38] H. Park, W. Choi, J. Phys. Chem. B 108 (2004) 4086–4093.
[39] Y. Yan, M. Zhang, K. Gong, L. Su, Z. Guo, L. Mao, Chem. Mater. 17 (2005) 3457–3463.
[40] E. Brasell, J. Phys. Chem. 72 (1968) 2477–2483.
[41] Z. Zhao, E.R. Malinowski, J. Chemometr. 13 (1999) 83–94.
[42] F. Gessner, C.C. Schmitt, M.G. Neumann, Langmuir 10 (1994) 3749–3753.
[43] D. Heger, J. Jirkovsky, P. Klan, J. Phys. Chem. A 109 (2005) 6702–6709.
[44] A.K. Ghosh, P. Mukerjee, J. Am. Chem. Soc. 92 (1970) 6413–6415.
[45] S. Jockusch, N.J. Turro, D.A. Tomalia, Macromolecules 28 (1995) 7416–7418.
[46] D. Severino, H.C. Junqueira, M. Gugliotti, D.S. Gabrielli, M.S. Baptista, Photochem. Photobiol. 77 (2005) 459–468.
[47] A. Mills, J. Wang, J. Photochem. Photobiol. A: Chem. 127 (1999) 123–134.
[48] K. Patil, R. Pawar, P. Talap, Phys. Chem. Chem. Phys. 2 (2000) 4313–4317.
[49] S. Bodoardo, L. Borello, S. Fiorilli, E. Garrone, B. Onida, C. Otero-Areán, N. Penazzi, G. Turnes-Palomino, Micropor. Mesopor. Mater. 79 (2005) 275–281.

Supplementary data 1

TEM and associated SAED of the MB/TiO_2 nanocomposite material. Planes assignation are also included.

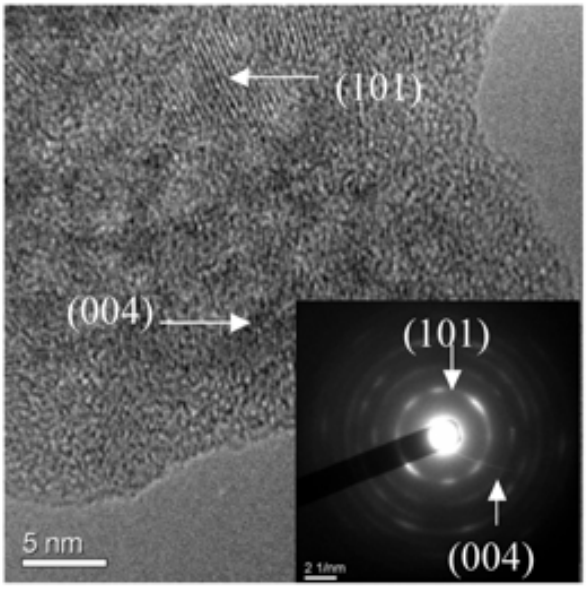

Supplementary data 2

Energy Dispersive Spectroscopy (EDS) X-ray microanalysis of the selected area in the MB/TiO_2 sample shown in supplementary data 1.

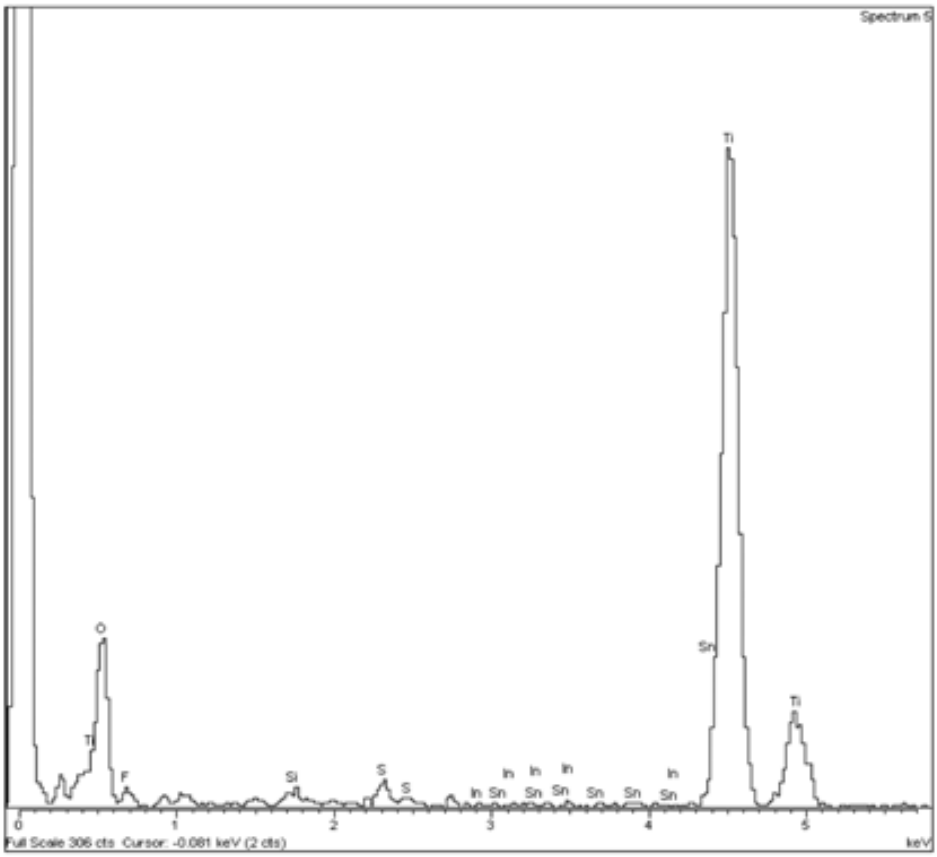

Spectrum processing :
Peak possibly omitted : 8.038 keV

Quantitation method : Cliff Lorimer thin ratio section.
Processing option : All elements analyzed (Normalised)
Number of iterations = 1

Standardless

Element	Peak Area	Area Sigma	k factor	Abs Corrn.	Weight%	Weight% Sigma	Atomic%
O K	256	38	1.810	1.000	17.75	2.25	38.67
F K	18	15	1.574	1.000	1.10	0.90	2.03
Si K	19	13	1.000	1.000	0.72	0.50	0.90
S K	49	17	0.940	1.000	1.75	0.61	1.90
Ti K	1913	70	1.050	1.000	76.91	2.82	55.97
In L	13	22	1.782	1.000	0.92	1.48	0.28
Sn L	12	21	1.818	1.000	0.85	1.48	0.25
Totals					100.00		

Supplementary data 3

Representation of the proposed growth mechanism of the *c* axis oriented MB/TiO_2 nanocomposite material, where a planar representation of the MB cationic dye is used.

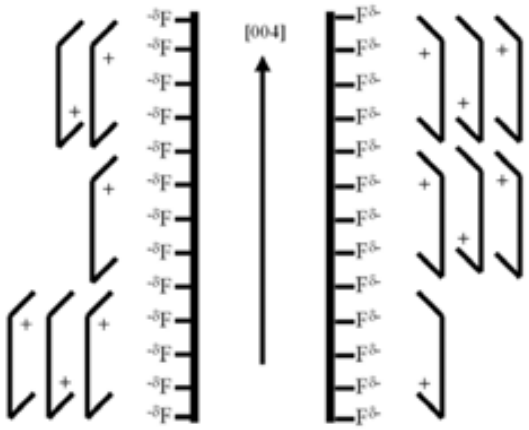

Supplementary data 4

Photographs from a typical light-activated oxygen indicator fabricated using a MB/TiO_2 film: (a) As-prepared MB/TiO_2 film, (b) Non-activated indicator: after spin-coating a solution of TEOA with the encapsulating polymer (hydroxyethyl cellulose), (c) UV-activated indicator and color recovery after different time of exposure to oxygen under ambient conditions: (d) 4 h, (e) 8 h, (f) 24 h, (g) 32 h and (h) 80 h.

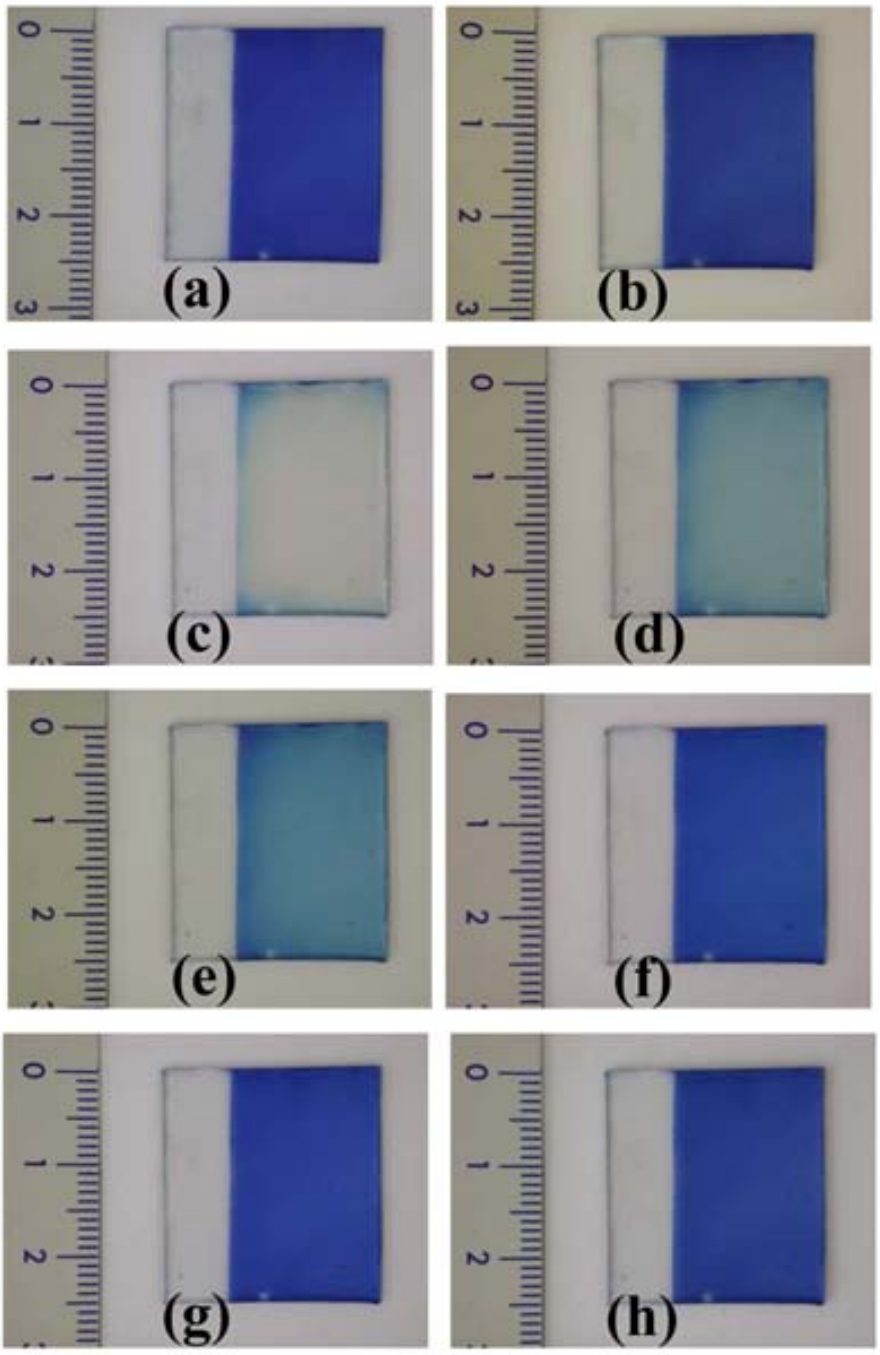

Available online at www.sciencedirect.com
ScienceDirect
Thin Solid Films 516 (2008) 3831–3835
thin solid films
www.elsevier.com/locate/tsf

Dopamine/TiO_2 hybrid thin films prepared by the liquid phase deposition method

David Gutiérrez-Tauste [a,*], Xavier Domènech [a], Concepción Domingo [b], José A. Ayllón [a]

[a] Departament de Química, Universitat Autònoma de Barcelona, Campus UAB, Edifici Cn, 08290 Cerdanyola del Vallès, Barcelona, Spain
[b] Instituto de Ciencia de Materiales (CSIC), Campus UAB, 08290 Cerdanyola del Vallès, Barcelona, Spain

Received 1 December 2006; received in revised form 31 May 2007; accepted 22 June 2007
Available online 4 July 2007

Abstract

Liquid phase deposition method is applied to one-step production of a hybrid material composed by dopamine(DA) and TiO_2 anatase. An optimized amount of the enediol derivative is added to a fluoride titania precursor aqueous solution in order to entrap this modifier within the growing TiO_2, yielding a DA/TiO_2 nanocomposite material. Uniform, well-adhered and brown-colored thin films are deposited on indium tin oxide covered glass substrate. The DA/TiO_2 hybrid material has been characterized by infrared spectroscopy, electronic microscopy, X-ray diffraction and UV–vis spectroscopy. The formation of the hybrid material seems to be reasonably explained by linkage of different TiO_2 nanocrystallites taking advantage of both enediol and amine groups of DA.

Keywords: Titanium oxide; Dopamine; Coatings; Hybrid nanocomposite; Liquid phase deposition (LPD); One-step deposition process; Low-temperature deposition process

1. Introduction

Liquid phase deposition (LPD) is a soft chemical technique applied initially to obtain amorphous titania films [1], but nowadays is also employed to produce different oxides thin films and powders [2–5]. LPD is a process based on the controlled hydrolysis of metallic fluoro-complexes. The addition of a fluoride scavenger such as boric acid shifts this chemical equilibrium of hydrolysis to form the corresponding metal oxide. This wet process allows the deposition of metal oxide thin films over large and complex surfaces and the obtention of metal oxide powders at relatively low temperatures avoiding thermal post-treatments [2,3]. LPD preparation of titanium dioxide (TiO_2) thin films and powders has been thoroughly studied by several groups, with special emphasis in determine factors that control nucleation and crystallinity [6–15].

Surface modification of TiO_2 semiconductor particles has attracted particular interest because of the application of these materials in fields as diverse as electrochromic [16] and photochromic [17] devices, and dye-sensitized solar cells [18]. TiO_2 film or powder preparation and surface modification are usually carried out separately in two steps, since common TiO_2 preparation methods require high temperatures that are incompatibles with the organic modifiers [16,19]. One-step deposition methods for hybrid TiO_2 materials are poorly reported in the literature [20–22]. However, one-step preparation methods of hybrid material with more easily crystallisable oxides such as ZnO have been described [23–25]. Therefore, development of more simple, low temperature and one-step methods applicable to the preparation hybrid organic-TiO_2 films and powders should be considered.

Compounds containing enediol units (e.g. catechol and its derivatives, that play key roles in many biological reactions [26]) have been known to chelate undercoordinated states of Ti on the surface of TiO_2 with the optimal geometry, resulting in a five-membered ring coordination complex [27,28]. These electron-donating bidentante ligands can confer new properties, shifting the optical response in the visible spectral region and improving effectiveness for charge separation of nanocrystalline TiO_2 (compared to unmodified semiconductor) [28,29]. The catechol derivate Dopamine (DA) has been widely studied

* Corresponding author. Tel.: +34 93 5812176; fax: +34 93 5812920.
E-mail address: davidg@qf.uab.es (D. Gutiérrez-Tauste).

0040-6090/$ - see front matter © 2007 Elsevier B.V. All rights reserved.
doi:10.1016/j.tsf.2007.06.165

as a robust biomimetic anchor for functional molecules, taking advantage of the presence of both enediol and alkyl-NH_2 groups. Diverse applications including light-induced site-specific TiO_2 redox chemistry architectures [30–32], surface-initiated polymerization to create antifouling coatings in metal substrates [26], linkage of small biomolecules onto ferromagnetic Fe_2O_3 nanoparticles [33] and DA selective moleculary imprinted materials [34–36] have been described.

The development of LPD technique has open a way for the preparation of organic-inorganic hybrid materials. Deki et al. have reported the LPD of alkyl sulfate and alkylbenzene sulfonate surfactants/TiO_2 [37] and copper phthalocyanine/TiO_2 hybrid films [38]. Recently, we have described the preparation of methylene blue/TiO_2 nanocomposite thin films used to fabricate light-activated oxygen indicators [39]. In this paper, we report an one-step route to obtain DA/TiO_2 hybrid nanocomposite thin films by the LPD technique. Aluminum(III) nitrate was employed as fluoride scavenger instead of the most commonly used boric acid, in order to increase the rate of film deposition [40].

2. Experimental details

2.1. Reagents and substrate

Ammonium hexafluorotitanate, aluminum nitrate and DA (analytical grade Aldrich, Panreac) were used as received without further purification. Acetone and ethanol (Panreac) were used for substrate cleaning. Water purified with a Milli-Q system (Millipore, conductivity < 0.05 μS/cm) was employed.

The used substrate was ITO (In_2O_3:Sn) conducting glass 13–18 Ω/sq, 1.1 mm thick (Optical Filters). Substrates were cleaned just before performing the deposition process [40]: 5 min ultrasonic cleaning in acetone, then 5 min in absolute ethanol, then in 30% nitric acid for 1 min and finally in water for 5 more min.

2.2. Preparation of films and powders

DA/TiO_2 films were deposited on ITO-covered glass placing vertically the substrates into a polyethylene vessel containing the fresh precursor solution: 10 mM $(NH_4)_2TiF_6$, 10 mM $Al(NO_3)_3 \cdot 9H_2O$ and 20 mM DA, at the natural pH of the system (pH = 2.0). The whole was sonicated for 1 min and kept at 80 °C for 4.5 h. A range of DA concentrations between 1 mM and 100 mM were also tried. After deposition, films were gently washed with water and dried with a nitrogen gas flow. DA/TiO_2 powders were obtained (as byproduct) by scrapping off a low-adhered films deposited on the surface of the polyethylene vessel. Powder samples were then collected with the aid of water, separated by centrifugation, washed with additional water and dried at 60 °C. Blank TiO_2 films and powders were prepared under similar experimental conditions, but without adding DA in the LPD precursor bath [40].

2.3. Characterization techniques

Attenuated Total Reflectance Fourier Transform Infrared (ATR-FTIR) spectra were performed with a Bruker apparatus (Tensor model equipped with MKII Golden Gate). The elemental analyses (C, H, N) were carried out by the staff of the Chemical Analyses Service of the Universitat de Barcelona on a Carlo Erba CHNS EA-1108 instrument. Films surface characteristics were investigated by Scanning Electron Microscopy (SEM) on gold covered samples, using a Hitachi S-570 microscope (operating voltage, 10–30 kV). For thickness measurements, samples were cut into pieces which results in breaking the TiO_2 film near the cut edge of the substrate. Films thickness was studied by SEM in these edges, taking into consideration the sample inclination with respect to the electron beam. X-ray Diffraction (XRD) spectra of powder samples were registered on a Rigaku Rotaflex RU-200B diffractometer with Cu K_α radiation. Grazing angle XRD spectra of the deposited films were recorded using a Siemens D-500 apparatus with Cu K_α radiation at incidence angle of 0.3. Electron diffraction patterns and Transmission Electron Microscopy (TEM) images were recorded in a JEOL 2011 microscope operating at 200 kV. Samples for TEM observations were prepared by scrapping off thin films deposited on ITO and sonicated for 15 min in ethanol to detach aggregates of the appropriate size for imaging. UV–vis absorbance data were obtained with a Helios series γ spectrophotometer (Thermo Electron corporation), using the respective bare substrate as the blank.

For comparative purposes, DA was adsorbed on TiO_2 Degussa P-25 (80% anatase–20% rutile, kindly gifted by Degussa). Adsorption equilibrium was established at similar conditions than those in the LPD bath from a suspension 10 mM TiO_2 P-25 and 20 mM DA. The initial pH was adjusted to 2.0 with diluted $HClO_4$ and the suspension was kept at 80 °C for 4.5 h. The powder obtained was separated by centrifugation, washed with water and dried at 60 °C.

3. Results and discussion

Our first goal was to find bath compositions and substrate preparation procedures that allow the deposition of optically transparent and well-adhered coatings of a DA/TiO_2 hybrid material. For that purpose, several assays varying DA concentrations in the LPD precursor bath were carried out. Using an optimized 20 mM DA concentration in the bath, uniform and brown-colored films were obtained. Films adhesion and stability were ascertained using ultrasound disruption.

Chemical equilibria of the LPD process are altered after DA addition. Although DA do not coordinate Al^{3+} cations at the acidic pH employed [41], the enediol chelate Ti^{4+} cations in the precursor bath (as denoted by the brown-colored solution obtained after DA addition). Ti^{4+} complexation with DA shifts LPD equilibria and make difficult the TiO_2 formation, according to Le Chatelier principle.

The addition of a very low DA concentration, leads to a very poor incorporation of DA into the coating and practically almost pure TiO_2 film is obtained. On the other hand, when DA is excessively concentrated in the precursor bath, the modifier make difficult the initial nucleation step and the posterior TiO_2 growth. Consequently, at DA concentration higher than 100 mM no film deposition is observed.

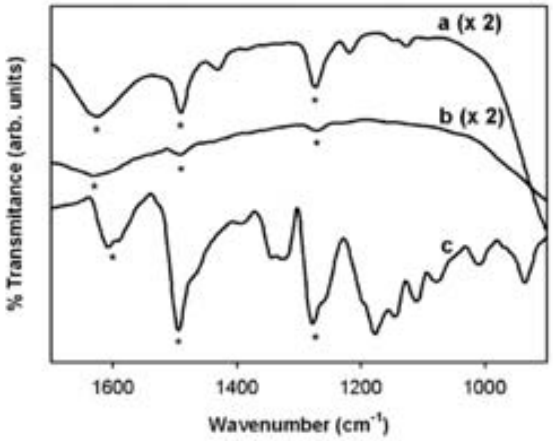

Fig. 1. ATR-FTIR spectra of: (a) DA/TiO_2 hybrid powder, (b) DA adsorbed on Degussa P-25 and (c) commercial DA hydrochloric salt. Spectra (a) and (b) are presented with 2× amplification. Mean absorption peaks are also marked with *.

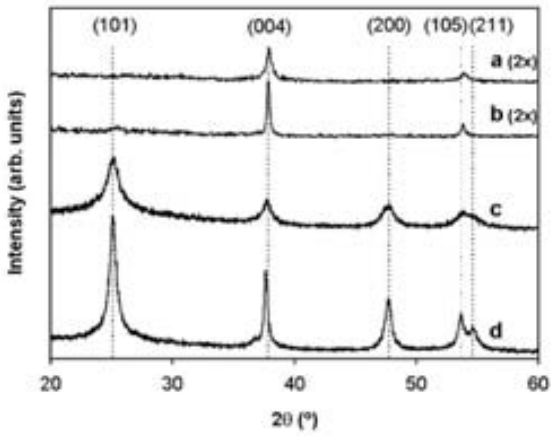

Fig. 3. Grazing angle XRD of DA/TiO_2 (a) and TiO_2 (b) thin films and XRD of DA/TiO_2 (c) and TiO_2 (d) powders.

The surface structure of the DA–TiO_2 complex was studied using infrared spectroscopy. Non-coordinated DA (Fig. 1c) present strong and overlaid infrared absorption peaks at ~1600 cm^{-1} (N–H bending and C=C ring stretch), ~1495 cm^{-1} (aromatic-C–H bending and aliphatic primary amine vibration, salt form) and ~1280 cm^{-1} (C–O stretching and aliphatic primary amine vibration) [11,42,43]. Similar infrared spectra are observed in the DA/TiO_2 hybrid thin films (not shown) and powders (Fig. 1a), and when DA is adsorbed on Degussa P-25 (Fig. 1b). Signals at ~1280 and ~1495 cm^{-1} appear in the DA coordinated materials with no absorption frequency modification. In addition, broad absorption bands at ~1630 cm^{-1} that cannot be unambiguously discerned, ascribed to contributions of O–H bending from adsorbed water molecules [28] plus N–H bending and C=C ring stretch vibrations from DA are also observed in the modified materials. Therefore, bidentate binding reported for the DA–TiO_2 complex at the nanoparticules surface is also confirmed in the DA/TiO_2 hybrid material. It must be also pointed out that DA/TiO_2 thin films present more intense infrared signals than samples obtained after absorption of DA on TiO_2 P-25 in similar conditions (pH and concentration), suggesting that DA is incorporated in higher proportion in the former case. An incorporation of 7% of DA in the hybrid material can be estimated from elemental analysis of powder samples.

Surface morphology and thickness of DA/TiO_2 hybrid films were studied by SEM (Fig. 2). DA/TiO_2 films (Fig. 2a) show dense and compact substrate coverage. The films present high optical transparency (see Fig. 4a, Transmittance UV–vis) and no cracks were observed. The particle size in the DA/TiO_2 samples is in the 10–50 nm range, being clearly lower with respect to TiO_2 samples [40]. These observations can be ascribed to the fact that the adsorption of DA on the TiO_2 particles limits its growth. A decrease in the mean particle size was also observed in our previous work when hybrid TiO_2 films were prepared by LPD, incorporating the cationic dye methylene blue [39]. An average deposition rate of 110 nm/h is estimated taking into account the films thickness (approximately 500 nm, Fig. 2c) and the deposition time in DA/TiO_2 samples. For comparison, a deposition rate of 150 nm/h was reported for TiO_2 blank films [40]. SEM observations point to the fact that addition of DA in

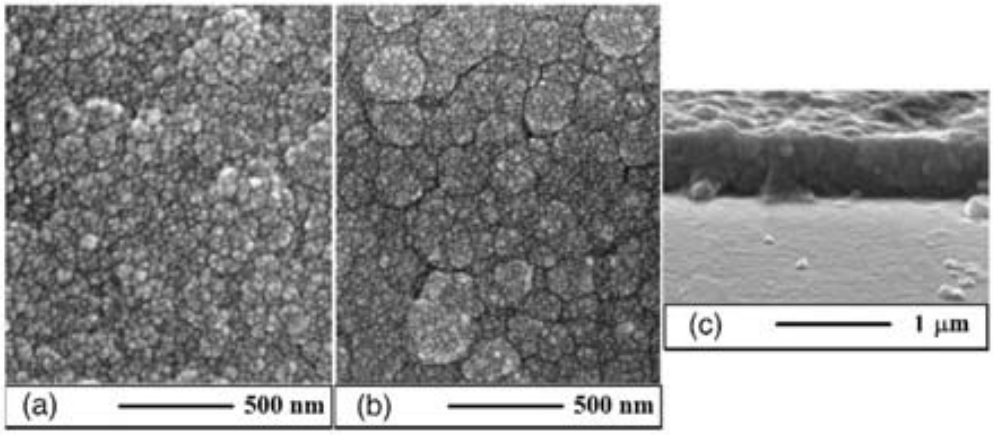

Fig. 2. SEM photographs showing surface morphology and thickness of DA/TiO_2 samples deposited on ITO-glass: using 20 mM optimal DA concentration (a) and (c) in the LPD precursor bath; and adding excess of DA (50 mM) with respect to the optimized DA concentration (b).

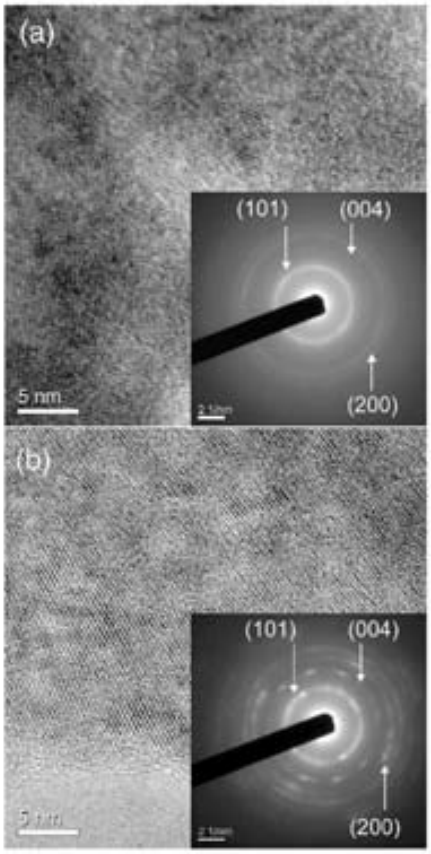

Fig. 4. TEM and associated SAED of DA/TiO_2 (a) and TiO_2 (b) thin films.

the LPD precursor bath limits the particle size and also decreases slightly the average deposition rate of the film. When DA concentration is slightly increased with respect to the optimal modifier concentration, the lower nucleation density leads to the deposition of a film that consists of hemispherical deposits whose collapse can be clearly observed, presenting morphology irregularities (see Fig. 2b).

XRD of DA/TiO_2 and TiO_2 thin films and powders are shown in Fig. 3, revealing peaks that may be assigned to the anatase structure [40,44]. Wider diffraction signals are observed in the DA/TiO_2 samples, evidencing that the size of TiO_2 crystallites (and also the mean particle size as was observed by SEM) decreases in the hybrid material. In all cases, the relative intensity of the (004) and (200) planes is noticeably increased with respect to the anatase standard patron corresponding to complete random order [45]. The preferential *c* axis growth is characteristic of TiO_2 films and powders prepared by LPD, and has been attributed to the preferential adsorption of fluoride to planes parallel to this direction [40,46]. In addition, the film samples (Fig. 3a and b) only present intensity for diffraction peaks perpendicular to anatase *c* axis, i.e. (004) and (105) planes, evidencing clear preferential TiO_2 nanocrystallites orientation with respect to the substrate in the c direction [40]. Niederberger et al. reported that DA seems to favor *a* axis growth, inducing the formation of nearly spherical TiO_2 particles [22]. However, this fact is only partially observed in DA/TiO_2 powder samples that present equal intensities for the (004) and (200) reflections. DA incorporation in TiO_2 LPD produces a material with both *a* and *c* preferential growth, which means that only slightly elongated crystallites are formed in the powder samples (compare Fig. 3c and d). Nevertheless when the hybrid DA/TiO_2 material is deposited on ITO substrate, dominating *c* axis preferential TiO_2 orientation is observed.

TEM and Selected-Area Electron Diffraction (SAED) studies were also carried out on DA/TiO_2 and TiO_2 thin films (Fig. 4a and b, respectively). The diffraction patterns (assigned to reflections of anatase TiO_2) indicate polycrystalline structures in both cases. Diffraction rings corresponding to lattice spacings of 3.5, 2.4 and 1.9 Å (assigned to (101), (004) and (200) reflections, respectively) are observed in the samples. The hybrid DA/TiO_2 material presents a continuous structure of lower size and more randomly oriented nanocrystallites than bare TiO_2, suggesting that DA can also link different TiO_2 crystallites and promote aggregation during hybrid material deposition, taking advantage of both enediol and amine groups [47]. Consequently, this fact could limit the application of the as-prepared hybrid material for anchoring functional molecules. However, no clear evidence of changes of the amine stretching frequencies was observed by infrared spectroscopy. Only isolated crystallites in an amorphous matrix were observed by TEM in our previous work in which hybrid methylene blue/TiO_2 films were prepared by LPD [39].

Typical UV–vis transmittance spectra of DA/TiO_2 and TiO_2 films are shown in Fig. 5. TiO_2 films are highly transparent in the visible region and only present the absorption corresponding to the semiconductor band gap (Fig. 5, dotted line). A noticeable decrease in transmittance in the visible region is observable in DA/TiO_2 coatings (Fig. 5, solid line) with respect to bare TiO_2 films, due to the brown coloration of the hybrid films. Nevertheless, electron injection from the ground state of the DA dye to the conduction band of TiO_2 by photoinduced charge-transfer excitation of the DA–TiO_2 complex is described in the literature [29,48], being the corresponding absorption in the visible range strongly dependent on the particle size, morphology and surface

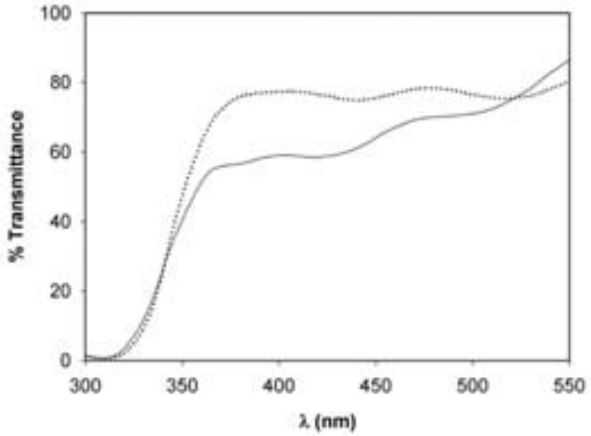

Fig. 5. UV–vis transmittance spectra of DA/TiO_2 (solid line) and TiO_2 (dotted line) thin films on ITO-covered glass.

states [28]. DA/TiO_2 hybrid films preserve the characteristic absorption oscillations in the visible range due to their regular morphology, according to SEM observations.

4. Conclusions

In the present work, a one-step and low temperature procedure to obtain DA/TiO_2 nanocomposite thin films on ITO-covered glass by LPD is presented. The material formation can be explained by linkage of TiO_2 crystallites by enediol and amine groups of DA.

DA incorporation in the growing TiO_2 limits the size of both anatase crystallites and the main particle of the nanocomposite, and slightly decreases the average deposition rate of the films. Moreover, typical *c* axis anisotropy of TiO_2 prepared by LPD is altered in the hybrid material; slightly elongated crystallites are formed with both *a* and *c* axis preferential growth in powder samples. However, *c* axis preferential TiO_2 orientation of thin films on ITO is attained during the film deposition. Infrared spectra suggest that DA is incorporated in DA/TiO_2 nanocomposite material in higher concentrations with respect to surface absorption on P-25.

The focus of our interest in the future investigations will be the development of applications of the promising DA/TiO_2 hybrid nanocomposite material.

Acknowledgements

This work has been financed by the Spanish National Plan of Research (CTQ2005-02808/PPQ project).

References

[1] H. Kawahara, H. Honda, Japanese patent 59141441 A (Nippon Sheet Glass), August 14, 1984.
[2] T.P. Niessen, M.R. De Guire, Solid State Ionics 151 (2002) 61.
[3] Y. Gao, K. Koumoto, Cryst. Growth Des. 5 (2005) 1983.
[4] H.Y.Y. Ko, M. Mizuhata, A. Kajinami, S. Deki, Thin Solid Films 491 (2005) 86.
[5] Y. Sakai, H. Norimatsu, Y. Norimatsu, Y. Saito, H. Inomata, T. Mizuno, Thin Solid Films 392 (2001) 294.
[6] Y. Masuda, T. Sugiyama, W.S. Seo, K. Koumoto, Chem. Mater. 15 (2003) 2469.
[7] Y. Masuda, S. Ieda, K. Koumoto, Langmuir 19 (2003) 4415.
[8] H. Kishimoto, K. Takahama, N. Hashimoto, Y. Aoi, S. Deki, J. Mater. Chem. 8 (1998) 2019.
[9] J.A. Ayllón, A.M. Peiró, L. Saadoun, E. Vigil, X. Domènech, J. Peral, J. Mater. Chem. 11 (2000) 1911.
[10] E. Vigil, L. Saadoun, J.A. Ayllón, X. Domènech, I. Zumeta, R. Rodríguez-Clemente, Thin Solid Films 365 (2000) 12.
[11] J.G. Yu, H.G. Yu, B. Cheng, X.J. Zhao, J.C. Yu, W.K. Ho, J. Phys. Chem., B 107 (2004) 13871.
[12] I. Zumeta, B. González, R. Espinosa, J.A. Ayllón, E. Vigil, Semicond. Sci. Technol. 19 (2004) L52.
[13] B. Herbig, P. Löbmann, J. Photochem. Photobiol., A Chem. 163 (2004) 359.
[14] J. Xiang, Y. Masuda, K. Koumoto, Adv. Mater. 16 (2004) 1461.
[15] H. Pizem, O. Gershevitz, Y. Goffer, A.A. Frimer, C.N. Sukenik, U. Sampathkumaran, X. Milhet, A. McIlwain, M.R. De Guire, M.A.B. Meador, J.K. Sutter, Chem. Mater. 17 (2005) 3205.
[16] S.Y. Choi, M. Mamak, N. Coombs, N. Chopra, G.A. Ozin, Nano Lett. 4 (2004) 1231.
[17] M. Biancardo, R. Argazzi, C.A. Bignozzi, Inorg. Chem. 44 (2005) 9619.
[18] M. Grätzel, Nature 414 (2001) 338.
[19] D. Gutiérrez-Tauste, I. Zumeta, E. Vigil, M.A. Hernández-Fenollosa, X. Domènech, J.A. Ayllón, J. Photochem. Photobiol., A Chem. 175 (2005) 165.
[20] M.H. Bartl, S.W. Boettcher, E.L. Hu, G.D. Stucky, J. Am. Chem. Soc. 126 (2004) 10826.
[21] R. Shacham, D. Avnir, D. Mandler, J. Sol-Gel Sci. Technol. 31 (2004) 329.
[22] J. Polleux, N. Pinna, M. Antonietti, C. Hess, U. Wild, R. Schlögl, M. Niederberger, Chem. Eur. J. 11 (2005) 3541.
[23] T. Oekermann, T. Yoshida, H. Minoura, K.G.U. Wijayantha, L.M. Peter, J. Phys. Chem., B 108 (2004) 8364.
[24] T. Pauporté, F. Bedioui, D. Lincot, J. Mater. Chem. 15 (2005) 1552.
[25] T. Jiu, H. Liu, H. Gan, Y. Li, S. Xiao, H. Li, Y. Liu, F. Lu, L. Jiang, D. Zhu, Synth. Met. 148 (2005) 313.
[26] X. Fan, L. Lin, J.L. Dalsin, P.B. Messersmith, J. Am. Chem. Soc. 127 (2005) 15843.
[27] T. Rajh, J.M. Nedeljkovic, L.X. Chen, O. Poluektov, M.C. Thurnauer, J. Phys. Chem., B 103 (1999) 3515.
[28] T. Rajh, L.X. Chen, K. Lukas, T. Liu, M.C. Thurnauer, D.M. Tiede, J. Phys. Chem. B 106 (2002) 10543.
[29] N.M. Dimitrijevic, Z.V. Saponjic, D.M. Bartels, M.C. Thurnauer, D.M. Tiede, T. Rajh, J. Phys. Chem., B 107 (2003) 7368.
[30] T. Rajh, Z. Saponjic, J. Liu, N.M. Dimitrijevic, N.F. Scherer, M. Vega-Arroyo, P. Zapol, L.A. Curtiss, M.C. Thurnauer, Nano Lett. 4 (2004) 1017.
[31] N.M. Dimitrijevic, Z.V. Saponjic, B.M. Rabatic, T. Rajh, J. Am. Chem. Soc. 127 (2005) 1344.
[32] L. Garza, Z.V. Saponjic, T. Rajh, N.M. Dimitrijevic, Chem. Mater. 18 (2006) 2682.
[33] C. Xu, K. Xu, H. Gu, R. Zheng, H. Liu, X. Zhang, Z. Guo, B. Xu, J. Am. Chem. Soc. 126 (2004) 9938.
[34] R. Makote, M.M. Collinson, Chem. Mater. 10 (1998) 2440.
[35] T.R. Ling, Y.Z. Syu, Y.-C. Tasi, T.-C. Chou, C.-C. Liu, Biosens. Bioelectron. 21 (2005) 901.
[36] T. Takeuchi, N. Murase, H. Maki, T. Mukawa, H. Shinmori, Org. Biomol. Chem. 4 (2006) 565.
[37] L. Li, M. Mizuhata, S. Deki, Appl. Surf. Sci. 239 (2005) 292.
[38] L. Li, M. Mizuhata, A. Kajinami, S. Deki, Synth. Met. 146 (2004) 17.
[39] D. Gutiérrez-Tauste, X. Domènech, N. Casañ-Pastor, J.A. Ayllón, J. Photochem. Photobiol., A Chem 187 (2007) 45.
[40] D. Gutiérrez-Tauste, X. Domènech, M.A. Hernández-Fenollosa, J.A. Ayllón, J. Mater. Chem. 16 (2006) 2249.
[41] F. Zhang, L. Yang, S. Bi, J. Liu, F. Liu, X. Wang, X. Yang, N. Gan, T. Yu, J. Hu, H. Li, T. Yang, J. Inorg. Biochem. 87 (2001) 105.
[42] M.N. Tahir, P. Theato, P. Oberle, G. Melnyk, S. Faiss, U. Kolb, A. Janshoff, M. Stepputat, W. Tremel, Langmuir 22 (2006) 5209.
[43] Y. Zeng, C. Li, C. Tang, X.-B. Zhang, G. Shen, R. Yu, Electroanalysis 18 (2006) 440.
[44] H. Pizem, C.N. Sukenik, U. Sampathkumaran, A.K. McIlwain, M.R. De Guire, Chem. Mater. 14 (2002) 2476.
[45] Powder Diffraction File, Joint Committee on Powder Diffraction Standards (JCPDS), card 21-1272.
[46] A.M. Peiró, E. Vigil, J. Peral, C. Domingo, X. Domènech, J.A. Ayllón, Thin Solid Films 411 (2002) 185.
[47] M. Niederberger, G. Garnweitner, F. Krumeich, R. Nesper, H. Cölfen, M. Antonietti, Chem. Mater. 16 (2004) 1202.
[48] E.L. Tae, S.H. Lee, J.K. Lee, S.S. Yoo, E.J. Kang, K.B. Yoon, J. Phys. Chem., B 109 (2005) 22513.

PART 4.4:

ALL-IN-ONE IONIC LIQUID LIKE PRECURSOR SOLUTIONS FOR TiO_2 POWDER PREPARATION

Publication 5:

Hexafluorotitanate salts containing organic cations: use as a reaction medium and precursor to the synthesis of titanium dioxide.

Chem. Commun. **2007**, 4659-4661.

4.4.1. INTRODUCTION

Ionic liquids (ILs) are organic salts with low melting points (<100ºC) that have received great deal of attention in many areas of chemistry and industry due to their potential as green recyclable alternative to conventional organic solvents in electrochemical, engineering and synthetic applications [1-4]. ILs present unique properties (tunable by selection of appropriate cation and anion) such as extremely low volatilility, wide liquid temperature range, good thermal stability, good dissolving ability, excellent microwave absorbing ability, high ionic conductivity and wide electrochemical window [5,6]. The formation of the liquid phase in ILs may be guided by the same principle governing the melting point of classical ionic compounds such as NaCl [7]. The much lower melting points of ILs compared to inorganic salts can be generally attributed to the cationic components, as a consequence of their low charge density (giving rise to weak Coulombic attraction forces) and steric difficulties to be fitted into a lattice [3,5]. It is worth emphasizing that the molecular flexibility and/or asymmetry built into at least one of the ions also opposes to the strong charge ordering due to the ionic interactions that would normally cause the system to crystallize [7,8].

Typical ILs are based on the combination of such asymmetric cations presenting low charge density (see some examples in Figure 4.4.1) with a great variety of anions such as $[BF_4]^-$, $[PF_6]^-$, $[AlCl_4]^-$, $[(CF_3SO_2)_2N]^-$, $[CF_3SO_3]^-$, $[CF_3COO]^-$ or $[CH_3COO]^-$ [4,7,9]. In principle, any charged cation and anion (including double charged species) could give rise to ILs [4]. However, 1,3-dialkylimidazolium cations have became the most extensively employed because of resulting ionic liquid systems present air and water stability and are liquid over a wide range of composition [4].

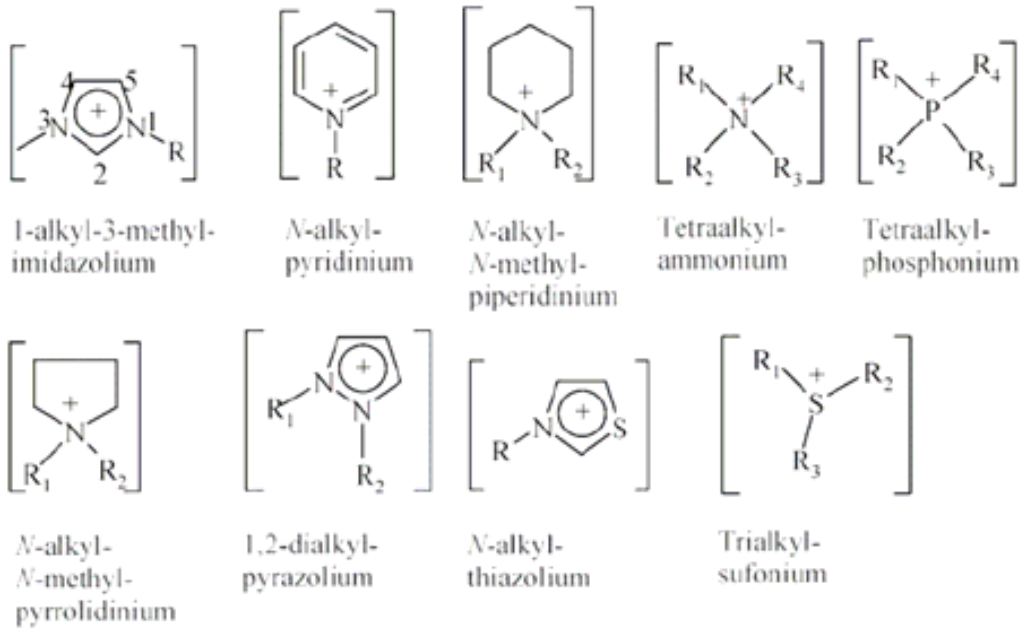

Figure 4.4.1. Cations most commonly used in ionic liquid systems (R refers to alkyl chains). Adapted from reference [4].

Unfortunately, widespread application of ionic liquids could be limited by inherent cost and purity issues, being their recyclability an economic imperative [10]. Abbott *et al.* have proposed deep eutectic solvents as alternative low-cost ILs by mixing quaternary ammonium salts with either hydrated (Cr) [11] and anhydrous halide salts of metals (Zn, Sn, Fe) [12,13] or hydrogen bond donors (such as amides, carboxylic acids or alcohols) [10,14]. As general view, ionic liquids are more expensive than conventional organic solvents, but it is thought that recycling them would result in processes economically viable [4]. However, Seddon *et al.* have recently reviewed industrial applications of ILs derived in many cases from close cooperation between academia and industry [4]. For instance, the industrial giant BASF designed the BASIL™ process (Biphasic Acid Scavenging utilizing Ionic Liquids) used for producing alkoxyphenylphosphines from chlorophenylphosphines and the corresponding alcohol (see Figure 4.4.2). In this multi-ton process, HCl generated as by-product is scavenged by 1-methylimidazol, *in situ* yielding the IL 1-methylimidazolium chloride that forms a biphasic system allowing IL recycling [15].

Air Products Inc. has designed the GASGUARD® technology for preparing high purity gases via complexation in 1,3-alkylmethylimadazolium based ionic liquids. Lewis acidic (*e.g.* BF_3(g)) and basic (*e.g.* PH_3(g) or AsH_3(g)) gases are stored in ionic liquids presenting the opposite Lewis acid-base behavior (*i.e.* basic ILs with $[BF_4]^-$ and acidic ILs with $[Cu_2Cl_3]^-$ or $[Cu_2Br_3]^-$, respectively). Finally, gases are recovered by means of vacuum [16]. IoLiTec (Ionic Liquid Technologies) commercializes ionic liquids and develops practical applications such as electrolytes for DSSCs consisting in common cations in combination with iodide and triiodide anions [17].

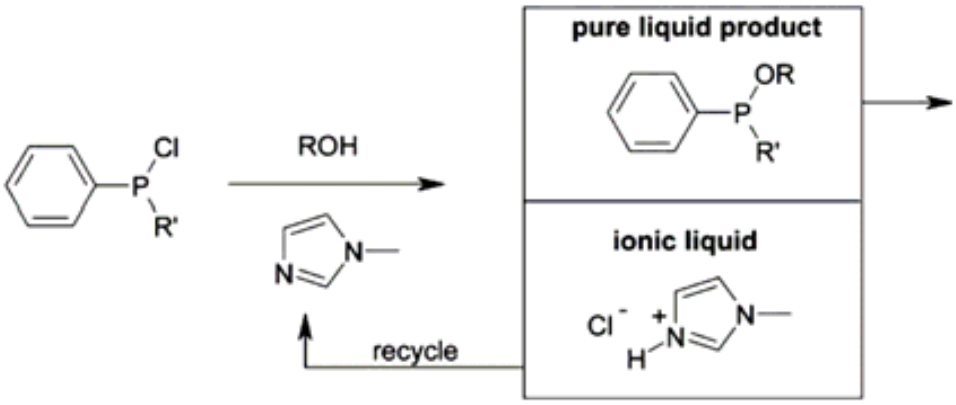

Figure 4.4.2. The BASIL™ process for preparing alkoxyphenylphosphines from chlorophenylphosphines and the corresponding alcohol [15].

In the context of inorganic synthesis, ILs have opened up a way for the crystallization of these materials, since they present several key advantages with respect to conventional solvents [1,2,7,18]: (i) ILs can have low interface tensions, resulting in high nucleation rates [2]; (ii) ILs dissolve many species since it provides both hydrophobic and hydrophilic regions [1]; (iii) ILs facilitate inorganic synthesis from very polar precursors under ambient conditions and under anhydrous or water-poor conditions [1,18]; (iv) Most important, ILs can act as entropic drivers since they exhibit self-organization as extended hydrogen bond network [2,7]. Thus, the modification of classical TiO_2 synthetic routes (*i.e.* sol-gel from Ti-alkoxides or $TiCl_4$ hydrolysis) employing imidazolium-based ILs have been reported for preparing TiO_2 directly

crystallized at low temperature, with different phases and morphologies [6,18-24]. For instance, Antonietti *et al.* reported the synthesis of spherical anatase nanoparticles with spongelike morphology from $TiCl_4$ hydrolysis in a mixture of water and 1-butyl-3-methylimidazolium tetrafluoroborate (80ºC, 12 hours aged) [24]. Kimikuza *et al.* carried out low-temperature interfacial synthesis of hollow amorphous TiO_2 microspheres by means sol-gel reactions in immiscible toluene/1-butyl-3-methylimidazolium hexafluoroborate mixtures [18]. However, ILs are typically employed as additives in mixtures with conventional solvents in these works, only partially exploiting the potential synthetic pathways in ILs.

On the other hand, some authors have just recently described a few examples of synthetic strategies for materials preparation based on the so-called "next generation" or "all-in-one" ILs that act as solvent, template and precursor at the same time [1,25-27]. In these systems, a metal center is directly included in either the cation or the anion constituting the corresponding IL, whose controlled destabilization gives rise to the desired inorganic. It is thought these precursor media can benefit low-temperature crystallization of inorganic compounds, since "all-in-one" ILs present a self-organized structure in the liquid state that is analogous to the alkylimidazolium-based ones and, hence, these novel IL media can be seen as "pre-organized" precursors. In this sense, one can thus imagine a rich and versatile chemistry following this strategy: exploring how to prepare ILs including a metal center and destabilizing them in order to prepare the desired inorganic with a defined phase, morphology and/or chemical composition [1]. For instance, Dai *et al.* controlled the morphology of ZnO nanostructures obtained by ionothermal treatment of a IL consisting of $[Zn\text{-}(NH_2R)_4][(CF_3SO_2)_2N]$ in tetramethylammonium hydroxide at 110ºC [26]. Taubert *et al.* prepared CuCl nanopellets by reducing [*N*-dodecyl-pyridinium]$_2$[$CuCl_4$] ILs with an ascorbic acid derivate (85-145ºC, 24h) [25]. However, to the best of our knowledge, no "all-in-one" synthetic approach had never been achieved for preparing titania.

In Publication 5: **Hexafluorotitanate salts containing organic cations: use as a reaction medium and precursor to the synthesis of titanium dioxide.** *Chem. Commun.* **2007**, 4659-4661, the knowledge of ILs and Liquid Phase Deposition was combined for preparing TiO_2 nanoparticles. Firstly, $[NR_4]_2TiF_6$ stable IL-like precursor solutions with only a small fraction of water were produced by the straightforward modification of commercial hexafluorotitanic acid (HFTA) with organic derivates containing a tetraalkylammonium cation. And secondly, TiO_2 nanocrystalline was then obtained at low temperature (85ºC) by destabilizing this $[NR_4]_2TiF_6$ precursor solutions in analogous way to classic LPD procedures with boric acid (that is, as previously commented, the common fluoride scavenger in the major part of LPD studies).

4.4.2. MAIN RESULTS AND DISCUSSION

In the first step, $[NR_4]_2TiF_6$ IL-like precursor solutions were prepared with two different quaternary ammonium salts by reacting with HFTA in a 2:1 molar ratio in a Teflon-covered plastic bottle, according to Equations 4.4.A and 4.4.B. Betaine (Bet; $(CH_3)_3$-N^+-CH_2-COO^- or strictly the betainium $BetH^+$ cation obtained after carboxylate protonation) and choline (Cho^+; $(CH_3)_3$-N^+-CH_2-CH_2OH) chloride were initially chosen as cheap and easily accessible cationic building blocks for forming the titania IL precursor. The melting point of the resulting solutions depended on the NR_4^+ cation: $[Cho]_2TiF_6$ precursor solutions were stable even at room temperature, whereas $[BetH]_2TiF_6$ ones became solid at temperatures lower than 60 ºC. Both tetraalkylammonium compounds are commodity chemicals produced annually on a multi-ton scale, being specially relevant their use as animal feed additives or additionally in the case of the betaine, as precursor for the synthesis of surfactants [5]. $BetH^+$ and Cho^+ cations only differ in the carboxylic acid and hydroxyl groups, respectively and, in fact, the former is a metabolite that is formed by oxidation of choline [28].

$$2\ Bet + H_2TiF_6 \longrightarrow [BetH]_2TiF_6\ (exothermic) \qquad (4.4.A)$$

$$2\ ChoCl + H_2TiF_6 \longrightarrow [Cho]_2TiF_6 + 2\ HCl\ (endothermic) \qquad (4.4.B)$$

It is thought that the resulting highly concentrated $[NR_4]_2TiF_6$ precursor solutions (only 21 wt.% of water content) are similar to ILs. The ions concentration of such $[NR_4]_2TiF_6$ solutions was clearly higher than in IL co-solvent assisted TiO_2 synthetic approaches [19-21]. Our precursor media possess certain parallelism with the deep eutectic mixtures (hydrated metal salts and choline chloride, so-called "ionic liquid analogues") described by Abbott *et al.* [11]. In such deep eutectic mixtures, the water content ranged, depending on the composition, from 25 to 35 wt.% although its origin arises from the hydrated nature of metal halides employed.

In the second step, stoichiometric 1.5 equivalents (with respect to Ti) of the fluoride scavenger boric acid were added to the as-prepared $[NR_4]_2TiF_6$ precursor solutions and a low-temperature (85ºC) aging treatment of the mixture was carried out for variable time periods (from 18 to 90 h). The clear initial solution gradually became turbid and nanocrystalline TiO_2 as final product was thus formed with this strategy, that can conceptually be seen as high-concentration LPD (Equation 4.4.C). The samples finally evidenced a quasi-solid "cheese-like" appearance (see Figure 4.4.3). The product was then dispersed in water, and TiO_2 was recovered by centrifugation and thoroughly washed with water. The non-dried samples formed a colloidal aqueous dispersion, whose aggregation was easily avoided by adding either acid or base. It is worth emphasizing here that TiO_2 yield was almost 100% and, most important, the ratio TiO_2 mass obtained/volume of the reaction mixture was really advantageous (approximately 1 g/10 ml). It is believed that this point could be specially interesting from an industrial point of view, since it represents a clear advantage with respect to other reported low-temperature nanocrystalline TiO_2 preparation procedures, in which diluted precursor solutions are commonly employed [19,29-31].

$$2\,[NR_4]_2TiF_6\,(aq) + 3\,H_3BO_3\,(s) \longrightarrow 2\,TiO_2\,(s) + 3\,[NR_4]BF_4\,(aq) + \ldots \quad (4.4.C)$$

Figure 4.4.3. Final quasi-solid TiO_2 paste with "cheese-like" appearance (from $[Cho]_2TiF_6$ medium) in the 30 ml Teflon-covered plastic reactor employed. Titania yield was almost 100%; TiO_2 mass obtained/volume of reaction mixture was 1g / 10ml, approx.

The positive role of the tetraalkylammonium cations in the precursor became evident at this point, since the blank experiment (*i.e.* direct reaction between HFTA and H_3BO_3 under similar experimental conditions) gave rise to the preparation of a titanium oxyfluoride instead of nanocrystalline titania. The result of the blank experiment was consistent with previous studies of high-concentration aqueous LPD (see zone (III) in Figure 1.7.1, Section 1.7) [29,32]. In addition, it was also found that boric acid presented higher solubility in the $[NR_4]_2TiF_6$ media rather than only in HFTA, also supporting the IL-like behavior of the initial precursor mixture.

4.4.2.A. Materials characterization

One common drawback in titania preparation procedures employing imidazolium-based ILs is the cleaning post-treatment *i.e.* habitually, the entrapped IL and other organics are extracted for long times by refluxing or hydrothermally processing the as-prepared TiO_2 in an organic solvent such as acetonitrile [19-22]. Alternatively, although our approach for titania preparation simply included short time

water extractions as cleaning procedures, no important contamination was found as seen by ATR-FTIR spectroscopy (see Figure 4.4.4) and C, N elemental analysis (in the 1.5-2 wt.% range).

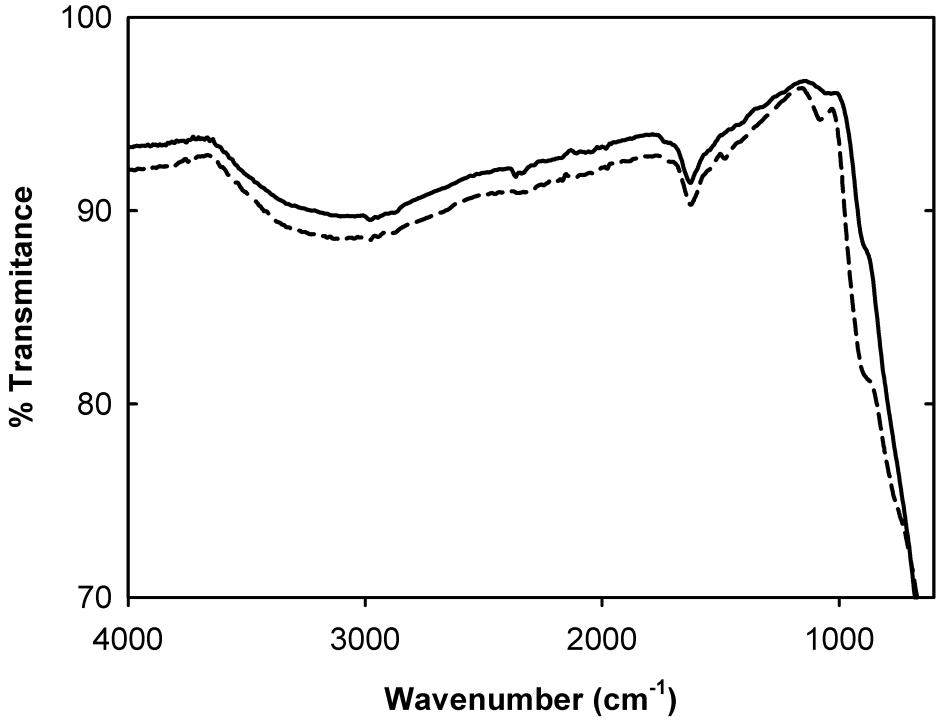

Figure 4.4.4. ATR-FTIR spectra of the water-cleaned nanocrystalline TiO_2 prepared from $[NR_4]_2TiF_6$ destabilization with boric acid. $[NR_4^+]$ = $BetH^+$ (solid line) and Cho^+ (dashed line).

As-prepared TiO_2 materials were additionally characterized by means of XRD, TEM and nitrogen adsorption/desorption. Significant differences were found by employing $BetH^+$ and Cho^+ as tetraalkylammonium cations under similar experimental conditions (Table 4.4.1), supporting the idea that each cation had a specific directing growth role in the final TiO_2 formed.

Table 4.4.1. Summary of XRD, TEM and nitrogen adsorption/desorption characterization of nanocrystalline titania, prepared from $[NR_4]_2TiF_6$ destabilized with boric acid at 85ºC during different aging times. [a]Estimated from (101) anatase reflection using the Scherrer equation.

Characterization	$[NR_4^+]$=$BetH^+$ (18h)	$[NR_4^+]$=Cho^+ (18h)	$[NR_4^+]$=Cho^+ (90h)	Comment
XRD [crystallite size][a]	anatase [~8 nm]	anatase/TiO_2-B	almost pure anatase	no typical *c* axis preferential growth of LPD
HR-TEM [crystallite size]	spherical nanocrystallites [5-7 nm]	irregular distribution [10-60 nm]	irregular distribution [10-100 nm] + nanorods [~15x60 nm]	-
nitrogen adsorption/desorption [BET surface area]	[~200 m^2/g]	-	[~110 m^2/g]	-

To summarize, on one hand, $BetH^+$ gave rise to a narrow size distribution of quasi-spherical anatase nanocrystals (5-7 nm) that do not evolve after a preparation time of 18 h. On the other hand, a mixture of anatase and TiO_2-B polymorphs was obtained after the same aging period but using $[Cho]_2TiF_6$ precursor solutions instead. However, in this latter case, almost pure anatase was observed for samples treated for longer times (90 h), suggesting a transformation from TiO_2-B to anatase phase during the process of synthesis. Moreover, titania nanorods consisting of ordered and twinned needle-like crystallites were also observed (see Figure 4.4.5) in samples aged 90 h from choline-based precursor solutions, which are potentially interesting, *e.g.* in DSSCs, since they have already shown inherently good electron transport properties [33,34]. It is thought the observed differences can be reasonably explained by the coordination capability of the carboxylate group of betaine toward metal ions and/or metal oxides, that is better than the aliphatic alcohol function of choline [5].

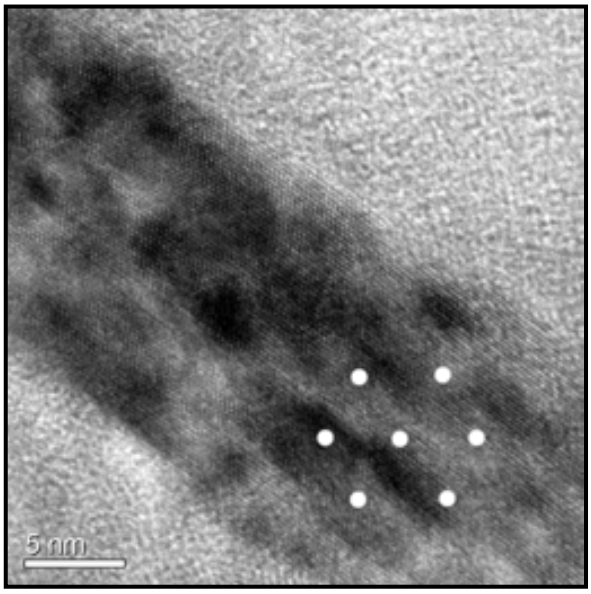

Figure 4.4.5. HR-TEM image and simulated electron diffraction pattern of a titania nanorod observed in samples obtained from $[Cho]_2TiF_6$ precursor solutions destabilized with boric acid for 90 h. Simulated electron diffraction pattern evidenced quasi-hexagonal symmetry. Corresponding lattice spacing was 2.37 Å, which can be assignable to either anatase (004) or TiO_2-B (401) reflections, according to JCPDS 21-1272 and 35-0088 patterns, respectively. HR-TEM image simulations are currently under investigation in order to discern crystalline structure.

It is assumed that some controversy can be surely derived from the "all-in-one" method for preparing TiO_2 in terms of affinity/contradiction with respect to Green Chemistry principles. The main drawback of the method is the toxicity and the corrosive character associated to both HFTA and the concentrated IL-like precursor solutions. On the other hand, high-yield titania crystallization was carried out at low temperature with no special equipment and, organic solvents were replaced by low-cost chemicals and only a water-based cleaning procedure was employed. In addition, a key advantage of the method is its inherent versatility since: (i) the crystal size and structure of the final product can be varied by carefully choosing a cation within the large tetraalkylammonium family of compounds; (ii) the commercial availability of H_2ZrF_6 and H_2SiF_6 makes the method potentially suitable for the preparation of the respective metal oxides in a analogous way; (iii) the destabilization process can be MW-activated, decreasing the reaction times from hours up to minutes and (iv) one-step synthesis of TiO_2 functionalized with enediol derivates has been achieved. IL-like nature of the resulting $[NR_4]BF_4$ by-product can be reasonably considered, whose recovering might result in a product with added value. Certainly, although special care should be taken in

the manipulation of the media, the IL-like precursor solutions method is specially attractive and open the door to further investigations, whose preliminary results are promising.

4.4.3. CONCLUSIONS

$[NR_4]_2TiF_6$ stable IL-like precursor solutions with only a small fraction of water are produced by the straightforward modification of commercial hexafluorotitanic acid (HFTA) with organic derivates containing a tetraalkylammonium cation. Nanocrystalline TiO_2 is quantitatively prepared by $[NR_4]_2TiF_6$ destabilization with boric acid at low temperature (85ºC) in a high-concentration LPD process. The crystal size and structure of the final titania product has shown to be dependent on the tetraalkylammonium cation present in the initial IL-like precursor solution. As relevant result, residual organics seem to be removed only by means of water cleaning procedures without requiring, for example, refluxing in an organic solvent for long times. The versatility, simplicity, low-cost as well as low-temperature processing represent important advantages of the proposed method and reasonably justify further investigations in the field of metal oxides synthesis.

4.4.4. REFERENCES

[1] Antonietti, M.; Kuang, D.; Smarly, B.; Zhou, Y. *Angew. Chem. Int. Ed.* **2004**, *43*, 4988-4992.

[2] Taubert, A.; Li, Z. *Dalton Trans.* **2007**, 723-727.

[3] Avalos, M.; Babiano, R.; Cintas, P.; Jiménez, J.L.; Palacios, J.C. *Angew. Chem. Int. Ed.* **2006**, *45*, 3904-3908.

[4] Plechkova, N.V.; Seddon, K.R. *Chem. Soc. Rev.* **2008**, *37*, 123-150.

[5] Nockerman, P., Thijs, B.; Pittois, S.; Thoen, J.; Glorieux, C.; Van Hecke, K.; Van Meervelt, L.; Kirchner, B.; Binnemans, K. *J. Phys. Chem. B* **2006**, *110*, 20978-20992.

[6] Ding, K.; Miao, Z.; Liu, Z.; Zhang, Z.; Han, B.; An, G.; Miao, S.; Xie, Y. *J. Am. Chem. Soc.* **2007**, *129*, 6362-6363.

[7] Dupont, J.; Suarez, P.A.Z. *Phys. Chem. Chem. Phys.* **2006**, *8*, 2441-2452.

[8] Reichert, W.M.; Hollbrey, J.D.; Vigour, K.B.; Morgan, T.D.; Broker, G.A.; Rogers, R.D. *Chem. Commun.* **2006**, 4767-4779.

[9] Lee, S.S. *Chem. Commun.* **2006**, 1049-1063.

[10] Abbott, A.P.; Boothby, D.; Capper, G.; Davies, D.L.; Rasheed, R.K. *J. Am. Chem. Soc.* **2004**, *126*, 9142-9147.

[11] Abbott, A.P.; Capper, G.; Davies, D.L.; Rasheed, R.K. *Chem. Eur. J.* **2004**, *10*, 3769-3774.

[12] Abbott, A.P., Capper, G.; Davies, D.L.; Rasheed, R. *Inorg. Chem.* **2004**, *43*, 3447-3452.

[13] Abbott, A.P.; Capper, G.; McKenzie, K.J.; Ryder, K.S. *J. Electroanal. Chem.* **2007**, *599*, 288-294.

[14] Abbott, A.P.; Capper, G.; Davies, D.L.; McKenzie, K.J.; Obi, S.U. *J. Chem. Eng. Data* **2006**, *51*, 1280-1282.

[15] BASF, BASIL process: www.corporate.basf.com/en/innovationen/preis/2004/basil.htm.

[16] GASGUARD® technology, Air Products: www.airproducts.com/markets/Electronics/Newsletter/SolutionsUpdate2.htm.

[17] IoLiTec: www.iolitec.de.

[18] Nakashima, T.; Kimikuza, N. *J. Am. Chem. Soc.* **2003**, *125*, 6386-6387.

[19] Yoo, K.; Choi, H.; Dionysiou, D.D. *Chem. Commun.* **2004**, 2000-2001.

[20] Yoo, K.; Choi, H.; Dionysiou, D.D. *Catal. Commun.* **2005**, *6*, 259-262.

[21] Choi, H.; Kim, Y.J.; Varma, R.S.; Dionysiou, D.D. *Chem. Mater.* **2006**, *18*, 5377-5384.

[22] Liu, Y.; Li, J.; Wang, M.; Li, Z.; Liu, H.; He, P., Yang, X.; Li, J. *Crys. Growth Des.* **2005**, *5*, 1643-1649.

[23] Yu, N.; Gong, L.; Song, H.; Liu, Y.; Yin, D. *J. Solid State Chem.* **2007**, *180*, 799-803.

[24] Zhou, Y.; Antonietti, M. *J. Am. Chem. Soc.* **2003**, *125*, 14960-14961.

[25] Taubert, A. *Angew. Chem. Int. Ed.* **2004**, *43*, 5380-5382.

[26] Zhu, H.; Huang, J.F.; Pan, Z.; Dai, S. *Chem. Mater.* **2006**, *18*, 4473-4477.

[27] Dobbs, W.; Suisse, J.M.; Douce, L., Welter, R. *Angew. Chem. Int. Ed.* **2006**, *45*, 4179-4182.

[28] Nyyssola, A.; Kerovuo, J.; Kaukinen, P.; Von Weymarn, N.; Reinikainen, T. *J. Biol. Chem.* **2000**, *275*, 22196-22201.

[29] Deki, S.; Aoi, Y.; Hiroi, O.; Kajinami, A. *Chem. Lett.* **1996**, *6*, 433.

[30] Niederberger, M.; Bartl, M.H.; Stucky, G.D. *Chem. Mater.* **2002**, *14*, 4364-4370.

[31] Niederberger, M.; Garnweitner, G.; Krumeich, F.; Nesper, R.; Cölfen, H.; Antonietti, M. *Chem. Mater.* **2004**, *16*, 1202-1208.

[32] Maeda, K.; Shimodaira, Y.; Lee, B.; Teramura, K.; Lu, D.; Kobayashi, H.; Domen, K. *J. Phys. Chem. C* **2007**, *111*, 18264-18270.

[33] Kamat, P.V. *J. Phys. Chem. C* **2007**, *111*, 2834-2860.

[34] Dürr, M.; Schmid, A.; Obermaier, M.; Rosselli, S.; Yasuda, A.; Nelles, G. *Nat. Mater.* **2005**, *4*, 607-611.

COMMUNICATION www.rsc.org/chemcomm | ChemComm

Hexafluorotitanate salts containing organic cations: use as a reaction medium and precursor to the synthesis of titanium dioxide†

David Gutiérrez-Tauste,[a] Xavier Domènech,[a] Concepción Domingo[b] and José A. Ayllón*[a]

Received (in Cambridge, UK) 29th June 2007, Accepted 1st October 2007
First published as an Advance Article on the web 10th October 2007
DOI: 10.1039/b709578c

The straightforward modification of commercial hexafluorotitanic acid with organic derivatives containing a tetraalkylammonium cation produced stable precursor solutions with only a small fraction of water, which were then used as a reaction medium for the synthesis of nanocrystalline TiO_2.

In the search for low cost and easy to implement methods to prepare nanocrystalline titanium dioxide (TiO_2), we are exploring the use of new techniques that avoid the use of organic solvents and/or controlled atmospheres. TiO_2 is a strategic material, with numerous applications in the areas of coatings and sensors. Its use in photocatalysis and dye-sensitized solar cells (DSSCs) is especially relevant to the solution of several problems, such as water contamination and energy supply. Hence, the search for new preparation methods that allow control over the microstructural and morphological parameters, and thus the properties of TiO_2, is encouraged. In this Communication, we describe how the simple modification of commercial hexafluorotitanic acid (HFTA) (60 wt% in water, Aldrich) with organic derivatives containing a tetraalkylammonium cation produces stable precursor solutions that include only a small fraction of water. These titania precursors, after reacting with boric acid (a common fluoride scavenger) at low temperature (85 °C), were quantitatively transformed into nanocrystalline TiO_2.

Ionic liquids (ILs) are new tools for designing alternative strategies in chemical synthesis and separation processes. Several advantages have also been established for materials preparation.[1] For instance, ILs can stabilize nanoparticles, they work as templates in zeolite crystallization and allow materials that are usually produced under hydrothermal conditions to be prepared in non-pressurized reactors.[1,2] The direct crystallization of TiO_2 at low temperature with complex morphologies like microspheres, in presence of ILs based on the butylmethylimidazole cation, has been reported.[3]

Other described materials preparation methods are based on ILs with a metal center, which simultaneously act as a solvent, molecular precursor and crystal growth driving agent.[4] This attractive "all-in-one" synthesis strategy, never reported before for TiO_2 preparation, has been pursued in this work. The use of salts containing a hexafluorotitanate anion and a tetraalkylammonium cation, present in numerous ILs, has been explored. These salts were prepared from commercial, low cost and easy to handle chemicals such as HFTA[5] and two organic derivatives: betaine (Bet; $Me_3N^+–CH_2–CO_2^-$) and choline (Cho^+; $Me_3N^+–CH_2–CH_2OH$) chloride.

Betaine, which can act as a base, forming the $HBet^+$ cation after carboxylate protonation, was firstly chosen for assay. In a typical synthesis procedure, 2.93 g (24.9 mmol) of Bet was dissolved in 3.35 g (12.2 mmol) of a 60 wt% HFTA solution in an exothermic reaction. The container was a plastic bottle, internally covered with Teflon and heated in a double boiler. The obtained viscous $(HBet)_2TiF_6$ solution, containing only 21 wt% of water, was stable over 60 °C. Due to the low proportion of water present, the obtained medium can be considered similar to that of ILs, and especially close to those formed from hydrated transition metal salts.[6] The concentration of ions was also higher than in previously described TiO_2 preparation procedures, in which ILs were used only as minor components of the initial reaction mixture.[3a,b,e]

HFTA and, most frequently, the derived ammonium salt are used to produce TiO_2 films by the Liquid Phase Deposition (LPD) method.[7,8] In this process, boric acid is employed as a fluoride scavenger, allowing a controlled hydrolysis of the precursor. In this work, a similar procedure was used to transform the new $(HBet)_2TiF_6$ precursor into TiO_2. 1.5 equivalents of boric acid, with respect to Ti, were added to the solution. The mixture was aged at 85 °C over 18 h, and gradually acquired a white paste texture. The sample did not evolve after this aging period. It was then dispersed in water, and the solid part was separated by centrifugation and thoroughly washed with water. The TiO_2 yield was almost 100%. The non-dried samples formed a colloidal aqueous suspension, which was easily stabilized against aggregation by the addition of a diluted base ($N(C_4H_9)_4OH$) or acid (HCl, $HClO_4$).

Characterization by high-resolution transmission electron microscopy (HR-TEM; Fig. 1a) showed that the obtained material consisted of nanocrystals (5–7 nm) with a narrow size distribution. A selected-area electron diffraction analysis of the sample (Fig 1b) pointed to the anatase crystal phase.

Samples dried at 85 °C presented a candy-like aspect due to particle aggregation. The small size and clean surface of the obtained nanoparticles facilitated their sintering at very low temperatures. According to ATR-FTIR characterization (not shown), the obtained TiO_2 contained only traces of organic species; below 1.5% according elemental analysis (C, N). XRD analysis (Fig. 2a) confirmed that the precipitated solid was anatase.

[a]*Departamento de Química, Universidad Autónoma de Barcelona, Campus UAB, 08193 Bellatera, Spain. E-mail: JoseAntonio.Ayllon@uab.es; Fax: +34 93581 2920; Tel: +34 93581 2176*
[b]*Instituto de Ciencia de Materiales de Barcelona, CSIC, Campus UAB, 08193 Bellaterra, Spain*

† Electronic supplementary information (ESI) available: Details of the characterization techniques employed and additional figures (Fig. S1 and S2). See DOI: 10.1039/b709578c

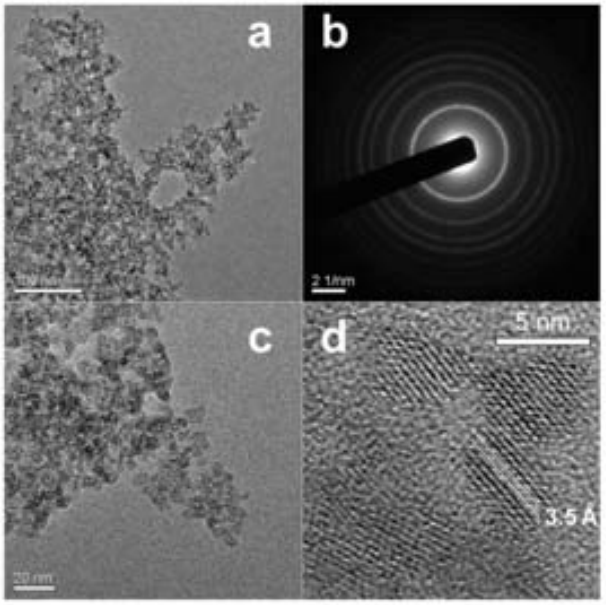

Fig. 1 Representative HR-TEM photographs.

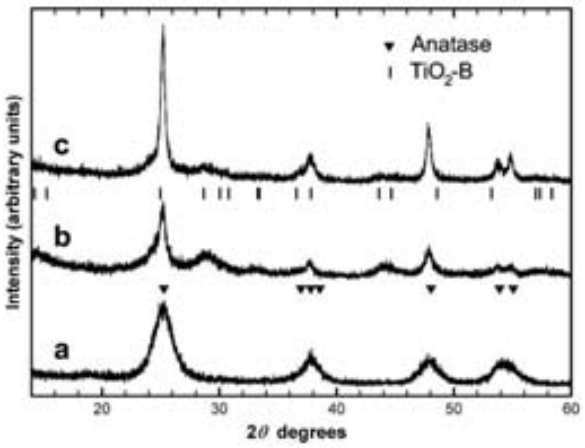

Fig. 2 XRD patterns of TiO_2 samples obtained from (a) $(HBet)_2TiF_6$ and from (b,c) $(Cho)_2TiF_6$. Symbols between traces signal the positions of the peaks corresponding to anatase (▼) and TiO_2–B (|).

The size of the nanoparticles, estimated from the peak width (Scherrer equation) of the XRD pattern, agreed with the value obtained from TEM characterization. Preferential growth of (004) is usually observed in anatase grown by LPD.[9] However, this preferential growth was not observed in the prepared samples, denoting that the growth medium used differed significantly from that of a diluted aqueous solution. The low temperature N_2 gas adsorption/desorption isotherm (BET analysis) of the TiO_2 nanoparticles showed a H2 type hysteresis loop, characteristic of mesoporous materials (Fig. 3a). The pore size distribution, calculated from the adsorption branch (Fig. 3b),[10] denoted the presence of pores in the 3–8 nm range. The estimated value of the specific surface area (S_a) was around 200 $m^2\ g^{-1}$.

Under similar experimental conditions, but in the absence of the $HBet^+$ organic cation, the reaction between concentrated

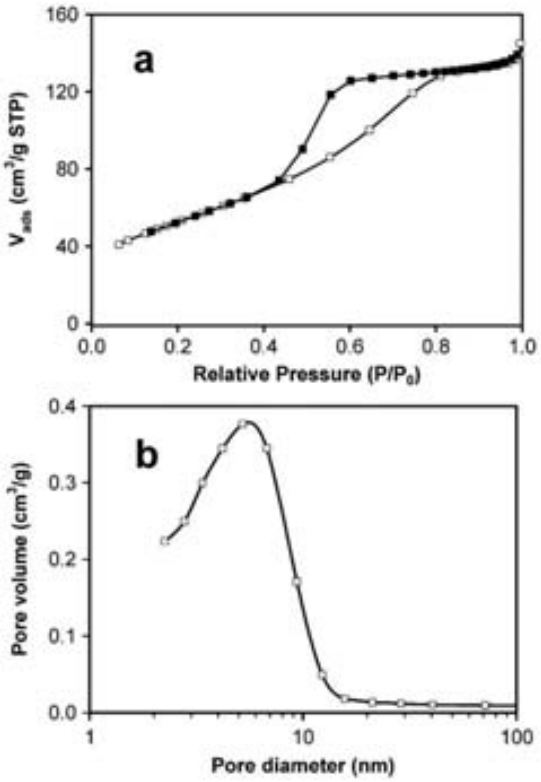

Fig. 3 (a) The N_2 gas adsorption (□)/desorption (■) isotherm and (b) the pore size distribution calculated from the adsorption branch of the isotherm of TiO_2 samples obtained from $(HBet)_2TiF_6$.

HFTA and boric acid (initially only partially dissolved) produced a titanium oxyfluoride. This compound could be described as $HTiOF_3$ according to the similarities between its XRD pattern and that of the corresponding $(NH_4)TiOF_3$ and other structurally related compounds (Fig. S1†).[11] It should be taken into account that, in our experiments, there was no ammonium source. $HTiOF_3$ is considered to be a product of the thermal decomposition of $(NH_4)TiOF_3$, although no direct preparation method has been described.[12] Therefore, it can be concluded that the $HBet^+$ cation enhanced the solubility of boric acid in the concentrated HFTA solution, allowing complete defluorination of the precursor and simultaneous control of the size of the precipitated particles. This fact is considered to be critical for the formation of nanocrystalline anatase.

In a second assay, the synthesis of TiO_2 was performed under similar experimental conditions, but using the Cho^+ cation instead of Bet. A $(Cho)_2TiF_6$ solution was prepared from HFTA and ChoCl, and HCl was liberated as a gas. This path was preferable to the reaction between HFTA and choline hydroxide, which is highly exothermic and produces additional water. The obtained viscous $(Cho)_2TiF_6$ solution was stable, even at room temperature. After the addition of boric acid and thermal treatment at 85 °C over an aging period of 18 h, a mixture of anatase and TiO_2–B polymorphs was obtained (Fig. 2b). Upon increasing the reaction time to 90 h, almost pure anatase was obtained (Fig. 2c). HR-TEM (Fig. S2†) confirmed the coexistence

of TiO_2–B and anatase after 18 h. The TiO_2 particles obtained after 90 h were larger and more irregular than those obtained using the $HBet^+$ cation, which led to a wider pore size distribution and lower S_a.

In summary, nanocrystalline TiO_2 was produced by adding organic derivatives, such as betaine or choline chloride, to commercial solutions of HFTA and using boric acid as a defluorinating agent. Although precautions should be taken due to the toxicity and corrosive character of both the precursor and fluorides, the method presents numerous advantages: all chemicals used are low cost, no organic solvent is needed, neither an inert atmosphere nor pressurized reactors are required, and the by-products can be washed with water. The ratio between TiO_2 yield and the required reaction volume is also advantageous. The aim of this Communication has been to describe a generic method for the preparation of nanometric crystals of TiO_2. A key advantage of this method is its versatility, since the crystal size and structure of the final product can be modified by careful choice of organic cation. Due to its high ionic content, the precursor mixture is, remarkably, able to absorb MW radiation, and using this heating procedure, the time necessary to produce the nanoparticles can be significantly reduced from hours to minutes. The method can also be used to prepare organic capped nanoparticles in a single step, *e.g.* by adding an enediol, such as catechol, to the initial solution. A comprehensive study will be reported elsewhere.

This work was supported by the Spanish National Plan of Research (CTQ2005-02808/PPQ project).

Notes and references

1 M. Antonietti, D. Kuang, B. Smarsly and Y. Zhou, *Angew. Chem., Int. Ed.*, 2004, **43**, 4988.
2 W. M. Reichert, J. D. Holbrey, K. B. Vigour, T. D. Morgan, G. A. Broker and R. D. Rogers, *Chem. Commun.*, 2006, 4767.
3 (*a*) K. Yoo, H. Choi and D. D. Dionysiou, *Chem. Commun.*, 2004, 2000; (*b*) K. S. Yoo, H. Choi and D. D. Dionysiou, *Catal. Commun.*, 2005, **6**, 259; (*c*) S. Miao, Z. Miao, Z. Liu, B. Han, H. Zhang and J. Zhang, *Microporous Mesoporous Mater.*, 2006, **95**, 26; (*d*) K. Ding, Z. Miao, Z. Liu, Z. Zhang, B. Han, G. An, S. Miao and Y. Xie, *J. Am. Chem. Soc.*, 2007, **129**, 6362; (*e*) H. Choi, Y. J. Kim, R. S. Varma and D. D. Dionysiou, *Chem. Mater.*, 2006, **18**, 5377; (*f*) Y. Liu, J. Li, M. Wang, Z. Li, H. Liu, P. He, X. Yang and J. Li, *Cryst. Growth Des.*, 2005, **5**, 1643; (*g*) N. Yu, L. Gong, H. Song, Y. Liu and D. Yin, *J. Solid State Chem.*, 2007, **180**, 799; (*h*) T. Nakashima and N. Kimizuka, *J. Am. Chem. Soc.*, 2003, **125**, 6386; (*i*) Y. Zhou and M. Antonietti, *J. Am. Chem. Soc.*, 2003, **125**, 14960.
4 (*a*) A. Taubert and Z. Li, *Dalton Trans.*, 2007, 723; (*b*) H. Zhu, J.-F. Huang, Z. Pan and S. Dai, *Chem. Mater.*, 2006, **18**, 4473; (*c*) A. Taubert, *Angew. Chem., Int. Ed.*, 2004, **43**, 5380; (*d*) W. Dobbs, J.-M. Suisse, L. Douce and R. Welter, *Angew. Chem., Int. Ed.*, 2006, **45**, 4179.
5 M. F. Borin, T. da Silva, R. F. Felisbino and D. Cardoso, *J. Phys. Chem. B*, 2006, **110**, 15080.
6 A. P. Abbott, G. Capper, D. L. Davies and R. K. Rasheed, *Chem.–Eur. J.*, 2004, **10**, 3769.
7 M.-K. Lee and B.-H. Lei, *Jpn. J. Appl. Phys.*, 2000, **39**, L101.
8 S. Deki, Y. Aoi, O. Hiroi and A. Kajinami, *Chem. Lett.*, 1996, **6**, 433.
9 J. A. Ayllón, A. M. Peiró, L. Saadoun, E. Vigil, X. Domènech and J. Peral, *J. Mater. Chem.*, 2000, **10**, 1911.
10 J. C. Groen, L. A. A. Peffer and J. Pérez-Ramírez, *Microporous Mesoporous Mater.*, 2003, **60**, 1.
11 N. M. Laptash, I. G. Maslennikova and T. A. Kaidalova, *J. Fluorine Chem.*, 1999, **99**, 133.
12 L. Zhou, D. S. Boyle and P. O'Brien, *Chem. Commun.*, 2007, 144.

Supplementary Material (ESI) for Chemical Communications

Hexafluorotitanate salts containing organic cations: use as a reaction medium and precursor to the synthesis of titanium dioxide

By David Gutiérrez-Tauste, Xavier Domènech, Concepción Domingo and José A. Ayllón*

Electronic Supplementary Information

Experimental Details

Electron diffraction patterns and Transmission Electron Microscopy (TEM) images were recorded in a JEOL 2011 microscope operating at 200 kV. Attenuated Total Reflectance Fourier Transform Infrared (ATR-FTIR) spectra were performed with a Bruker apparatus (Tensor model equipped with MKII Golden Gate). The elemental analyses (C, H, N) were carried out by the staff of the Chemical Analyses Service of the Universitat de Barcelona on a Carlo Erba CHNS EA-1108 instrument. X-Ray Diffraction (XRD) spectra of powder samples were registered on a Rigaku Rotaflex RU-200B diffractometer with Cu K_α radiation.

Textural characterisation of the samples was performed in a Micromeritics ASAP 2000 instrument. The Brunauer-Emmett-Teller (BET) surface area and pore size distribution of the titania samples were obtained from nitrogen adsorption/desorption isotherms at 77 K. A sample (0.1–0.3 g) was outgassed under vacuum for 8 h at 393 K prior to each measurement. In the calculation of the pore size distribution for TiO_2 samples, cumulative surface areas calculated from the pore volume and the pore diameter were consistent with the specific surface areas obtained by the BET method.[s1] The mesopore size distributions were calculated by applying the Barret-Joyner-Hallenda (BJH) [s2] method to the adsorption branch of the isotherms.

(s1) Sing, K.S.W.; Everett, D.H.; Haul, R.A.W.; Moscou, L.; Pierotti, R.A.; Rouquérol, J.; Siemieniewska, T. *Pure Appl. Chem.* 1985, **57**, 603.

(s2) Barret, E.P.; Joyner, L.G.; Halenda, P.P. *J. Am. Chem. Soc.* 1951, **73**, 373.

Supplementary Material (ESI) for Chemical Communications

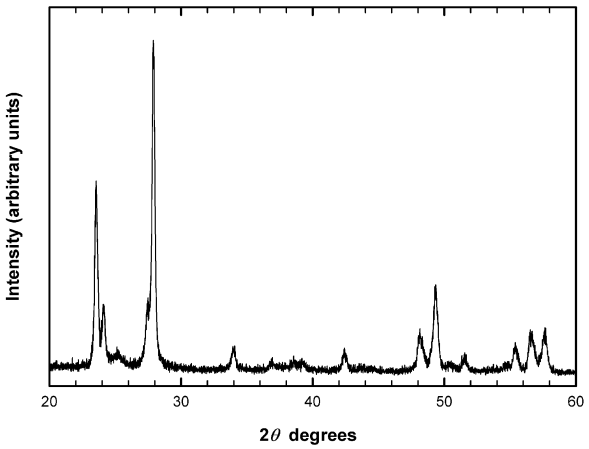

Figure S1. XRD pattern of a sample obtained from direct reaction between concentrated H_2TiF_6 and boric acid.

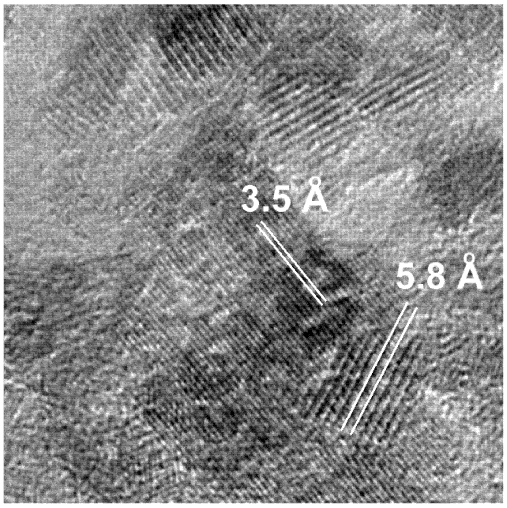

Figure S2. Representative HR-TEM image of a sample obtained from $(Cho)_2TiF_6$ after reacting with boric acid at 85ºC for 18 h, showing the coexistence of anatase and TiO_2-B.

CHAPTER 5:

CONCLUDING REMARKS

Solving technological limitations of titania concerning conventional high-temperature processing is necessary. In this work, novel low-temperature preparation routes for TiO_2 (and organic/TiO_2) powders and films have been explored following Green Chemistry guidelines. The as-prepared materials have been focused on practical applications in Dye-Sensitized Solar Cells and actuating materials. General conclusions and perspectives drawn from the work carried out can be summarized as follows, according to their respective Part in the foregoing Chapter 4:

PART 4.1: UV PREPARATION METHOD OF TiO_2 POROUS PHOTOELECTRODES FOR DSSCs

- To the best of our knowledge, all-plastic DSSCs in which TiO_2 porous photoelectrodes are processed by means of low-temperature strategies still remains quite low (max. η=7.4%) with respect to conventional high temperature annealing of rigid devices on thermostable substrates (~11%). Hence, further investigations in this research area should be attempted.

- Our proposal based on chemical necking of commercial P-25 nanoparticles via additional TiO_2 generated from UV degradation of a molecular precursor presents comparable features with respect to standard high temperature post-treatment in relatively large area devices.

PART 4.2: ALTERNATIVE FLUORIDE SCAVENGERS FOR TiO_2 LPD

- Fluoride scavengers others than boric acid for LPD are poorly reported in the literature. In this work, Al(III) and Fe(III) cations have been firstly studied for this role.

- Polycrystalline anatase TiO_2 films have been deposited with relative low times (3h) at a temperature of 80ºC on glass and ITO-glass. However, Al(III) seems the most suitable cation, since it has presented the highest average deposition rate, evidencing no incorporation of the cation within the film (by means of XPS), in contrast to Fe(III).

- Controlled glass corrosion by means of an aqueous solution of hexafluorotitanic acid has demonstrated positive effects as seed pretreatment for favoring posterior TiO_2 nucleation. Thus, homogeneity as well as degree of substrate coverage are enhanced in the subsequent TiO_2 LPD. One could infer this pretreatment might be of general use for improving quality of LPD deposits on glass.

PART 4.3: ONE-STEP ORGANIC/TiO_2 HYBRID THIN FILMS PREPARED BY LPD

- As proven in MB/TiO_2 and DA/TiO_2 materials, organic substances presenting either electrostatic affinity toward a fluorinated surface or chelating capability toward Ti(IV) sites at the surface are suitable candidates for one-step hybrid/TiO_2 Liquid Phase Deposition. Thus, LPD broadens horizons toward hybrid materials since TiO_2 synthesis is performed at low temperatures, not inducing thermal decomposition of organics.

- By means of entrapping organic substances within the growing titania, hybrid nanocomposite materials exhibiting different properties (*i.e.* nucleation, crystal growth, morphology, applications, *etc.*) can be reasonably expected. In this sense, novel actuating (or self-actuating) materials could be explored following similar strategies.

PART 4.4: ALL-IN-ONE IONIC LIQUID LIKE PRECURSOR SOLUTIONS FOR TiO_2 POWDER PREPARATION

- $[NR_4]_2TiF_6$ IL-like precursor solutions destabilized with boric acid at temperatures as low as 85ºC have achieved direct preparation of nanocrystalline TiO_2, suggesting a triple role of the media: solvent, precursor and crystal growth directing agent. It is worth emphasizing that, to the best of our knowledge, this all-in-one strategy had never been reported before for TiO_2.

- Although toxic and corrosive nature of the media seems to unfit Green Chemistry principles, inherent simplicity, versatility, low-cost and advantageous TiO_2 mass yielded/reactor volume ratio can be related to the desired guidelines. Further studies are justified since the method can be potentially designed from $[NR_4]_2MF_6$ (M=Ti, Si, Zr and NR_4^+=tetraalkylammonium cations) solutions, which could also be activated by microwave irradiation. Besides, one-step catechol capped TiO_2 nanoparticles have also been achieved, also suggesting a general via of organic/inorganic materials could be explored.

ANNEXE:

RESULTS WAITING FOR PUBLICATION

This section includes additional studies regarding to the preparation of nanocrystalline titania by destabilizing $[NR_4]_2TiF_6$ IL-like precursor solutions ($[NR_4^+]$=$BetH^+$, Cho^+) with boric acid at low temperature. It continues with the work done in Publication 5: **Hexafluorotitanate salts containing organic cations: use as a reaction medium and precursor to the synthesis of titanium dioxide.** *Chem. Commun.* **2007,** 4659-4661. First, the effects of varying temperature and time of the corresponding aging treatment on the titania crystallization process are briefly addressed in Annex A.1. Second, further studies of such home-made titania nanoparticles carried out at Material Science Laboratory of SONY Stuttgart Technology Center GmbH (Germany) are summarized in Annex A.2 (XPS characterization) and Annex A.3 (application in Dye-Sensitized Solar Cells).

A.1. TEMPERATURE AND TIME EFFECTS ON TITANIA CRYSTALLIZATION

As commented in Section 4.4, the crystal size and structure of the final titania produced by the IL-like precursor solutions method can be modified by carefully choosing the tetraalkylammonium cation. In a set of systematic experiments, a range of temperatures (65-120 ºC) and aging times (18-90 h) were also tested for both $BetH^+$ and Cho^+ cations.

On one hand, no significant dependence on the experimental parameters temperature and time was found in the case of $BetH^+$ cation. Thus, as shown in Publication 5, similar quasi-spherical nanoparticles with a relative narrow size distribution of 5-7 nm were obtained in all cases. Most probably, coordination of the carboxylate group of $BetH^+$ cation is responsible of such controlled crystallization process [1]. On the other hand, destabilization of $[Cho]_2TiF_6$ precursor solutions with boric acid exhibited a richer crystallization chemistry.

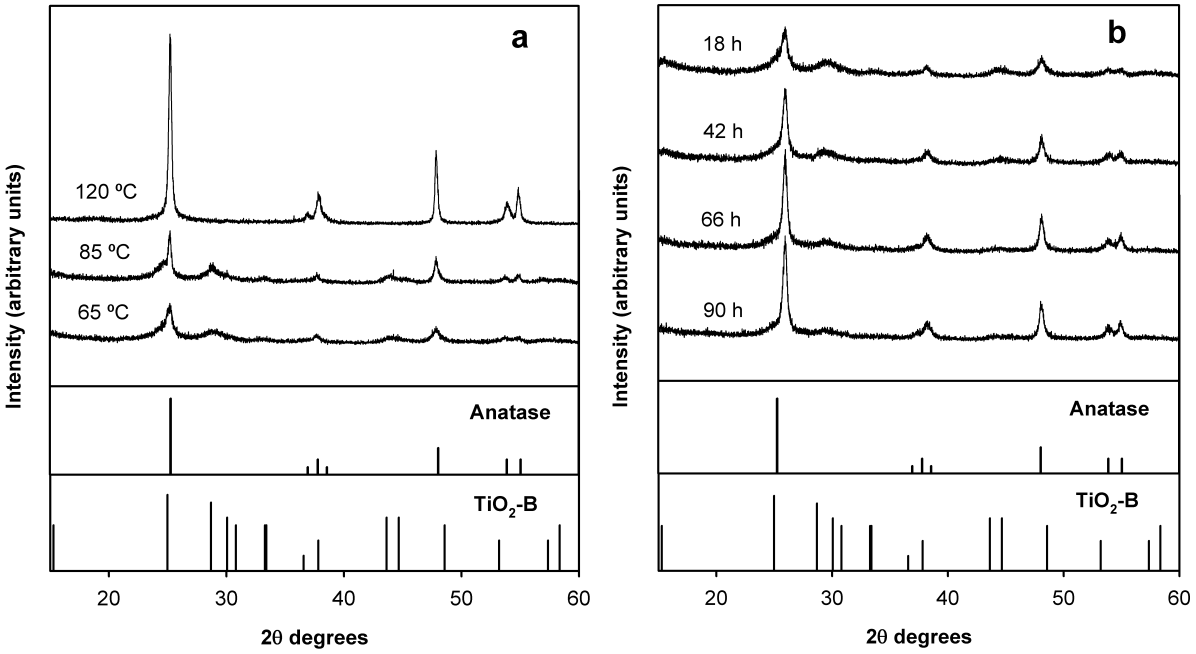

Figure A.1. XRD patterns of titania nanoparticles prepared from the destabilization of $[Cho]_2TiF_6$ precursor solutions (1 equivalent) with boric acid (1.5 equivalents): (a) temperature dependence, preparation time of 18 h; (b) time dependence, T=65ºC. JCPDS patterns of pure anatase (21-1272) and TiO_2-B (35-0088) are also included.

First, the dependence of the as-prepared titania nanoparticles from the $[Cho]_2TiF_6$ precursor solutions on aging temperature became evident for samples treated for 18 h (Figure A.1.a). Aging temperatures below 100 ºC gave rise to an irregular mixture of anatase and TiO_2-B phases. Nevertheless, taking into consideration the intensity of the peaks corresponding to each phase, the anatase/TiO_2-B ratio between samples treated at 65 ºC and 85 ºC was approximately equivalent. According to Scherrer equation, wider XRD signals of samples aged at 65 ºC evidenced smaller crystallite size as a consequence of a lower aging temperature. In principle, one might consider that this effect can be ascribed to a decrease in media viscosity with temperature [2]. Alternatively, at the highest temperature tested (120 ºC), stronger and narrower XRD signals assigned to pure anatase phase were observed. In this case, it is believed that the lower viscosity in combination with the increasing precursor media concentration (due to a significant water evaporation) gave rise to a situation in which formation of anatase crystallites was favored.

Second, it was also found that growing titania nanoparticles prepared form IL-like precursor solutions based on choline suffered an evolution depending on treatment time at a certain temperature. As example, Figure A.1.b shows the evolution according to the aging time of a sample prepared at 65 ºC. Taking into consideration the intensity of anatase and TiO_2-B XRD signals, we suppose a growing mechanism of the final large anatase crystallites by self-assembly of initial anatase and fresh anatase crystallites derived from a TiO_2-B transformation. It is thought that XRD and TEM studies of early stages might clarify how these phenomena occur and allow us to propose a low-temperature one-step synthetic approach toward the preparation of pure TiO_2-B. This metastable polymorph has attracted attention as host material for lithium storage [3,4] or humidity sensor material [5]. Unfortunately, TiO_2-B is generally prepared by three-step procedures (including solvothermal treatments of precursors in high-concentration NaOH aqueous solutions, followed by acid-washing and annealing treatments), in which the final product consists of anatase/TiO_2-B bicrystalline mixtures [5-7].

A.2. XPS CHARACTERIZATION

The composition of the as-prepared and sintered titania nanoparticles (at 450ºC for 30 min, as in Annex A.3 for DSSCs preparation) was studied by means of XPS. Samples were prepared on FTO-glass by placing a drop of a 2% ethanol based suspension and drying at 85ºC, a process that was repeated three times in order to maximize substrate coverage. Degussa P-25 reference samples for comparative purposes were prepared in the same way. The measurements were done on a Kratos Axis Ultra system with a monochromated Al K_α X-ray source and a charge neutralizer. All the binding energies were referenced to the C1s peak at 284.8 eV. As expected, the XPS results showed that titania samples contain not only Ti and O elements, but also some F, N and C contamination (Table A.1). According to ATR-FTIR results commented in Publication 5, no significant N and C contribution assignable to NR_4^+ cations was found in the as-prepared samples. It has to be taken into account that XPS peaks for C1s are always observed due to the adventitious hydrocarbon [8,9]. However,

the N content was significantly decreased after sintering due to the thermal decomposition of residual tetraalkylammonium derivates.

Table A.1. XPS composition analysis (at.% and Ti/F ratios) of titania samples prepared from $[NR_4]_2TiF_6$ IL-like precursor solutions destabilized with boric acid at 85ºC (aging times are indicated in brackets). [a]As-prepared, [b]sintered at 450ºC for 30 min.

Sample	F	O	Ti	N	C	Ti/F
$[NR_4^+]$=$BetH^+$ (18h)[a]	8.6	53	26	1.7	10	**3.0**
$[NR_4^+]$=Cho^+ (18h)[a]	11	50	26	1.5	11	**2.3**
$[NR_4^+]$=Cho^+ (90h)[a]	9.0	53	27	1.2	11	**3.0**
$[NR_4^+]$=$BetH^+$ (18h)[b]	1.0	59	28	0.6	8.7	**28**
$[NR_4^+]$=Cho^+ (18h)[b]	0.8	60	29	0.6	9.8	**35**
$[NR_4^+]$=Cho^+ (90h)[b]	1.1	59	29	0.5	9.9	**26**

The interest was then centered in the fluorine content, that is the most usual contaminant in TiO_2 materials prepared by LPD [8,9]. Although it has been previously noted that fluorine is practically not detected at the surface of FTO by XPS [10], blank experiments under the same experimental conditions were carried out in order to be on the safe side. The maximum F contribution from the FTO (F_{FTO} at.% max.) was calculated for each sample, taking into account the observed Sn at.% in the samples and the Sn/F ratio obtained in the FTO. In the worst case, the at.% of the observed fluorine was 24 times higher than the F_{FTO} at.% max. Hence, no significant contribution in the F signal was assured. The titania samples presented in all cases (as-prepared and sintered) F1s XPS symmetric signals centered at 685 eV, a value of binding energy associated to fluorine chemisorbed on the TiO_2 surface (≡Ti-F) [11-14]. Fluorine can be partially

eliminated by soaking the samples in 0.1 M NaOH for 1 night. In principle, substitutional F-doping in TiO_2 is dismissed since no peak located at 688 eV was observed, at least in the near surface region sampled by XPS (*i.e.* up to 10 nm [8,10,15]). Whereas noticeable amount of fluorine was detected in the as-prepared samples (only presenting a Ti/F atomic ratio of 2-3), peak intensities for F1s decreased significantly (Ti/F=25-35) when the annealing treatment was carried out (also with no F-doping). In fact, F-doping thermally induced at 450 ºC from initial surface fluorination has been reported to occur for longer sintering times (4 h) [16]. Most probably, during the sintering process fluorine element in the as-prepared materials gradually evaporates as HF gas [8]. However, no total fluoride disappearance was achieved in any case. At this point, became evident that the followed water-cleaning procedure allowed almost total NR_4^+ removal (as seen in Section 4.4) but was not effective enough for eliminating chemisorbed fluorine. However, surface fluorination of TiO_2 could be desirable in photocatalysis since oxidation pathways via hydroxyl radical have been found to effectively improve their quantum yield [17-20].

A.3. APPLICATION IN DSSCs

Titania nanoparticles prepared by destabilizing $[NR_4]_2TiF_6$ IL-like precursor solutions with boric acid at 85ºC were tested in laboratory scale DSSCs. Sandwich type solar cells were built as follows (see Figure A.2.a). A 30 nm TiO_2 blocking layer was formed on FTO-glass by spray pyrolysis. Home-made TiO_2 nanoparticles were deposited on this blocking layer by repeating 8 times a process consisting of spraying 2% ethanol based suspensions and drying at 80ºC on a hot plate for 10 min. Afterwards, the photoelectrodes were sintered under standard conditions at 450ºC for half an hour as in XPS analysis) and subsequently sensitized with red dye Ru 535 TBA molecules[Φ], by means of self-assembly from a 0.3 mM solution in ethanol for 1 night. The samples were dipped in ethanol to desorb any excess of dye and, after drying, the porous layer was then interpenetrated with an acetonitrile based liquid electrolyte

[Φ] *cis*-*bis*(*iso*thiocyanato)*bis*(2,2'-bipyridyl-4,4'-dicarboxylato)ruthenium(II)-*bis*(tetrabutylammonium)

containing the redox I_3^-/I^- couple ($[I_3^-]$=186 mM). Finally, TiO_2 photelectrodes were assembled with a Pt mirror counter electrode placing a 30 μm spacer between them. Current-voltage characteristics were registered under illumination with white light from a sulfur lamp (IKL Celsius, Light Drive 1000) at an intensity of 100 mW/cm^2. The spectral mismatch factor, in comparison with sunlight, was evaluated to be about 0.7 for this lamp. In order to assure reliability of the measurements, at least five DSSCs were tested for each type of nanoparticles.

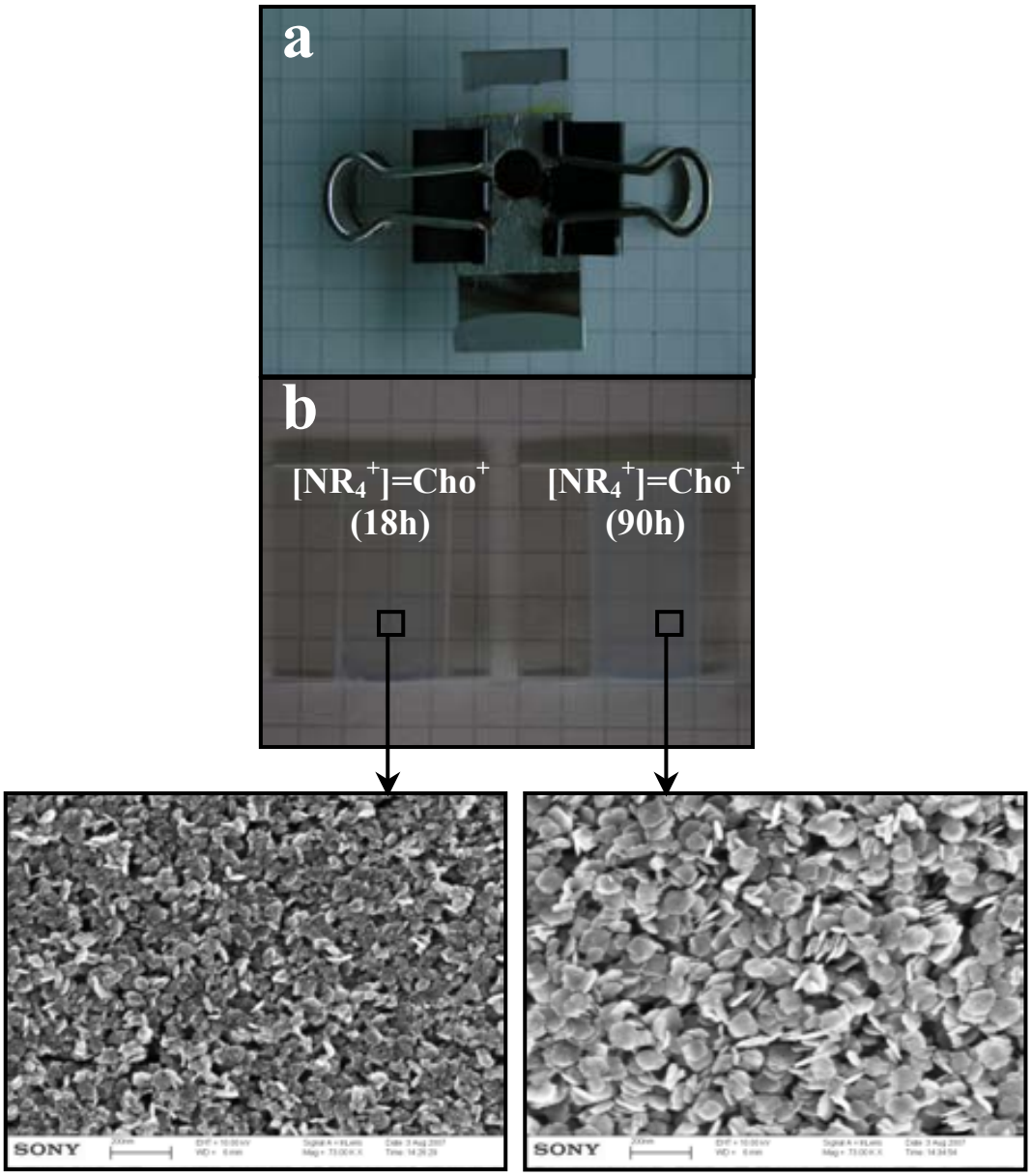

Figure A.2. (a) Laboratory scale DSSC once assembled, active area of 0.24 cm^2; (b) Macroscopic and SEM observations of TiO_2 photoelectrodes after sintering at 450ºC for 30 min according to the type of nanoparticle and aging time employed.

Porous titania photoelectrodes were successfully prepared via the low-cost and additive-free approach simply based on spraying a suspension of the corresponding home-made nanoparticles in ethanol. On the contrary, the desired porosity of the TiO_2 layers has to be habitually adjusted by burning a certain amount of organic content in the initial paste [21-23]. Samples with high transparency were obtained from titania nanoparticles prepared from $[Cho]_2TiF_6$ IL-like precursor solutions (Figure A.2.b), whereas nanoparticles obtained via the $[BetH]_2TiF_6$ route cracked during the consecutive spraying processes as a consequence of aggregate packing due to their small size and presented a hazy appearance. Therefore, no good electrical contact was expected in this latter case. SEM observations of $[Cho]_2TiF_6$ photoelectrodes show the presence of roughly shaped titania nanodisks in samples aged for 90 h. The formation of such nanostructures can be ascribed to two different self-assembly mechanisms of the nanoparticles either during storage of the suspension or during the sintering process. Further SEM studies are now being carried out to address the influence of the storage time of the titania suspensions in both ethanol and water.

The average performance of the devices built are summarized in Table A.2. As expected, particles prepared from $[BetH]_2TiF_6$ precursor solutions exhibited the worst overall efficiency. However, DSSCs fabricated with choline-derived nanoparticles presented remarkable performances in terms of J_{SC}, V_{OC}, FF and η. The highest value of power conversion efficiency (8.5 % approx.) was obtained for TiO_2 nanoparticles prepared from $[Cho]_2TiF_6$ IL-like precursor solutions destabilized with boric acid for 18 h. It is somehow surprising that such thin titania porous photoelectrodes (only 5 μm approx. and with surface area similar to samples aged at 90 h) showed high current density (17.6 mA/cm^2). In principle, according to MSL experience, one could have expected lower current density values since, as revealed UV-Vis spectroscopy, the amount of dye chemisorbed within the layer was limited. In fact, although optimal thickness of the TiO_2 porous layer mainly depends on the initial titania paste, sintering process and electrolyte, best power conversions have been usually found in devices with thicker films [24,25]. Therefore, improved power conversion efficiency can be reasonable expected by increasing the film thickness. In addition, it is known that

designing optimal structural engineering of the devices (*e.g.* tandem cells [26] or incorporation of scattering layers [27]) results in enhanced power conversion efficiencies.

Table A.2. Average performance parameters of DSSCs employing titania nanoparticles prepared from $[NR_4]_2TiF_6$ IL-like precursor solutions at 85ºC (aging times are indicated in brackets).

Sample	Thickness (µm)	Surface area (m^2/g)	J_{SC} (mA/cm^2)	V_{OC} (mV)	FF (%)	η (%)
$[NR_4^+]$=$BetH^+$ (18h)	8.8	150	14.5	689	66	6.6
$[NR_4^+]$=Cho^+ (18h)	4.9	100	17.6	744	65	8.5
$[NR_4^+]$=Cho^+ (90h)	6.9	110	15.6	742	68	7.8

The promising conversion efficiencies achieved justify further studies in the application of TiO_2 nanoparticles obtained via $[Cho]_2TiF_6$ IL-like precursor solutions in DSSCs, broadening the horizons of the "all-in-one" TiO_2 preparation method presented in Publication 5. Considering the total knowledge accumulated so far, one might consider additional questions taking as starting point nanoparticles obtained from $[Cho]_2TiF_6$ IL-like precursor solutions destabilized with boric acid at 85 ºC for 18 h: (i) Is there any synergic effect in the bicrystalline anatase/TiO_2-B structure?; (ii) According to the literature, TiO_2-B phase is metastable and slowly transforms into anatase at temperatures above 400-500ºC [28,29]. So, does this phase transformation occur during the sintering process carried out? Are the electrical contacts in the photoelectrodes improved as a consequence of that?; and (iii) Does the remaining fluorine chemisorbed on the titania surface after sintering have a positive role in the DSSCs working mechanism?

A.4. REFERENCES

[1] Nockerman, P., Thijs, B.; Pittois, S.; Thoen, J.; Glorieux, C.; Van Hecke, K.; Van Meervelt, L.; Kirchner, B.; Binnemans, K. *J. Phys. Chem. B* **2006**, *110*, 20978-20992.

[2] Reichert, W.M.; Hollbrey, J.D.; Vigour, K.B.; Morgan, T.D.; Broker, G.A.; Rogers, R.D. *Chem. Commun.* **2006**, 4767-4779.

[3] Zukalova, M.; Kalbac, M.; Kavan, L.; Exnar, I.; Grätzel, M. *Chem. Mater.* **2005**, *17*, 1248-1255.

[4] Armstrong, G.; Armstrong, A.R.; Canales, J.; Bruce, P.G. *Chem. Commun.* **2005**, 2454-2456.

[5] Wang, G.; Wang, Q.; Lu, W.; Li, J. *J. Phys. Chem. B* **2006**, *110*, 22029-22034.

[6] Kobayashi, M.; Petrykin, V.V.; Kakihana, M.; Tomita, K.; Yoshimura, M. *Chem. Mater.* **2007**, *19*, 5373-5376.

[7] Wang, Q.; Wen, Z.; Li, J.; *Inorg. Chem.* **2006**, *45*, 6944-6949.

[8] Yu, J.G.; Yu, H.G.; Cheng, B; Zhao, X.J.; Yu, J.C.; Ho, W.K. *J. Phys. Chem. B* **2004**, *107*, 13871-13879.

[9] Gutiérrez-Tauste, D.; Domènech, X.; Hernández-Fenollosa, M.A.; Ayllón, J.A. *J. Mater. Chem.* **2006**, *16*, 2249-2255.

[10] Andersson, A.; Johansson, N.; Bröms, P.; Yu, N.; Lupo, D.; Salaneck, W.R. *Adv. Mater.* **1998**, *10*, 859-863.

[11] Li, D.; Haneda, H.; Labhsetwar, N.K.; Hishita, S.; Ohashi, N. *Chem. Phys. Lett.* **2005**, *401*, 579-584.

[12] Li, D., Haneda, H.; Hishita, S.; Ohashi, N.; Labhsetwar, N.K. *J. Fluorine Chem.* **2005**, *126*, 69-77.

[13] Yu, J.C.; Yu, J.; Ho, W.; Jiang, Z.; Zhang, L. *Chem. Mater.* **2002**, *14*, 3808-3816.

[14] Huang, D.G.; Liao, S.J.; Liu, J.M.; Dang, Z.; Petrik, L. *J. Photochem. Photobiol. A: Chem.* **2006**, *184*, 282-288.

[15] Buschow, K.H.J.; Cahn, R.W.; Flemings, M.C.; Ilschner, B.; Kramer, E.J.; Mahajan, S. *Encyclopedia of Materials: Science and Technology.* Ed. Elsevier. **2001**. ISBN: 0-08-043152-6.

[16] Wang, D.; Li, W.; Zhang, M.; Tao, K. *Appl. Catal. A* **2007**, *317*, 105-112.

[17] Minero, C.; Mariella, V.; Maurino, V.; Pelizzetti, E. *Langmuir* **2000**, *16*, 2632-2641.
[18] Minero, C.; Mariella, G.; Maurino, V.; Vione, D.; Pelizzetti, E. *Langmuir* **2000**, *16*, 8964-8972.
[19] Park, H.; Choi, W. *J. Phys. Chem. B* **2004**, *108*, 4086-4093.
[20] Kim, H.; Choi, W. *Appl. Catal. B* **2007**, *69*, 127-132.
[21] Dürr, M.; Schmid, A.; Obermaier, M.; Yasuda, A.; Nelles, G. *J. Phys. Chem. A* **2005**, *109,* 3967-3970.
[22] Dürr, M.; Rosselli, S.; Yasuda, A.; Nelles, G. *J. Phys. Chem. B* **2006**, *110*, 21899-21902.
[23] Ito, S.; Cevey Ha, N.; Rothenberger, G.; Liska, P.; Comte, P.; Zakeeruddin, S.M.; Péchy, P.; Nazeeruddin, M.K.; Grätzel, M. *Chem. Comm.* **2006**, 4004-4006.
[24] Nazeeruddin, M.K.; Péchy, P.; Renouard, T.; Zakeeruddin, S.; Humphry-Baker, R.; Comte, P.; Liska, P.; Cevey, L.; Costa, E.; Shklover, V.; Spiccia, L.; Deacon, G.B.; Bignozzi, C.A.; Grätzel, M. *J. Am. Chem. Soc.* **2001**, *123*, 1613-1624.
[25] Grätzel, M. *Prog. Photovolt: Res. Appl.* **2006**, *14*, 429-442.
[26] Dürr, M.; Bamedi, A.; Yasuda, A.; Nelles, G. *Appl. Phys. Lett.* **2004**, *84*, 3397-3399.
[27] Tachibana, Y.; Hara, K.; Sayama, K.; Arakawa, H. *Chem. Mater.* **2002**, *14*, 2527-2535.
[28] Nuspl, G.; Yoshizawa, K.; Yamabe, T. *J. Mater. Chem.* **1997**, *7*, 2529-2536.
[29] Zhu, J.; Zhang, J.; Chen, F.; Anpo, M. *Mater. Lett.* **2005**, *59*, 3378-3381.